




Universitat Autònoma de Barcelona

**ADVERTIMENT.** L'accés als continguts d'aquesta tesi queda condicionat a l'acceptació de les condicions d'ús establertes per la següent llicència Creative Commons:  [http://cat.creativecommons.org/?page\\_id=184](http://cat.creativecommons.org/?page_id=184)

**ADVERTENCIA.** El acceso a los contenidos de esta tesis queda condicionado a la aceptación de las condiciones de uso establecidas por la siguiente licencia Creative Commons:  <http://es.creativecommons.org/blog/licencias/>

**WARNING.** The access to the contents of this doctoral thesis it is limited to the acceptance of the use conditions set by the following Creative Commons license:  <https://creativecommons.org/licenses/?lang=en>



# **Design and development of molecularly imprinted polymers and imprinted sensors**

Ferdia Bates

Doctoral Thesis

Doctoral Studies in Chemistry

Director: Manel del Valle Zafra

Departament de Química

Facultat de Ciències

2016



# Declaration

---

Thesis submitted to aspire for the doctoral degree

Ferdia Bates

Director's approval:

Dr. Manel de Valle Zafra Professor of Analytical Chemistry

Bellaterra (Ceerdanyola del Vallès), September 2016



## Funding acknowledgement

---

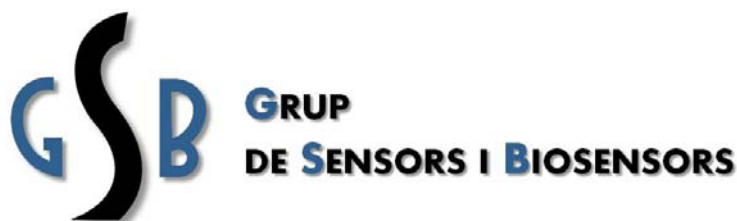
This present dissertation has been carried out in the laboratories of the Grup de Sensors i Biosensors of the Department de Química in the Universitat Autònoma de Barcelona, with the support of the Marie Curie Actions fellowship FP7-PEOPLE-2010-ITN- and the financial support of the Ministry of Economy and Innovation (MINECO) project “Electronic tongue fingerprinting: aplicaciones en el campo alimentario y de seguridad” (MCINN, CTQ2013-41577-P).

Grup de Senors i Biosensors

Unitat de Química Analítica

Department de Química Universitat Autònoma de Barcelona

Edifici Cn 08193, Bellatera



## Acknowledgments

For my Masters supervisor at Cranfield university, Doctor Yi Ge, my respected colleague and friend, I would like to offer my most heart-felt thanks; without Dr Ge's encouragement, advise and reference, I most probably would not have pursued a doctorate as a career choice.

I acknowledge Doctor Manel del Valle, my doctoral supervisor at the Autonomous University of Barcelona. For the lessons I have learned and the experience I have gained during our time together I extend my profound thanks. I am a better scientist because of them and I hope that the Barcelona laboratory has benefited from my time there.

To Andrea and Delfina, members of MC Team Barcelona, for the support, love and understanding you both have extended to me. We have all grown so much over our shared time and PhD projects together. And now we are all doctors!

To Professor Sergey Piletsky of the University of Leicester, I must also offer my sincerest gratitude for extending an invitation to work in his laboratory for several months. These resulted in a publication and a gargantuan increase in my knowledge of polymer chemistry. Even more thanks must be given for his suggestion and for originally putting me in touch with the University of Coruña which turned out to be such a fruitful collaboration.

To Doctor José Manuel López-Vilariño, of the University of Coruña; his drive and charisma, not to mention his excellent taste in music, allowed this collaboration to be so productive during my time

there.

A huge thank you to Maria Paredes Ramos for the great image on the front cover and also for the Spanish corrections in the resumen!

To Mirko Busato of the University of Verona, I must say a very big 'thank you' to the man who always had a clear explanation and solution to all my issues and problems with Linux and Gromacs.

To Vanessa, you more than anyone have helped me to arrive to this point. Thank you and 'poof!'.

To everyone who has helped and collaborated with me along this journey; if a philosophy doctorate is ultimately a search for knowledge, I hope we have found some together.



“Sucedió, pues, que como el amor en los mozos por la mayor parte no lo es, sino apetito, el cual, como tiene por último fin el deleite, en llegando a alcanzarle se acaba, y ha de volver atrás aquello que parecía amor, porque no puede pasar adelante del término que le puso naturaleza, el cual término no le puso a lo que es verdadero amor.”

“Now as love in a young man is, for the most part, nothing but appetite, and as pleasure is the ultimate end, it is terminated by enjoyment; and what seemed to be love vanishes, because it cannot pass the bounds assigned by nature; whereas true love admits of no limits.”

- Miguel de Cervantes Saavedra<sup>1</sup>

---

1 Miguel de Cervantes Saavedra, in Don Quixote



# **Table of Contents**

---



Declaration .....	III
Funding acknowledgement .....	IV
Acknowledgments.....	V
Table of Contents.....	IX
Abbreviations .....	XV
Summary .....	XXIII
Resumen.....	XXVII
1. Introduction.....	1
1.1 Molecularly Imprinted Polymers .....	5
1.1.1 MIP prehistory: Targeted detection and the start of the field .....	5
1.1.2 The birth and growth of a discipline .....	5
1.2. Molecular Imprinting Strategies .....	11
1.2.1 Covalent imprinting .....	11
1.2.2 Semi-covalent imprinting.....	14
1.2.3 Non-covalent imprinting .....	18
1.3 Polymerisation formats .....	23
1.3.1 Bulk form polymers .....	27
1.3.2 Polymer particles and polymer resins .....	29
1.3.3 Films, layers and membranes .....	37
1.4 Polymerisation mechanism .....	40
1.4.1 Condensation polymerisation.....	41
1.4.2 Addition polymerisation .....	42
1.5 Rational design of a molecular imprinting protocol .....	45



1.5.1 Porogenic solvents for molecular imprinting .....	46
1.5.2 Template solvation and stability .....	54
1.5.3 Selection of crosslinking monomer.....	56
1.5.4 Initiation rate .....	59
1.6 Transduction methods used for MIPs .....	62
1.6.1 MIPs in sensor arrays .....	64
1.7 Computational modelling for molecular imprinting .....	68
1.7.1 Computational chemistry .....	70
1.7.2 Model smelliness.....	73
1.7.3 The combinatorial approach.....	76
1.8 References .....	78
2. Objectives.....	101
3. Experimental.....	105
3.1 Materials.....	109
3.2 Instrumentation .....	110
3.2.1 Laboratory instrumentation.....	110
3.2.2 Computational instrumentation.....	111
3.3 Polymerisation Protocols .....	113
3.4 MIP immobilisation .....	114
3.5 Detection parameters.....	116
3.6 Computational Chemistry .....	118
3.6.1 Preparation of virtual molecules .....	118
3.6.2 Virtual Screening .....	122
3.6.3 Simulation of molecular dynamics .....	126
3.7 References.....	129
4. Results and discussion .....	133
4.1 Voltammetric sensor for theophylline using sol-gel immobilised molecularly imprinted polymer particles.....	137
4.1.1 Particle synthesis and sol-gel immobilisation.....	137
4.1.2 Optimisation and determination of deposition, drying and regeneration sol-gel conditions .....	138
4.1.3 Electrochemical Characterisation .....	143
4.2 Computational design of molecularly imprinted polymer for direct detection of melamine in milk .....	149
4.2.1 Solvation of melamine into the porogen and the use of computational modelling.....	149
4.2.2 Thermodynamic calculation of stoichiometric ratio and MIP composition .....	155
4.2.3 Selection of initiator and polymerisation temperature .....	157
4.2.4 Mobile phase selection and polymer characterisation .....	158
4.2.5 Testing on spiked real milk samples .....	162

4.3 Virtual Screening of Receptor Sites for Molecularly Imprinted Polymers.....	165
4.3.1 Detection of hypoxanthine using a theophylline-imprinted polymer .....	166
4.3.2 Detection of Tetrahydrocannabinol using Catechin-Imprinted Polymers .....	171
4.3.3 Design of a Bisphenol A –Imprinted Polymers .....	182
4.4 References.....	189
5. Conclusions and future work .....	195
5.1 Conclusions.....	197
5.2 Ongoing and future work .....	199
5.2.1 Virtually matched, triggerable polymer sensor arrays for electronic tongues .....	199
5.2.2 Augmentation of the computational power.....	200
5.2.3 Improvement of virtual screening of imprinted receptors .....	202
5.2.4 Incorporation of Open-Source Modelling Techniques into Online screening platform for MIP design .....	203
5.2.5 Application of an array of CIT imprinted polymer pastilles to a GSB artificial neural network.....	205
6. Publications.....	207
Annex .....	229



# Abbreviations

---



## Abbreviations

$\Delta H$	The heat of vaporisation
$\alpha$	Imprint factor
$\delta$	Hildebrand solubility parameter
$\delta_d$	Inherent dispersion or van der Waals forces
$\delta_h$	The hydrogen bonding capacity
$\delta_p$	Dipolar interaction or polarity
$\delta_T$	Total Hansen solubility parameter
$\epsilon$	Magnitude of the well energy potential
$\zeta$	The distance at which the inter-atomic potential can be defined as zero
$\zeta_s$	HPLC separation Factor
<b>2VP</b>	2 vinylpyridine
<b>4VP</b>	4 vinylpyridine
$\text{\AA}$	Angstrom
<b>A</b>	The pre-exponential factor which relates temperature to the rate coefficient

<b>AA</b>	Acrylic acid
<b>AC</b>	Aromatic carbon atom (Autodock ligand.pdbqt)
<b>ACE</b>	Acetaminophen
<b>ACPYPE</b>	AnteChamber PYthon Parser interfacE
<b>ACR</b>	Acrylamide
<b>ADT</b>	Autodock Tools
<b>AD4</b>	Autodock 4
<b>AIBN</b>	Azobisisobutyronitrile
<b>AICN</b>	1,1' azobis-cyclohexanecarbonitrile
<b>AIVN</b>	2,2'-Azobis (2,4-dimethylvaleronitrile)
<b>AMBER</b>	Assisted Model Building with Energy Refinement
<b>AMPSA</b>	Acrylamido-2-methyl-1-propanesulfonic acid
<b>B<sub>max</sub></b>	Apparent number of receptor binding sites
<b>C</b>	Enthalpy of vaporisation
<b>CAF</b>	Caffeine
<b>CAT</b>	Catechin hydrate
<b>CHARMM</b>	Chemistry at HARvard Macromolecular Mechanics
<b>CIT</b>	Technological Research Centre (Centro de Investigaci3n Tecnol3gicas)
<b>COSMOS</b>	Computer Simulation of Molecular Structure
<b>DCCA</b>	Drying chemical control additives
<b>DEAEM</b>	<i>N,N</i> -diethylamino ethyl methacrylate
<b>DMF</b>	Dimethylformamide
<b>DMSO</b>	Dimethyl Sulfoxide
<b>DNA</b>	Deoxyribonucleic acid
<b>DVB</b>	Divinylbenzene
<b>ECMIPS</b>	Electrochemical molecularly imprinted polymer sensors
<b>EGDMA</b>	Ethylene glycol dimethacrylate

<b>EGMP</b>	Ethylene glycol methacrylate phosphate
<b>ET</b>	Electronic Tongue
<b><math>E_a</math></b>	Activation energy
<b>FET</b>	Field effect transistor
<b>FM</b>	Functional monomer
<b>FP</b>	First principals
<b>GAFF</b>	Generalised Amber Force Field
<b>GO</b>	Geometric optimisation
<b>GROMOS</b>	GRoningen MOlecular Simulation computer program package
<b>GSB</b>	Sensors and Biosensor research group (Grup de Sensores I Biosensores)
<b>GUI</b>	Graphic User Interface
<b>HD</b>	Hydrogen donor atom (Autodock ligand.pdbqt)
<b>HEMA</b>	Hydroxyethyl methacrylate
<b>HPLC</b>	High performance liquid chromatography
<b>IA</b>	Itaconic acid
<b>IF</b>	Imprint factor
<b><math>k_x</math></b>	Retention factor of the molecule numerically referenced in the subscript
<b><math>K_d</math></b>	Affinity constant
<b><math>k_d</math></b>	Rate constant
<b>L</b>	Column length
<b>LINCS</b>	Linear constraint solver
<b>LOD</b>	Limit of detection
<b>MAA</b>	Methacrylic acid
<b>MBAA</b>	N,N', acrylamide, methylenebisacrylamide
<b>MD</b>	Molecular dynamics
<b>MeCN</b>	Acetonitrile
<b>MIP</b>	Molecularly imprinted polymers



<b>MIP-NP</b>	Imprinted polymer nanoparticle
<b>MW</b>	Molecular weight
<b>nm</b>	Nanometer
<b>N</b>	Theoretical plate number for stationary phase of a column
<b>NA</b>	Nitrogen acceptor atom (Autodock ligand.pdbqt)
<b>NIP</b>	Non-imprinted polymer
<b>NP</b>	Nanoparticles
<b>NMR</b>	Nuclear Magnetic Resonance
<b>NPHS</b>	Non-polar hydrogen atoms
<b>NPEDMA</b>	N-phenylethylene diamine methacrylamide
<b>OA</b>	Oxygen acceptor atom (Autodock ligand.pdbqt)
<b>OLPS</b>	Optimized Potentials for Liquid Simulations
<b>PBC</b>	Periodic boundary conditions
<b>PME</b>	Particle mesh Ewald
<b>QCM</b>	Quartz crystal microbalance
<b>R</b>	Universal gas constant
<b>R<sup>2</sup></b>	Coefficient of regression
<b>r</b>	Distance between two atoms
<b>SAR</b>	Structure activity relationship
<b>SAW</b>	Surface acoustic wave
<b>SPE</b>	Solid phase extract
<b>SPR</b>	Surface plasmon resonance
<b>STW</b>	Surface transverse wave
<b>T</b>	Absolute temperature respectively
<b>THC</b>	Tetrahydrocannabinol
<b>TRIGLYME</b>	Triethylene glycol dimethyl ether
<b>t<sub>r</sub></b>	Analyte retention time at maximum peak height

<b>t<sub>0</sub></b>	Column dead volume
<b>TB</b>	Tight binding
<b>TEOS</b>	Tetraethyl orthosilicate
<b>TFAA</b>	Trifluoromethylacrylic acid
<b>THF</b>	Tetrahydrofuran
<b>TLC</b>	Thin layer chromatography
<b>TORSDORF</b>	Torsional degrees of freedom of a ligand molecule in the Autodock file format
<b>TRIM</b>	Trimethylolpropane trimethylacrylate
<b>UAB</b>	Autonomous University of Barcelona (Universitat Autònoma de Barcelona)
<b>UDC</b>	University of La Coruña (Universidade da Coruña)
<b>UoL</b>	Univeristy of Leicester
<b>V<sub>m</sub></b>	Solvent-molar volume
<b>VD</b>	1-vinylimidazole
<b>VdW</b>	Van der Waals
<b>VI</b>	1-vinylimidazole
<b>VINA</b>	Referring to the Autodock VINA scoring algorithm
<b>VMD</b>	Visual Molecular Viewer
<b>v/v</b>	Volume per volume
<b>V(r)</b>	Lennard-Jones potential for two particles at a distance 'r'
<b>w<sub>h</sub></b>	Width of peak at half the maximum peak height
<b>w/w</b>	Weight per weight



## Summary

---



This thesis was predominantly undertaken to study and investigate molecular imprinted polymers (MIPs) with a view to their use as high longevity sensing elements in sensor arrays. The research line of the thesis was intended to lead to the integration of these imprinted arrays into an Electronic Tongue (ET) sensing system which is the area of expertise of the research group in which this project was primarily executed. Having initially executed a review of the literature, focusing initially on the application of the MIPs to an electrochemical device, an imprinted voltammetric sensor and a complimentary sensing procedure was developed using a combination of protocols extracted from the literature. This sensor, described in *Article 1*, had good selectivity toward the primary analyte, theophylline, and specificity against structural analogues. Though the design of the sensor allowed for significantly improved regeneratibility of the sensor relative to similar systems in the literature, the insulating nature of the polymers used in the MIP reduced the electron transfer rate at the sensor surface and thus resulted in a reduction in sensitivity.

Following this initial experimental study, a secondment was undertaken in the University of Leicester under the supervision of Professor Sergey Piletsky. During this period, an intensive study of the design process of molecular imprinting, aided by an in-house computational molecular modelling platform, was conducted focusing on the design of an imprinted receptor for the low solubility 'model template', melamine. This MIP was successfully synthesised, characterised and used in the detection of melamine in milk samples, as detailed in *Article 2*.

Further development of computational modelling techniques for the evaluation of MIP modelling techniques was also achieved with a view to create a virtual evaluation technique for the design of imprinted receptor sites optimised for the requirements of their application to an ET sensor array using the skills acquired during the Leicester secondment as detailed in *Article 3*.

As detailed in the final chapter of this thesis, the insight into the imprinting process which was acquired during the research has been used to design a sensor array system which meets the specifications of ET experimental runs. This takes the form of the introduction of the research topic computationally selected polyelectrolytes, immobilised onto a voltammetric electrode surface via highly robust conducting graphite ink. Additional recommendations are also made to further enhance the on-going MIP projects within the laboratory, such as the separation of the MIP and the electrode to increase MIP regeneratibility. Some final suggestions for some other inter-institutional collaboration are also presented which aim to creating portable ET system for in-field sample collection and analysis.



# Resumen

---





Esta tesis se ha hecho principalmente para estudiar e investigar polímeros impresos (MIPs) con la intención de usarlos como sensores de larga vida. La línea de investigación de esta tesis es la dirigida a conseguir la integración de estas formaciones impresas dentro de una lengua electrónica (ET), que es la rama de especialización en la que se ha desarrollado principalmente este proyecto. Después de hacer una revisión de la literatura, que inicialmente se centraba en la aplicación de MIPs a un equipo electroquímico, un sensor voltamétrico impreso y un procedimiento sensitivo complementario, el procedimiento se creó a través de una combinación de protocolos tomados de la literatura. Este sensor, descrito en el *Artículo 1*, presentaba una buena selectividad hacia el analito primario, teofilina, además de la especificidad requerida frente a sus análogos estructurales. Aunque el diseño del sensor permitía una mejor regeneración de la superficie respecto a otros sistemas parecidos encontrados en la literatura, el comportamiento de los polímeros usados en el MIP retardaba la tasa de transferencia de electrones en la superficie del sensor. Por culpa de este fenómeno, la sensibilidad del sensor se reducía.

Justo después de estos experimentos iniciales, se hizo una colaboración con el grupo del Profesor Sergey Piletsky en la Universidad de Leicester (UoL) de Reino Unido. Durante este período, se realizó un estudio intensivo del proceso de diseño de impresión molecular asistido por un sistema computacional de modelización molecular ‘inhouse’. Se puso énfasis en el diseño de un receptor impreso para la molécula de baja solubilidad melanina, que se toma como ‘template modelo’. El MIP resultante se caracterizó y usó para la detección de melanina en muestras de leche, tal y como se describe y detalla en el *Artículo 2*.

Más tarde, utilizando los conocimientos adquirido durante la estancia en Leicester, se desarrollaron nuevas técnicas de modelización computacional para la evaluación de los métodos utilizados en la modelización de MIPs, con el objetivo de obtener una técnica de evaluación virtual para el diseño de receptores impresos, optimizados para los requerimientos necesarios para su posterior aplicación en un sensor ET, tal como se detalla en el *Artículo 3*.

Tal y como se detalla en el capítulo final de esta tesis, la experiencia y conocimientos adquiridos durante la investigación, se usaron para diseñar un grupo de sensores que funcionan asociados a ET. Este desarrollo podría ampliarse profundizando en la selección computacional de polielectrolitos, que luego serían inmovilizados en la superficie de un electrodo voltamétrico mediante una tinta de grafito conductora, de elevada robustez y estabilidad.

En este sentido, también se proponen otras recomendaciones para lograr la mejora de la capacidad de regeneración de los MIPs utilizados, por ejemplo mediante la separación de MIP y electrodo. Finalmente, se presentan algunas sugerencias para colaboraciones institucionales, con el propósito de crear un sistema ET móvil, que permita recoger y analizar muestras en campo.



# **Chapter 1 – Introduction**

---



## 1. Introduction

The aim of this PhD thesis was to investigate the plausibility of the application of molecularly imprinted polymers (MIPs) to the electronic tongue paradigm, ideally using efficient, and relatively low-cost electrochemical detection techniques incorporating durable, reusable sensor arrays. To test this hypothesis, the project had to be divided into its two constituent parts which were the design and synthesis of robust and efficient receptor, or sensing element, and the optimal application of it to an appropriate transduction method. It is perhaps most important to note that for the final system to operate efficiently, not only must both of these components be confirmed to function in and of themselves, but also both the receptor and the transduction platform must not unduly inhibit each other when combined.

When confronting an analytical challenge, *id est*, the detection of analytes in real samples rather than those created in a laboratory used for characterisation purposes, the accuracy of the result depends on either the efficacy of the preparation of the sample and minimisation of unknown variables, or on the efficacy of the sensing method and the interpretation of the results. In real world scenarios, targeted compounds are often present at trace levels and/or in complex matrices. The combat of these issues can lead the researcher either to attempt to concentrate or purify the targeted compound in anticipation of detection, employing MIPs as extraction tools. Alternatively, direct

detection of the untreated target-compound's signal in the presence of interferants can be achieved using the excellent trace-level performance of MIPs in concert with computational algorithms for the interpretation of the results from several conciliatory MIP sensors. One of the most widely known uses of these computational algorithms can be seen in the field of electronic tongues, which is the area expertise of the Barcelona laboratory from which this PhD project was conducted. The harmonious combination of both of these *pre*- and *post*-analysis sample treatments would potentially lead to a system whose whole was truly greater than the sum of its parts.

Using the acronym 'MIPs' does not help in the understanding of what such an entity is. Starting with the most the most basic of definition, MIPs are always polymers, or a chain of repeating finite units. An artificial molecular receptor, or imprint, is created by mixing a molecular template with one or more monomers, the structure of one of which contains some manner of functional group, referred to as the functional monomer (FM). These FM molecules have the capacity to form bonds with chemical groups or features on the structure of the template molecule. Complementary forces between these molecules draw them together and compel them to form what is often referred to as the 'pre-polymerisation complex'. A co-monomer is then added, at which point a polymerisation reaction is initiated. The polymerisation of the co-monomer around the pre-polymerisation complex rigidly locks its morphology in place. Upon termination of the polymerisation reaction, the template molecule can be removed from the now secured complex, thus creating an artificial receptor on the surface of the polymer, tailored to the template molecule and thus capable of preferentially re-binding to that same molecule and its analogues (Figure 1.1).

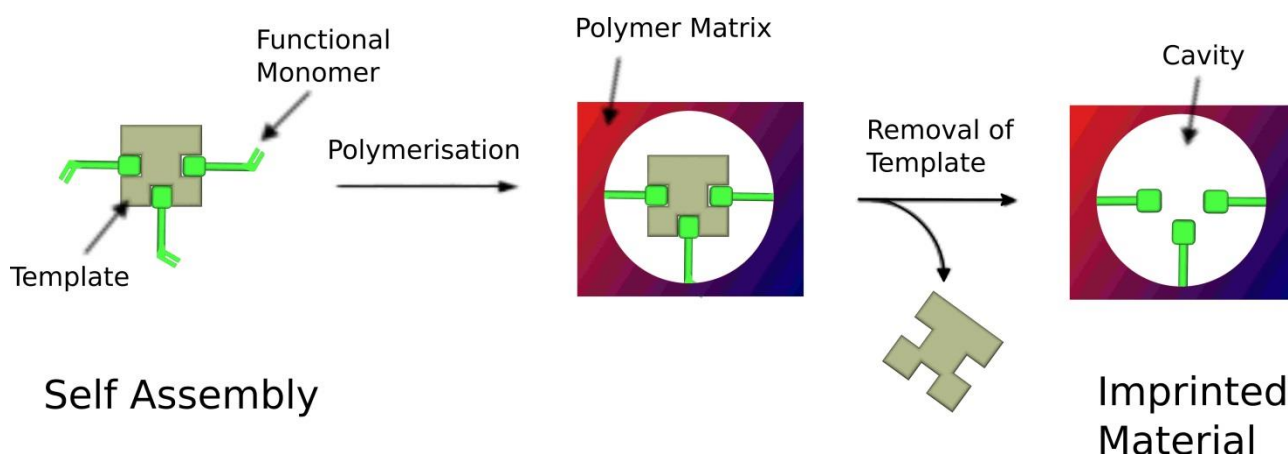


Figure1.1: Simple schematic representation of the molecular imprinting process

## **1.1 Molecularly Imprinted Polymers**

### **1.1.1 MIP prehistory: Targeted detection and the start of the field**

The concept of triggered or specific molecular reactions within a structure is more than a century old. The phrase 'lock and key', used to describe the preferential interaction between a ligand and an enzyme was first coined by Nobel Laureate, Emil Fischer in 1894 [1]. This analogy was and is a highly useful manner in which to visualise and simply explain the docking interaction between the enzyme receptor and the ligand; because the two components are in close proximity to each other, and assuming the relatively low energy or shallow field of the attractive forces at play between them, the morphology of the ligand is obliged to closely adhere to that of the enzyme in order to instigate its function. From such beginnings, the expansive field of biochemistry grew, with the mechanisms of biomolecular processes being understood from this basis.

This field has progressed from observation and understanding, to active application and exploitation of these recognition properties, to the field of biosensing which ranges from microbial enzymes [2] to bespoke biomolecular structures, tailored to specific target-molecules. Monoclonal antibodies [3], engineered binding proteins [4], nanobodies [5] and aptamers [6] to name but a few. Though this entire field is priced in the tens of billions of dollars, these biostructures invariably suffer from identical problems of high synthetic cost, substrate sensitivity and low thermal and dynamic stability. One of the most promising efforts to solve these issues can be seen in the rapid growth of the field of MIPs [7].

### **1.1.2 The birth and growth of a discipline**

The field of molecular imprinting, embodying the design, synthesis and application of MIPs, is one of the most exciting and dynamic facets of modern chemistry. There has been a steady and tireless annual growth, increasing by an order of magnitude over the past two decades, in both the journal papers published and the patents filed which reference this discipline (Figure 1.2). This can be taken as a clear indication to expansive potential and interest which it has garnered.



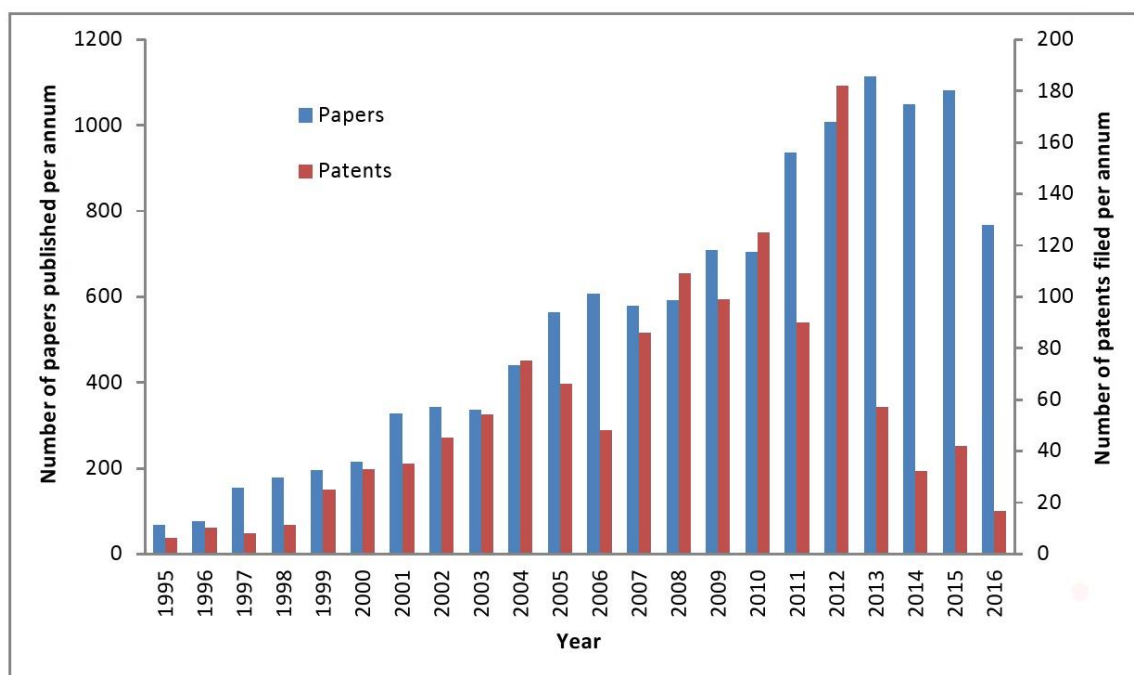


Figure 1.2: Number of papers and patents published on the topic of molecularly imprinted polymers from 1995 to June 2016 [8]

Though the widespread international dissemination of the molecular imprinting technique and growth of the field has largely occurred from the 1990's onward, the origins of the field can be traced back long before this. It has been accepted that the first example of molecular imprinting, the 'publication-zero', was reported in 1931, by Soviet chemist M.V. Polyakov who observed some curious absorption properties exhibited by a specimen while investigating silica gel matrices. He noted that when the polymerisation process was initiated in the presence of certain additives, such as benzene and toluene, the resulting silica particles displayed superior binding capacity towards those specific additives relative to other structural analogues. This ability was reported to be akin to some sort of material 'memory' [9].

Following this initial report, came a steady trickle of publications, averaging from one to three each year, though the technique failed to gain significant popularity due to the low repeatability of the synthetic protocols and the quite low selectivity that these silica-based MIPs displayed. It was not until the 1970's when Wulff and Sarhan [10] and Takagishi and Klotz [11] simultaneously reported

the first instances of molecularly imprinting occurring in organic polymer matrices that the scientific community upgraded their academic curiosity to attention and engagement.

From this threshold, the imprinting technique has been developed for a diverse range of templates, including atoms, ions, simple molecules, macromolecules, viruses, micro-organisms and even particles. To expand on the basic definition offered at the start of this introduction and shown in Figure 1.1, a template structure is used to create a tailored receptor site which is formed during polymerisation. The removal of the template molecule or structure leaves behind a cavity, capable of some degree of subsequent rebinding or recognition of the template or its analogue [12–14]. Most notably from this expanded definition, which is graphically represented in Figure 1.3, the affinity of the receptor site toward the template can be a cumulative effect from a number of different molecular forces including non-covalent, covalent, electrostatic, Van der Waals or ionic interactions not necessarily originating from the functional groups within the FM. Indeed, it has been definitively shown by Spivak et al. that the binding mechanism of molecularly imprinted receptors can be a cooperative effect of two, three or more finite molecules which together have the capacity to distinguish between structural analogues of identical molecular weight, differing only in shape [15].

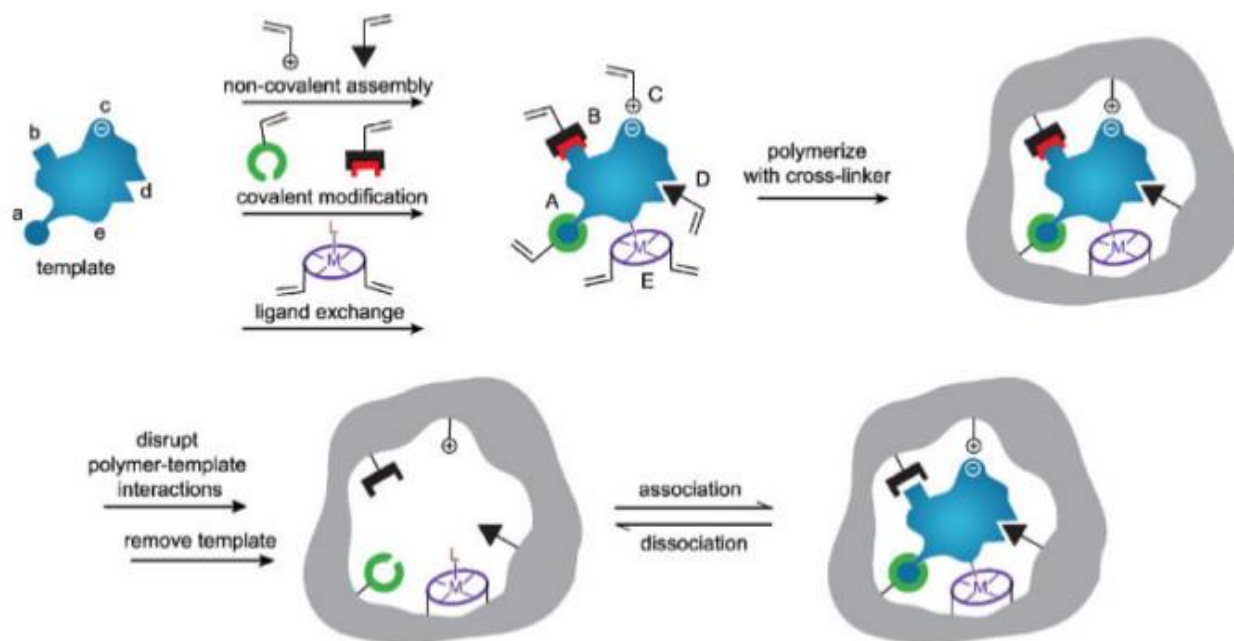


Figure 1.3: A schematic example of the formation of a multivalent imprinted receptor employing several functionalities on the template together with those present in the other molecules within the polymerisation solutions. These can include formation of receptor features using (A) covalent and (B) semi-covalent bonds, (C) electrostatic forces, (D) van der Waals interactions or (E) co-ordination with a metal centre via ligand exchange (denticity) (adapted from [12])

This rapid growth in popularity of MIPs is due to the aforementioned advantages they hold against their biological counterparts. While they can offer comparable efficacy, reproducibility and sensitivity, they also offer significantly greater tolerance to extreme temperatures and are cited to be able to maintain their functionality having endured temperatures well above the typical physiological or ambient temperatures required by biologically-based sensors [16], even going so high as 150°C which significantly broadens MIP's potential scope of application as well as allowing for ever more effective receptor cleaning, renewal or regeneration and sterilisation [17]. Tolerance to extreme pH levels allows MIPs to operate in conditions optimised to maximise the signal of the analyte, which is often outside of the biocompatible range, rather than to accommodate the receptor itself [18]. The ability to function in organic and aqueous solvents also allows for a diverse number of parallel applications [19, 20] as well as the ability to imprint a larger range of molecules with greater ease further enhances the MIP's repertoire of talents [21]. Finally, the cost of manufacture for MIPs is significantly cheaper than the biomolecular alternative and, while the ultimate cost can often depend on the purchase or refinement price of the molecular template, the difference may be

measured and compared using orders of magnitude. In addition to this low synthetic cost, MIPs are highly dynamically stable and can be stored for several years without any observable loss in receptor functionality [22].

Given the numerous advantages which are exhibited but MIPs as a technology, it is quite surprising that industry has been so slow to commercialise these seemingly perfect artificial receptors. This trend may be seen in the contrast between the number of published articles and the number of patented items which incorporate molecular imprinting into their novelty (Figure 1.2). The reason for this can be attributed to the general widespread inability to produce a class of MIP receptor with proven performance in practical applications. Though the advantages are clear to see in laboratory trials, MIPs have not demonstrated a sufficient competitive advantage over the existing state-of-the-art of analytical chemistry or separation solutions currently on the market to inspire widespread commercial adoption [23]. These issues are low receptor homogeneity [24], significant retardation of receptor performance in aqueous media due to MIP hydrophobia [25] as well as the notable absence of a universal protocol. On this final point, particular note should be taken of the development of an automated synthesis system developed by Professor Sergey Piletsky's research group which heralds a substantial advance towards the widespread ability to standardise the synthetic procedure to produce a regulated and thus commercially viable product [26], a schematic of this system can be seen in (Figure 1.4).

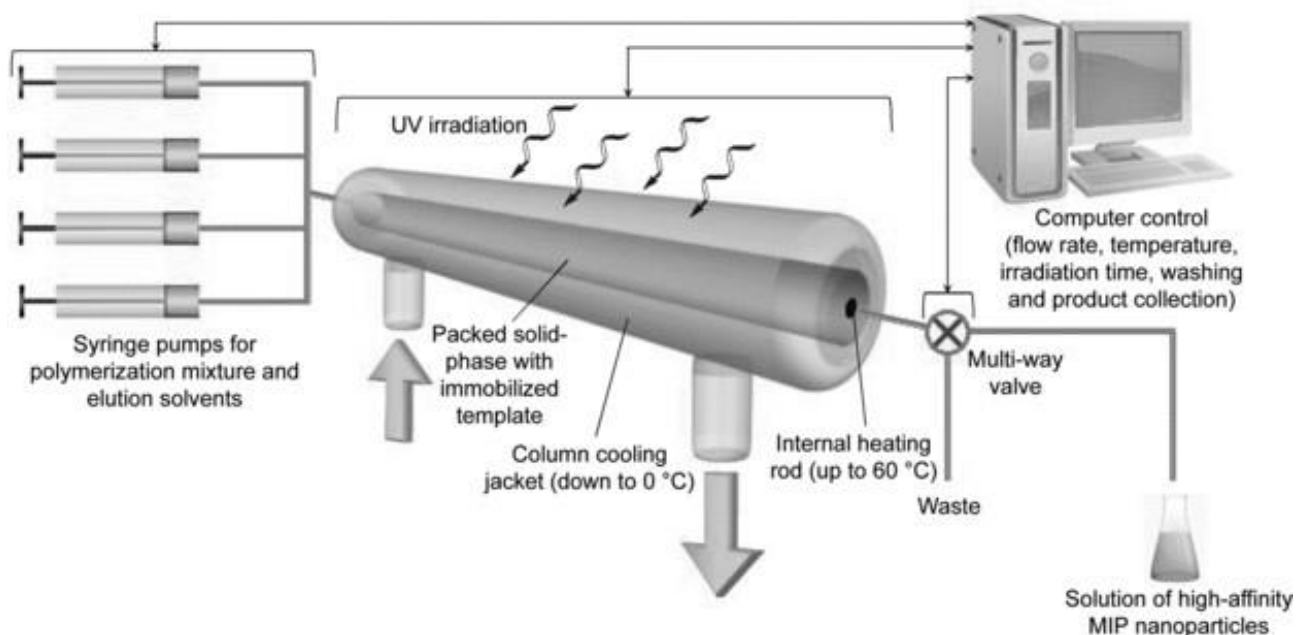


Figure 1.4: A schematic of the automated synthesis MIP system developed by the Professor Piletsky's laboratory [26]

Despite of this progress, MIPs as a commercial venture remains in its infancy with the selection of products currently on the market being related to solid phase extract (SPE). Not surprisingly, it can be quite a challenge to find such speciality companies given that they are often small start-up ventures coming from established academic laboratories. A brief list of some companies can be seen in (Table 1.1).

Table 1.1: List of some MIP companies

<b>Company name</b>	<b>location</b>	<b>Foundation year</b>	<b>Sample activities</b>	<b>Current status</b>
MIP Technologies	Lund, Sweden	1999	Separation and extraction of substances from food, chemical and pharmaceutical products; Provides support to 'SupelMIP' products currently sold by Sigma Aldrich	On the market
Semorex	North Brunswick, New Jersey and Ness Ziona, Israel	2001	The development of novel targeted therapeutics for cancer patients and diagnosis for systemic fungal infections; development stage company	Development Stage
POLYIntell	Rouen, France	2004	Polymer company specialising in SPE used for purification and sensing; 'AFFINIMIP' product solution offered in addition to existing range	On the market
NanoMyP	Granada, Spain	2011	Pre-characterised micro particles and, functionalised core-shell particles for pre-specified applications. Spin out company from the University of Granada	On the market
MIP Diagnostics Ltd.	Leicester, UK	2015	Development of nanoMIP 'plastic antibodies' for point-of-care diagnostics and in field based testing; Spin out company from University of Leicester research group	Development Stage

## 1.2. Molecular Imprinting Strategies

To continue to use Fischer's lock and key analogy, if the MIP receptor and the template are the lock and key respectively, then the molecular or atomic interactions through which the polymerised complex is formed and maintained can be described as the bits within the lock. The stronger and closer the fit between the two components during synthesis, the more detailed and secure the imprint will be. Just as there are a plethora of types of key for different scenarios and conditions, so too are there numerous types of imprinting strategies in the literature.

### 1.2.1 Covalent imprinting

Molecular imprinting via covalent forces is one of the oldest formats used in artificial receptor design. It involves the formation of a covalent bond between the template and functional monomer molecule which is then secured in place via polymerisation with a co-polymer. The template may then be removed via hydrolysis or a similar treatment to cleave the chemical bonds securing it to the newly formed polymer to create the imprinted receptor.

In their ground breaking research, which incidentally was also the first report of molecular imprinting using organic polymers, as detailed above, (Section 1.1.2), Wulff and Sarhan imprinted D-glyceric acid [10,27] using molecules with polymerisable vinyl groups as well as boronic acid and amine-based functionalities as the imprinting mechanism along with an additional monomer, divinylbenzene (DVB), whose sole functional group consists of an aromatic ring and thus could be used to crosslink the polymer in such a way as to physically secure the structure of the receptor site while not affecting or disrupting the primary template-FM esters of the molecular imprint (Figure 1.5). This imprinted polymer was then used to demonstrate the selective capture of the template and an analogue, thus proving the concept and viability of an entirely organic imprinted polymer. It is noteworthy that this work and those following it during the 1980's used FMs that were generally referred to as amino acid derivatives containing one or more polymerisable vinyl groups in their structures [28, 29]. This process was a great advance from the inorganic MIPs of the prior decades through the increase of accessible reaction sites on the augmented surface area of the 3-dimensional macroporous polymer structure. However, the imprintable templates were still limited to those moieties of the source amino acids. This led to them being referred to as 'Enzyme Analogues' rather than the versatile 'Plastic Antibodies' (see section 1.3.2) which constitute the current state of the art.

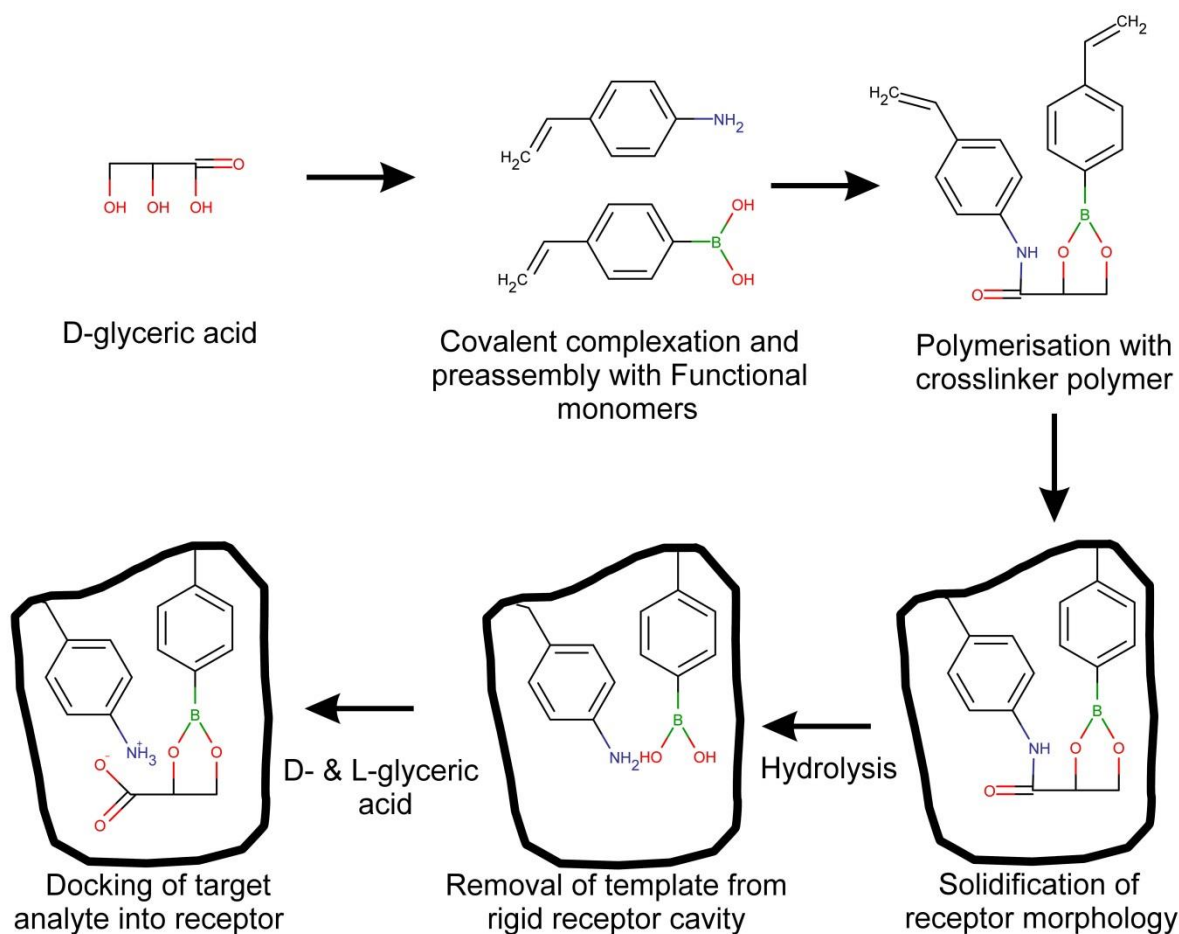


Figure 1.5: An example of a typical covalent imprinting protocol showing the imprinting of D-glyceric acid using 2, 3-O-p-vinylphenylboronic and a derivative of p-vinylanilide for the selective detection of D- and L-glyceric acid as reported by Wulff and Sarhan [10, 27].

One very notable advantage of the covalent imprinting approach is the durability of the template-FM complex during polymerisation. The covalent bonds holding the primary complex together means that imprinting can be executed with a greatly increased level of precision than the more commonly employed non-covalent method, which invariably must incorporate a 'factor of safety' to compensate for the disruption of template-FM complexes by competing solvent and co-monomer interactions. Though the non-covalent imprinting strategy is now by far the most used method, contemporary covalent imprinting is still used in order to produce a higher affinity receptor and a more homogeneous population of binding sites whilst also minimising the number of non-specific sites during the polymerisation process [30]. The price that must be paid for this high specificity and affinity is an increased difficulty in the rebinding or removal of the template due to the strength of the formed and reformed covalent bonds between the template and the FMs [31]. Regarding the post-polymerisation removal of the template, recoveries can vary from 50% to 85 – 95%,

depending on the type of polymer structure which is being cleaned. This range comes from the need to break only the template-FM covalent bonds without compromising the structure of the receptor and bulk polymer [32]. Though cleavage of boronic acid esters can be achieved using water or alcohol, cleaning of covalently imprinted MIPs is often done with the use of concentrated acids or bases [33, 34], high pressure, supercritical CO<sub>2</sub> can similarly be employed to increase the removal rate, exploiting the fluid's inherent high diffusivity and low viscosity to permeate the polymer matrix and extract the template with minimal damage to the structure [35]. FM's containing boronic acid groups are highly suitable, and thus are the most commonly used, for covalent imprinting events. Polymers containing boronic acid-based compounds were already in use as the stationary phase in chromatographic separations thus making them easily purchasable and cost effective. Though capable of forming robust and versatile connections with the template via formation of ester bonds, boronic acid-based FM's do, however suffer from slow bond formation ( $t_{0.5}$  100 – 600 s in water), obliging long incubation times to ensure ligand capture [32]. For this reason, it common to pair a boronic acid functional group with a charged amine or piperidine group, either in an aqueous buffer solution or incorporating it into the receptor (Figure 1.5) which allows bond reformation in a matter of minutes. Nowadays, the majority of contemporary reports of covalently imprinted polymers in the literature have used boronic acid based functional monomers, capable of bonding to diols, polyols, saccharides, sialic and mandelic acid, such as (4-Vinylphenyl)boronic acid [36–39], or (3-Acrylamidophenyl)boronic acid [40,41]. Several other functionalities including Schiff's bases, ketals, esters and disulphides, all having polymerisable vinyl groups within their structure, have been successfully used to covalently imprint aldehydes, amines, ketones and disulphides [32,42]. This work, having been principally though not exclusively carried out by the respective research groups of Professors Günter Wulff and Kenneth Shea during the 1980's, detailed the use of the bespoke functional monomers 1-(4-Vinylphenyl)methenamine [43,44], 4-Vinylbenzaldehyde [28,29,45,46], 2-(4-ethenylphenyl)propane-1,3-diol [47–50], p-vinylbenzyl alcohol [51–53], and 4-mercaptomethylstyrene [54,55] as FM's; The molecular structures of these covalent FM's can be seen in Figure 1.6.



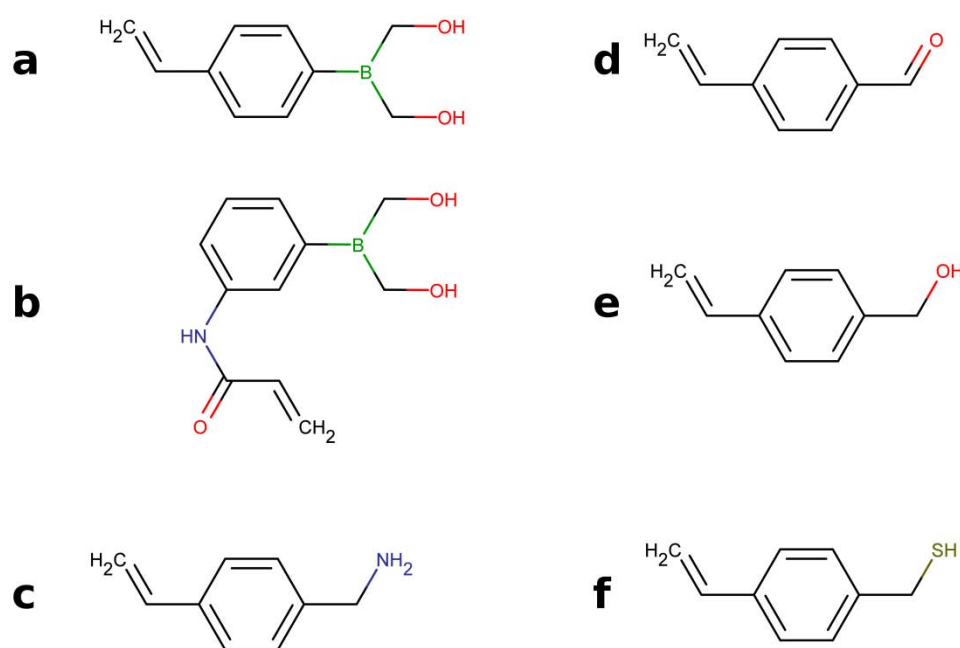


Figure 1.6: Examples of some previously used functional monomers for covalent imprinting; a: 4-Vinylphenylboronic acid, b: 3-(Acrylamido)phenylboronic acid, c: 1-(4-Vinylphenyl)methanamine, d: 4-Vinylbenzaldehyde, e: p-vinylbenzyl alcohol, f: 4-mercaptomethylstyrene

### 1.2.2 Semi-covalent imprinting

The semi-covalent approach to molecular imprinting is a manifestation of the effort made to meld the advantages of both the covalent and non-covalent (Section 1.2.3) imprinting approaches whilst excluding their respective failings and disadvantages. Semi-covalently imprinted polymers are those MIPs which have been covalently imprinted but then have had the features involved in the covalent complex replaced with non-covalent functionalities which are still advantageously placed to capture the target molecule. This switch of binding mechanism allows for the high receptor uniformity of covalent MIPs to be combined with the versatility of use and application of non-covalent MIPs, namely that the rebinding event is not contingent on any kinetic parameters other than diffusion [56].

Though the origins of the semi-covalent technique can be attributed to, as with so much of the field, Günter Wulff in the 1970's [10,27], the first use of the most commonly used 'sacrificial spacer'

method was reported by Whitcombe et al in 1995 [57], in which a 4-vinylphenyl carbonate ester was used to covalently imprint cholesterol. Upon removal of the template via hydrolytic cleavage of said ester, the remaining oxygen molecule was protonated to create carbonyl functional group, capable of forming dipole and hydrogen bonds with cholesterol (Figure 1.7). The work reported 'remarkable uniformity' in the receptor population with respect to binding affinity and noted the applicability of the technique to the imprinting of smaller sized molecules with a lack of functional groups or with an otherwise poor capacity to form durable pre-polymerisation complexes via a purely non-covalent approach.

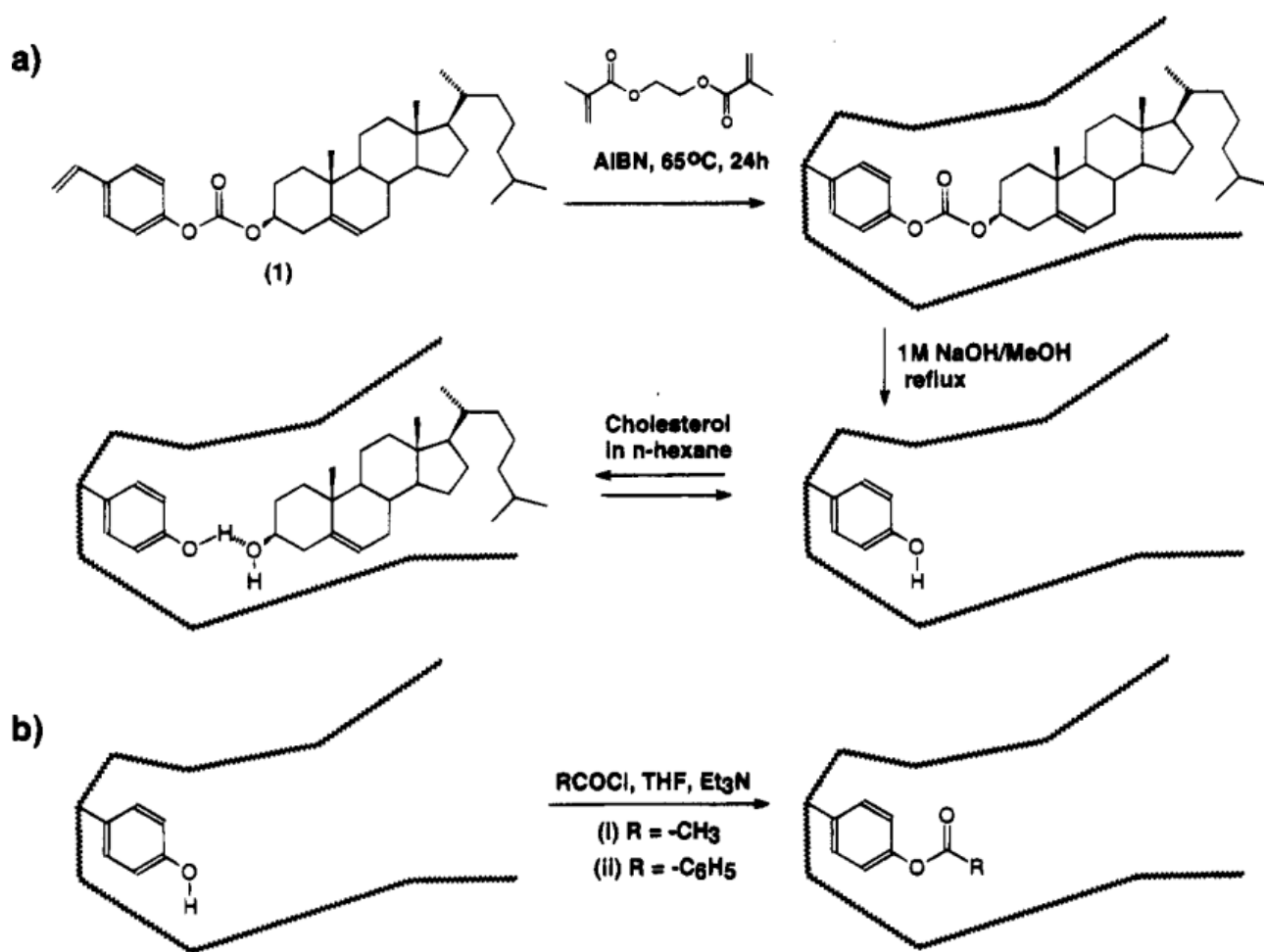


Figure 1.7: Schematic of (a) covalent imprinting and non-covalent rebinding of cholesterol using 4-vinylphenyl carbonate ester and carbonyl functionality respectively; (b) post-polymerisation modification the carbonyl in the receptor to facilitate subsequent covalent binding of cholesterol as reported by Whitcombe et al. [57]

Following this ground breaking work, the reported pre-polymerisation complexation mechanisms used have greatly diversified with the easy replacement of the covalent functionality with a dipole being the principal condition. The two principal methods of semi-covalent imprinting are either to directly bind the template to the functional monomer via various, though most commonly carboxylic esters [30, 58, 59] (Figure 1.8), or to employ the use one of a diverse number sacrificial spacers, though most often a carbonate functionality [60]. The former may provide an arguably more direct adhesion to the morphology of the template though this close adhesion may also lead to crowding and steric hindrance within the receptor thus negatively affecting its binding behaviour and capacity.

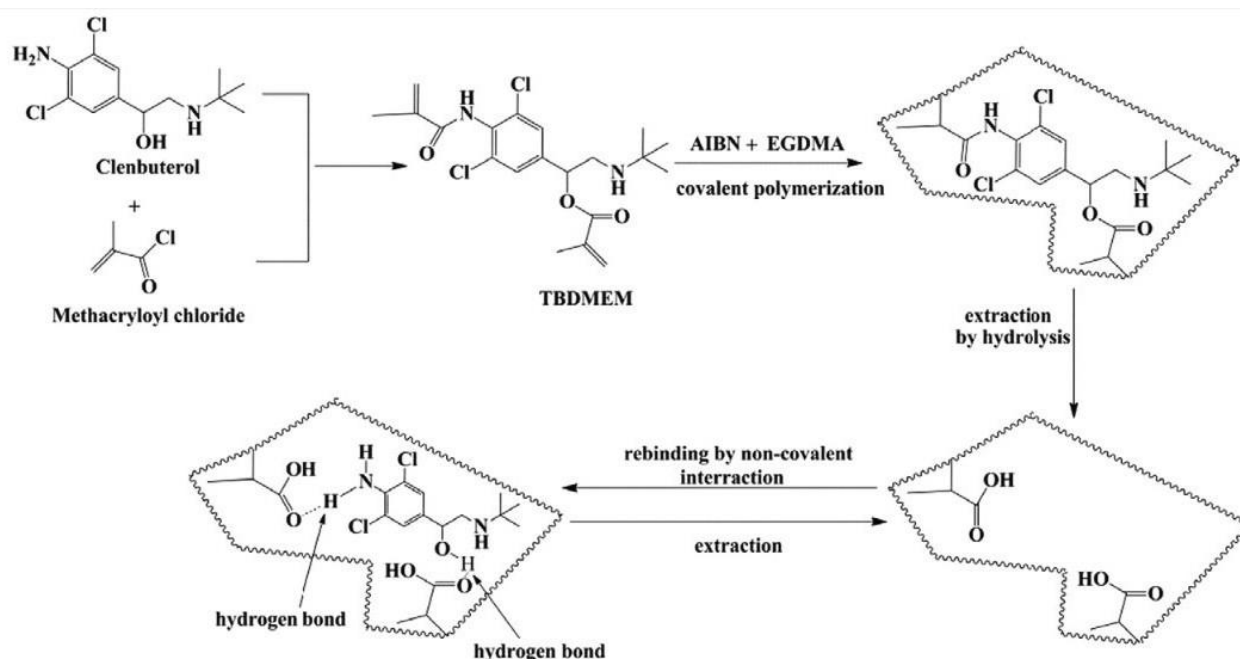
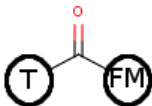
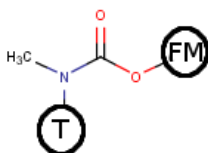
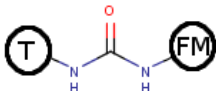
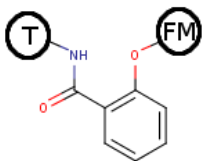



Figure 1.8: An example of semi covalent imprinting via direct linkage of the functional monomer to the template using carboxylic and amide esters [30]

Sacrificial spacers can also act as a buffer bond between the template and the base of the functional monomer group. This is to say that a diverse number of functional groups and bonds may be employed and optimised for the synthesis process both for binding with the template functionality and in anticipation for the most efficient or the most desired dipole. Five of the most commonly referenced sacrificial spacers are described in Table 1.2.

Table 1.2: Description and application of some commonly used sacrificial spacers and their uses in binding the template molecule 'T' to the functional monomer 'FM'

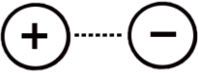

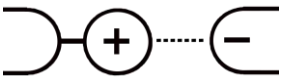
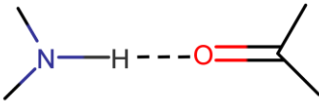
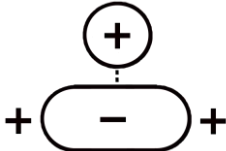
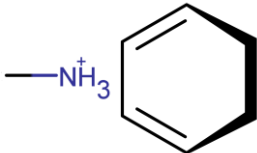

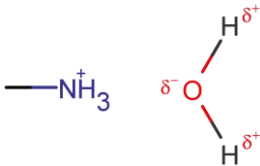
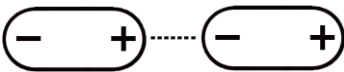
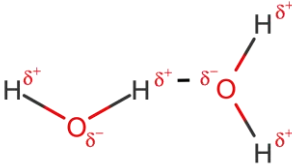
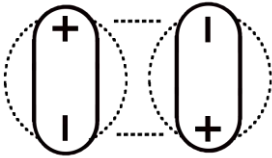
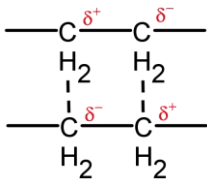
Sacrificial Spacer functionality	Schematic representation	Description of use	References
Carbonate ester		One of the most commonly used spacers; generally a carbonyl group is placed between a polymerisable phenol group and an alcohol functionality on the template structure	[60–63]
Carbamate		Used to introduce hydroxyl or amine groups into receptor	[64–66]
Urea		Introduces an amine group into receptor; can also weakly hydrogen-bond to aromatic chlorine	[67]
Salicylamide		Useful for imprinting amine-based templates	[59,67]
Silyl ether		Useful strategy to imprint molecules which may not otherwise be imprinted by (non)covalent techniques due to weak hydrogen bond formation or due to not being capable of forming labile covalent bonds	[35,68,69]

### 1.2.3 Non-covalent imprinting

Inspired by the diverse range of non-covalent interactions found in biochemistry, this third and final imprinting approach is by far the most widely used and referenced in the literature. This is because of the ease with which it can be performed in a non-specialised laboratory and also, as is the case with the semi-covalent imprinting approach (Section 1.2.2), the facile and versatile manner in which these MIPs can be used and implemented thanks to their ability to rapidly re-bind or re-dock their template molecule in non-specialised solutions. As with much of the field of molecular imprinting,

this strategy too originated out of the Mosbach laboratory in the 1980's [70–72]; given the high accessibility of this technique, its dissemination and use within the scientific community was one of the main factors causing the exponential growth in publications seen over the past twenty years (Figure 1.2). The umbrella term of 'non-covalent imprinting' can be applied to a wide range on interactions and bond types all of which may be included within its definition (Table 1.3).

Table 1.3: The various bond types and interactions which are employed in the non-covalent imprinting processes

Type of Interaction	Model	Example	Approximate Binding energy
Charge-Charge			$\leq 60 \text{ kcal} \cdot \text{mol}^{-1}$
Hydrogen Bond			$\leq 40 \text{ kcal} \cdot \text{mol}^{-1}$
Cation- $\pi$			$\leq 40 \text{ kcal} \cdot \text{mol}^{-1}$
Charge-Dipole			$\leq 8 \text{ kcal} \cdot \text{mol}^{-1}$
Dipole-Dipole			$\leq 1 \text{ kcal} \cdot \text{mol}^{-1}$
van der Waals			$0.1\text{-}1 \text{ kcal} \cdot \text{mol}^{-1}$

The popularity of the non-covalent imprinting approach comes from the lower bond energies exhibited by the bond types employed which allow for the rapid and more efficient post-polymerisation removal of the template which increases the user-friendly nature of this technique.

However, this approach is uniquely vulnerable to binding site heterogeneity which occurs when ideal template-functional monomer complexes are broken or compromised due to interference and competitive binding from the solvent or cross-linking monomer. Equally, this interference can come from the substantial increase in thermal energy often introduced into the solution during the polymerisation process with thermal polymerisation being the most common energy source to the polymerisation process employed. This vulnerability leads to a variety of receptor types ranging from high to low affinity (Figure 1.9). Strategies to maximise receptor homogeneity are discussed in greater detail in a later section (see Section 1.5).

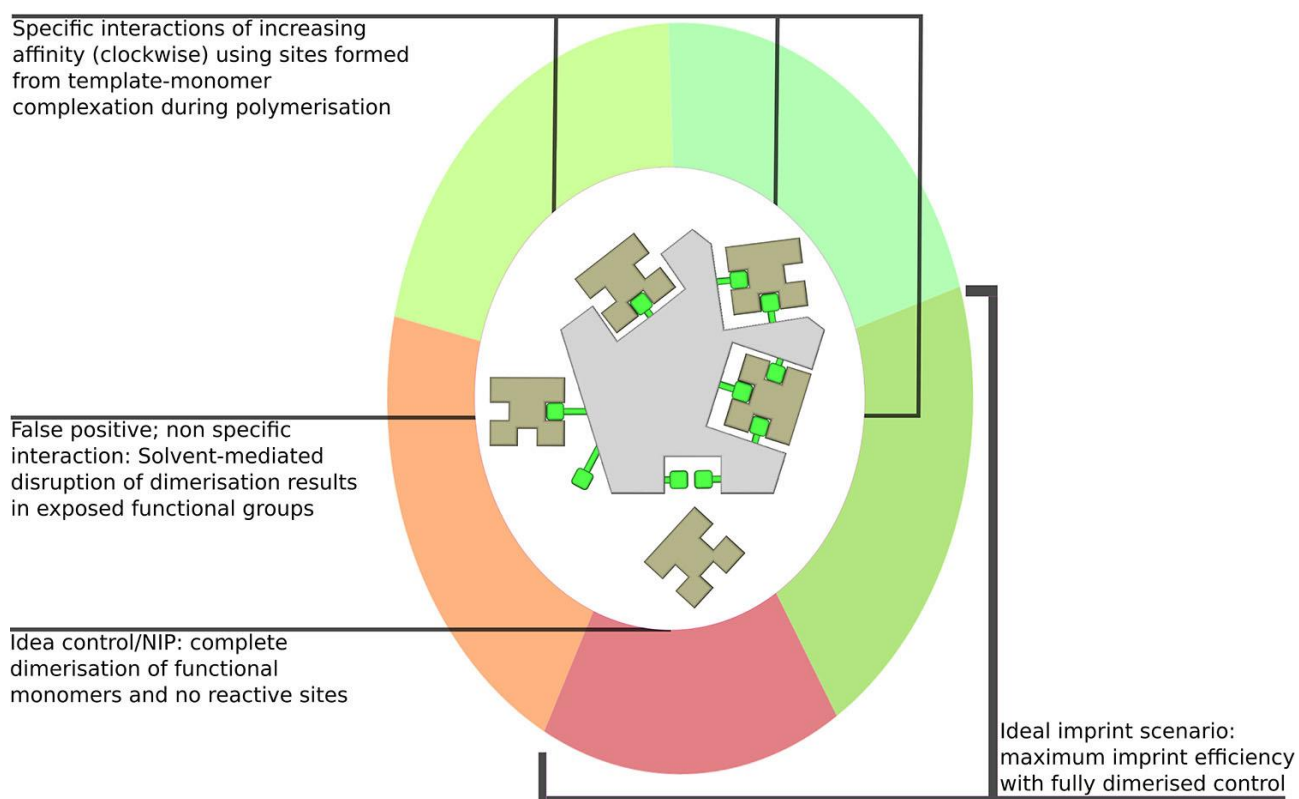


Figure 1.9: The range of receptor site affinities which occur within a standard non-covalently imprinted polymer

Though methacrylic acid (MAA) is far and away the most used and reported FM due to its versatility, low cost, stability and ease of use, it is highly important and advantageous to match the most suitable FM to the template so as to maximise the performance of the resulting MIP. While this may be quite obvious at times, such as selecting an aromatic or anionic group to imprint a cation [73], the selection process becomes a great deal more nuanced when selecting a functional group to produce a complex with maximum affinity, and thus maximum probability to endure the polymerisation process, and produce a robust receptor cavity. When matching an FM to the



template, the chemical nature of the template should be considered, an acidic functional monomer for an alkaloid template molecule might perform superiorly for example or a basic FM for a template containing acidic moieties and so on. Some of the more commonly used and referenced functional monomers are given below, grouped into acidic (Figure 1.10), basic (Figure 1.11) and neutral (Figure 1.12) functionalities.

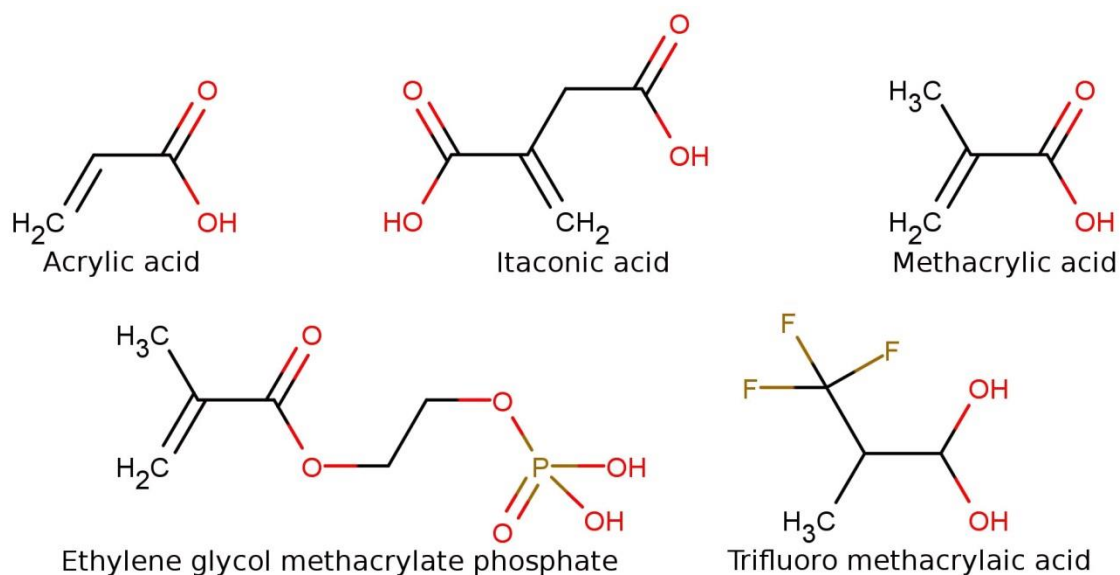


Figure 1.10: Commonly used functional monomers containing acidic functional groups

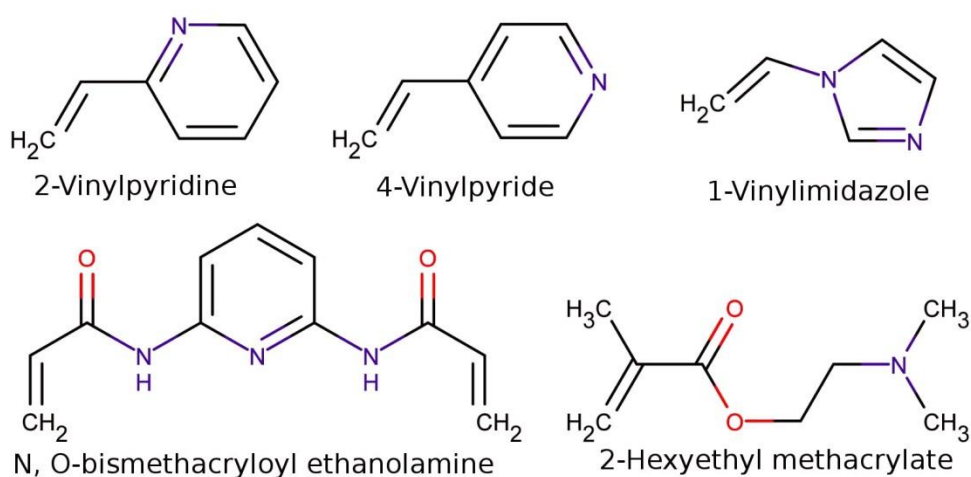


Figure 1.11: Commonly used functional monomers containing basic functional groups

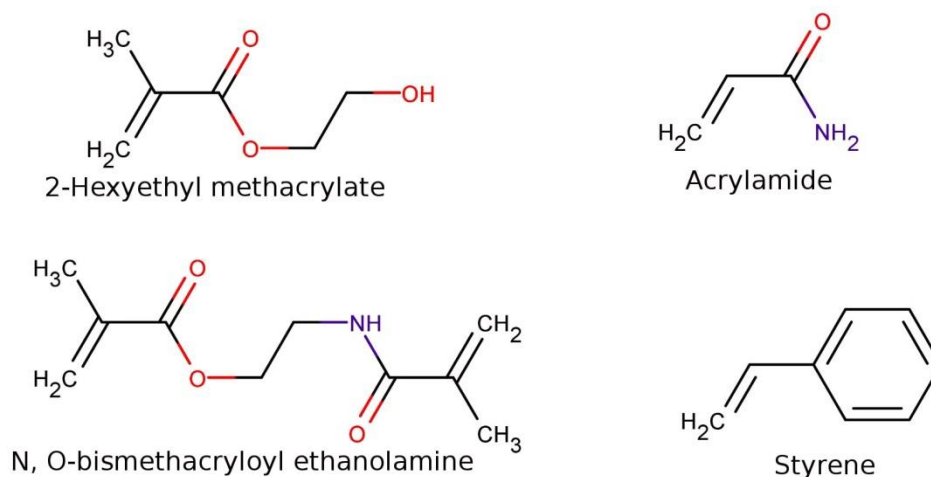


Figure 1.12: Commonly used functional monomers containing neutral functional groups

Though this method for FM selection can be used as a good starting point in polymer design, it is extremely rudimentary and should not be thought of as an infallible qualifier but rather an answer to the often repeated advice of 'when in doubt, use MAA'. The locations of functional groups both on the monomer and within the template's structure also contribute not only to the strength of the primary bond but also the cumulative effect that interactions between multiple functional groups will have on the overall receptor-template affinity. A good example of this can be seen in DNA sequences whereby the cytosine-guanine base-pair forms a stronger complex than thymine-adenine due to the former's ability to form three, albeit longer, hydrogen bonds as opposed to the latter's two shorter bonds with each of the bases only being able to bind with their complementary pair [74]. This concept is discussed further below (see Section 1.7).

### 1.3 Polymerisation formats

While a polymer chain itself is simplicity incarnate, the final forms it can take are diverse and are applied to a wide range of areas and applications. It cannot be stressed enough that one must consider the ultimate objective or purpose of the polymer before selecting the polymerisation format for the molecular imprint. There are a number of requirements regarding template solubility, component miscibility and interference that are discussed in a following section (Section 1.5); Table 1.4 shows the advantages, disadvantages and principal area of application for each polymerisation format. These diverse formats all form in identical cumulative fashions whereby progressive stages of chain growth and collapse form polymer nuclei before precipitating into the solution to form

particles. Depending on solvent type and quantity, thermodynamic properties of the solute, polymerisation type, polymerisation rate and initiation method, particle growth can continue in free solution or a polymer solid is formed (Figure 1.13 a). It is also possible to attach polymer chains to functionalised surfaces to form shells, discrete nanoparticles or layers (Section 1.3.2 & 1.3.3; Figure 1.13 b). What follows is a brief description of each of these main imprinted polymer formats.

Table 1.4: Applications, advantages and disadvantages of each of the main MIP formats

<b>Polymer format</b>	<b>Main Application</b>	<b>Advantage</b>	<b>Disadvantage</b>
Ground Monolith particles		Most straight forward polymer formulation & versatile	Requires high template solubility; Results in highly irregular particles; poor mass transfer properties
Precipitation		Generally spherical particles; relatively homogeneous size distribution; Most straight forward polymer particle formulation; no stabiliser (surfactant) needed	Final particle size highly dependent on component thermodynamics; The need to thermodynamically facilitate precipitation limits monomer-porogen compatibility
Suspension polymerisation	Materials for chromatography & assays	Particle size can be controlled by synthesis parameters; water-compatible process	Requires integrated mechanical mixing for suspension & stabilizing agents
Emulsion polymerisation		Better heat control of process; water-compatible process	Requires emulsifying surfactant for synthesis
Solid-phase synthesised nanoparticles		'Soluble' particles suitable for in vitro applications. Affinity separation isolates the best-formed receptors, leading to the highest specificity and sensitivity of contemporary MIP formats	Low capacity & yield
Core-shell/ & multi-step swelling polymerisation	Chromatography, assays & sensors	Particle size can be controlled; large sizes can be obtained – results in highly uniform material suitable as a column packing media	Time consuming multiple step process to grow particles to size; a stabilizer is often necessary
Particles in thin polymer layers	Thin layer chromatography & sensors	Separation of particle and layer synthesis gives more leeway for facile optimisation; sub-frit sized particles can be used & the size effect is minimised	Separation of synthesis steps increases inter-device irregularly
Thin polymer films, layers & membranes	Electro- & Chemo-sensor surfaces and selective membranes	Highly suitable for specific sensor applications; greatest level of interface between transducer & MIP; Individual properties can be tuned accordingly	Poor control of layer thickness; susceptible to the 'gate effect'

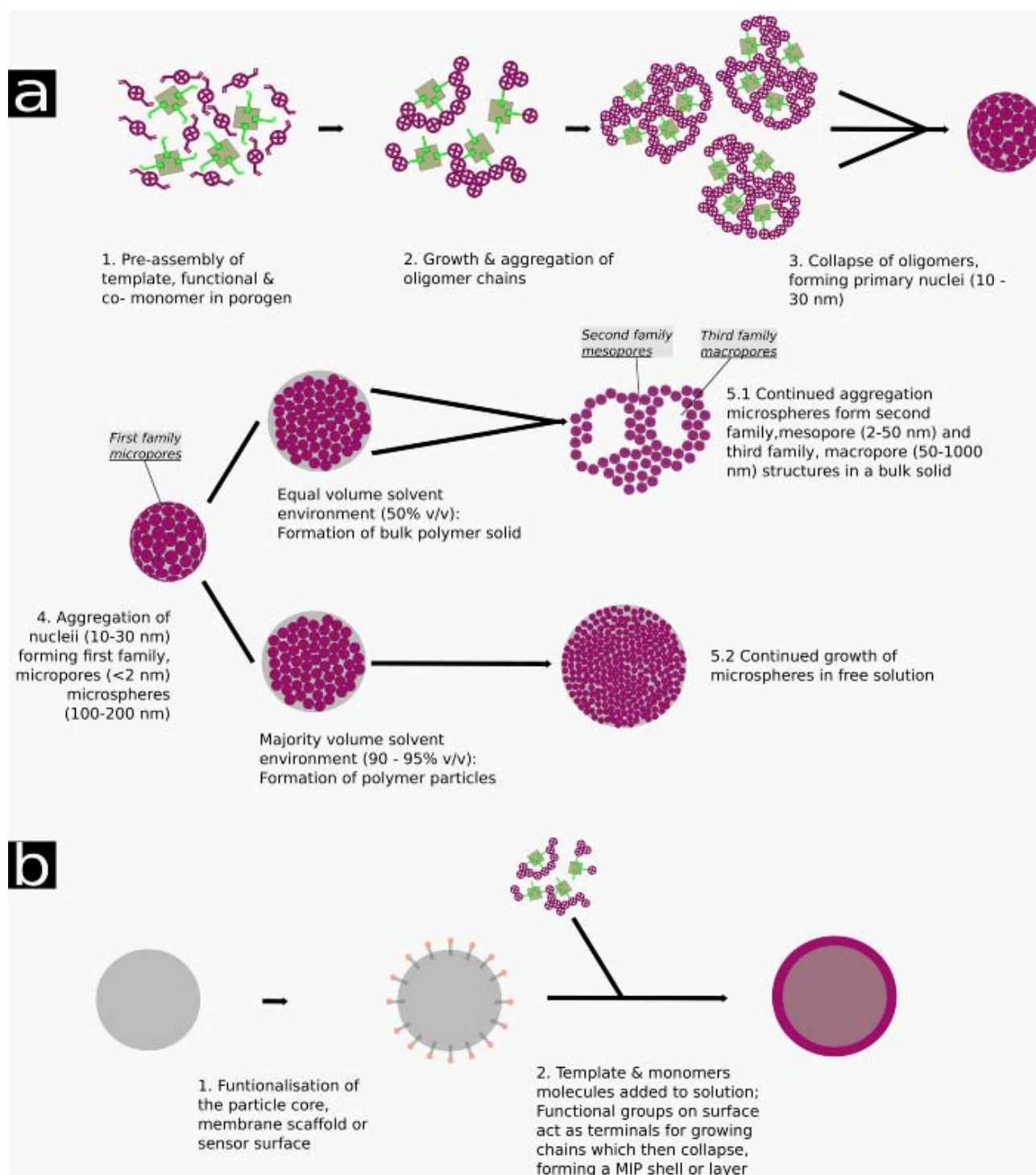


Figure 1.13: Schematic showing the growth and collapse of polymer chains to form particulate and bulk polymers (a) and, in the presence of a functionalised surface, the formation of polymer layers, shells and membranes (b)

### 1.3.1 Bulk form polymers

Bulk imprinted polymers are perhaps one of the most widely used formats for MIPs due to its rapid protocol and low-tech requirements with respect to laboratory equipment. The most common method of post-polymerisation processing this MIP format is to break and grind the polymer 'brick' into micron-sized monoliths with a size range controlled by the mesh size of the sieves used isolate the usable particles from the fines. This size range is typically from 5 – 50  $\mu\text{m}$  between the upper and lower size limit, which are generally approximately 100 and 20  $\mu\text{m}$  respectively. This size range can be tuned with respect to the final application which is most often the stationary phase of conventional and capillary columns for liquid and electrochemical chromatography, thin layer chromatography (TLC) plates and solid phase extraction (SPE) cartridges [75–77].

The latter use of SPE, similar to the use of narrowly sized MIPs for imprinted sorbent assays, are particularly popular due to their circumvention of the chromatographic limitations associated with bulk form MIPs. These are peak broadness asymmetry brought about by the inherent poor mass transfer properties and receptor heterogeneity of bulk form MIPs. The use of MIPs for SPE also allows for larger scale batch applications consisting of many parallel binding events and processes [78, 79].

Even with the apparent simplicity of bulk imprinting, there are still some inherent attenuating factors to the efficacy of this polymer format; the most immediately obvious of these being the low usable yield which can be collected within the size desired range. This is due to the unavoidable production of under-sized fine particles during the grinding process which then must be discarded. While these fines may be somewhat limited with the use of the manual mortar and pestle method of breaking down the polymer brick, this labour intensive method is, more often than not, skipped over for an automated method where possible, leading to an average yield of 20% w/w useful particles per synthesis [80]. The creation of a hard, brittle polymer brick occurs as a consequence of the need for a high level of chemical crosslinking within the individual polymer chains to support and strengthen the imprinted receptor sites within the MIP structure (see Section 1.5 & Figure 1.28). In addition to this low yield, the material stress which is induced by the mechanical grinding process can also negatively affect the integrity of the imprinted receptors within the MIP by the physical alteration, damage or reorientation of receptor components while also producing irregularly shaped particles which can reduce the packing efficiency when they are placed into the column or cartridge [81]. The requirement to break the polymer into monolith particles is also obliged due to majority of the receptors being located deep within the pore structure of the MIP and also to limit the amount of

permeation inhibition (retardation of mass transport and diffusion) due to non-specific, lower affinity interactions and sorption in shallower recesses of the pore structure, a phenomenon referred to as the gate effect [82, 83]. Additionally, the closed nature of the pore structure, even after breakage into monolith particles, can retain template molecules even after aggressive washing protocols. This 'bleeding' effect leads to inaccurate results, false positives and a reduction in the apparent number of receptor binding sites ( $B_{\max}$ ), especially at low concentrations; the very range where MIPs should be most efficient and effective [17,84].

While improved accessibility to these receptor sites can be facilitated with the use of a non-reactive linear polymer to increase pore depth and connectivity throughout the polymer structure [85, 86], additional disadvantages remain. The inadequate dispersal of heat during radical polymerisation, caused by the autoacceleration phenomenon, also serves as a barrier to the use of this imprinting technique on industrial scales and relegates the format to analytical laboratory quantities.

A major step forward in the state-of-the-art for bulk form MIPs can be seen in the work of Dr José Vilariño and his research team at the University of Coruña in the north of Spain whereby the advantageous simplicity and high  $B_{\max}$  of MIPs are exploited while the aforementioned negative factors stemming from mechanical grinding are removed. The crux of their method is the formation of highly porous polymer structures, a few millimetres in size (Figure 1.14), described as MIP 'disks' or 'pills'. While the use of linear polymers creates a permeable surface and access to the receptor sites therein, removing the need to mechanically break the polymer, thus leaving receptor morphology intact and undamaged, the distribution of the polymerisation process across several individual moulds also minimises autoacceleration-associated *in-situ* temperature increases. These MIP-pills have been tested on several systems including detection of Bisphenol A in aqueous solutions [87], cannabinoids in urine and saliva [88, 89] and plastic additives in olive oil [90].



Figure 1.14: Sample of MIP-pastilles as described in [87–90]

### 1.3.2 Polymer particles and polymer resins

Polymer microparticles or resins are essentially condensates of a polymerised solution of monomers at low concentration, approximately 5 – 10%. A practical minimum of 2% monomer concentration must be present in a solution in order to allow the growing linear oligomer chains to interpenetrate with each other, chemically crosslink (Section 1.5.4) and precipitate into the solution [91]. As they are formed in the presence of a non-reactive porogenic solvent, they have a structure of micropores which may be up to 2 nm in size, as dictated by oligomer-solvent miscibility and compatibility [92]. Rather counter intuitively, these particles are actually classed as 'macroporous' structures due to a definition originally defined in the 1970's which states that this classification includes all polymers to have permanent pore structures greater than 50 Å in size [93].

Their shapes, dictated by thermodynamic forces rather than mechanical grinding, are invariably more homogeneous than their bulk-polymer counterparts. However, the lack of larger second or third family pore structures (Figure 1.13) greatly reduces their accessible surface area, which can reduce their column efficiency, while maintaining the binding site heterogeneity (see Section 1.2.3) synonymous with all MIP syntheses except for next generation 'nano-MIPs' where receptor affinity separations can be conducted [94].

In parallel to the single-receptor nano-MIP particles which, by definition are minute, A progression of MIP particle synthesis protocols have been developed with the general trend toward larger and



more uniform particle sizes, first with the tuning of binary organic porogen mixtures to delay the theta point (Section 1.5.1), then with organic-inorganic porogen mixtures in the form of suspension and emulsion polymerisations. Simultaneously, cores or seeds with functionalised surfaces have been optimised to provide scaffold structures onto which the MIP layers can be anchored (Figure 1.13 b).

### **Precipitation Polymerisation**

Precipitation polymerisation is essentially an identical procedure to bulk polymerisation at a concentration one order of magnitude lower (Figure 1.13 a). Integrated mechanical stirring is also generally used though this can be a source of particle size heterogeneity due to the turbulence this internal movement can introduce. The effect can be minimised with the use of an external movement, such as that provided by a rotovap or kugelrohr, which maintains a laminar motion within the solution itself [95]. The most immediately notable aspect of precipitated MIP particles relative to their NIP controls is the, at times, substantial size difference that can manifest between them [96]. It is interesting that the effect of template solubility on the thermodynamics of the polymerisation process is often just viewed as a curiosity given that the enhanced recognition ability of a MIP towards its imprint was originally described an effect caused by *additives*, the template molecule, to the polymerisation mixture (Section 1.1.2).

In one very interesting case, Castell and co-workers compensated for the size increase observed in the MIP by modifying the proportions of the binary porogen used. The solubility of the molecular template, propranolol, caused a size decrease in the MIP due to its low solubility in the porogenic solvent, acetonitrile-toluene. In order to reduce this size difference, the proportion of thermodynamically 'good' solvent (see Section 1.5.1) toluene, was reduced from 17.5 to 10% of the total solvent content. The particle sizes resulting from a thermally mediated polymerisation process were 3.6 and 3.9  $\mu\text{m}$  for the MIP and NIP respectively [97]. It is, however, risky to introduce any additional variability between the MIP and its control for the obvious reason of decreased comparability. Variation of the polymerisation rate via careful selection of the initiator is a much more secure method by which to match MIPs with comparable NIPs when using such simplistic polymerisation protocols (Section 1.5.4).

## Suspension Polymerisation

Particle synthesis via suspension polymerisation allows for the largest, most uniform particles of all the imprinting protocols discussed here. The formed particles are essentially bulk-form polymer 'bricks', containing an identical pore structure, whose size and shape have been limited by prefabricated polymerisation vessels. A typical synthesis, shown in Figure 1.15, is carried out in a continuous phase which may be either aqueous or organic. The polymerisable phase is immiscible with the continuous phase and is mechanically dispersed throughout the continuous phase at which point a stabiliser is added and the polymerisation process takes place. Capable of producing particle sizes between 3 and 50  $\mu\text{m}$ , the final size of the particles is dictated by the size of the globules formed which are 'suspended' in place using the stabilising surfactant. These globules or droplets become *in situ* polymerisation vessels and achieve their uniform shape via the dispersion forces within the bi-phasic solution. It is the propensity of the two phases to their entropic minima that obliges the additional use of a stabilising agent which can sometimes be a source of contamination if the polymer is inadequately washed. In addition to achieving large MIP particle sizes, the NIP can be grown to an identical degree by controlling droplet size rather than modifying the porogen as was discussed above [98,99].

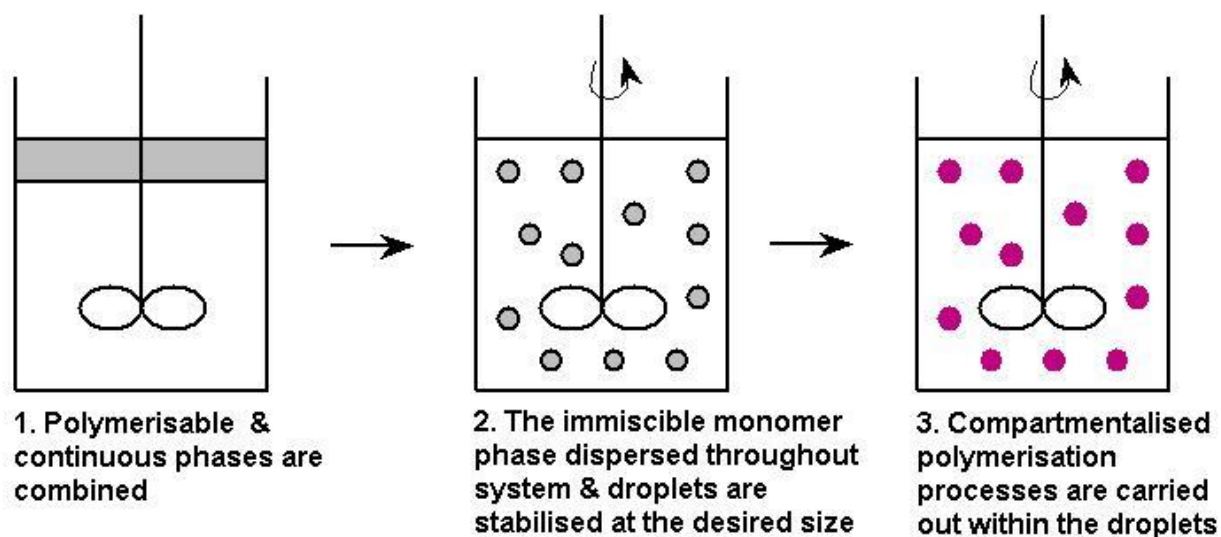


Figure 1.15: A generic polymerisation protocol executed in suspension

A notable synthesis using an aqueous continuous phase was reported by Lai et al who communicated a successful imprinting event using 4-aminopyridine, MAA, EGDMA, AIBN and chloroform as template, FM, crosslinker, initiator and porogen respectively. This solution was added drop-wise directly into an aqueous solution containing polyvinyl alcohol as a stabilising

agent. Control of the mass flow rate, through the regulation of drop-rate ensured a homogeneous distribution of the organic phase within the droplets. Under constant stirring at 600RPM, the particles were polymerised at 60°C for 24 hours. The resulting MIP and NIP were of sufficient size, 8 – 25  $\mu\text{m}$ , to be packed into a HPLC column for characterisation [100].

### **Core-shell Polymerisation**

Core-shell polymerisation can be further divided into two subcategories, seed and grafting approaches. The former refers to the use of a scaffold, often but not always a polystyrene particle, which can then be swollen in a suitable solvent to provide further surface area. Exposed terminal double bonds on the surface of these particles can then anchor the growing imprinted polymer chains to the surface of the particle, thus forming an imprinted polymer layer [101,102]. The latter approach, the grafting method, uses non-polymer cores which must have their surfaces modified with a functional group immediately prior to their use. An example of both of these approaches can be seen in Figure 1.16.

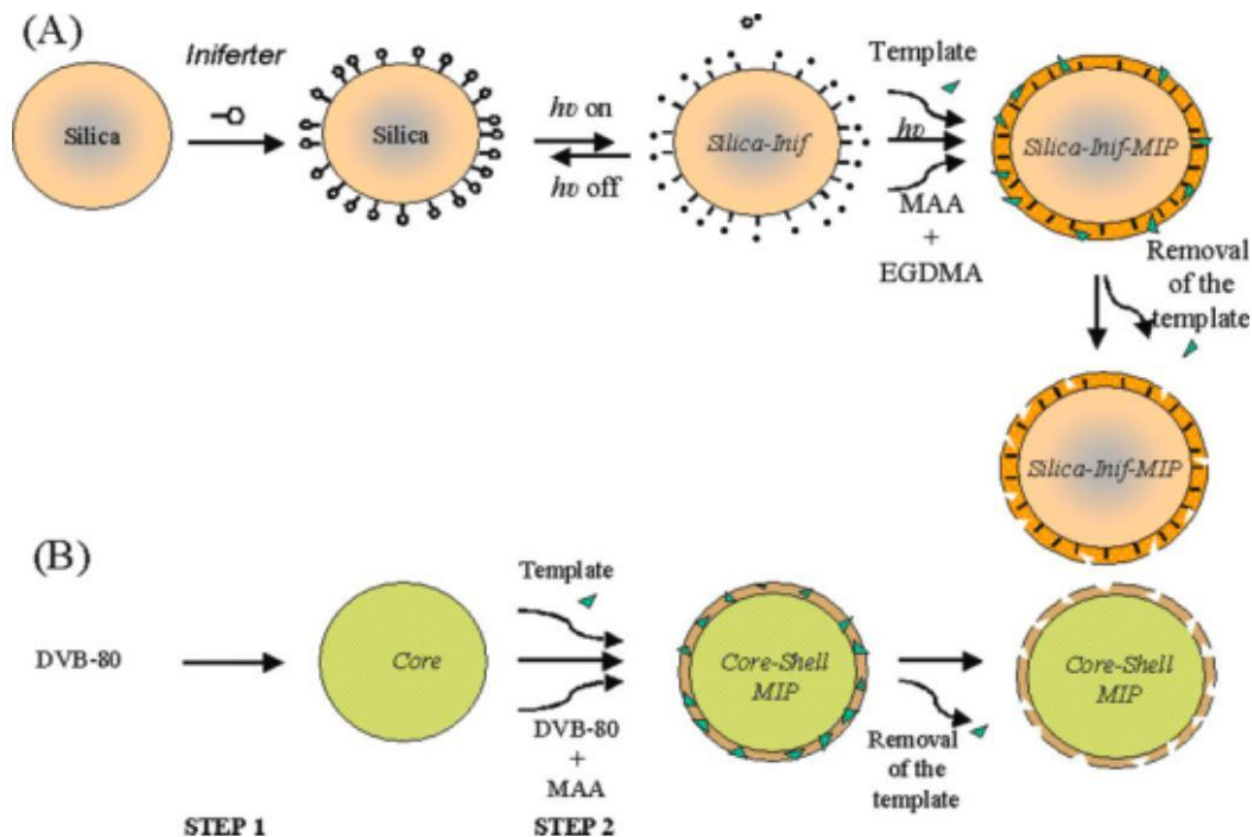


Figure 1.16: Schematic of the seed and grafting methods of core-shell molecular imprinting using surface-modified silica particles (A) and DVB polymer (B) [103]

While the use of a polymer core of the same composition as the shell is a more facile process, the use of an inorganic silica core can introduce a highly defined prefabricated pore structure without the need to further optimize the polymerisation process. The immobilisation of an iniferter on the core surface is also highly advantageous as the use of living polymerisation (see section 1.4.2) allows for the highest control over polymer growth, layer or shell thickness and the gate effect [38,83].

The solid core can be used to support the imprinted receptors, thus removing the need to maximise chemical cross-linkages using elevated polymerisation temperatures (see section 1.4.2). This allows large column-compatible particles to be produced and imprinted with thermally-sensitive or biological template molecules while isolating receptors to the accessible surface of the particles only [104,105]. A final noteworthy point for this imprinting technique is the ability to introduce additional functionalities into the particles via the core to increase the versatility and range of applications for these particles. Multifunctional MIP assays and sensors have been reported in the

literature, incorporating quantum dot [105], gold [106], carbon power [107], carbon nanotubes [108,109] or magnetic nanoparticles [110].

## **Emulsion Polymerisation**

One of the most common requests on chemistry message boards regarding MIP synthesis methods is to clearly define where emulsion and suspension polymerisation techniques differ. One of the most common errors in answering this is to conflate superficial similarities, such as that both are bi-phasic systems of immiscible solvents, with an interchangeability of the two procedures. The two phases of the reaction mixtures are an aqueous continuous phase and an organic mixture of monomer and crosslinker. Polymer emulsions differ distinctly from all of the other techniques discussed because of the location of the polymerisation initiator molecule in the aqueous phase. The use of a hydrophilic initiator to polymerise organic monomers completely negates the potential for temperature increases related to autoacceleration (see section 1.5.1) and thus allows for a constant temperature to be maintained which might otherwise decrease laboratory safety or, even worse, negatively affect the polymer structure and the imprinted receptors. A surfactant or stabiliser must be used to stabilise the emulsion ahead of polymerisation. Sizes are nanoscopic and typically in the range of 50 to 500 nm which can be regulated using sonication or elevated pressure homogenisation treatments [111–113].

A key criticism towards this imprinting protocol is always the potential for post-polymerisation contamination of the MIP particles by the molecular surfactant employed in the stabilisation of the pre-polymerisation emulsion. A solution to this issue was offered by the use of nanoparticles (NP), often silica, to form a Pickering emulsion (Figure 1.17). This is an emulsion stabilised by NP rather than a conventional molecular surfactant to facilitate increased particle sizes. The larger NP are also easier to separate from the MIP particles, relative to molecular surfactants. From this point, it is a small additional step to attach the template molecule to these emulsion-stabilising nanoparticles in order to easily remove and reuse the template in future imprinting procedures while also localising all the formation of receptors to easily accessible parts of the surface of the MIP.

The size range of these NP-stabilised emulsified droplets, however, is typically two to three orders of magnitude larger than the droplets stabilised with a molecular-surfactant [114–116]. Additional surfactants are sometimes also used when a low solubility template destabilises the emulsion to otherwise produce heterogeneous distributions [113].

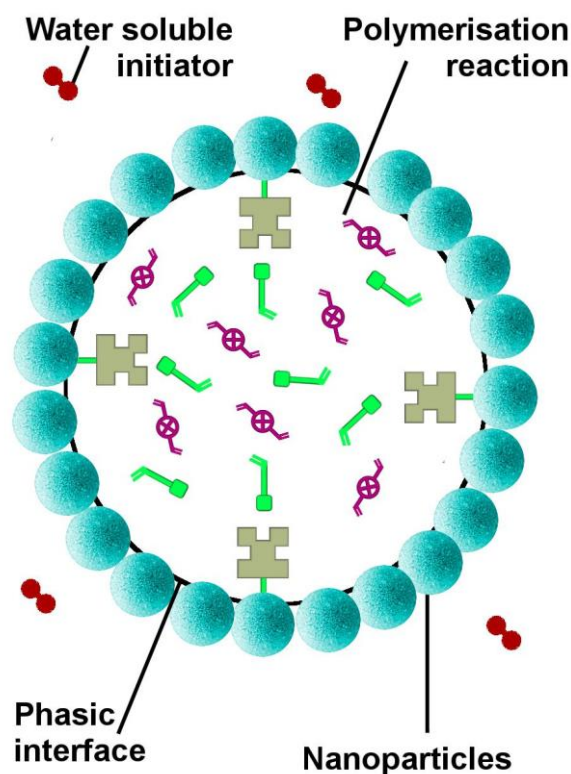


Figure 1.17: Schematic representation of a NP-stabilised emulsion for imprinting NP-immobilised templates for better control of receptor location

### Solid-Phase Polymerisation

Solid-phase imprinting protocols are yet another enhancement and improvement on previous techniques with a very small albeit very important, distinction. The silica particles used to immobilise the template are micron sized and thus remain as a distinct phase in the solution. This allows for affinity separations to be executed on the MIP with respect to their receptor affinity ( $B_{\max}$ ) and thus a more homogeneous, controllable product can be isolated.

Solid phase synthesis has its roots in the 1950's in the field of peptide synthesis and earned Bruce Merrifield the Nobel prize for Chemistry in 1984 [117], whose goal was to localise the polymerisation of amino acids to the surface of a solid-phase in order to have greater control over the process. It can be immediately obvious just how compatible such a technique would be to an artificial polymer which seeks to mimic natural receptors such as those present in (poly)-peptides. A typical procedure, shown in Figure 1.18, consists of the mixing all the components together with the silica-immobilised template molecule, followed by an extremely short polymerisation period, often

as short as 100 to 200 seconds exposure to the energy source. This short polymerisation period secures the template-FM conformation in place but does not allow the polymer chains to progress past the initial nucleus stage (Figure 1.13), thus leaving the imprinted polymer nanoparticle (MIP-NP) dissolved in solution and greatly more analogous to the existing biological assays which these MIP-NPs seek to compete against. The solid-phase can then be washed to remove unreacted monomer species and low affinity MIP-NPs. Having already separated the best formed, highest quality MIP receptors still attached to the solid-phase, these can be isolated and concentrated ahead of their characterisation and use. The ability to perform concentrating procedures additionally allows for the synthesis of the MIP-NPs to be conducted as extremely low template concentrations thus allowing for the direct imprinting of low solubility templates, such as melamine as is shown in Figure 1.18 below. This concentrating step, followed by the affinity separation of the receptors, also allows for receptors based on hydrogen-bonded template-FM complexes to be synthesised directly in water or aqueous buffer as any low affinity receptors below the affinity threshold can be washed away though. Naturally, this can reduce the yield of the MIP-NPs [26,118–120].

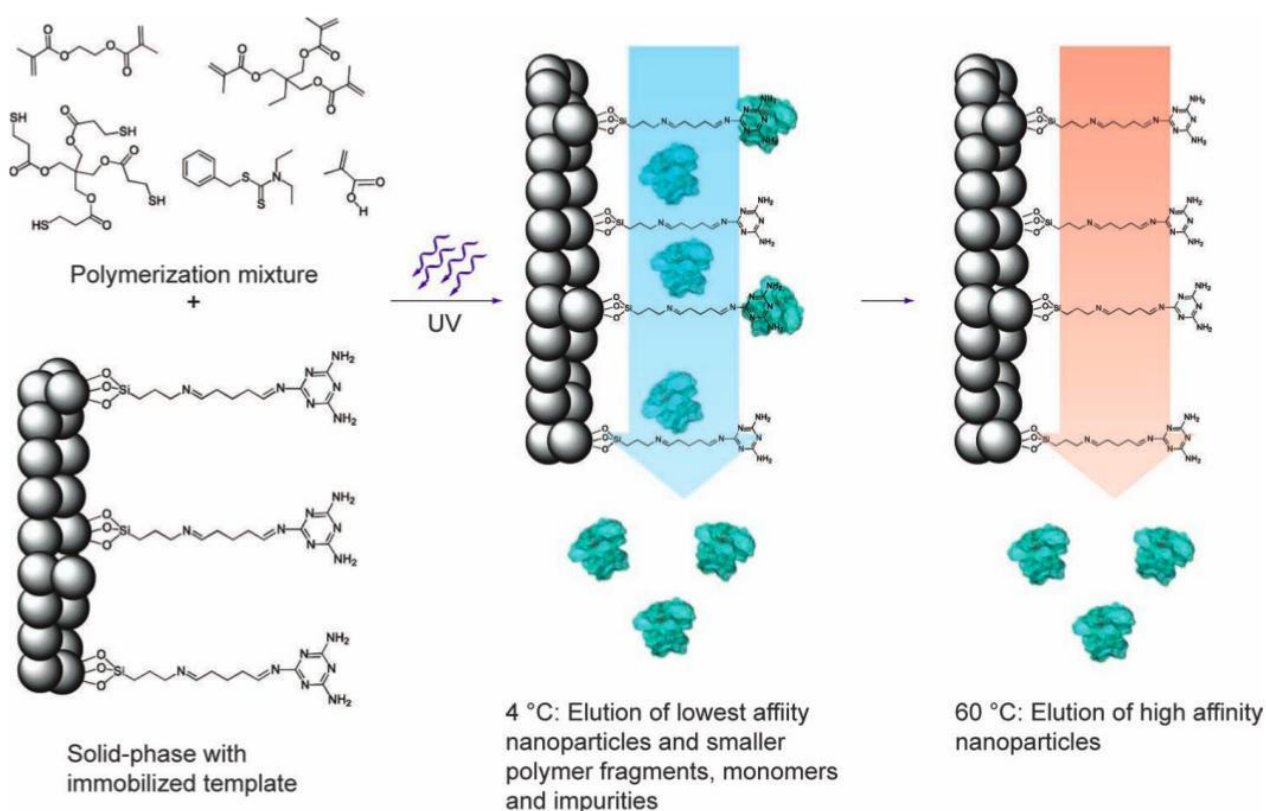


Figure 1.18: Schematic representation of the solid phase synthesis and affinity separation method for MIP-NPs [26]

### 1.3.3 Films, layers and membranes

Films and membranes differ in that membranes are generally free standing and thus must have enough structural rigidity to support their own weight and the stresses of the analyte moving through it. MIP films or layers, on the other hand, are deposited on a functionalised surface which serves as a signal transducer, a structural support or both. NIP layers can also immobilise MIP particles or gels, sometimes providing the structural support to hold the form of the receptor that would otherwise be secured by high levels of chemical cross-linkages between the polymer chains surrounding the receptor site. These layers or structures can be formed on a surface within a voltage gradient using electroactive monomers, by using surface functionalization in pre-treatments identical to those employed in core-shell synthesis, or else by the use of a non-interacting set of surfaces to form a moulded free-standing polymer membrane.

#### **In situ electropolymerisation**

Polymerisation of electroactive monomers can be induced by the application of a sufficient voltage potential. The electropolymer formed this way can be either conducting, such as polyphenylene and polypyrrole, or insulating, such as polyphenol or polyenylenediamine. For imprinted electropolymers, an FM is required with both an electropolymerisable moiety and an appropriate functional group (Figure 1.19) [121,122]. As the voltage flows toward the surface of the sensor, an extremely uniform coverage and layer thickness can be achieved by the immediate termination of the reaction via the removal of the voltage gradient when the desired polymerisation level has been reached. The magnitude of the voltage gradient also allows for the control of the polymerisation rate and thus the pore structure. Because of this, electropolymerisation, besides the obvious application to electrochemical sensors, is also used to create homogeneous imprinted layers for piezoelectric analyte detection (QCM) [123–125]. The popularity of sensing techniques, other than the most intuitive electrochemical one stems from the frequent need to dope electropolymers with an ionic species in order to achieve optimal degrees of electrical conductivity in the polymer layer, which, of course can have additional negative effects on the capture and retention of the target analyte in the imprinted receptor [121]. Additionally, as the reaction is mediated by electrical potential, no additional radical initiator molecule is required. Imprinted electropolymer films have been used in several forms and applications using voltammetry [126], including EIS [127] and amperometry [128].



One of the most interesting investigations into imprinted electropolymers was reported by the research group of Professor Piletsky within this last decade. In which a novel dual-function monomer is developed and used in an imprinted sensor. This monomer, N-phenylethylene diamine methacrylamide (NPEDMA) shown in Figure 1.19, contains both a electropolymerisable aniline moiety, as well as a terminal double bond which may be polymerised via more conventional radical addition polymerisation methods. The combination of these two polymerisable groups in one molecule allows for the creation of highly efficient and rapid voltammetric sensors which are less susceptible to resistivity or capacitance by the creation of an initial electropolymerised layer of densely packed pendant methacrylamide double bonds, facilitating a greatly reduced polymerisation time and layer thickness required to form an imprinted layer. This imprinted nano-layer lead to imprinted voltammetric sensors extending their LOD as low as 29 nM [127,129–132].

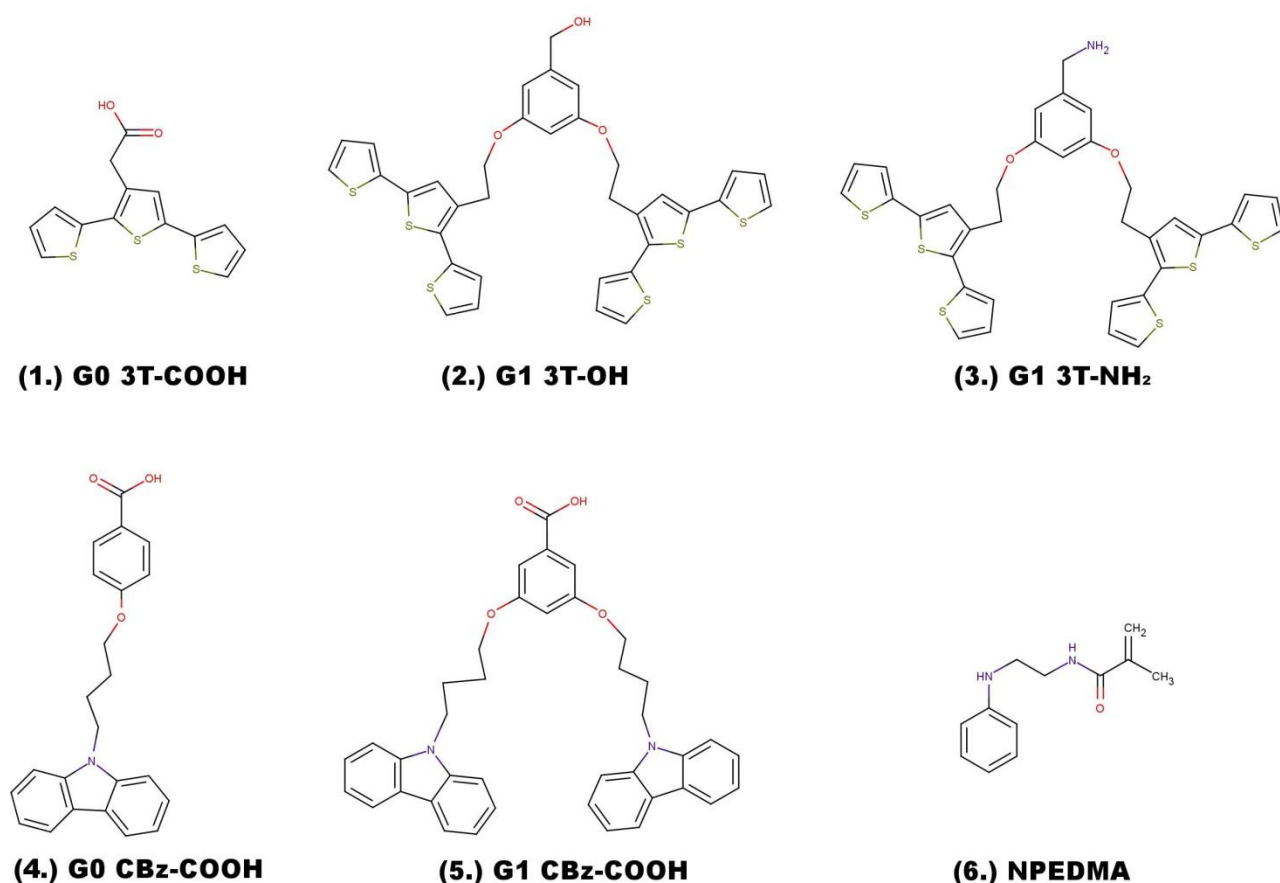


Figure 1.19: Molecular structure of some electropolymerisable functional monomers used in the literature for the creation of imprinted sensors using terthiophene (1 - 3) and carbazole (4 & 5) moieties; NPEDMA, as used in the creation of MIP nano-layers for ultrasensitive imprinted voltammetric sensors, incorporating an *electro*- and *radical*- polymerisable moieties (6) [121,130]

## **Grafting approaches**

Imprinted polymer layers can be immobilised on sensor surfaces by first adding polymerisable groups to the surface through one of many pre-treatments. These pre-treatments are identical to those used in core-shell MIP particle technique discussed above. Suitable functional groups include carboxylic groups depositing through prolonged acid treatment [109], salinisation (Si-OH) [133] or coating with Indium tin oxide [134], which can then connect with growing polymer radical species via the appropriate coupling reaction. Layer thicknesses are most often kept below 500 nm due to the cumulative gate effect whereby it becomes increasingly difficult for even the template molecule to access the receptor due to non-specific dipole and van der Waals interactions of the polymer support [111]. Because of this need to minimise layer thickness, several other protocols report directly immobilising an iniferter species on the surface of the sensor so that living polymerisation (see section 1.4) can be carried out and control final chain weight and layer thickness [103,135,136].

## **Imprinted Moulded Membranes**

The use of a mould to regulate and limit polymer thickness is an elegant solution to the previously discussed issues relating to bulk imprinting whereby a solid brick must be broken into irregular monoliths ahead of its use. To guarantee an effective fluid through-flow, interconnected pore structures are created during polymerisation by the inclusion of a non-reactive linear polymer, such as polyethylene glycol. This enhanced porosity makes such membranes ideal for thin layer chromatography (TLC) while the 'mould' or scaffold can be as simple as two glass slides placed together [137]. Additional functionalities, such as fluorescent dyes, can also be incorporated into the membrane as a sensing mechanism [138]. With the need to incorporate some strength and rigidity into the membrane structure while also providing a sufficient cross-section to achieve practical results, the thickness of these membrane layers can be as thick as 1 mm [82,139–141].

## **MIPs in host polymer layer**

The final method of imprinting to be discussed is the creation of an 'imprinted' layer via the immobilisation of already-imprinted materials within a non-imprinted polymer layer. This

technique immediately has a notable advantage in that the imprinting and deposition events are separated, thus increasing its versatility, especially in the scenario that the conditions for the imprinting and layer deposition processes cannot be reconciled. This might be due to such issues as required polymerisation conditions or template solubility. This method also allows for structurally weak imprinted polymers, which could not support a receptor in free solution, to be used when supported by the underlying sensor surface. In recent years, MIP-NPs have been immobilised in this way in an attempt to increase low concentration detection of targeted molecular species as was done by Kamra et al using an epoxy-silane layer to immobilise the MIP-NPs [133]. Agarose gel has also been used to immobilise older generations of MIP microparticles to a sensor surface [142].

Finally, imprinted receptor sites have been created using the polymerisation of various combinations of melamine, chloranil and aminononzoic acid. This process, conducted under reflux at 160°C, forms a linear polymer, devoid of any receptor-supporting crosslinks. This renders the receptor unusable in the absence of a solid structural support. The imprinted receptor is, however, electroactivated thus making it highly attractive as a modifier for electrochemical sensors for which the receptors can be switched on and off to allow for easy sensor regeneration. The development team devised the use of a conductive sol-gel matrix to act simultaneously as the MIP support and transducer, producing an efficient voltammetric sensor used to detect trace levels of uric acid [143], barbituric acid [144] and creatine [145].

#### **1.4 Polymerisation mechanism**

The mechanism by which polymerisation occurs and how the reaction is initiated and maintained impacts the properties of the polymer greatly. There are two broad categories in this respect; condensation and addition polymerisation. Condensation polymerisation, also known as step growth polymerisation, implies chain growth via the condensing of the monomer, losing some part of its structure as it is incorporated into the polymer chain. Addition polymerisation requires the addition of an external molecule to initiate and propagate the reaction and incorporates the entire monomer structure into the polymer chain. A brief explanatory discussion follows.

### 1.4.1 Condensation polymerisation

Perhaps the most well-known condensation polymer reaction is that of nucleic acid chains in the formation of nucleic acids and polypeptides with the latter forming the biological receptors which MIPs seek to mimic. Imprinted sol-gel layers are formed from the condensation of monomeric silane molecules. With the polymerisation rate being moderated using the pH of the solution which balances the proportion of hydrolysis and condensation reactions occurring (Figure 1.20). At low pH, the rate of silane hydrolysis is slow while condensation is fast so that growth is favoured over crosslinking, resulting in high molecular weight polymer chains. At high pH, conversely, hydrolysis outpaces condensation thus leading to short-length, highly cross-linked chains which tend to form heterogeneous aggregates in the solution. Because sol-gels are mostly imprinted on supports in the form of a layer, high levels of crosslinks are not needed for structural support [146,147]. The reaction rate can be additionally slowed and controlled by adding drying chemical control additives (DCCA) such as DMF, THF or formamide. Direct imprinting into a sol-based polymer is typically limited to ion imprinting, due to the underlying requirement for an aqueous continuous phase additional salts makes such polymerisation impractical for the formation of any complexes based on hydrogen- or dipole-dipole bonds [148].

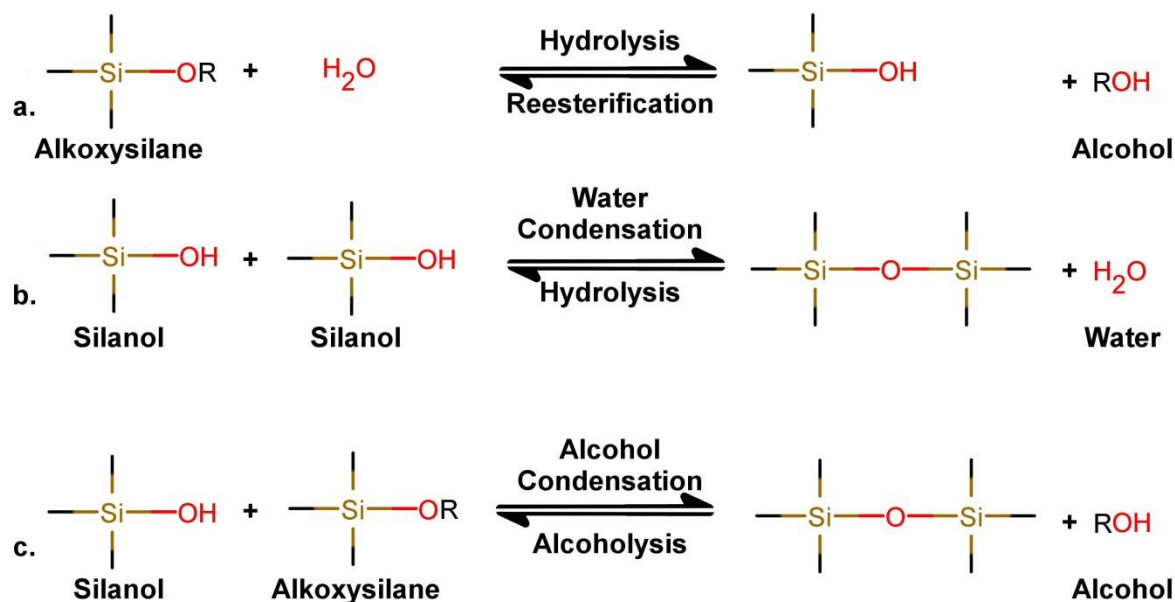


Figure 1.20: Schematic representation of the sol-gel hydrolysis and condensation mechanisms [146]

### 1.4.2 Addition polymerisation

Radical addition polymerisation is the most widely used polymerisation method for MIP synthesis due to its simplicity and versatility. It can, in turn be subdivided via the means of by which the reaction is initiated. The most commonly used initiating energy source is thermal and UV, though several other electromagnetic wavelengths can also be employed to modify the polymer properties including visible, mid-IR and ionising photons. The use of X- and gamma-rays and even electron beams allow for the inducement of the polymerisation reaction in the absence of molecular initiators or catalysts as well as tighter control over surface properties and degree of crosslinking by supplying a continuous, controlled quantity of radicals to the reaction until the desired structural properties are achieved [149,150]. Additionally, REDOX catalysts such as hydrogen peroxide, hydroxides of potassium, calcium or sodium, or pyridine can also be used when the template contains or is a radical scavenging functionality [151,152].

REDOX polymerisation can also be induced in certain monomers via the application of electrical potential. The use of this technique for molecular imprinting is somewhat attenuated due to the necessity of in-house synthesis of the FMs required for the imprinting process [121]. What follows is a brief description of these techniques, principally divided into the free radical chain polymerisation method and the electrochemically mediated REDOX method.

#### Free radical chain polymerisation

Terminal or free radical polymerisation consists of 3 steps: initiation, propagation and termination. Firstly, the radical initiator or catalyst must first be activated with the application of an energy source, such as is depicted in (Figure 1.21).

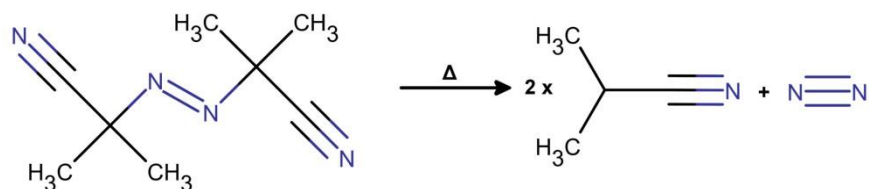


Figure 1.21: Decomposition of the commonly used radical initiator Azobisisobutyronitrile (AIBN) to form radicals, usable in a chain polymerisation

The polymerisation process involves the placement of a radicalised initiator fragments into contact with the monomers in the solution which then can accept the radical via its the vinyl groups which then combine together to form a growing oligomer chain. These chains, as their weights increase, have an increasing probability of combining with another oligomer chain rather than a single monomer thus leading to the unification of two radicals and the termination of the reaction (Figure 1.22). This random addition of various chain lengths results in a divergent reaction with thermodynamic equilibrium forces dictating ultimate polymer weight and particle size.

The structural properties of the polymer are determined by the rate of chain formation. Low, slow rates favouring long physically cross-linked (tangled and finite) chains which produce a soft polymer with low surface area, unable to support an imprinted receptor site and liable to solvent-related swelling which can open up cavities and pores within the structure otherwise known as 'solvent porosity' which can cause template bleeding and osmotic shock to the polymer [153]. High, fast rates of polymerisation form a rigid, brittle polymer containing shorter, chemically cross-linked chains which can support a highly intricate hierarchical pore structure and consequently a substantial surface area to host imprinted receptor sites. As the life span of radical species can vary from 0.1 – 10 s, by balancing the reaction between propagation and termination, the structural properties of the polymer can be controlled [154].

While the rule of thumb is that increasing the temperature increases the rate of initiator decomposition and the creation of radicals, each initiator has an inherent rate constant ( $k_d$ ) which is given by the Arrhenius equation, shown below:

$$k_d = Ae^{\frac{-E_a}{RT}}$$

Equation 1

Where  $A$  is the pre-exponential factor which relates temperature to the rate coefficient,  $E_a$  is the activation energy and  $R$  and  $T$  are the universal gas constant and the absolute temperature respectively. What should be noted from this equation is the existence of a minimum working temperature for the initiator which is followed by an optimal window of radical propagation which increases along a line defined by the rate coefficient. The importance of this relationship with respect to the selection of the initiator for a polymerisation of a molecular imprint is discussed in greater detail in section 1.5.4.

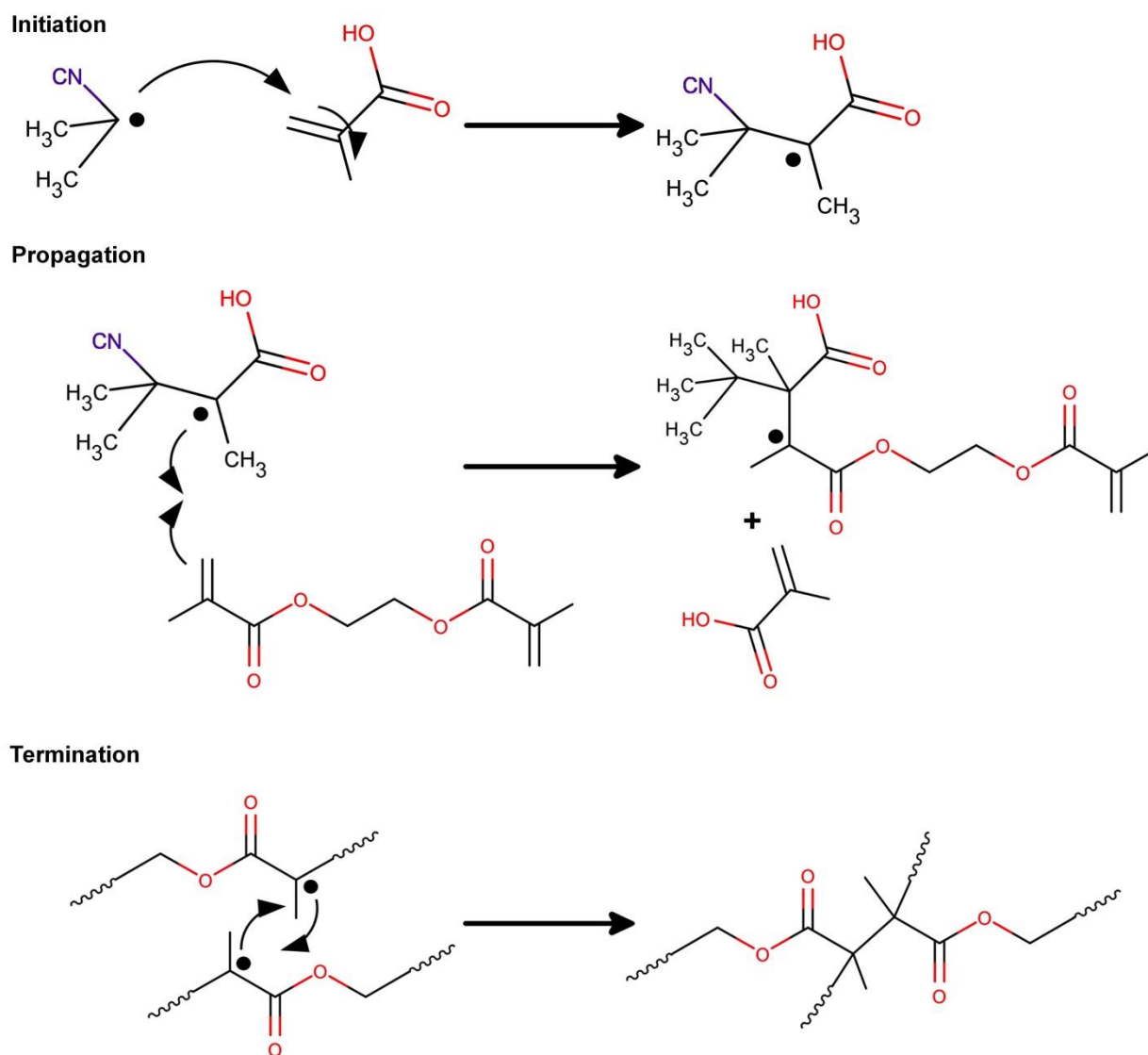


Figure 1.22: The co-polymerisation initiation, propagation and termination mechanism for methacrylate monomers (MAA & EGDMA) using AIBN as a radical initiator

### Living addition polymerisation

Living free radical polymerisation is one of the other principal initiation mechanisms used for molecular imprinting due to its ability to start and stop the polymerisation process as required. This is possible due to the localisation of the polymerisation reaction, id est the radical initiator, to the ends of growing chains, rather than in free solution as is the case with free radical addition polymerisation. This is most useful when precision layer thicknesses or particle sizes are required. To facilitate this process, an 'iniferter' is used in place of a simple radical initiator. This molecule

combines the function of initiator, transfer agent (propagator) and terminator into one and is thus appropriately named an 'ini-fer-ter'. This iniferter is coupled and immobilised to an existing substrate and the polymerisation is conducted similarly to that of a free radical polymerisation except that all growth is kept in one location, each addition can be predicted as one unit length and the number of actively growing chains is constant throughout the reaction. This is as opposed to the chaos of the random addition of chains of arbitrary sizes as occurs in free radical addition, in which the number of active chains must be determined using instantaneous steady assumptions such as the Bodenstein approximation [127,155–157].

## **Electropolymers**

Electropolymerisation, as the name suggests, uses a potential to induce polymerisation instead of a decomposing radical initiator with the magnitude of the voltage potential dictating polymerisation rate rather than an initiator's  $k_d$ . While conventional organic monomers are typically insulating in nature, thus resisting any transfer of charge through their structures, highly mobile valence electrons in conducting monomers allow them to serve as iniferters themselves in the presence of a voltage potential. However, though many conducting monomers may permit the throughflow of electrons at a sufficient rate to induce a polymerisation reaction, conductivity on a level sufficient to create an electrosensor must often be achieved only with the doping of the polymer with a conducting ionic species [122].

## **1.5 Rational design of a molecular imprinting protocol**

The unique contribution that each component makes to the thermodynamic equilibrium of the template monomer complex in the pre-polymerisation solution and throughout the polymerisation process has a substantial effect on the structural morphology, mechanical strength, and the surface area of the MIP. The process involved in optimising an imprinting protocol is intricate. While, with respect to a non-covalently imprinted polymer, it is preferable to conduct the reaction in an apolar environment to minimise disruption to the template-FM complex, this is often not possible due to template solubility. Thus a compromise must be found between effective receptor sites and pore formation. What follows is a brief discussion of each of the main factors which should be considered when designing an imprinting protocol.



### 1.5.1 Porogenic solvents for molecular imprinting

The need for a pore structure tuned to the application cannot be overstated. In SPE or chromatographic procedures, an effective, well-formed three family pore system can physically block larger interferants from interacting with the imprinted receptors via the gate effect.

For example, Koeber and colleagues stated their EGDMA-MIP was polymerised in toluene, a very thermodynamically good solvent for EGDMA. The resulting pore structure was highly defined though impenetrable to molecules weighing greater than 15 kDa and thus performs a preliminary filtration step upon the analyte before it reaches the MIP receptors [158,159]. This intricate pore structure makes these same MIP particles almost impossible to completely regenerate when immobilised to a sensor surface without destroying the sensor itself [142,160]. For this reason, MIP layers tend to be polymerised more slowly, often using photoinitiation to reduce the chemical crosslinks within the polymer and the hierarchical pore structure along with it which can resist any mechanical washing procedures via the capillary effect.

The requirement to disperse receptor sites throughout the MIP structure as well as augment the surface area and pore structure is the core function of the porogenic solvent. This solvent provides an *in situ* scaffold, around which a pore can be formed during polymerisation, as well as a solvation medium in which the template can be dissolved [92,161]. The presence of a non-reactive solvating medium facilitates the mixing and complexation of the template and FM, and thus the subsequent formation of template-specific imprinted binding sites.

As was previously discussed in section 1.3, once the polymerisation process is initiated, oligomer chains increase in length, growing more thermodynamically unstable until phase transition occurs and they precipitate into the solution. This precipitation causes the collapse of the previously dispersed oligomer which then forms the primary nucleus round which further chain collapse can continue depending on the solubility of the template and its effect on the stability of the oligomer to which it is complexed. If there is sufficient solvent volume, these nuclei will remain particulate until the reaction is spent, aggregating only to the extent of forming microporous (<2nm) microspheres (100 – 200 nm) [162]. If, however, the volumes of the polymer and solvent are similar, typically in equal parts for bulk imprinting [25], these microparticles continue to aggregate, forming a larger network, eventually fusing together to form a macro porous solid which may then be broken into monolith particles.

The selection of the porogen must take into account the format of the polymer being produced which dictates the proportion of porogen to be used with respect to the polymerisable fraction of the solution with the maximum, as previously stated, being 98% v/v above which point the polymer concentration is too low to facilitate chain entanglement or interpenetration [91]. While monomer concentrations above this threshold will ensure chain interpenetration, it does not guarantee polymer precipitation. Though with high concentrations of polymerisable media, such as are present during a bulk polymerisation (typically 50% v/v), precipitation can be forced by solidification of the solution itself around the porogenic solvent, the influence of the thermodynamic miscibility and compatibility of the solvent and polymerisable phases must be taken into account.

### **Thermodynamic goodness**

The measure of the ‘goodness’ of a polymerisable phase with respect to a prospective porogenic solvent can be further defined as the degree to which these two phases can mix and the ease with which solution homogeneity is maintained. As can be guessed, ‘good’ implies comparable parameters while ‘bad’ implies the opposite. A good solvent is miscible with both the monomer and polymer when it is the continuous phase while at lower concentrations it delays precipitation of the polymer significantly longer than its ‘bad’ counterpart. This is because, in addition to parameter compatibility, molecular weight is inversely proportional to miscibility and solubility. While the connotations of ‘good’ are of course favourable. If particles are the desired format, then a ‘less good’ solvent should be used to ensure the collapse and precipitation of the polymer chain to form solid particulate structures (Figure 1.23).

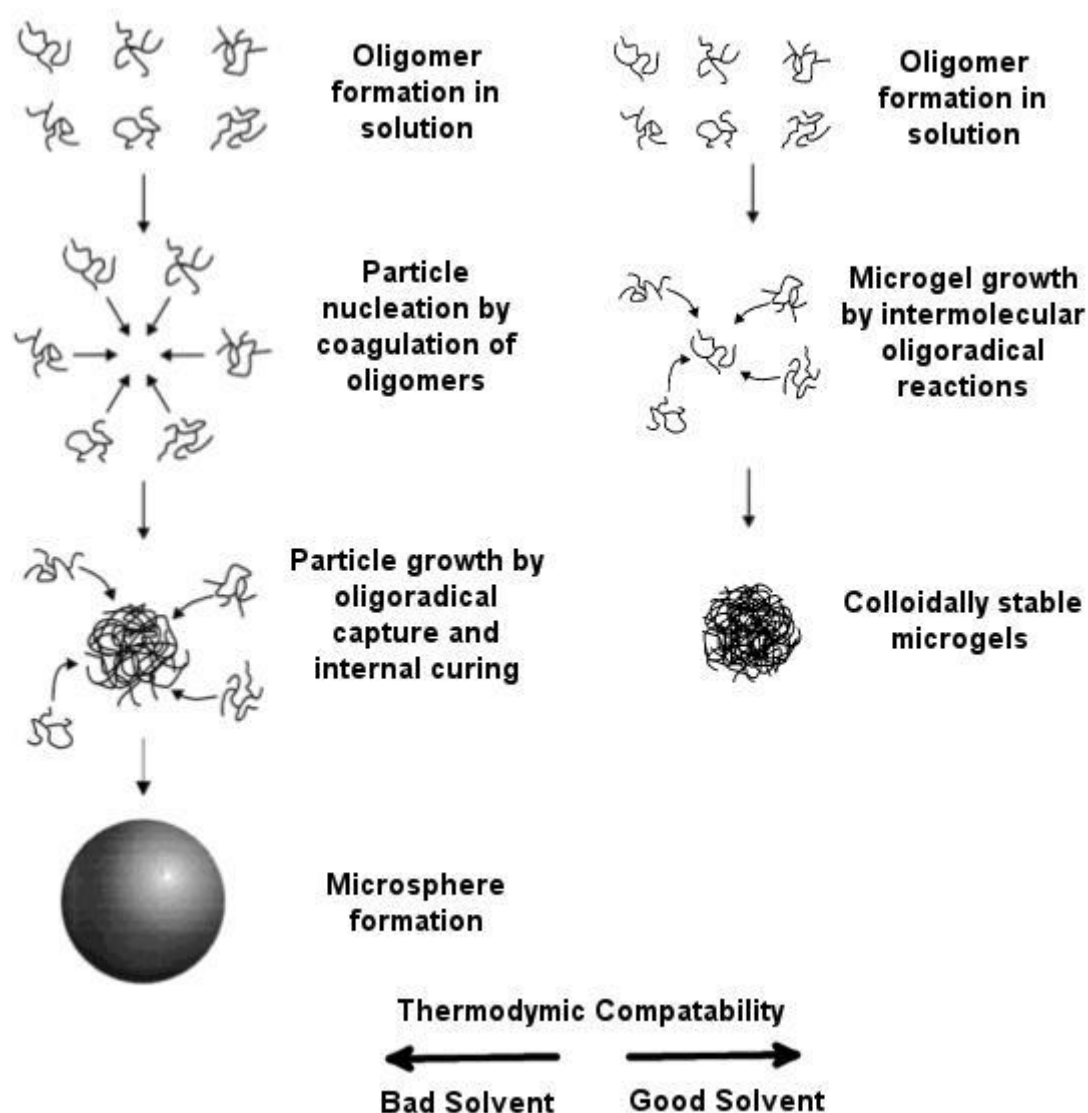


Figure 1.23: Importance of porogen selection on particle and pore formation; (adapted from: [163])

When a bulk polymer is being designed, a highly defined and rigid pore structure is required to maximise the accessible internal surface area. The use of a ‘good’ porogen allows for a complex hierarchical rigid pore structure to be formed even at lower polymerisation rates [158]. While the use of an extremely compatible solvent can block the precipitation of the polymer, in the case of a bulk polymerisation, the polymer chains can be placed in such density and proximity to each other that they can form extremely high molecular weight structures while still being supported by the porogen. This allows for the use of porogens such as toluene [98], DMF [164] or chlorine [165] to form methacrylate and vinylbenzene polymer solids, two of the most commonly used co-polymers for molecular imprinting, even though they share extremely similar properties (Table 1.5). The measure of solvent goodness is relative to monomer or polymer in question. By resolving the monomer's properties to the origin of a multidimensional graph (Figure 1.24). Boundary conditions

can be set by the sphere created by the modulus of the parameters on each axis. Both good and bad porogenic solvents can be combined in order to achieve the desired physical properties and particle size by the adjustment of the polymer precipitation point [166]. Tuning of porogen mix changes the theta point which is the point at which chain collapse occurs. This in turn permits an extended growth period for the chains in the solution and thus produces higher chain weights [95,167–169]. These miscibility or solubility parameters are named after the scientists who devised them, Hansen and Hildebrand.

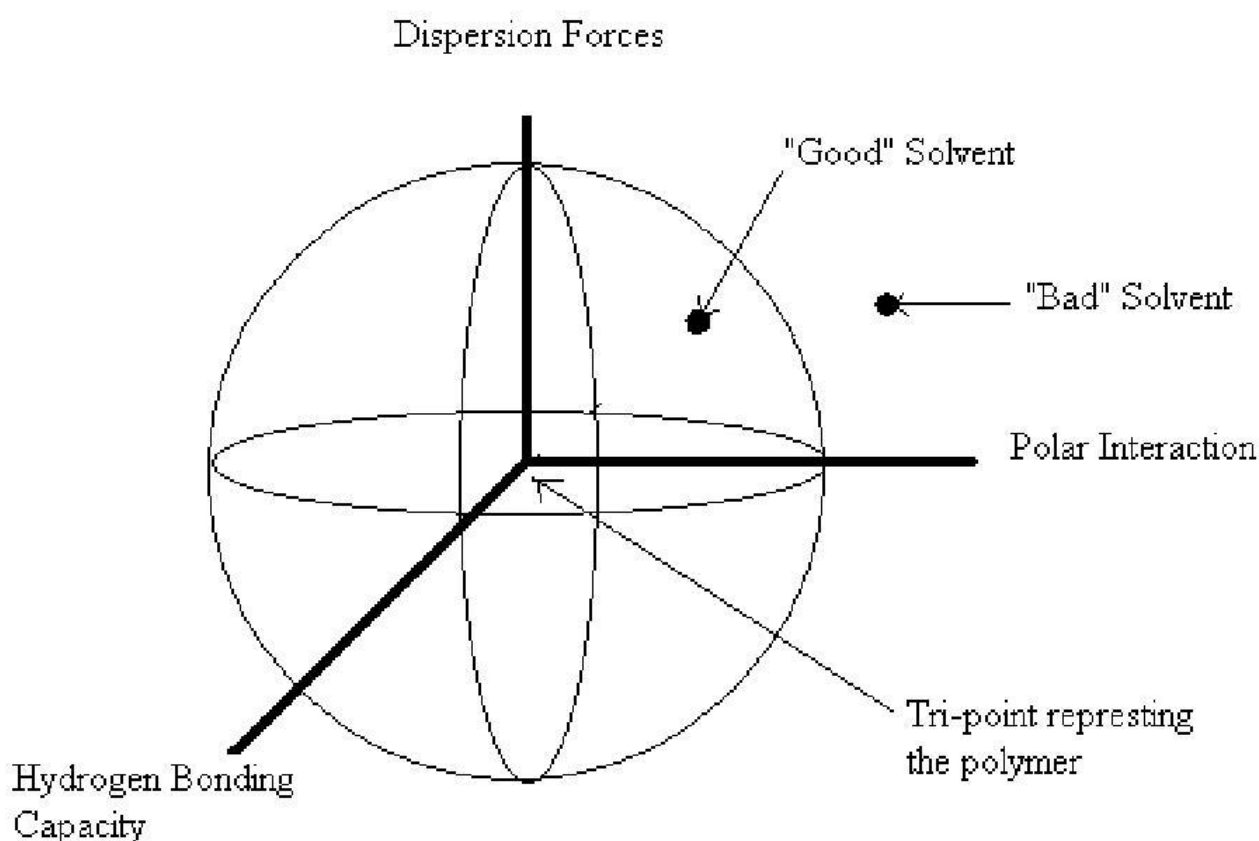


Figure 1.24: Good and bad solvent relative to the parameters of the polymer [92]

### Hildebrand and Hansen solubility parameter theory

The ability to predict the interaction behaviour and miscibility of two solvent compounds is clear for any composite solution. Whereas a rudimentary indication can be found in solvent polarity and hydrophobicity, this is highly limiting when control of complex systems is desired; such as is the case with molecular imprinting. The idea of a solubility parameter was first proposed by one Joel H.

Hildebrand in 1936 who proposed that a systematic description of the miscibility behaviour of solvents could be estimated as the square root of the cohesive energy density, or enthalpy of vaporisation 'C', of both solvents given by equation 2.

$$\delta = \sqrt{C} = \sqrt{\frac{\Delta H - RT}{V_m}}$$

Equation 2

The enthalpy of vaporisation 'C', in turn is derived from the heat of vaporisation ' $\Delta H$ ', gas constant ' $R$ ', temperature ' $T$ ' and solvent-molar volume ' $V_m$ '. This parameter, though a marked improvement on the binary notion of polarity and hydrophobicity alone, the Hildebrand parameter ' $\delta$ ' was still unable to adequately define the intrinsic properties of a solvent which drive compatibility and miscibility. With this in mind, Charles M. Hansen, in 1966, expanded on Hildebrand's parameter to empirically define solvent properties of inherent dispersion or van der Waals forces ' $\delta_d$ ', dipolar interaction or polarity ' $\delta_p$ ' and the hydrogen bonding capacity ' $\delta_h$ ' and modifying the original Hildebrand parameter to be ' $\delta_T$ '. These are related to the Hildebrand parameter by equation 3.

$$\delta = \delta_T = \sqrt{(\delta_d^2 + \delta_p^2 + \delta_h^2)}$$

Equation 3

This expansion of the original model in to three components led to Hansen's equation being referred to as the 3 dimensional solubility model. The separation of these three parameters allows for the tuning of solution to ensure effective mixing of the components whilst also facilitating the minimisation of any interfering forces from secondary compounds. In the case of non-covalent molecular imprinting, this is absolutely paramount in that interference with the primary template-

FM must be minimised whilst simultaneously facilitating the solvation capacity required to maintain an adequately dispersed solution, free of precipitate [170]. A list of common porogens and other solvents and compounds relevant to this study are given in Table 1.5.

Table 1.5: A list of solvents common and uncommon solvents to be used as porogens; Hansen solubility parameters and other characteristics influencing a compound's performance as a porogen or dispersing solvent with respect to miscibility with monomers relevant to this current study

		Hansen Solubility Parameters (MPa <sup>0.5</sup> ) [171,172]				Relative Polarity [173]	Hydrogen bonding strength [174]	Molecular weight (g/mol)	Viscosity at 25°C (cP) [175]	Boiling point (°C) [175]	Vapour pressure at 25°C (kPa) [175]
		$\delta_d$	$\delta_p$	$\delta_h$	$\delta_T$						
Commonly used porogens	Acetonitrile	15.3	18.0	6.10	24.39	0.460	Poor	41.05	0.37	82	11.8
	Chloroform	17.8	3.10	5.70	18.95	0.259	Poor	119.38	0.53	61	26.2
	DMF	17.4	13.7	11.3	4.86	0.386	Moderate	73.09	0.92	153	0.44
	Toluene	18.0	1.4	2.0	18.2	0.099	Poor	92.14	0.551	110.6	5.4
	Ethanol	15.8	8.80	19.4	26.50	0.654	Strong	46.07	1.2	78	5.95
Seldom used porogenic solvents	Methanol	15.1	12.3	22.3	29.61	0.762	Strong	32.04	0.6	65	16.9
	Ethylene Glycol	17.0	11.0	26.0	32.90	0.790	Strong	62.07	16.2	197	0.01
	Water	15.6	16.0	42.3	47.81	1.000	Strong	18.02	1.0	100	3.17
	DMSO	18.4	16.4	10.2	26.68	0.444	Moderate	78.13	2.0	189	0.08
Commonly used monomers	MAA	15.8	2.80	10.2	19.00	N/A	N/A	86.06	0.14	161	0.13
	IA	16.6	8.40	18.1	25.96	N/A	N/A	130.01	N/A	381	N/A
	EGDMA	16.4	5.40	8.60	19.30	N/A	N/A	198.22	0.32	100	0.13
	DVB	18.6	1.00	7.00	19.90	N/A	N/A	130.19	1.0	195	0.11

## **Pore formation and vapour pressure**

To ensure a well-formed and rigid pore structure, porogen vapour pressure must be minimised. Simultaneously, to ensure a rigid and highly cross-linked structure, the rate of polymerisation must be kept at a specified level to ensure chemical, rather than physical crosslinking and chain termination or vice versa. Pore rigidity maintains the position of the functional groups within the artificial receptor whilst overall porosity ensures receptor accessibility through increased mass transfer rates and pore diffusion [176]. While increased pressure may augment the rate of chemical crosslinking through the increased production of radical species, the vaporisation of the solvent during polymerisation inhibits the formation of an accessible primary pore network and reduces porosity. Conversely, a low polymerisation rate also reduces the permanent pore structure through the preferential formation of physical cross linkages, also known as chain entanglement. This lower rate, typical of photo-mediated polymerisations, produces a less rigid polymer more susceptible to solvent related swelling or 'solvent porosity' [24, 91, 166].

As aforementioned, pore formation occurs when droplets of the porogen are entrapped by the collapse of the previously dispersed polymer chains when precipitation into the solution occurs. This entrapment of droplets of the porogen occurs on a larger scale when these microspheres fuse together and then again when the solution completely solidifies. These three events produce first, second and third family pore structures within the polymer which has already been touched upon (Section 1.3, Figure 1.13). Low vapour pressure solvents are thus desirable and used as porogens where possible during syntheses of MIPs when the polymerisation is thermally initiated (Table 1.5). As the reaction for radial polymerisation is conducted in a sealed environment to prevent oxygen related inhibition of the polymerisation process [177], any increase in pressure in the closed system when it is brought to the reaction temperature will also increase the risk of an explosion. As with the issue of autoacceleration, discussed below, this associated risk can be minimised by reducing the size of the reaction vessel. The polymerisation rate is also proportional to pressure and can be accelerated by vapour induced pressurisation which may in fact inhibit the formation of second and third family pore structures and reduce the post polymerisation MIP performance [16]. In other words, the vaporisation of the porogen implies that it is not available to support the formation of pore structures and thus cannot serve its primary purpose. Vapour pressure however only appears to affect the morphology and mechanical structure of the polymer thus, if sufficient rigidity is provided by an external support or a sufficiently cross-linked internal chain network, the actual binding and selectivity behaviour of the imprinted receptor is not dependent on a particular porosity [178].



### **Viscosity and auto acceleration**

Solvent viscosity is a parameter of high importance due to its influence on mixing behaviour as well as the mass and reaction kinetics of the solution. Low initial solvent viscosity is favoured in order to minimise the increase in viscosity as the molecular weight of the polymer chains increases within the solution during the gelation stage of polymerisation. This is caused by the growth of a loose network of polymer chains, which restrict the mobility of the radical species, trapping them inside a finite area [179]. Due to the exothermic nature of radical polymerisation, the resulting build-up of heat further accelerates the rate of the process, forming more radical species. This chain reaction is referred to as autoacceleration or the Trommsdorff effect [166] and is an inherent part of the radical polymerisation process. It can be controlled by the fraction of radical initiator added (Section 1.5.4) to the solution to induce the reaction which is kept at approximately 0.5 – 1% w/w of the polymerisable phase. When an adequate quantity of initiator is present, and the same decrease in diffusion kinetics which would cause autoacceleration to occur in turn inhibits the propagation reaction by which the radical species are formed, resulting in a decrease of the polymerisation rate, referred to as autodeceleration [180], and the movement of the process toward polymer curing, in which the polymer gel achieves complete phase separation from the porogenic solvent. While it is a normal part of the polymerisation process, if too much heat is created through autoacceleration due to an overly viscous solution, polymer porosity can be reduced by an overly rapid polymerisation rate [16]. If the polymerisation reaction is on a sufficiently large scale, an explosion may occur.

Because viscosity is also linked to increased molecular weight of the porogenic solvent and can reduce the dispersion of the pore scaffold-droplets in addition to contributing to the autoacceleration effect low molecular weight porogens, such as non-reactive polymer solvents or polymer porogens, can be added to the solutions to reduce viscosity in a similar manner in which higher molecular weight non-reactive polymers are added during the synthesis of polymer layers to ensure an interconnected pore network [92].

### **1.5.2 Template solvation and stability**

The need to dissolve, stabilise and maintain the template molecule in the solution at elevated concentrations leads to proportionally augmented levels of frustration observably in the scientist during the design stage of a MIP. While an ideal porogenic solvent is defined by several variables, discussed above, the perfect porogen does not always equate to an ideal solvation medium for the

chosen template. In these scenarios, a non-reactive solubility enhancer can be added to dissolve the template at the required concentration. This however, can often lead to a poorer MIP due to the interference to the template-FM primary complex caused of this solubility enhancer. Disruption of the template-FM complex was observed and reported by Professor Mosbach's research group when theophylline's solubility in chloroform was enhanced using acetic acid. The acetic acid was seen, however, to significantly inhibit the primary theophylline-MAA complexes from forming polymerised imprinted receptors [181]. Other examples of template solubility enhancement in concert with the preservation of the template-FM primary complex include the use of a binary solvent phase to delay the saturation point of the template in the solution [182]. One other strategy is to switch the template-FM binding mode from high energy hydrogen bonds to weaker though uncontested van der Waals forces when the only apparently suitable solvent also has a very high hydrogen bonding capacity [183]. Perhaps the most effective of manner in which to improve template solubility without negatively affecting formation of the MIP receptors is to directly exploit the stabilising effect of the FM on the template. The enhancing effect that the FM has on template solubility can be as high as a doubling or tripling in the template's solubility in the porogen [184]. The object of using the FM alone to dissolve the template can be used to confirm that there is a template-FM interaction which is stronger than any template-porogen interactions. In other words, the fact that the template dissolves into the solvent only in the presence of the FM is an encouraging sign that some form of imprinted receptor site can be formed using that combination of those molecular components. As has been shown in Figure 1.9, the effect of the porogen and any other non-polymerisable interferants present in the solution will ultimately block or disrupt the formation of 'ideal' receptors which are those with the maximum number of FM groups interacting with the most unique functionalities on the structure of the template. The solvent interactions can act not only to create range of heterogeneous receptor sites of varying affinity and specificity, but also block the formation of FM-FM dimers in the NIP by forming solvent-FM complexes. These interactions result in exposed functional groups on the surface of the NIP follow the post-polymerisation removable of the porogen. These exposed FM dipoles and groups both dilute the observable imprinting effect of the MIP, which is calculated relative to the NIP, and also lead to increased levels of interference, reduced specificity and poorer overall performance [25].

In bulk imprinting, where template concentrations are significantly augmented, and where the thermodynamic characters of the crosslinker and the solvent are very similar, unstable or low solubility templates and template-FM complexes can often be stabilised by the addition the crosslinking monomer which typically accounts for up to 40% of the total volume of the pre-polymerisation solution. This solubility enhancing effect can be enhanced even further by the use of

a crosslinker. *Di*-, *Tri*-, and *Tetra*- EGDMA, discussed further in section 1.5.3 below, exhibit increasing hydrophilic character. These monomers can be used as cross-linkers when a low solubility template or an unstable template-FM complex is being imprinted [185,186]. However, the presence of an increasing number of oxygen atoms might also augment the probability of non-specific binding since they can each be employed as acceptor atoms in the formation of a hydrogen bond. Even with the evidence already given regarding the influence of the imprinting of molecular 'shape' and not only functional groups [15], the sheer volume of crosslinking polymer which is present in the MIP can contribute to non-specificity if the template-crosslinker affinity is significant [25].

One final method to bypass poor template solubility is to negate its use completely, using a more soluble structural analogue in its place. This strategy has been employed as a solution to high cost, thermal sensitivity or structural incompatibility to the imprinting process (i.e. tautomeric structure). The 'dummy' imprinting of a structural 'mimic', in fact, a quite common imprinting strategy with various cases being detailed in the literature a brief number of examples can be seen in Table 1.6.

Table 1.6: A small number of examples of dummy templates used to form MIPs to target molecules otherwise unsuitable to the imprinting processes

Template molecule	Target molecule	Reference
Cyromazine	Melamine	[187,188]
6-Aminopenicillanic acid	Penicillin	[189]
Trialkylmelamine	Atrazine	[115]
Catechin hydrate	Tetrahydrocannabinol	[88,89]
Theophylline	Hypoxanthine	[190,191]

### 1.5.3 Selection of crosslinking monomer

By design, the crosslinking polymer of a MIP should be complementary and not competing with the primary bonds holding the template-FM complex together. The correct proportion of crosslinker, normally devoid of high affinity functional groups, can be likened to the complementary role played by the aromatic functionalities within nucleotides as a DNA strand relaxes to its stable double-helix

structural state. While the primary binding mechanism between base pairs on complimentary strands is driven by hydrogen-bonding, each of the bases is secured in a horizontal position by its neighbour above and below. The cumulative effect of this  $\pi$ - $\pi$  stacking is a high stability platform with sufficient strength to maintain the highly complex structures to hold in close proximity to the primary (hydrogen) bonds of the DNA [74].

The molar proportion of template to FM to crosslinker is normally taken as 1:4:16 respectively which works out at approximately 80 mol% of the total solids for the crosslinker and 19 mol% for the FM. Proportions in this range have been shown to provide the greatest separation factor for MIPs relative to their controls [192]. The 1 to 4 ratio between FM and crosslinker is done to ensure the rigidity of the polymer which is directly responsible, in the absence of an external support, for maintaining receptor morphology. Interestingly, the use of excessive quantities of cross-linking polymer has also been seen to negatively affect the receptor site by introducing too much bulk into the pore structure which acts to reduce the closeness of geometric fit between the template molecules and the imprints made in the polymer [193].

Quantity alone, however, does not exclusively dictate the efficacy of the MIP when experimentally tested. Choice of the monomer also significantly alters the performance of the MIP. Ethylene glycol dimethacrylate (EGDMA) and divinylbenzene (DVB), shown in Figure 1.25, are two of the most widely known and used crosslinking monomers used in molecular imprinting. As shown in Figure 1.26, they have significantly differing effects on the performance of the MIP. While DVB, containing one aromatic functionality within its structure, poses negligible interference to the primary hydrogen-bond based template-FM complex, the poly-DVB's tendency to form a denser, more closely packed and less porous structure through  $\pi$ - $\pi$  stacking of its aromatic rings serves to decrease the accessible surface area of the MIP and thus reduce the number of accessible receptor sites available to capture the analyte from the solution [194]. The long, linear structure of EGDMA, on the other hand, allows for greatly increased entrapment of the porogen which, in turn, creates a much more easily accessible, larger surface area. This enhancement occurs even in the presence of additional oxygen atoms with EGDMA's structure which can act as acceptor atoms in hydrogen bonds (see Table 1.9) and thus can directly compete with the template-FM complex, disrupting the formation of receptor sites and also posing a greater risk of a-specific binding at the MIP's surface.

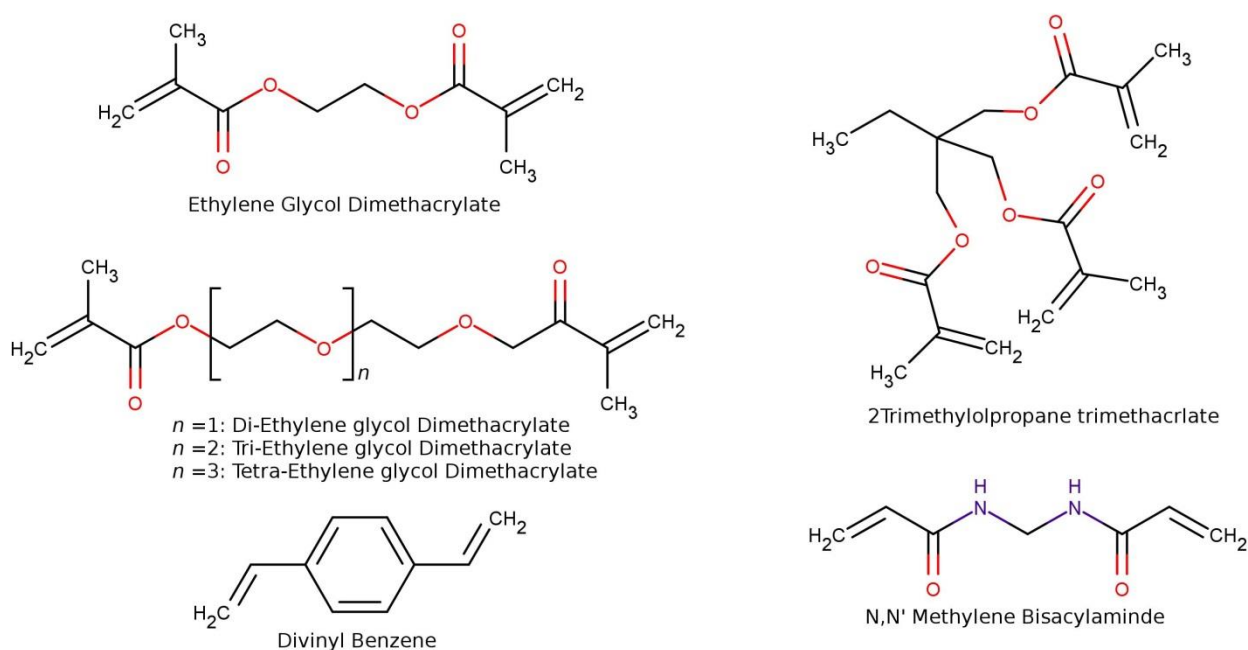


Figure 1.25: The structures of some common crosslinking monomers used for molecular imprinting

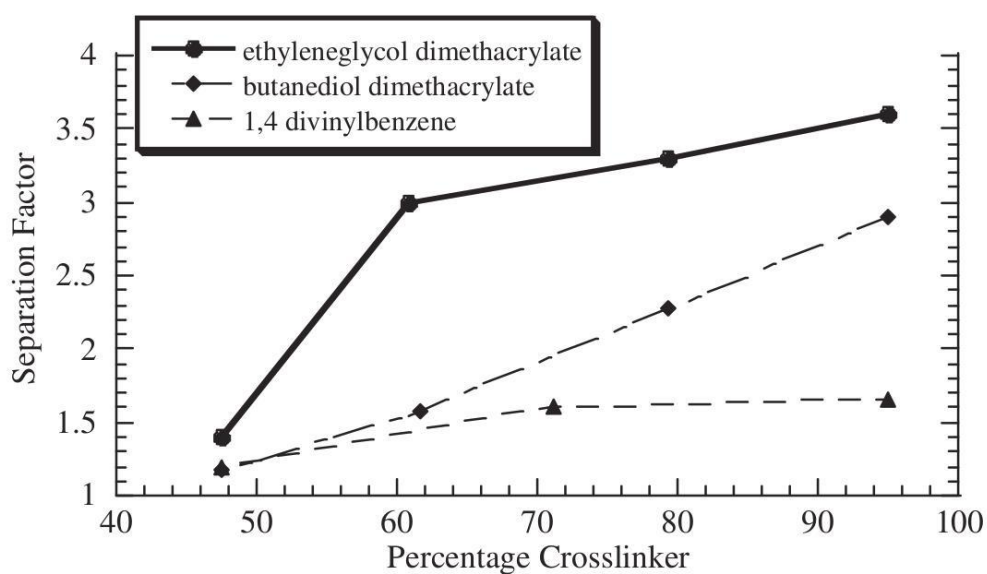


Figure 1.26: Selectivity versus amount of crosslinker for covalently imprinted polymers [162]

### 1.5.4 Initiation rate

The actual crosslinking of polymer chains during the polymerisation process should not be confused with the crosslinking monomer. The latter is a monomer containing two polymerisable groups, it can actually be cross-linked to varying degrees by the rate of the polymerisation reaction with is ultimately dictated by the decomposition rate of the initiator molecule. As can be seen in Figure 1.27, the difference between a linear (physically cross-linked or entangled chains) or low density, structurally weak polymer which requires a support, and a structurally rigid polymer, capable of supporting receptor sites unaided, is found in the level of interconnectivity between finite polymer chains, occurring during the polymerisation reaction.

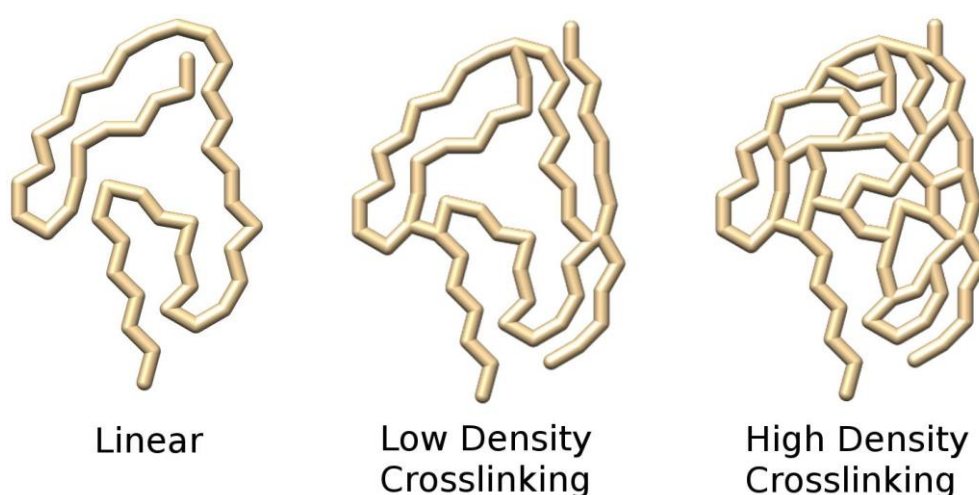


Figure 1.27: Polymer chains resulting from increasing polymerisation rate from linear (slow) to minimally and highly cross-linked (high)

It is, more often than not, most important to ensure rapid chemical crosslinking of the monomers around the template-FM complexes in order to form robust structures, resistant to solvent-related swelling. This is often achieved with the use of a thermally mediated radical polymerisation process. The use of an elevated temperature affects the quality of polymer in two ways. Firstly, increased incidence of radicals leads to more frequent polymer chain termination within the solution; shorter chain lengths result in a more robust structure, less susceptible to solvent related swelling [195,196]. Secondly, the increased temperature can also augment the solubility of the template in accordance with Le Chatelier's equilibrium principal, which can delay the precipitation of the short-chain oligomers into the solution relative to the control which can reduce the pore quality and polymer surface area.

The rate of radical creation in photo-mediated polymerisation is actually faster than thermal energy sources, being proportional to the intensity of the incident light; however, the propagation rate is lower and thus so is the mechanism by which chemical cross-linkages occur [174]. The distinct advantage of this photo-polymerisation method is the ability to perform polymerisations at temperatures as low as  $-20^{\circ}\text{C}$  [197] which may be required to stabilise the template or the template-FM complex in the solution ahead of polymerisation. Indeed, the use of low temperature polymerisation protocols is observed to produce a MIP with approximately double the amount binding sites  $B_{\text{max}}$ , though a corresponding halving in the apparent affinity constant  $K_d$  of these sites relative to thermally initiated MIPs [24]. From this proportional relation between  $K_d$  and  $B_{\text{max}}$  with respect to polymerisation temperature, it can be inferred that, while higher temperature polymerisations may destroy many lower energy template-FM complexes, the augmented mobility that this thermal energy provides to the system also allows the remaining complexes to orientate themselves into a more optimal conformation prior to being physically secured in place by the growing polymer chains.

The need for a minimal support structure is clear and whether this is integrated via the aforementioned promotion of chemical crosslinking or through the use of an external support. The results of both equate to the same if the mechanical stress resulting from the removal of the template is not compensated for upon removal of the template from the receptor site. The consequences inadequately providing for this necessity is shown in Figure 1.28. The most insidious scenario of those shown must be the inadequate removal of the template which may be released during the subsequent use of the MIP in a phenomenon known as template bleeding [17,84].

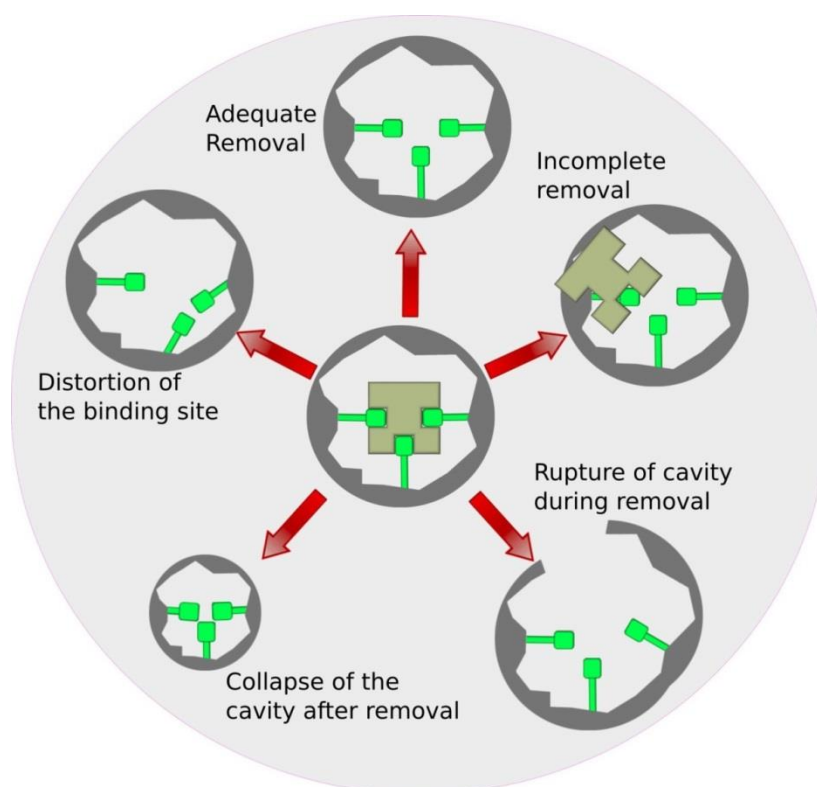


Figure 1.28: Schematic showing the outcomes from insufficient crosslinking in which the MIP is then structurally weak or susceptible to incomplete template removal, solvent related swelling and subsequent template bleeding

The polymerisation rate can also magnify any positive or negative thermodynamic effects which the template molecule may have on the MIP solution in contrast to the NIP. Thus special attention should be paid to the decomposition rate of the initiator molecule at the desired polymerisation temperature so as to adjust the polymerisation rate to minimise this effect, making the results produced by the MIP and NIP more comparable [198].



## **1.6 Transduction methods used for MIPs**

The method of transduction of a MIP sensor is at least of equal importance to the synthesis of a robust and optimal MIP structure. While electrochemical sensing techniques often the most cost effective, facile and robust methods of transduction, the monomers used in molecular imprinting are most often electrical insulators themselves. This can make the quantity of MIP, used to modify the sensor surface, inversely proportional to the sensitivity of the electrochemical sensor itself. For this reason, many laboratories use alternative methods such as the piezoelectric quartz crystal microbalance (QCM), surface acoustic wave (SAW) or surface transverse wave (STW). Other methods such as surface plasmon resonance (SPR) and field effect transistor (FET) are also frequently used. Each one of these possesses their own strengths and weaknesses inherent to the detection strategy which are summarised in Table 1.7. Perhaps the most common sensing strategy incorporate the use of MIPs are optical as the MIP can be used in assay in free solution, as a pre-concentration mechanism (SPE) or as the solid phase in chromatography apparatus.

Table 1.7: A summary of the most commonly used techniques for the transduction of MIP based chemosensors (adapted from [199,200])

Transduction method	Sensing scheme	Advantage	Disadvantage	Reference
Optical	Absorbance or fluorescence	Non-destructive, Improved S/N ratio via multiplexing,	Susceptible to photo-bleaching	[201,202]
SPR	Coupling angle reflectivity	Applicable to biosensing	miniaturisation	[203,204]
QCM, SAW & STW	Piezoelectric sensing	Cheap & universal detection principal	Sensitive to temperature & viscosity, liable to cross sensitivity	[123–125]
FET	Field-effect	Wide working range & low detection limit	Requires reference electrode	[205]
Electrochemical Impedance spectroscopy	Electrical impedance	Low LOD	Poor reproducibility, laborious optimisation	[206,207]
Conductometry	Change in conductivity	No additional reagents or markers required	Analyte must be electroactive	[208]
Potentiometry	Potential difference between two electrodes	No additional reagents or markers required	Analyte must be ionisable	[39,209]
Amperometry	Current at constant potential	Low LOD Most commonly used ECMIPS	Fouling of sensor surface reduces detectable signal	[210,211]
Voltammetry	Current at varied potential	Rapid, cheap detection	poor electron transfer due to isolating MIP material	[40,212,213]

### 1.6.1 MIPs in sensor arrays

When viewing the progress made in the application of MIPs to sensor arrays, one must also be aware of the specific start point of the research trajectory or rather, the specific generation of MIP technology which is employed in the sensors which is most often non-covalent in nature. Their popularity and widespread use relies on their inherent simplicity and low cost, widely available component reagents and, most importantly, the unspecialised equipment and skill set required in the synthetic process. The availability and applicability of the technique to numerous template molecules using an essentially identical protocol has proven to be the key practical advantage that has led to the explosive growth in the field of molecular imprinting that has already been discussed at the start of this chapter (Section 1.1.1). Due to this apparently universal protocol, many reported imprinting protocols are not optimised, employing instead the 'rule of thumb' ratio of 1:4:16 discussed previously (Section 1.5.3) for template, FM and crosslinker quantities without excessive thought on synthesis optimisation to the sensing environment. This can often lead to the already mentioned effects of high incidence of non-specific binding, receptor hydrophobia, template bleeding, slow kinetics, poor affinity or all of the above [214].

Indeed, the concepts of molecular imprinting and sensor arrays can appear to be divergent as the former seeks to achieve the highest possible selectivity of a sensor material by the act of literally imprinting the likeness of the target within the sensor. Sensor arrays, on the other hand, seek to improve accuracy, ultimately equitable to selectivity, by the collaborative effort of several sensors each of which exhibit some comparable cross response to the target. The apparent superfluity of this combination was summed up by Professor Sergey Piletsky, the most highly published author by number in the field of molecular imprinting [13], when he asked<sup>1</sup> whether the ultimate goal of a MIP sensor array would be to create 'bad' MIPs, alluding to the potential of a loose-loose scenario of the performance of intentionally designed low specificity MIPs being further reduced by immobilisation of the polymers on a sensor surface and by the transduction method. This comment highlights a curious point of debate which can occur between the engineer and the scientist with respect to research trajectories and the development of a practical system. At what point must one exit the ideal conditions of the laboratory and enter the imperfect world of real samples and unknown interferants? A definitive answer to this does not exist. A conscious decision must be made between a highly optimised and consequently delicate MIP which must be applied with precision under highly controlled conditions, such as the *in vivo* application of a MIP [215], and a dependable, more generic MIP whose inherent flaws are patched and solved on an ad-hoc, after-the-

---

<sup>1</sup> : 3<sup>rd</sup> CHEBANA Summer School, Biarritz, France, 1 – 7 September, 2013

fact basis which is the more widely employed strategy reported on in the literature. As Shimizu and Stephenson put it in their review on the subject, placing MIPs in an array form serves to 'compensate for', rather than solve, the observed low selectivities and elevated cross-reactivities seen in MIP sensor systems [216].

The crux of the issue of application of the MIP to the sensor array has always been to find a way in which to maintain imprinted receptor integrity while maximising signal transduction and regenerability. The latter being needed in order to produce the large data sets needed in order to solve cluttered signals from the complex mixtures of molecules present in real samples. The reward for solving these issues would be to explain and exploit “nature's tricks” which is to explain the complex mechanism used by the physiological sensors for analytes in fluid, namely, the nose and tongue [217]. As shown in (Figure 1.29), a sensor array uses both specific and non-specific receptors to determine the concentration of one or more of molecules by the processing of the variation in response from sensor to sensor represented, in this case, by colour.

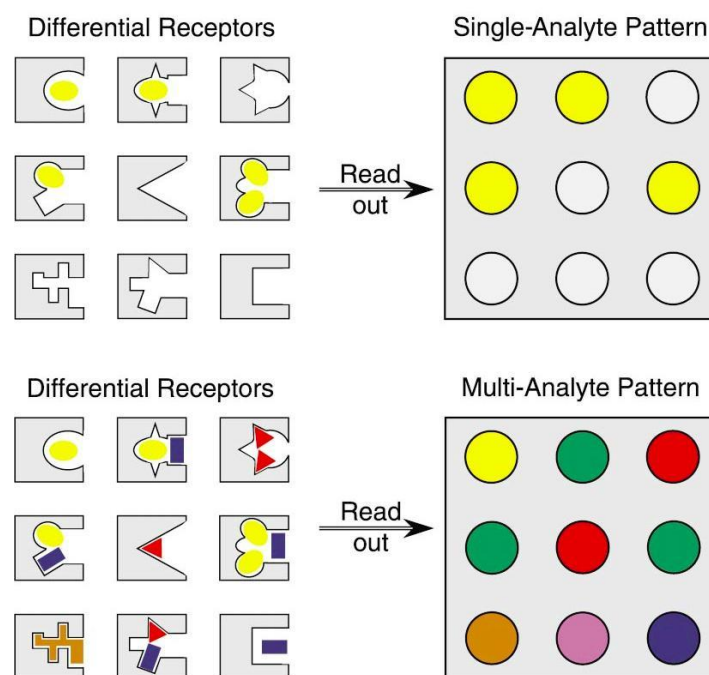


Figure 1.29: Variation in signal produced by a sensor array in a homogeneous and heterogeneous solution of analytes (modified from: [217])

As summarised in Table 1.8, there are a number of array systems based on MIP sensors. The detection strategy of each of the systems presented speaks to the inherent limitations of MIP sensors already discussed in previous sections. All but one array system employ non-electrochemical methods, opting instead for more MIP-compatible piezoelectric, absorbance and fluorescence based sensing techniques. The issue of sensor regenerability are solved by using flow systems [149,218], volatile analytes [219–221], MIPs in free solution [222–224], limiting the receptors used in each measurement and compensating for the signal loss for the finite lifetime of the sensor [225] or by controlling pore structure using physical scaffolds [124]. In the latter, equilibrating time is extended greatly due to diffusion limitations of the fluid throughout the micropore structure of the MIP layer.

Table 1.8: Summaries of publications reporting on molecular imprinted sensor arrays

Target system	Imprinted templates	Sensor system	Data processing	Ref.
E-nose measuring Volatile organic compounds from plant-degradation	water, limonene, ethyl acetate, propanol, butanol	MIP layer deposition on QCM electrodes	Principal component analysis	[221] [219]
E-nose measuring terpenes in herbs	Limonene, $\alpha$ - & $\beta$ -pinene, estragole, eucalyptol, terpinene	MIP layer deposition on QCM electrodes	Principal component analysis	[220]
Detection of bittering compounds in tonic water	Quinine, sacchrine	Precipitated MIP particles in PVC layer on QCM electrodes in flow system at varying pH	N/A	[218]
Detection of albuterol (performance enhancing drug) in biological samples	Albuterol	Thin MIP layer electrode with complimentary NIP, platinum & glassy carbon voltammetric electrodes	Numerical analysis	[225]
Proof-of-concept screening platform for high-throughput screening of sensors	dansyl-l-phenylalanine	Microfluidic array of 14 NIPs; UV absorbance measured with CCD camera; separate MIP sensor created from the results	N/A	[149]
Characterisation of sensor array with potential applications in physiological and environmental scenarios	$Zn^{2+}$ , $Cd^{2+}$	Ion-imprinted Silica layers impregnated with organic fluorophore to indicate binding events	Principal component analysis	[224]
Detection of aromatic amines and distinction between diastereomers, pharmaceuticals and structural analogues	( $\pm$ )-propranolol, (+)-pseudoephedrine, (2)-ephedrine, R-(2)-2-phenylglycinol, benzylamine, $\alpha$ -methylbenzylamine, and 2-(dimethylaminomethyl)-3-hydroxypyridine	7 methacrylate MIPs in free solution; Colorimetric sensing of complex binding through displacement of a non-specific fluorescent dye (benzofurazan) from MIP receptors	Linear discriminant analysis	[222] [223]
Detection of aspartame against peptide analogues	aspartame	MIP thin film using bead scaffold to form a structural array in place of a macropore system on a QCM electrode	N/A	[124]

### 1.7 Computational modelling for molecular imprinting

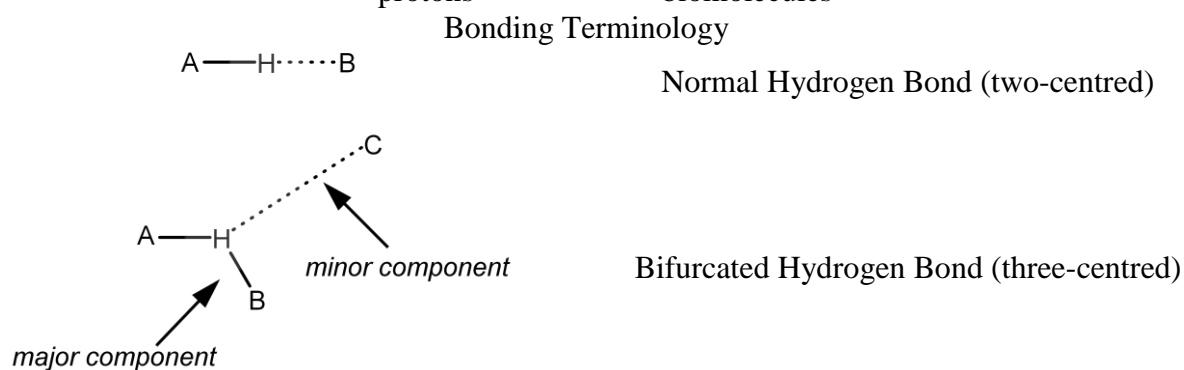
Virtual screening using specialized computational models can serve as an accelerative tool in the pre-polymerization selection process; such models can provide accurate predictions of the primary binding energy of candidate FMs for a selected template. A preliminary refining of a large library of monomers can be made over the course of a day by a computational algorithm which would otherwise take weeks or months in the laboratory. On a numerical scale, a two-component system of 100 monomers results in more than 5000 possible combinations[194]; a decidedly unviable number for experimental screening. The main, overbearing and ever-present issue that goes in-hand with the attempt to model and predict the highly complex interactions of physical chemistry with an analogous virtual system is the question of accuracy. The compromise between computational price, processor-load and faithful replication of the quantum effects driving the observed inter-atomic behaviour is an extremely delicate one [226].

Given the large variety of components and conditions used in MIP synthesis, the *ab initio* incorporation of computational modelling is highly attractive in order to reduce the laboratory workload, design time and consumed materials. This can be done by providing an affinity ranking for functional monomers and porogenic solvents based on the primary site of hydrogen bonding, shown to be an accurate indicator of post-polymerisation performance [227]. This prediction of the strength of the electrostatic bonds between the template and each of the components can be used to determine whether solvent or co-monomer can disrupt or interfere with the formation of complex between the template and the FM and as a consequence, affect the affinity and specificity of MIP receptor.

Indeed, the efficacy of computational models is such that there have been successful reports of 'virtual imprinting' whereby a monomer is virtually matched to the target molecule based on the quality of the hydrogen bonds formed (Table 1.9) and then, a non-imprinted polymer (NIP) is used in place of a MIP. This further accelerates the design process and has proven to be an effective strategy for targeting compounds which may not necessarily be prime candidates for the conventional imprinting process [226,228]. The link between favourable NIP binding properties and a successful imprinting event, in other words that high primary or nonspecific affinity between the template and FM increases the probability of effective imprinted receptors being formed, has long been established [227].

Table 1.9: Table stating the defining features of hydrogen bonding strength and quality [229]

	Strong	Medium	Weak
Bond energy (kJ·mol <sup>-1</sup> )	14-40	4-14	0-4
Interaction type:	Mostly covalent	Mostly electrostatic	electrostatic
Bond lengths (Å)	A—H = H···B	A—H < H···B	A—H << H···B
A---B	2.2-2.5	2.5-3.2	3.2-4.0
H···B	1.2-1.5	1.5-2.2	2.2-3.2
Bond angle (θ)	175 - 180	130 - 180	90 - 150
Reduction in IR stretch frequency	25%	10 - 25%	< 10%
Examples	Proton sponges, HF complexes, hydrated protons	Carboxylic acids, alcohols, biomolecules	C-H···O/N O/N-H···π



Over 25% of H-bonds in carbohydrates are multifurcated; more in amino acids and proteins

Dynamic simulation of molecular interactions can also provide extremely useful insights into events within the polymerisation solutions. This can be either in the pre-polymerisation design phase where maximum or ideal stoichiometric ratios between the template molecule and the FM can be calculated and then used in the calculation of molar ratios within the synthesis protocol to replace the experimental determination through Job Plot analysis [113,230–232], or the simulation of the polymerisation even itself in which the durability of the template-FM complexes can be tested in the solvent and crosslinker molecules, at polymerisation temperatures as well as predicting the diversity or heterogeneity of the receptors which may be predicted to be formed during the polymerisation process [233–235].



### **1.7.1 Computational chemistry**

Computational chemistry performs simulations of inter-atomic and molecular interactions in order to study the behaviour of system. The development process of such a computational system can be seen summarised in (Figure 1.30). This progression can be understood as a steady tightening of the boundary conditions on the interaction of interest. If one thinks of an experimental system in a laboratory as a simplification of a naturally occurring system, from a boundless environment to a controlled one, then from that precedent, the further progression from experimentation in a physically constructed artificial environment to experimentation in a virtual environment is perhaps not so drastic or abrupt. Just as is the case in experimental chemistry, the design and development of computational chemistry models must make approximations and simplifications of highly complex phenomena in order to reduce the computational-cost, or the workload, to a level compatible with the processing power of available computing systems.

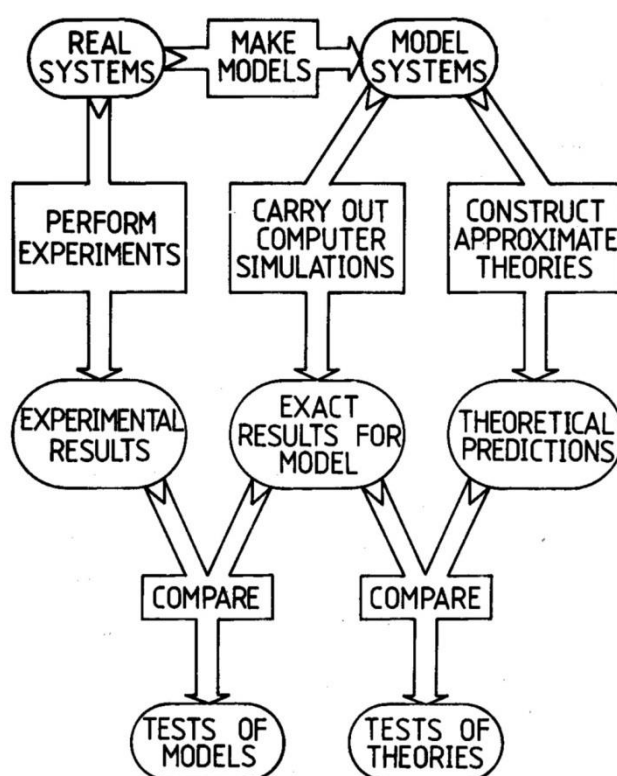


Figure 1.30: A schematic depicting the basis on which predictive computer models are created from and tested using experimentally acquired empirical data (adapted from: [236])

The resolution of the system or the degree to which the model must be simplified depends on the size of the system with respect to number of mobile atoms and the simulation time with the two of these being directly proportional to each other. As shown in Figure 1.31, three broad categories of modelable systems can be defined the first principals (FP), tight binding (TB) and empirical molecular dynamics (MD) methods.

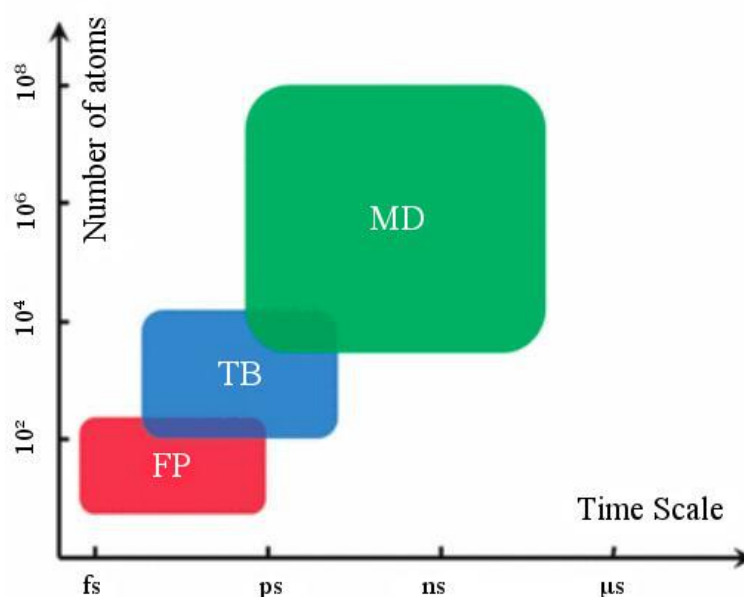


Figure 1.31: Graphic showing the relationship between the scale and size of the system of interest, the time required to achieve quality simulations and the level of detail in which the system can be represented [237]

The FP method might also be referred to as the *ab initio* method in which all quantum mechanical properties are modelled from the Schrödinger equation in order to achieve the greatest degree of accuracy in the predictions made by the model. However, given the level of detail into which this model goes, current computational capacities limit this method to small systems of up to approximately 100 atoms. For larger system up to 10,000 atoms, the semi-empirical TB method can be used. This method is based on the Hamiltonian matrix mathematical model and constructed using a low number of basic material functions. These can be used to calculate eigenvalues and wave functions from which additional parameters such as charge density, band structure and absorbance spectra can be extrapolated. In this intermediary model, quantum properties and effects such as superposition are still observable thus making it highly useful for modelling one and two dimensional nanostructures. For systems any larger than this, as are the systems representing molecular imprinting events, more coarsely defined environments based on empirical data must be relied on [237].

Because of the empirical nature of these environmental systems, the properties of each object are heavily dependent on the conditions under which they were originally observed and optimised; for example, protein or DNA interactions in water. Table 1.10 shows the specialisation of a selection of the most common force fields currently described in the literature. These force fields can be viewed as large tables of atomic properties, bond types and energies which can then be observed interacting

with each other under specified ambient conditions of pressure, temperature, time, charged state etcetera.

Table 1.10: Description of some commonly used force fields for molecular dynamics simulations

<b>Force field name</b>	<b>Optimised environment</b>	<b>Reference</b>
Tripos	Organic molecules & proteins	[238]
AMBER	Mainly used for modelling of proteins & DNA	[239]
CHARMM	Small and macromolecules	[240]
GROMOS	General purpose system for biomolecular systems	[241]
OPLS	Specialised liquid simulations	[242]
COSMOS	Organic, inorganic & biological molecules	[243]

### 1.7.2 Model smelliness

The concept of 'smell' when discussing mathematical models and functions in computational code is used to describe the accuracy with which the model represents the system on which it is base in terms such as level of abstraction, accuracy of boundary conditions and over- or under-definition of parameters [244]. This can become a significant issue if the system must be modified to a secondary environment or if it is being further simplified in order to reduce the computational load on the processor available to the scientist. It is a fine line to tread when the fitting of experimental and to theoretical models can be attributed to 'luck' and stands to the testimony of just what a feat the creation of an accurate theoretical model is [245].

The very nature of this level of molecular modelling, which is essentially simplistic mathematical functions with applied empirical constants to suitably weight key parameter, has led the majority of the force fields to make some key approximations which reduce the accuracy of their predictions [246]. Perhaps the most notable of these approximations can be taken as the common use of the Lennard-Jones potential equation to describe molecular interactions between atoms, shown in equations 4 and hypothetically plotted in Figure 1.32.

$$V(r) = 4\epsilon \left[ \left( \frac{\sigma}{r} \right)^a - \left( \frac{\sigma}{r} \right)^b \right]$$

Equation 4

Where  $\epsilon$  is defined as the magnitude or 'depth' of the well energy potential and  $\sigma$  is the distance at which the inter-atomic potential can be defined as zero. Finally, the superscripts 'a' and 'b' are versatile operators which may be modified depending on the modelling function. For example, 12-6, 12-10 potentials can be used to represent van der Waals and dipole or hydrogen bonds receptively [246,247]. An extended 12-10-6 triplicate function can be used to model a function, repulsive at medium distances, which can be used to represent the desolvation energy penalty which occurs when a receptor removes a ligand from free solution [248].

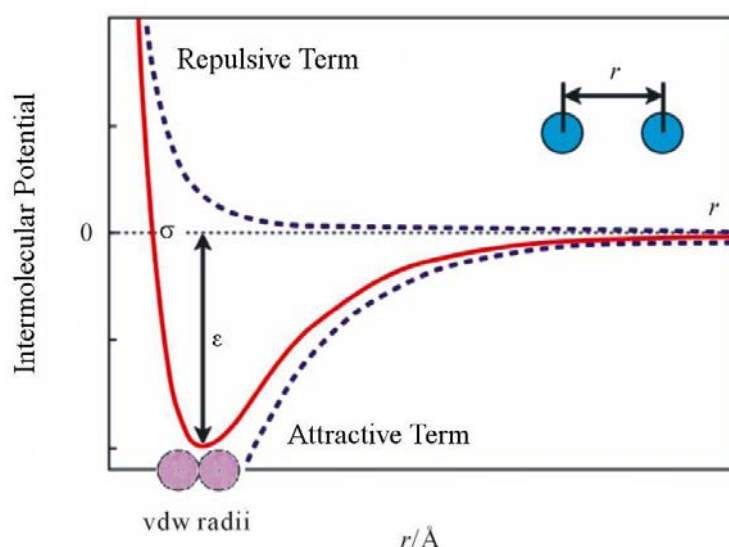


Figure 1.32: Schematic of the plotted Lennard-Jones potential mathematical function (adapted from: [249])

The scenario to which a model is applicable can be further narrowed with the use of additional approximations such as the united atom model, where non-polar hydrogen atoms are merged to their heavier root atoms for the modelling of larger proteins and other macromolecules [250], or the embedded atom model which can be used to simulate bulk materials and surfaces [251]. This necessary simplification of interactions can predictably lead to model incapacity or ignorance of certain background interactions [252].

Two levels of system coarseness and docking search strategies can be seen in the in Figure 1.33 which compares the highly detailed though computationally more expensive SYBYL modelling suite an Leap Frog search algorithm, developed by Tripos and available through the Certara parent company, with the open source computationally lighter Autodock suite developed by the Scripps institute. SYBYL is built on top of a bespoke force field developed by Tripos itself and, given its primary application to physiological molecules, its high resolution definition of various bond types as well as, for example, 6 distinct atomic states for carbon, is highly defined and can produced detailed results. Autodock, on the other hand, is slightly smelly by comparison. The cutting of computational cost allows the Scripps institute to provide the Autodock suite as an open-source, freely downloadable software package. The compromise between computational cost and accuracy must be complemented by an appropriate effort in the laboratory to confirm the predictions of the computation model. This is referred to as the combinatorial approach.

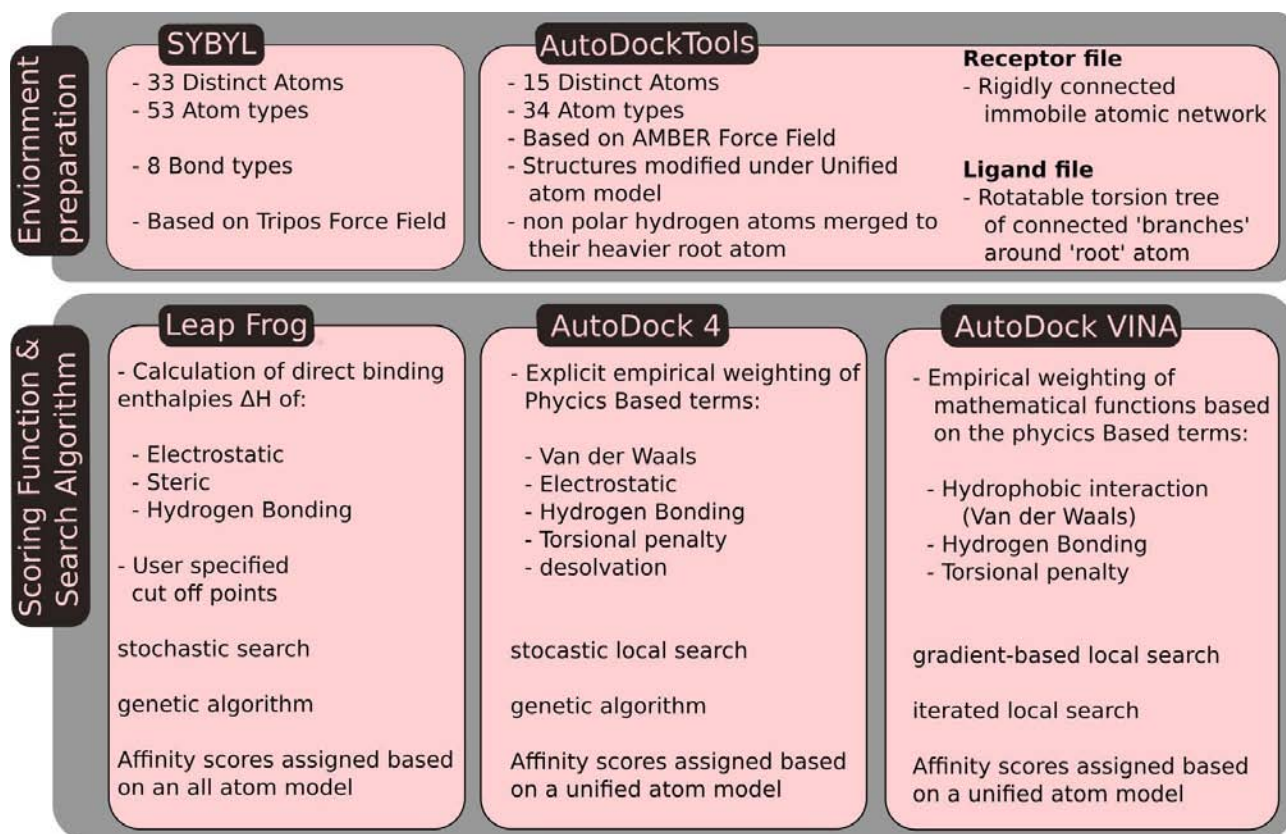


Figure 1.33: comparison between the SYBYL and open-source Autodock molecular docking suites

### 1.7.3 The combinatorial approach

When observing the results predicted by a computational model, it is most important to remember value and necessity of the combinatorial approach. This is to say that the use and incorporation of computational algorithms into the research and development process is most powerful when it is done in harmony with conventional and thus can complement the accuracy and speed of the research rather than leading to discrepancies between experiential observations and virtually predicted, overly abstracted results. This can be seen in the already mentioned use of virtual modelling to determine template-FM stoichiometry rather than the most labour intensive experimental method of Job plot analysis. Alternatively, the screening of virtual libraries of FM molecules against a candidate template molecule can also greatly reduce the need to experimentally test these combinations on well plates or automated MIP fabrication devices [253]. Computational energy minimisations can also be used to determine complex molecular structures and intermolecular bond location and directionality which may differ significantly between structural analogues to the structure activity relationship (SAR) paradox [254]. This change in location can be

the cause of some significant headaches when designing a polymer imprinted with a dummy template (see section 1.5.2).

The ability to predict the location of such bond locations has also allowed for the combination of multiple FM in one single MIP receptor. Accurate prediction of the location of various template-FM bonding site permits the inclusion of two or more FM molecules each of which target separate features in the template's structure. The presence of multiple functionalities within a receptor introduces the possibility for chiral separations of analogues [255–257]. More impressively still, mimicking of multivalent biological receptors also becomes possible by analysing the interacting amino acids and relevant structures of natural receptors, determined most often through x-ray crystallographic analysis, and then matching it to a FM with the appropriate functionality, improved and specialised MIP receptors can be created, a brief summary some examples of this combinatorial and biomimetic approach can be seen in Table 1.11.



Table 1.11: Short summary of biomimetic and multivalent MIP receptors utilising the combinatorial approach

Template	Bioreceptor mimic	Monomer 1	Monomer 2	Reference
Cocaine	Dopamine transporter	acrylamide	Itaconic acid	[252]
Deoxyephedrine	Dopamine transporter	HEMA	Itaconic acid	
Methadone	$\mu$ opioid receptor	HEMA	Itaconic acid	
Morphine	$\mu$ opioid receptor	HEMA	MAA	
Amino acid derivatives	N/A	2VP	MAA	[258]
Amino acid derivatives	N/A	2VP	acrylamide	[259]
Theophylline & Chlorogenic acid	N/A	3-aminopropyltriethoxysilane	MAA	[260]
catechol	Tyrosinase	urocanic acid ethyl ester	CuCl <sub>2</sub>	[137]
Bisphenol A	N/A	2-acrylamido-2-methylpropanesulfonic acid	styrene	[261]
adenosine 5'-monophosphate (AMP)	adenylate kinase	2-(dimethylamino)ethyl methacrylate	acrylamide	[262]

A more recent report published this year has even detailed the application of a neural network to the analysis of a complex virtual system to predict several optimal sensor parameters including pH, absorbent mass and time, eluent volume and extraction time, heralding a greater level of integration of such models into all stages of the MIP design process [263].

## 1.8 References

- [1] E. Fischer, Einfluss der Configuration auf die Wirkung der Enzyme, Berichte Dtsch. Chem. Ges. 27 (1894) 2985–2993. doi:10.1002/cber.18940270364.
- [2] S.F. D'Souza, Microbial biosensors, Biosens. Bioelectron. 16 (2001) 337–353. doi:10.1016/S0956-5663(01)00125-7.
- [3] J.K.H. Liu, The history of monoclonal antibody development – Progress, remaining challenges and future innovations, Ann. Med. Surg. 3 (2014) 113–116. doi:10.1016/j.amsu.2014.09.001.

- 
- [4] B. Wang, M. Barahona, M. Buck, J. Schumacher, Rewiring cell signalling through chimaeric regulatory protein engineering, *Biochem. Soc. Trans.* 41 (2013) 1195–1200. doi:10.1042/BST20130138.
- [5] S. Muyldermans, Nanobodies: Natural Single-Domain Antibodies, *Annu. Rev. Biochem.* 82 (2013) 775–797. doi:10.1146/annurev-biochem-063011-092449.
- [6] K.-M. Song, S. Lee, C. Ban, Aptamers and Their Biological Applications, *Sensors*. 12 (2012) 612–631. doi:10.3390/s120100612.
- [7] A.P.F. Turner, Biosensors: sense and sensibility, *Chem. Soc. Rev.* 42 (2013) 3184. doi:10.1039/c3cs35528d.
- [8] M.J. Whitcombe, MIPdatabase – All database items, 2016 [http://mipdatabase.com/all\\_items.php](http://mipdatabase.com/all_items.php) (accessed June 9, 2016).
- [9] M.V. Polyakov, Adsorption properties and structure of silica gel, *Zhurnal Fizieskoj Khimii Akademiya SSSR*. 2 (1931) 799–805.
- [10] G. Wulff, A. Sarhan, The use of polymers with enzyme-analogous structures for the resolution of racemates, *Angew. Chem. Int. Ed. Engl.* 11 (1972) 341. doi:10.1002/anie.197203341.
- [11] T. Takagishi, I.M. Klotz, Macromolecule-small molecule interactions; introduction of additional binding sites in polyethyleneimine by disulfide cross-linkages, *Biopolymers*. 11 (1972) 483–491. doi:10.1002/bip.1972.360110213.
- [12] C. Alexander, H.S. Andersson, L.I. Andersson, R.J. Ansell, N. Kirsch, I.A. Nicholls, et al., Molecular imprinting science and technology: a survey of the literature for the years up to and including 2003, *J. Mol. Recognit.* 19 (2006) 106–180. doi:10.1002/jmr.760.
- [13] M.J. Whitcombe, N. Kirsch, I.A. Nicholls, Molecular imprinting science and technology: a survey of the literature for the years 2004–2011, *J. Mol. Recognit.* 27 (2014) 297–401. doi:10.1002/jmr.2347.
- [14] G. Wulff, Fourty years of molecular imprinting in synthetic polymers: origin, features and perspectives, *Microchim. Acta*. 180 (2013) 1359–1370. doi:10.1007/s00604-013-0992-9.
- [15] D.A. Spivak, R. Simon, J. Campbell, Evidence for shape selectivity in non-covalently imprinted polymers, *Anal. Chim. Acta*. 504 (2004) 23–30. doi:10.1016/S0003-2670(03)00946-2.
- [16] N.W. Turner, C.I. Holdsworth, S.W. Donne, A. McCluskey, M.C. Bowyer, Microwave induced MIP synthesis: comparative analysis of thermal and microwave induced polymerisation of caffeine imprinted polymers, *New J. Chem.* 34 (2010) 686. doi:10.1039/b9nj00538b.
- [17] A. Ellwanger, L. Karlsson, P.K. Owens, C. Berggren, C. Crecenzi, K. Ensing, et al., Evaluation of methods aimed at complete removal of template from molecularly imprinted polymers, *The Analyst*. 126 (2001) 784–792. doi:10.1039/b009693h.

- [18] C. Baggiani, F. Trotta, G. Giraudi, G. Moraglio, A. Vanni, Chromatographic characterization of a molecularly imprinted polymer binding theophylline in aqueous buffers, *J. Chromatogr. A.* 786 (1997) 23–29. doi:10.1016/S0021-9673(97)00537-2.
- [19] B. Mattiasson, L. Ye, eds., *Molecularly Imprinted Polymers in Biotechnology*, Springer International Publishing, Cham, 2015. <http://link.springer.com/10.1007/978-3-319-20729-2> (accessed January 14, 2016).
- [20] L.I. Andersson, Application of molecular imprinting to the development of aqueous buffer and organic solvent based radioligand binding assays for (s)-propranolol, *Anal. Chem.* 68 (1996) 111–117. doi:10.1021/ac950668+.
- [21] S. Piletsky, S. Pilsetskey, I. Chianella, MIP-based Sensors, in: S. Li, Y. Ge, S.A. Piletsky, J. Lunec (Eds.), *Mol. Imprinted Sens. Overv. Appl.*, 1st ed, Elsevier, Amsterdam ; Boston, 2012: pp. 35–56.
- [22] G. Vasapollo, R.D. Sole, L. Mergola, M.R. Lazzoi, A. Scardino, S. Scorrano, et al., Molecularly Imprinted Polymers: Present and Future Prospective, *Int. J. Mol. Sci.* 12 (2011) 5908–5945. doi:10.3390/ijms12095908.
- [23] I. Mijangos, F. Navarro-Villoslada, A. Guerreiro, E. Piletska, I. Chianella, K. Karim, et al., Influence of initiator and different polymerisation conditions on performance of molecularly imprinted polymers, *Biosens. Bioelectron.* 22 (2006) 381–387. doi:10.1016/j.bios.2006.05.012.
- [24] O.K. Castell, D.A. Barrow, A.R. Kamarudin, C.J. Allender, Current practices for describing the performance of molecularly imprinted polymers can be misleading and may be hampering the development of the field, *J. Mol. Recognit.* 24 (2011) 1115–1122. doi:10.1002/jmr.1161.
- [25] J. Li, G. Wei, Y. Zhang, Molecularly imprinted polymers as recognition elements in sensors, in: S. Li, Y. Ge, S.A. Piletsky, J. Lunec (Eds.), *Mol. Imprinted Sens. Overv. Appl.*, 1st ed, Elsevier, Amsterdam ; Boston, 2012: pp. 35–56.
- [26] A. Poma, A. Guerreiro, M.J. Whitcombe, E.V. Piletska, A.P.F. Turner, S.A. Piletsky, Solid-Phase Synthesis of Molecularly Imprinted Polymer Nanoparticles with a Reusable Template-“Plastic Antibodies,” *Adv. Funct. Mater.* 23 (2013) 2821–2827. doi:10.1002/adfm.201202397.
- [27] G. Wulff, A. Sarhan, K. Zabrocki, Enzyme-analogue built polymers and their use for the resolution of racemates, *Tetrahedron Lett.* 14 (1973) 4329–4332. doi:10.1016/S0040-4039(01)87213-0.
- [28] G. Wulff, J. Vietmeier, Enzyme-analogue built polymers .25. Synthesis of macroporous copolymers from  $\alpha$ -amino-acid based vinyl compounds, *Makromol. Chem.-Macromol. Chem. Phys.* 190 (1989) 1717–1726.
- [29] G. Wulff, J. Vietmeier, Enzyme-analogue built polymers, 26. Enantioselective synthesis of amino acids using polymers possessing chiral cavities obtained by an imprinting procedure with template molecules, *Makromol. Chem.-Macromol. Chem. Phys.* 190 (1989) 1727–17345.

- [30] Y. Tang, J. Lan, X. Gao, X. Liu, D. Zhang, L. Wei, et al., Determination of clenbuterol in pork and potable water samples by molecularly imprinted polymer through the use of covalent imprinting method, *Food Chem.* 190 (2016) 952–959. doi:10.1016/j.foodchem.2015.06.067.
- [31] Y.-W. Tang, G.-Z. Fang, S. Wang, J.-L. Li, Covalent imprinted polymer for selective and rapid enrichment of ractopamine by a noncovalent approach, *Anal. Bioanal. Chem.* 401 (2011) 2275–2282. doi:10.1007/s00216-011-5280-0.
- [32] G. Wulff, A. Biffis, Molecular imprinting with covalent or stoichiometric non-covalent interactions, in: B. Sellergren (Ed.), *Mol. Imprinted Polym. Man-Made Mimics Antibodies Their Appl.* Anal. Chem., 1st ed, Elsevier, Amsterdam ; New York, 2001: pp. 71–112.
- [33] T. Kobayashi, S.S. Leong, Q. Zhang, Using polystyrene-co-maleic acid for molecularly imprinted membranes prepared in supercritical carbon dioxide, *J. Appl. Polym. Sci.* 108 (2008) 757–768. doi:10.1002/app.27734.
- [34] T. Ikegami, T. Mukawa, H. Nariai, T. Takeuchi, Bisphenol A-recognition polymers prepared by covalent molecular imprinting, *Anal. Chim. Acta.* 504 (2004) 131–135. doi:10.1016/j.aca.2003.08.032.
- [35] M. Soares da Silva, R. Viveiros, A. Aguiar-Ricardo, V.D.B. Bonifácio, T. Casimiro, Supercritical fluid technology as a new strategy for the development of semi-covalent molecularly imprinted materials, *RSC Adv.* 2 (2012) 5075. doi:10.1039/c2ra20426f.
- [36] N. Henry, R. Delépée, J.-M. Seigneuret, L.A. Agrofoglio, Synthesis of water-compatible imprinted polymers of in situ produced fructosazine and 2,5-deoxyfructosazine, *Talanta.* 99 (2012) 816–823. doi:10.1016/j.talanta.2012.07.035.
- [37] T. Takeuchi, N. Murase, H. Maki, T. Mukawa, H. Shinmori, Dopamine selective molecularly imprinted polymers via post-imprinting modification, *Org. Biomol. Chem.* 4 (2006) 565. doi:10.1039/b514432a.
- [38] Y. Yoshimi, A. Narimatsu, K. Nakayama, S. Sekine, K. Hattori, K. Sakai, Development of an enzyme-free glucose sensor using the gate effect of a molecularly imprinted polymer, *J. Artif. Organs.* 12 (2009) 264–270. doi:10.1007/s10047-009-0473-4.
- [39] H.A. Zayas, A. McCluskey, M.C. Bowyer, C.I. Holdsworth, Potentiometric determination of acid dissociation constants of novel biaryl monomers, *Anal Methods.* 7 (2015) 8206–8211. doi:10.1039/C5AY01673H.
- [40] S. Hong, L.Y.S. Lee, M.-H. So, K.-Y. Wong, A Dopamine Electrochemical Sensor Based on Molecularly Imprinted Poly(acrylamidophenylboronic acid) Film, *Electroanalysis.* 25 (2013) 1085–1094. doi:10.1002/elan.201200631.
- [41] Z. Lin, L. Sun, W. Liu, Z. Xia, H. Yang, G. Chen, Synthesis of boronic acid-functionalized molecularly imprinted silica nanoparticles for glycoprotein recognition and enrichment, *J Mater Chem B.* 2 (2014) 637–643. doi:10.1039/C3TB21520B.
- [42] H.V.R. Burri, D. Yu, An Assay Study of Molecular Recognition of Amino Acids in Water: Covalent Imprinting of Cysteine, *J. Biomed. Sci. Eng.* 8 (2015) 805–814. doi:10.4236/jbise.2015.812077.

- [43] G. Wulff, B. Heide, G. Helfmeier, Enzyme-analog built polymers. 20. Molecular recognition through the exact placement of functional groups on rigid matrixes via a template approach, *J. Am. Chem. Soc.* 108 (1986) 1089–1091. doi:10.1021/ja00265a045.
- [44] G. Wulff, B. Heide, G. Helfmeier, Enzyme-analogue built polymers, 24 On the distance accuracy of functional groups in polymers and silicas introduced by a template approach, *React. Polym. Ion Exch. Sorbents.* 6 (1987) 299–310. doi:10.1016/0167-6989(87)90101-2.
- [45] G. Wulff, Selective binding to polymers via covalent bonds. The construction of chiral cavities as specific receptor sites, *Pure Appl. Chem.* 54 (1982). doi:10.1351/pac198254112093.
- [46] G. Wulff, W. Best, A. Akelah, Enzyme-analogue built polymers, 17 Investigations on the racemic resolution of amino acids, *React. Polym. Ion Exch. Sorbents.* 2 (1984) 167–174. doi:10.1016/0167-6989(84)90132-6.
- [47] K.J. Shea, T.K. Dougherty, Molecular recognition on synthetic amorphous surfaces. The influence of functional group positioning on the effectiveness of molecular recognition, *J. Am. Chem. Soc.* 108 (1986) 1091–1093. doi:10.1021/ja00265a046.
- [48] K.J. Shea, D.Y. Sasaki, On the control of microenvironment shape of functionalized network polymers prepared by template polymerization, *J. Am. Chem. Soc.* 111 (1989) 3442–3444. doi:10.1021/ja00191a059.
- [49] K.J. Shea, D.Y. Sasaki, An analysis of small-molecule binding to functionalized synthetic polymers by <sup>13</sup>C CP/MAS NMR and FT-IR spectroscopy, *J. Am. Chem. Soc.* 113 (1991) 4109–4120. doi:10.1021/ja00011a009.
- [50] K.J. Shea, D.Y. Sasaki, G.J. Stoddard, Fluorescence probes for evaluating chain solvation in network polymers. An analysis of the solvatochromic shift of the dansyl probe in macroporous styrene-divinylbenzene and styrene-diisopropenylbenzene copolymers, *Macromolecules.* 22 (1989) 1722–1730. doi:10.1021/ma00194a037.
- [51] J. Damen, D.C. Neckers, Stereoselective syntheses via a photochemical template effect, *J. Am. Chem. Soc.* 102 (1980) 3265–3267. doi:10.1021/ja00529a073.
- [52] K.J. Shea, E. Thompson, Template synthesis of macromolecules. Selective functionalization of an organic polymer, *J. Org. Chem.* 43 (1978) 4253–4255. doi:10.1021/jo00415a064.
- [53] K.J. Shea, E.A. Thompson, S.D. Pandey, P.S. Beauchamp, Template synthesis of macromolecules. Synthesis and chemistry of functionalized macroporous poly(divinylbenzene), *J. Am. Chem. Soc.* 102 (1980) 3149–3155. doi:10.1021/ja00529a044.
- [54] G. Wulff, I. Schulze, Directed Cooperativity and Site Separation of Mercapto Groups in Synthetic Polymers, *Angew. Chem. Int. Ed. Engl.* 17 (1978) 537–538. doi:10.1002/anie.197805371.
- [55] G. Wulff, I. Schulze, Enzyme-analogue built polymers. IX. Polymers with mercapto groups of definite cooperativity, *Isr. J. Chem.* 17 (1978) 291–297.
- [56] N. Kirsch, M.J. Whitcombe, The Semi-Covalent Approach, in: M. Yan, O. Ramström (Eds.), *Mol. Imprinted Mater. Sci. Technol.*, Marcel Dekker, New York, 2005: pp. 93–122.

- [57] M.J. Whitcombe, M.E. Rodriguez, P. Villar, E.N. Vulfson, A New Method for the Introduction of Recognition Site Functionality into Polymers Prepared by Molecular Imprinting: Synthesis and Characterization of Polymeric Receptors for Cholesterol, *J. Am. Chem. Soc.* 117 (1995) 7105–7111. doi:10.1021/ja00132a010.
- [58] S.N.N.S. Hashim, R.I. Boysen, L.J. Schwarz, B. Danylec, M.T.W. Hearn, A comparison of covalent and non-covalent imprinting strategies for the synthesis of stigmasterol imprinted polymers, *J. Chromatogr. A.* 1359 (2014) 35–43. doi:10.1016/j.chroma.2014.07.034.
- [59] J.U. Klein, M.J. Whitcombe, F. Mulholland, E.N. Vulfson, Template-Mediated Synthesis of a Polymeric Receptor Specific to Amino Acid Sequences, *Angew. Chem. Int. Ed.* 38 (1999) 2057–2060. doi:10.1002/(SICI)1521-3773(19990712)38:13/14<2057::AID-ANIE2057>3.0.CO;2-G.
- [60] A. Beltran, R.M. Marcé, P.A.G. Cormack, F. Borrull, Synthetic approaches to parabens molecularly imprinted polymers and their applications to the solid-phase extraction of river water samples, *Anal. Chim. Acta.* 677 (2010) 72–78. doi:10.1016/j.aca.2010.07.021.
- [61] X. Li, Y. Tong, L. Jia, H. Guan, Fabrication of molecularly cholesterol-imprinted polymer particles based on chitin and their adsorption ability, *Monatshefte Für Chem. - Chem. Mon.* 146 (2015) 423–430. doi:10.1007/s00706-014-1369-4.
- [62] P. Qi, J. Wang, L. Wang, Y. Li, J. Jin, F. Su, et al., Molecularly imprinted polymers synthesized via semi-covalent imprinting with sacrificial spacer for imprinting phenols, *Polymer.* 51 (2010) 5417–5423. doi:10.1016/j.polymer.2010.09.037.
- [63] Y. Tong, H. Guan, S. Wang, J. Xu, C. He, Syntheses of chitin-based imprinting polymers and their binding properties for cholesterol, *Carbohydr. Res.* 346 (2011) 495–500. doi:10.1016/j.carres.2010.12.013.
- [64] A.L. Graham, C.A. Carlson, P.L. Edmiston, Development and Characterization of Molecularly Imprinted Sol–Gel Materials for the Selective Detection of DDT, *Anal. Chem.* 74 (2002) 458–467. doi:10.1021/ac0106142.
- [65] A. Katz, M.E. Davis, Molecular imprinting of bulk, microporous silica, *Nature.* 403 (1999) 286–289.
- [66] M.A. Khasawneh, P.T. Vallano, V.T. Remcho, Affinity screening by packed capillary high performance liquid chromatography using molecular imprinted sorbents, *J. Chromatogr. A.* 922 (2001) 87–97. doi:10.1016/S0021-9673(01)00932-3.
- [67] M. Lübke, M.J. Whitcombe, E.N. Vulfson, A Novel Approach to the Molecular Imprinting of Polychlorinated Aromatic Compounds, *J. Am. Chem. Soc.* 120 (1998) 13342–13348. doi:10.1021/ja9818295.
- [68] N. Kirsch, C. Alexander, M. Lübke, M. Whitcombe, E. Vulfson, Enhancement of selectivity of imprinted polymers via post-imprinting modification of recognition sites, *Polymer.* 41 (2000) 5583–5590. doi:10.1016/S0032-3861(99)00782-X.
- [69] N. Kirsch, C. Alexander, S. Davies, M. Whitcombe, Sacrificial spacer and non-covalent routes toward the molecular imprinting of “poorly-functionalized” N-heterocycles, *Anal. Chim. Acta.* 504 (2004) 63–71. doi:10.1016/S0003-2670(03)00510-5.

- [70] L.I. Andersson, K. Mosbach, Enantiomeric resolution on molecularly imprinted polymers prepared with only non-covalent and non-ionic interactions, *J. Chromatogr.* 516 (1990) 313–322.
- [71] R. Arshady, K. Mosbach, Synthesis of substrate-selective polymers by host-guest polymerization, *Makromol. Chem.* 182 (1981) 687–692.
- [72] O. Norrlöw, M. Glad, K. Mosbach, Acrylic polymer preparations containing recognition sites obtained by imprinting with substrates, *J. Chromatogr. A.* 299 (1984) 29–41. doi:10.1016/S0021-9673(01)97819-7.
- [73] C. Branger, W. Meouche, A. Margaillan, Recent advances on ion-imprinted polymers, *React. Funct. Polym.* 73 (2013) 859–875. doi:10.1016/j.reactfunctpolym.2013.03.021.
- [74] C.E. Carraher, R.B. Seymour, Naturally Occurring Polymers - Animals, in: Carraher's Polym. Chem., 8th ed, CRC Press, Boca Raton, FL, 2011: pp. 321–380.
- [75] S. Ahuja, H. Rasmussen, Molecularly Imprinted Polymers as Sorbents for Separations and Extractions, in: *HPLC Method Dev. Pharm.*, Elsevier, Academic Press, Amsterdam; Boston, 2007: pp. 479–504. [http://www.123library.org/book\\_details/?id=35052](http://www.123library.org/book_details/?id=35052) (accessed March 8, 2016).
- [76] S. Emara, Simultaneous determination of caffeine, theophylline and theobromine in human plasma by on-line solid-phase extraction coupled to reversed-phase chromatography, *Biomed. Chromatogr.* 18 (2004) 479–485. doi:10.1002/bmc.341.
- [77] P.T. Vallano, V.T. Remcho, Highly selective separations by capillary electrochromatography: molecular imprint polymer sorbents, *J. Chromatogr. A.* 887 (2000) 125–135. doi:10.1016/S0021-9673(99)01199-1.
- [78] J. Matsui, T. Takeuchi, Techniques for the in situ preparation of imprinted polymers, in: B. Sellergren (Ed.), *Mol. Imprinted Polym. Man-Made Mimics Antibodies Their Appl. Anal. Chem.*, Elsevier, Amsterdam; New York, 2001: pp. 325–340. <http://public.eblib.com/choice/publicfullrecord.aspx?p=313711> (accessed March 8, 2016).
- [79] B. Sellergren, K.J. Shea, Origin of peak asymmetry and the effect of temperature on solute retention in enantiomer separations on imprinted chiral stationary phases, *J. Chromatogr. A.* 690 (1995) 29–39. doi:10.1016/0021-9673(94)00905-O.
- [80] O. Brüggemann, K. Haupt, L. Ye, E. Yilmaz, K. Mosbach, New configurations and applications of molecularly imprinted polymers, *J. Chromatogr. A.* 889 (2000) 15–24. doi:10.1016/S0021-9673(00)00350-2.
- [81] V.B. Kandimalla, H. Ju, Molecular imprinting: a dynamic technique for diverse applications in analytical chemistry, *Anal. Bioanal. Chem.* 380 (2004) 587–605. doi:10.1007/s00216-004-2793-9.
- [82] S.. Piletsky, T.. Panasyuk, E.. Piletskaya, I.. Nicholls, M. Ulbricht, Receptor and transport properties of imprinted polymer membranes – a review, *J. Membr. Sci.* 157 (1999) 263–278. doi:10.1016/S0376-7388(99)00007-1.

- [83] Y. Yoshimi, R. Ohdaira, C. Iiyama, K. Sakai, "Gate effect" of thin layer of molecularly-imprinted poly(methacrylic acid-co-ethyleneglycol dimethacrylate), *Sens. Actuators B Chem.* 73 (2001) 49–53. doi:10.1016/S0925-4005(00)00671-7.
- [84] C. Baggiani, L. Anfossi, C. Giovannoli, Solid phase extraction of food contaminants using molecular imprinted polymers, *Anal. Chim. Acta.* 591 (2007) 29–39. doi:10.1016/j.aca.2007.01.056.
- [85] M. Azenha, B. Szefczyk, D. Loureiro, P. Kathirvel, M.N. D. S. Cordeiro, A. Fernando-Silva, Computational and Experimental Study of the Effect of PEG in the Preparation of Damascenone-Imprinted Xerogels, *Langmuir.* 29 (2013) 2024–2032. doi:10.1021/la304706t.
- [86] Z. Xu, X. Huang, L. Wan, Molecularly imprinted membranes, in: *Surf. Eng. Polym. Membr., Zhejiang University Press ; Springer, Hangzhou : Berlin ; New York, 2009: pp. 225–262.*
- [87] M.C. Cela-Pérez, M.M. Castro-López, A. Lasagabáster-Latorre, J.M. López-Vilariño, M.V. González-Rodríguez, L.F. Barral-Losada, Synthesis and characterization of bisphenol-A imprinted polymer as a selective recognition receptor, *Anal. Chim. Acta.* 706 (2011) 275–284. doi:10.1016/j.aca.2011.09.002.
- [88] M.C. Cela-Pérez, F. Bates, C. Jiménez-Morigosa, E. Lendoiro, A. de Castro, A. Cruz, et al., Water-compatible imprinted pills for sensitive determination of cannabinoids in urine and oral fluid, *J. Chromatogr. A.* 1429 (2016) 53–64. doi:10.1016/j.chroma.2015.12.011.
- [89] E. Lendoiro, A. de Castro, H. Fernández-Vega, M.C. Cela-Pérez, J.M. López-Vilariño, M.V. González-Rodríguez, et al., Molecularly imprinted polymer for selective determination of  $\Delta^9$ -tetrahydrocannabinol and 11-nor- $\Delta^9$ -tetrahydrocannabinol carboxylic acid using LC-MS/MS in urine and oral fluid, *Anal. Bioanal. Chem.* (2014). doi:10.1007/s00216-013-7599-1.
- [90] M.S. Dopico-García, C. Cela-Pérez, J.M. López-Vilariño, M.V. González-Rodríguez, L.F. Barral-Losada, An approach to imprint irganox 1076: Potential application to the specific migration test in olive oil, *J. Appl. Polym. Sci.* 119 (2011) 2866–2874. doi:10.1002/app.32964.
- [91] D.C. Sherrington, Preparation, structure and morphology of polymer supports, *Chem. Commun.* (1998) 2275–2286. doi:10.1039/a803757d.
- [92] M.H. Mohamed, L.D. Wilson, Porous Copolymer Resins: Tuning Pore Structure and Surface Area with Non Reactive Porogens, *Nanomaterials.* 2 (2012) 163–186. doi:10.3390/nano2020163.
- [93] I.M. Abrams, J.R. Millar, A history of the origin and development of macroporous ion-exchange resins, *React. Funct. Polym.* 35 (1997) 7–22. doi:10.1016/S1381-5148(97)00058-8.
- [94] L. Ye, New Frontiers in Molecular Imprinting: From Micro- to Nanofabrication, in: L. Ye (Ed.), *Mol. Imprinting Princ. Appl. Micro- Nanostructured Polym.*, Pan Stanford Publications, Singapore, 2013: pp. 1–24.
- [95] J. Wang, P.A.G. Cormack, D.C. Sherrington, E. Khoshdel, Monodisperse, molecularly imprinted polymer microspheres prepared by precipitation polymerization for affinity



- separation applications, *Angew. Chem. Int. Ed Engl.* 42 (2003) 5336–5338. doi:10.1002/anie.200352298.
- [96] F. Bates, M. del Valle, Voltammetric sensor for theophylline using sol–gel immobilized molecularly imprinted polymer particles, *Microchim. Acta.* 182 (2015) 933–942. doi:10.1007/s00604-014-1413-4.
- [97] O.K. Castell, C.J. Allender, D.A. Barrow, Novel biphasic separations utilising highly selective molecularly imprinted polymers as biorecognition solvent extraction agents, *Biosens. Bioelectron.* 22 (2006) 526–533. doi:10.1016/j.bios.2006.07.017.
- [98] A.G. Mayes, K. Mosbach, Molecularly Imprinted Polymer Beads: Suspension Polymerization Using a Liquid Perfluorocarbon as the Dispersing Phase, *Anal. Chem.* 68 (1996) 3769–3774. doi:10.1021/ac960363a.
- [99] N. Pérez-Moral, A.G. Mayes, MIP Formats for Analytical Applications, in: S. Piletsky, A.P.F. Turner (Eds.), *Mol. Imprinting Polym.*, Landes Bioscience, Georgetown, Tex, 2006: pp. 1–11.
- [100] J.-P. Lai, X.-Y. Lu, C.-Y. Lu, H.-F. Ju, X.-W. He, Preparation and evaluation of molecularly imprinted polymeric microspheres by aqueous suspension polymerization for use as a high-performance liquid chromatography stationary phase, *Anal. Chim. Acta.* 442 (2001) 105–111. doi:10.1016/S0003-2670(01)01115-1.
- [101] Z. Tan, J. Ma, H. Chen, N. Ji, G. Zong, Synthesis of monodisperse crosslinked poly(styrene-co-divinylbenzene) microspheres by precipitation polymerization in acetic acid, *J. Appl. Polym. Sci.* 124 (2012) 3799–3806. doi:10.1002/app.35397.
- [102] Q. Yan, Y. Bai, Z. Meng, W. Yang, Precipitation Polymerization in Acetic Acid: Synthesis of Monodisperse Cross-Linked Poly(divinylbenzene) Microspheres, *J. Phys. Chem. B.* 112 (2008) 6914–6922. doi:10.1021/jp711324a.
- [103] F. Barahona, E. Turiel, P.A.G. Cormack, A. Martín-Esteban, Chromatographic performance of molecularly imprinted polymers: Core-shell microspheres by precipitation polymerization and grafted MIP films via iniferter-modified silica beads, *J. Polym. Sci. Part Polym. Chem.* 48 (2010) 1058–1066. doi:10.1002/pola.23860.
- [104] K. Hosoya, K. Yoshizako, N. Tanaka, K. Kimata, T. Araki, J. Haginaka, Uniform-size Macroporous Polymer-based Stationary Phase for HPLC Prepared through Molecular Imprinting Technique., *Chem. Lett.* (1994) 1437–1438. doi:10.1246/cl.1994.1437.
- [105] D. Liu, Q. Yang, S. Jin, Y. Song, J. Gao, Y. Wang, et al., Core–shell molecularly imprinted polymer nanoparticles with assistant recognition polymer chains for effective recognition and enrichment of natural low-abundance protein, *Acta Biomater.* 10 (2014) 769–775. doi:10.1016/j.actbio.2013.10.007.
- [106] R. Ahmad, N. Griffete, A. Lamouri, N. Felidj, M.M. Chehimi, C. Mangeney, Nanocomposites of Gold Nanoparticles@Molecularly Imprinted Polymers: Chemistry, Processing, and Applications in Sensors, *Chem. Mater.* 27 (2015) 5464–5478. doi:10.1021/acs.chemmater.5b00138.

- [107] B.B. Prasad, R. Madhuri, M.P. Tiwari, P.S. Sharma, Imprinted polymer–carbon consolidated composite fiber sensor for substrate-selective electrochemical sensing of folic acid, *Biosens. Bioelectron.* 25 (2010) 2140–2148. doi:10.1016/j.bios.2010.02.016.
- [108] P.-Y. Chen, P.-C. Nien, C.-W. Hu, K.-C. Ho, Detection of uric acid based on multi-walled carbon nanotubes polymerized with a layer of molecularly imprinted PMAA, *Sens. Actuators B Chem.* 146 (2010) 466–471. doi:10.1016/j.snb.2009.11.035.
- [109] H. Wang, H. Zhao, X. Quan, S. Chen, Electrochemical Determination of Tetracycline Using Molecularly Imprinted Polymer Modified Carbon Nanotube-Gold Nanoparticles Electrode, *Electroanalysis.* 23 (2011) 1863–1869. doi:10.1002/elan.201100049.
- [110] X. Wang, L. Wang, X. He, Y. Zhang, L. Chen, A molecularly imprinted polymer-coated nanocomposite of magnetic nanoparticles for estrone recognition, *Talanta.* 78 (2009) 327–332. doi:10.1016/j.talanta.2008.11.024.
- [111] N. Iqbal, P.A. Lieberzeit, Artificial receptors for mass-sensitive sensors: Targeting analytes from surface, nanoparticles, and bioanalytes by molecular imprinting, in: S. Li, Y. Ge, S. Piletsky, J. Lunec (Eds.), *Mol. Imprinted Sens. Overv. Appl.*, 1st ed, Elsevier, Amsterdam ; Boston, 2012: pp. 195–235.
- [112] E. Kellens, H. Bové, M. Conradi, L. D’Olieslaeger, P. Wagner, K. Landfester, et al., Improved Molecular Imprinting Based on Colloidal Particles Made from Miniemulsion: A Case Study on Testosterone and Its Structural Analogues, *Macromolecules.* (2016). doi:10.1021/acs.macromol.6b00130.
- [113] J. Yang, Y. Li, J. Wang, X. Sun, R. Cao, H. Sun, et al., Molecularly imprinted polymer microspheres prepared by Pickering emulsion polymerization for selective solid-phase extraction of eight bisphenols from human urine samples, *Anal. Chim. Acta.* 872 (2015) 35–45. doi:10.1016/j.aca.2015.02.058.
- [114] M. Gan, J. Pan, Y. Zhang, X. Dai, Y. Yin, Q. Qu, et al., Molecularly imprinted polymers derived from lignin-based Pickering emulsions and their selectively adsorption of lambda-cyhalothrin, *Chem. Eng. J.* 257 (2014) 317–327. doi:10.1016/j.cej.2014.06.110.
- [115] C. Giovannoli, C. Passini, L. Anfossi, F.D. Nardo, G. Spano, V. Maurino, et al., Comparison of binding behavior for molecularly imprinted polymers prepared by hierarchical imprinting or Pickering emulsion polymerization: Other Techniques, *J. Sep. Sci.* 38 (2015) 3661–3668. doi:10.1002/jssc.201500511.
- [116] J. Li, X. Hu, P. Guan, X. Zhang, L. Qian, N. Zhang, et al., Preparation of L-phenylalanine-imprinted solid-phase extraction sorbent by Pickering emulsion polymerization and the selective enrichment of L-phenylalanine from human urine, *J. Sep. Sci.* (2016) n/a-n/a. doi:10.1002/jssc.201600055.
- [117] A.R. Mitchell, Bruce Merrifield and solid-phase peptide synthesis: A historical assessment, *Biopolymers.* 90 (2008) 175–184. doi:10.1002/bip.20925.
- [118] F. Canfarotta, A. Poma, A. Guerreiro, S. Piletsky, Solid-phase synthesis of molecularly imprinted nanoparticles, *Nat. Protoc.* 11 (2016) 443–455. doi:10.1038/nprot.2016.030.

- [119] A. Poma, A. Guerreiro, S. Caygill, E. Moczko, S. Piletsky, Automatic reactor for solid-phase synthesis of molecularly imprinted polymeric nanoparticles (MIP NPs) in water, *RSC Adv.* 4 (2014) 4203–4206. doi:10.1039/C3RA46838K.
- [120] E. Yilmaz, K. Haupt, K. Mosbach, The Use of Immobilized Templates—A New Approach in Molecular Imprinting, *Angew. Chem. Int. Ed.* 39 (2000) 2115–2118. doi:10.1002/1521-3773(20000616)39:12<2115::AID-ANIE2115>3.0.CO;2-V.
- [121] R. Pernites, R. Ponnappati, M.J. Felipe, R. Advincula, Electropolymerization molecularly imprinted polymer (E-MIP) SPR sensing of drug molecules: Pre-polymerization complexed terthiophene and carbazole electroactive monomers, *Biosens. Bioelectron.* 26 (2011) 2766–2771. doi:10.1016/j.bios.2010.10.027.
- [122] P.S. Sharma, A. Pietrzyk-Le, F. D'Souza, W. Kutner, Electrochemically synthesized polymers in molecular imprinting for chemical sensing, *Anal. Bioanal. Chem.* 402 (2012) 3177–3204. doi:10.1007/s00216-011-5696-6.
- [123] A. Pietrzyk, S. Suriyanarayanan, W. Kutner, R. Chitta, F. D'Souza, Selective Histamine Piezoelectric Chemosensor Using a Recognition Film of the Molecularly Imprinted Polymer of Bis(bithiophene) Derivatives, *Anal. Chem.* 81 (2009) 2633–2643. doi:10.1021/ac8025652.
- [124] B.D.B. Tiu, R.B. Pernites, S.B. Tiu, R.C. Advincula, Detection of aspartame via microsphere-patterned and molecularly imprinted polymer arrays, *Colloids Surf. Physicochem. Eng. Asp.* 495 (2016) 149–158. doi:10.1016/j.colsurfa.2016.01.038.
- [125] A. Wojnarowicz, P.S. Sharma, M. Sosnowska, W. Lisowski, T.-P. Huynh, M. Pszona, et al., An electropolymerized molecularly imprinted polymer for selective carnosine sensing with impedimetric capacity, *J Mater Chem B.* 4 (2016) 1156–1165. doi:10.1039/C5TB02260F.
- [126] L. Peng, A. Yarman, K. Jetzschmann, J.-H. Jeoung, D. Schad, H. Dobbek, et al., Molecularly Imprinted Electropolymer for a Hexameric Heme Protein with Direct Electron Transfer and Peroxide Electrocatalysis, *Sensors.* 16 (2016) 272. doi:10.3390/s16030272.
- [127] D. Lakshmi, A. Bossi, M.J. Whitcombe, I. Chianella, S.A. Fowler, S. Subrahmanyam, et al., Electrochemical Sensor for Catechol and Dopamine Based on a Catalytic Molecularly Imprinted Polymer-Conducting Polymer Hybrid Recognition Element, *Anal. Chem.* 81 (2009) 3576–3584. doi:10.1021/ac802536p.
- [128] C.-L. Choong, J.S. Bendall, W.I. Milne, Carbon nanotube array: A new MIP platform, *Biosens. Bioelectron.* 25 (2009) 652–656. doi:10.1016/j.bios.2008.11.025.
- [129] M. Akbulut, D. Lakshmi, M.J. Whitcombe, E.V. Piletska, I. Chianella, O. Güven, et al., Microplates with Adaptive Surfaces, *ACS Comb. Sci.* 13 (2011) 646–652. doi:10.1021/co200073w.
- [130] F. Berti, S. Todros, D. Lakshmi, M.J. Whitcombe, I. Chianella, M. Ferroni, et al., Quasi-monodimensional polyaniline nanostructures for enhanced molecularly imprinted polymer-based sensing, *Biosens. Bioelectron.* 26 (2010) 497–503. doi:10.1016/j.bios.2010.07.063.
- [131] S. Des Azevedo, D. Lakshmi, I. Chianella, M.J. Whitcombe, K. Karim, P.K. Ivanova-Mitseva, et al., Molecularly Imprinted Polymer-Hybrid Electrochemical Sensor for the

Detection of  $\beta$ -Estradiol, *Ind. Eng. Chem. Res.* 52 (2013) 13917–13923.  
doi:10.1021/ie302999j.

- [132] D. Lakshmi, M. Akbulut, P.K. Ivanova-Mitseva, M.J. Whitcombe, E.V. Piletska, K. Karim, et al., Computational Design and Preparation of MIPs for Atrazine Recognition on a Conjugated Polymer-Coated Microtiter Plate, *Ind. Eng. Chem. Res.* 52 (2013) 13910–13916. doi:10.1021/ie302982h.
- [133] T. Kamra, S. Chaudhary, C. Xu, N. Johansson, L. Montelius, J. Schnadt, et al., Covalent immobilization of molecularly imprinted polymer nanoparticles using an epoxy silane, *J. Colloid Interface Sci.* 445 (2015) 277–284. doi:10.1016/j.jcis.2014.12.086.
- [134] L.M. Kindschy, E.C. Alcolija, A molecularly imprinted polymer on indium tin oxide and silicon, *Biosens. Bioelectron.* 20 (2005) 2163–2167. doi:10.1016/j.bios.2004.08.028.
- [135] B. Rückert, A.J. Hall, B. Sellergren, Molecularly imprinted composite materials via iniferter-modified supports, *J. Mater. Chem.* 12 (2002) 2275–2280. doi:10.1039/b203115a.
- [136] S. Sasaki, T. Ooya, Y. Kitayama, T. Takeuchi, Molecularly imprinted protein recognition thin films constructed by controlled/living radical polymerization, *J. Biosci. Bioeng.* 119 (2015) 200–205. doi:10.1016/j.jbiosc.2014.06.019.
- [137] T.A. Sergeyeva, O.A. Slinchenko, L.A. Gorbach, V.F. Matyushov, O.O. Brovko, S.A. Piletsky, et al., Catalytic molecularly imprinted polymer membranes: Development of the biomimetic sensor for phenols detection, *Anal. Chim. Acta.* 659 (2010) 274–279. doi:10.1016/j.aca.2009.11.065.
- [138] T. A. Sergeyeva, L.A. Gorbach, O. A. Slinchenko, L.A. Goncharova, O.V. Piletska, O. O. Brovko, et al., Towards development of colorimetric test-systems for phenols detection based on computationally-designed molecularly imprinted polymer membranes, *Mater. Sci. Eng. C.* 30 (2010) 431–436. doi:10.1016/j.msec.2009.12.012.
- [139] T.A. Sergeyeva, O.O. Brovko, E.V. Piletska, S.A. Piletsky, L.A. Goncharova, L.V. Karabanova, et al., Porous molecularly imprinted polymer membranes and polymeric particles, *Anal. Chim. Acta.* 582 (2007) 311–319. doi:10.1016/j.aca.2006.09.011.
- [140] T.A. Sergeyeva, O.V. Piletska, S.A. Piletsky, L.M. Sergeeva, O.O. Brovko, G.V. El'ska, Data on the structure and recognition properties of the template-selective binding sites in semi-IPN-based molecularly imprinted polymer membranes, *Mater. Sci. Eng. C.* 28 (2008) 1472–1479. doi:10.1016/j.msec.2008.04.006.
- [141] N. Wu, L. Feng, Y. Tan, J. Hu, An optical reflected device using a molecularly imprinted polymer film sensor, *Anal. Chim. Acta.* 653 (2009) 103–108. doi:10.1016/j.aca.2009.08.043.
- [142] S. Kröger, A.P.F. Turner, K. Mosbach, K. Haupt, Imprinted Polymer-Based Sensor System for Herbicides Using Differential-Pulse Voltammetry on Screen-Printed Electrodes, *Anal. Chem.* 71 (1999) 3698–3702. doi:10.1021/ac9811827.
- [143] A.K. Patel, P.S. Sharma, B.B. Prasad, Electrochemical sensor for uric acid based on a molecularly imprinted polymer brush grafted to tetraethoxysilane derived sol-gel thin film graphite electrode, *Mater. Sci. Eng. C.* 29 (2009) 1545–1553. doi:10.1016/j.msec.2008.12.008.

- [144] A.K. Patel, P.S. Sharma, B.B. Prasad, Voltammetric sensor for barbituric acid based on a sol–gel derivated molecularly imprinted polymer brush grafted to graphite electrode, *Int. J. Pharm.* 371 (2009) 47–55. doi:10.1016/j.ijpharm.2008.12.016.
- [145] A.K. Patel, P.S. Sharma, B.B. Prasad, Trace-level sensing of creatine in real sample using a zwitterionic molecularly imprinted polymer brush grafted to sol–gel modified graphite electrode, *Thin Solid Films*. 518 (2010) 2847–2853. doi:10.1016/j.tsf.2009.09.009.
- [146] C.J. Brinker, Hydrolysis and condensation of silicates: Effects on structure, *J. Non-Cryst. Solids*. 100 (1988) 31–50. doi:10.1016/0022-3093(88)90005-1.
- [147] D.Y. Sasaki, Molecular imprinting approaches using inorganic matrices, in: B. Sellergren (Ed.), *Mol. Imprinted Polym. Man-Made Mimics Antibodies Their Appl. Anal. Chem.*, Elsevier, Amsterdam; New York, 2001: pp. 213–244.  
<http://public.eblib.com/choice/publicfullrecord.aspx?p=313711> (accessed March 23, 2016).
- [148] K. Tsukagoshi, M. Murata, M. Maeda, Imprinting polymerisation for recognition and separation of metal ions, in: B. Sellergren (Ed.), *Mol. Imprinted Polym. Man-Made Mimics Antibodies Their Appl. Anal. Chem.*, Elsevier, Amsterdam; New York, 2001: pp. 245–270.  
<http://public.eblib.com/choice/publicfullrecord.aspx?p=313711> (accessed March 23, 2016).
- [149] O.Y.F. Henry, S.A. Piletsky, D.C. Cullen, Fabrication of molecularly imprinted polymer microarray on a chip by mid-infrared laser pulse initiated polymerisation, *Biosens. Bioelectron.* 23 (2008) 1769–1775. doi:10.1016/j.bios.2008.02.010.
- [150] S.S. Milojković, D. Kostoski, J.J. Čomor, J.M. Nedeljković, Radiation induced synthesis of molecularly imprinted polymers, *Polymer*. 38 (1997) 2853–2855. doi:10.1016/S0032-3861(97)85624-8.
- [151] J. Czulak, A. Jakubiak-Marcinkowska, A. Trochimczuk, Polymer Catalysts Imprinted with Metal Ions as Biomimics of Metalloenzymes, *Adv. Mater. Sci. Eng.* 2013 (2013) 1–9. doi:10.1155/2013/464265.
- [152] L.M. Pedroso, M.M.C.A. Castro, P. Simões, A. Portugal, Melamine/epichlorohydrin prepolymers: syntheses and characterization, *Polymer*. 46 (2005) 1766–1774. doi:10.1016/j.polymer.2004.12.046.
- [153] P.D. Brown, S.K. Gill, L.J. Hope-Weeks, Influence of solvent on porosity and microstructure of an yttrium based aerogel, *J. Mater. Chem.* 21 (2011) 4204. doi:10.1039/c0jm03178j.
- [154] A. van Herk, Introduction to Radical (co)Polymerisation, in: A. van Herk (Ed.), *Chem. Technol. Emuls. Polym.*, Blackwell Pub., Oxford; Ames, Iowa, 2005: pp. 25–45.  
<http://public.eblib.com/choice/publicfullrecord.aspx?p=284287> (accessed March 30, 2016).
- [155] A. Bossi, M.J. Whitcombe, Y. Uludag, S. Fowler, I. Chianella, S. Subrahmanyam, et al., Synthesis of controlled polymeric cross-linked coatings via iniferter polymerisation in the presence of tetraethyl thiuram disulphide chain terminator, *Biosens. Bioelectron.* 25 (2010) 2149–2155. doi:10.1016/j.bios.2010.02.015.
- [156] P.K. Ivanova-Mitseva, V. Fragkou, D. Lakshmi, M.J. Whitcombe, F. Davis, A. Guerreiro, et al., Conjugated Polymers with Pendant Iniferter Units: Versatile Materials for Grafting, *Macromolecules*. 44 (2011) 1856–1865. doi:10.1021/ma102692h.

- [157] M. Wulkow, The simulation of molecular weight distributions in polyreaction kinetics by discrete Galerkin methods, *Macromol. Theory Simul.* 5 (1996) 393–416. doi:10.1002/mats.1996.040050303.
- [158] R. Koeber, C. Fleischer, F. Lanza, K.-S. Boos, B. Sellergren, D. Barceló, Evaluation of a Multidimensional Solid-Phase Extraction Platform for Highly Selective On-Line Cleanup and High-Throughput LC–MS Analysis of Triazines in River Water Samples Using Molecularly Imprinted Polymers, *Anal. Chem.* 73 (2001) 2437–2444. doi:10.1021/ac001483s.
- [159] Y. Suzuki, T. Curstedt, G. Grossmann, T. Kobayashi, R. Nilsson, K. Nohara, et al., The role of the low-molecular weight (less than or equal to 15,000 daltons) apoproteins of pulmonary surfactant, *Eur. J. Respir. Dis.* 69 (1986) 336–345.
- [160] T. Alizadeh, M.R. Ganjali, M. Zare, P. Norouzi, Development of a voltammetric sensor based on a molecularly imprinted polymer (MIP) for caffeine measurement, *Electrochimica Acta.* 55 (2010) 1568–1574. doi:10.1016/j.electacta.2009.09.086.
- [161] M.T. Gokmen, F.E. Du Prez, Porous polymer particles—A comprehensive guide to synthesis, characterization, functionalization and applications, *Prog. Polym. Sci.* 37 (2012) 365–405. doi:10.1016/j.progpolymsci.2011.07.006.
- [162] D. Spivak, Optimization, evaluation, and characterization of molecularly imprinted polymers, *Adv. Drug Deliv. Rev.* 57 (2005) 1779–1794. doi:10.1016/j.addr.2005.07.012.
- [163] R.S. Frank, J.S. Downey, K. Yu, H.D.H. Stöver, Poly(divinylbenzene- *alt* -maleic anhydride) Microgels: Intermediates to Microspheres and Macroscopic Cross-Linking Copolymerization, *Macromolecules.* 35 (2002) 2728–2735. doi:10.1021/ma001927m.
- [164] E.V. Piletska, N.W. Turner, A.P.F. Turner, S.A. Piletsky, Controlled release of the herbicide simazine from computationally designed molecularly imprinted polymers, *J. Controlled Release.* 108 (2005) 132–139. doi:10.1016/j.jconrel.2005.07.016.
- [165] G. Bunte, J. Hürttlen, H. Pontius, K. Hartlieb, H. Krause, Gas phase detection of explosives such as 2,4,6-trinitrotoluene by molecularly imprinted polymers, *Anal. Chim. Acta.* 591 (2007) 49–56. doi:10.1016/j.aca.2007.02.014.
- [166] C.E. Carraher, R.B. Seymour, Carraher's polymer chemistry, 8th ed, CRC Press, Boca Raton, FL, 2011.
- [167] F. Puoci, F. Iemma, R. Muzzalupo, U.G. Spizzirri, S. Trombino, R. Cassano, et al., Spherical molecularly imprinted polymers (SMIPs) via a novel precipitation polymerization in the controlled delivery of sulfasalazine, *Macromol. Biosci.* 4 (2004) 22–26. doi:10.1002/mabi.200300035.
- [168] R.H. Schmidt, A.-S. Belmont, K. Haupt, Porogen formulations for obtaining molecularly imprinted polymers with optimized binding properties, *Anal. Chim. Acta.* 542 (2005) 118–124. doi:10.1016/j.aca.2005.03.064.
- [169] Á. Valero-Navarro, M. Gómez-Romero, J.F. Fernández-Sánchez, P.A.G. Cormack, A. Segura-Carretero, A. Fernández-Gutiérrez, Synthesis of caffeic acid molecularly imprinted polymer microspheres and high-performance liquid chromatography evaluation of their

- sorption properties, *J. Chromatogr. A.* 1218 (2011) 7289–7296.  
doi:10.1016/j.chroma.2011.08.043.
- [170] M. Belmares, M. Blanco, W.A. Goddard, R.B. Ross, G. Caldwell, S.-H. Chou, et al., Hildebrand and Hansen solubility parameters from Molecular Dynamics with applications to electronic nose polymer sensors, *J. Comput. Chem.* 25 (2004) 1814–1826.  
doi:10.1002/jcc.20098.
- [171] A.F.M. Barton, *CRC handbook of solubility parameters and other cohesion parameters*, 2nd ed, CRC Press, Boca Raton, 1991.
- [172] T. Renkecz, K. Lázló, V. Horvaáth, Molecularly imprinted microspheres prepared by precipitation polymerization at high monomer concentrations, *Mol Impr.* 2 (2014) 1–17.  
doi:10.2478/molim-2014-0001.
- [173] C. Reichardt, T. Welton, *Solvents and solvent effects in organic chemistry*, 4th, updated and ed ed., Wiley-VCH, Weinheim, Germany, 2011.
- [174] B. Sellergren, A.J. Hall, Fundamental aspects on the sythesis and characterisation of imprinted network polymers, in: B. Sellergren (Ed.), *Mol. Imprinted Polym. Man-Made Mimics Antibodies Their Appl. Anal. Chem.*, Elsevier, Amsterdam; New York, 2001: pp. 21–57. <http://public.eblib.com/choice/publicfullrecord.aspx?p=313711> (accessed April 4, 2016).
- [175] Chemical Rubber Company, D.R. Lide, eds., *CRC handbook of chemistry and physics: a ready-reference book of chemical and physical data*, 85. ed, CRC Press, Boca Raton, 2004.
- [176] H. Kim, K. Kaczmarek, G. Guiochon, Mass transfer kinetics on the heterogeneous binding sites of molecularly imprinted polymers, *Chem. Eng. Sci.* 60 (2005) 5425–5444.  
doi:10.1016/j.ces.2005.04.057.
- [177] V.A. Bhanu, K. Kishore, Role of oxygen in polymerization reactions, *Chem. Rev.* 91 (1991) 99–117. doi:10.1021/cr00002a001.
- [178] H. Yan, K.H. Row, Characteristic and Synthetic Approach of Molecularly Imprinted Polymer, *Int. J. Mol. Sci.* 7 (2006) 155–178. doi:10.3390/i7050155.
- [179] K. Ito, A Theory Generalized to Cage Effects in Radical Formation for Determining Initiator Efficiency, *Polym. J.* 17 (1985) 421–426. doi:10.1295/polymj.17.421.
- [180] K.. Berchtold, L.. Lovell, J. Nie, B. Hacıoğlu, C.. Bowman, The significance of chain length dependent termination in cross-linking polymerizations, *Polymer.* 42 (2001) 4925–4929.  
doi:10.1016/S0032-3861(00)00723-0.
- [181] G. Vlatakis, L.I. Andersson, R. Müller, K. Mosbach, Drug assay using antibody mimics made by molecular imprinting, *Nature.* 361 (1993) 645–647. doi:10.1038/361645a0.
- [182] H.-H. Yang, W.-H. Zhou, X.-C. Guo, F.-R. Chen, H.-Q. Zhao, L.-M. Lin, et al., Molecularly imprinted polymer as SPE sorbent for selective extraction of melamine in dairy products, *Talanta.* 80 (2009) 821–825. doi:10.1016/j.talanta.2009.07.067.

- [183] N. Yusof, S. Rahman, M. Hussein, N. Ibrahim, Preparation and Characterization of Molecularly Imprinted Polymer as SPE Sorbent for Melamine Isolation, *Polymers*. 5 (2013) 1215–1228. doi:10.3390/polym5041215.
- [184] W.M. Mullett, E.P. Lai, Determination of theophylline in serum by molecularly imprinted solid-phase extraction with pulsed elution, *Anal. Chem.* 70 (1998) 3636–3641. doi:10.1021/ac980264s.
- [185] M.-M. Zheng, R. Gong, X. Zhao, Y.-Q. Feng, Selective sample pretreatment by molecularly imprinted polymer monolith for the analysis of fluoroquinolones from milk samples, *J. Chromatogr. A*. 1217 (2010) 2075–2081. doi:10.1016/j.chroma.2010.02.011.
- [186] A. Gryshchenko, C. Bottaro, Development of Molecularly Imprinted Polymer in Porous Film Format for Binding of Phenol and Alkylphenols from Water, *Int. J. Mol. Sci.* 15 (2014) 1338–1357. doi:10.3390/ijms15011338.
- [187] L. He, Y. Su, X. Shen, Y. Zheng, H. Guo, Z. Zeng, Solid-phase extraction of melamine from aqueous samples using water-compatible molecularly imprinted polymers, *J. Sep. Sci.* 32 (2009) 3310–3318. doi:10.1002/jssc.200900407.
- [188] H. Yan, X. Cheng, N. Sun, T. Cai, R. Wu, K. Han, Rapid and selective screening of melamine in bovine milk using molecularly imprinted matrix solid-phase dispersion coupled with liquid chromatography-ultraviolet detection, *J. Chromatogr. B*. 908 (2012) 137–142. doi:10.1016/j.jchromb.2012.09.022.
- [189] J. Matsui, K. Fujiwara, T. Takeuchi, Atrazine-Selective Polymers Prepared by Molecular Imprinting of Trialkylmelamines as Dummy Template Species of Atrazine, *Anal. Chem.* 72 (2000) 1810–1813. doi:10.1021/ac9911950.
- [190] M.C. Cela-Pérez, L. Barbosa-Pereira, X. Vecino, M. Pérez-Ameneiro, A.L. Latorre, J.M. López-Vilariño, et al., Selective removal of ATP degradation products from food matrices II: Rapid screening of hypoxanthine and inosine by molecularly imprinted matrix solid-phase dispersion for evaluation of fish freshness, *Talanta*. 135 (2015) 58–66. doi:10.1016/j.talanta.2014.12.037.
- [191] A.L. Latorre, M. Concepción Cela Pérez, S.F. Fernández, J.M. López Vilariño, M.V. González Rodríguez, Selective removal of ATP degradation products from food matrices I: Design and characterization of a dummy molecularly imprinted specific sorbent for hypoxanthine, *React. Funct. Polym.* 91–92 (2015) 51–61. doi:10.1016/j.reactfunctpolym.2015.04.004.
- [192] E. Yilmaz, K. Mosbach, K. Haupt, Influence of functional and cross-linking monomers and the amount of template on the performance of molecularly imprinted polymers in binding assays, *Anal. Commun.* 36 (1999) 167–170. doi:10.1039/a901339c.
- [193] M. Schaeperl, D.W. Lewis, Probing the Structural and Binding Mechanism Heterogeneity of Molecularly Imprinted Polymers, *J. Phys. Chem. B*. 119 (2015) 563–571. doi:10.1021/jp506157x.
- [194] K. Karim, F. Breton, R. Rouillon, E. Piletska, A. Guerreiro, I. Chianella, et al., How to find effective functional monomers for effective molecularly imprinted polymers?, *Adv. Drug Deliv. Rev.* 57 (2005) 1795–1808. doi:10.1016/j.addr.2005.07.013.



- [195] C.E. Carraher, R.B. Seymour, Crosslinking, in: Carraher's Polym. Chem., 8th ed, CRC Press, Boca Raton, FL, 2011: pp. 44–47.
- [196] S.H. Lee, W.G. Lee, B.G. Chung, J.H. Park, A. Khademhosseini, Rapid Formation of Acrylated Microstructures by Microwave-Induced Thermal Crosslinking, *Macromol. Rapid Commun.* 30 (2009) 1382–1386. doi:10.1002/marc.200900199.
- [197] L. Schweitz, L.I. Andersson, S. Nilsson, Capillary Electrochromatography with Predetermined Selectivity Obtained through Molecular Imprinting, *Anal. Chem.* 69 (1997) 1179–1183. doi:10.1021/ac9607929.
- [198] Sigma Aldrich, Free radical initiators - thermal initiators, 2015. [http://www.sigmaaldrich.com/content/dam/sigma-aldrich/docs/Aldrich/General\\_Information/thermal\\_initiators.pdf](http://www.sigmaaldrich.com/content/dam/sigma-aldrich/docs/Aldrich/General_Information/thermal_initiators.pdf) (accessed September 24, 2015).
- [199] F.L. Dickert, O. Hayden, Non-covalent molecularly imprinted sensors for vapours, polyaromatic hydrocarbons and complex mixtures, in: Börje Sellergren (Ed.), *Mol. Imprinted Polym. Man-Made Mimics Antibodies Their Appl. Anal. Chem.*, Elsevier, Amsterdam; New York, 2001: pp. 503–525. <http://public.eblib.com/choice/publicfullrecord.aspx?p=313711> (accessed March 31, 2016).
- [200] S. Li, ed., *Molecularly imprinted sensors: overview and applications*, 1st ed, Elsevier, Amsterdam ; Boston, 2012.
- [201] M.C. Moreno-Bondi, E. Benito-Pena, B. San Vicente, F. Navarro-Villoslada, M.E. de Leon, G. Orellana, et al., Molecularly imprinted polymers as selective recognition elements for optical sensors based on fluorescent measurements, in: *IEEE*, 2003: pp. 975–978. doi:10.1109/SENSOR.2003.1216930.
- [202] S.A. Piletsky, E. Terpetschnig, H.S. Andersson, I.A. Nicholls, O.S. Wolfbeis, Application of non-specific fluorescent dyes for monitoring enantio-selective ligand binding to molecularly imprinted polymers, *Fresenius J. Anal. Chem.* 364 (1999) 512–516. doi:10.1007/s002160051377.
- [203] A. Kugimiya, T. Takeuchi, Surface plasmon resonance sensor using molecularly imprinted polymer for detection of sialic acid, *Biosens. Bioelectron.* 16 (2001) 1059–1062.
- [204] X.-Y. Xu, X.-G. Tian, L.-G. Cai, Z.-L. Xu, H.-T. Lei, H. Wang, et al., Molecularly imprinted polymer based surface plasmon resonance sensors for detection of Sudan dyes, *Anal Methods.* 6 (2014) 3751–3757. doi:10.1039/C3AY42230E.
- [205] Z. Iskierko, M. Sosnowska, P.S. Sharma, T. Benincori, F. D'Souza, I. Kaminska, et al., Extended-gate field-effect transistor (EG-FET) with molecularly imprinted polymer (MIP) film for selective inosine determination, *Biosens. Bioelectron.* 74 (2015) 526–533. doi:10.1016/j.bios.2015.06.073.
- [206] D. Cai, L. Ren, H. Zhao, C. Xu, L. Zhang, Y. Yu, et al., A molecular-imprint nanosensor for ultrasensitive detection of proteins, *Nat. Nanotechnol.* 5 (2010) 597–601. doi:10.1038/nnano.2010.114.

- [207] B. Khadro, C. Sanglar, A. Bonhomme, A. Errachid, N. Jaffrezic-Renault, Molecularly imprinted polymers (MIP) based electrochemical sensor for detection of urea and creatinine, *Procedia Eng.* 5 (2010) 371–374. doi:10.1016/j.proeng.2010.09.125.
- [208] S.A. Piletsky, E.V. Piletskaya, A.V. Elgersma, K. Yano, I. Karube, Y.P. Parhometz, et al., Atrazine sensing by molecularly imprinted membranes, *Biosens. Bioelectron.* 10 (1995) 959–964. doi:10.1016/0956-5663(95)99233-B.
- [209] T. Alizadeh, R.E. Sabzi, H. Alizadeh, Synthesis of nano-sized cyanide ion-imprinted polymer via non-covalent approach and its use for the fabrication of a CN<sup>−</sup>-selective carbon nanotube impregnated carbon paste electrode, *Talanta*. 147 (2016) 90–97. doi:10.1016/j.talanta.2015.09.043.
- [210] J. de R.M. Neto, W. de J.R. Santos, P.R. Lima, S.M.C.N. Tanaka, A.A. Tanaka, L.T. Kubota, A hemin-based molecularly imprinted polymer (MIP) grafted onto a glassy carbon electrode as a selective sensor for 4-aminophenol amperometric, *Sens. Actuators B Chem.* 152 (2011) 220–225. doi:10.1016/j.snb.2010.12.010.
- [211] W.-M. Yeh, K.-C. Ho, Amperometric morphine sensing using a molecularly imprinted polymer-modified electrode, *Anal. Chim. Acta.* 542 (2005) 76–82. doi:10.1016/j.aca.2005.01.071.
- [212] M. Cieplak, K. Szwabinska, K.C. Chandra, P. Borowicz, K.R. Noworyta, F. D'Souza, et al., Selective Electrochemical Sensing of Human Albumin By Semi-Covalent Imprinting, *ECS Meet. Abstr.* MA2015-01 (2015) 2309.
- [213] Y. Li, J. Liu, M. Liu, F. Yu, L. Zhang, H. Tang, et al., Fabrication of ultra-sensitive and selective dopamine electrochemical sensor based on molecularly imprinted polymer modified graphene@carbon nanotube foam, *Electrochem. Commun.* 64 (2016) 42–45. doi:10.1016/j.elecom.2016.01.009.
- [214] F. Lanza, B. Dirion, B. Sellergren, Combinatorial Approaches to Molecular Imprinting, in: M. Yan, O. Ramström (Eds.), *Mol. Imprinted Mater. Sci. Technol.*, Marcel Dekker, New York, 2005: pp. 225–248. <http://www.crcnetbase.com/isbn/9780824753535> (accessed April 5, 2016).
- [215] Y. Hoshino, H. Koide, T. Urakami, H. Kanazawa, T. Kodama, N. Oku, et al., Recognition, Neutralization, and Clearance of Target Peptides in the Bloodstream of Living Mice by Molecularly Imprinted Polymer Nanoparticles: A Plastic Antibody, *J. Am. Chem. Soc.* 132 (2010) 6644–6645. doi:10.1021/ja102148f.
- [216] K.D. Shimizu, C.J. Stephenson, Molecularly imprinted polymer sensor arrays, *Curr. Opin. Chem. Biol.* 14 (2010) 743–750. doi:10.1016/j.cbpa.2010.07.007.
- [217] J.J. Lavigne, E.V. Anslyn, Sensing A Paradigm Shift in the Field of Molecular Recognition: From Selective to Differential Receptors, *Angew. Chem. Int. Ed.* 40 (2001) 3118–3130. doi:10.1002/1521-3773(20010903)40:17<3118::AID-ANIE3118>3.0.CO;2-Y.
- [218] H. Sun, Z.H. Mo, J.T.S. Choy, D.R. Zhu, Y.S. Fung, Piezoelectric quartz crystal sensor for sensing taste-causing compounds in food, *Sens. Actuators B Chem.* 131 (2008) 148–158. doi:10.1016/j.snb.2007.12.014.

- [219] F.L. Dickert, P.A. Lieberzeit, P. Achatz, C. Palfinger, M. Fassnauer, E. Schmid, et al., QCM array for on-line-monitoring of composting procedures, *The Analyst*. 129 (2004) 432. doi:10.1039/b315356h.
- [220] N. Iqbal, G. Mustafa, A. Rehman, A. Biedermann, B. Najafi, P.A. Lieberzeit, et al., QCM-Arrays for Sensing Terpenes in Fresh and Dried Herbs via Bio-Mimetic MIP Layers, *Sensors*. 10 (2010) 6361–6376. doi:10.3390/s100706361.
- [221] P.A. Lieberzeit, A. Rehman, B. Najafi, F.L. Dickert, Real-life application of a QCM-based e-nose: quantitative characterization of different plant-degradation processes, *Anal. Bioanal. Chem.* 391 (2008) 2897–2903. doi:10.1007/s00216-008-2222-6.
- [222] N.T. Greene, K.D. Shimizu, Colorimetric Molecularly Imprinted Polymer Sensor Array using Dye Displacement, *J. Am. Chem. Soc.* 127 (2005) 5695–5700. doi:10.1021/ja0468022.
- [223] N.T. Greene, S.L. Morgan, K.D. Shimizu, Molecularly imprinted polymer sensor arrays, *Chem. Commun.* (2004) 1172. doi:10.1039/b401677g.
- [224] J. Tan, H.-F. Wang, X.-P. Yan, A fluorescent sensor array based on ion imprinted mesoporous silica, *Biosens. Bioelectron.* 24 (2009) 3316–3321. doi:10.1016/j.bios.2009.04.024.
- [225] H.-C. Huang, S.-Y. Huang, C.-I. Lin, Y.-D. Lee, A multi-array sensor via the integration of acrylic molecularly imprinted photoresists and ultramicroelectrodes on a glass chip, *Anal. Chim. Acta.* 582 (2007) 137–146. doi:10.1016/j.aca.2006.09.009.
- [226] F. Breton, R. Rouillon, E.V. Piletska, K. Karim, A. Guerreiro, I. Chianella, et al., Virtual imprinting as a tool to design efficient MIPs for photosynthesis-inhibiting herbicides, *Biosens. Bioelectron.* 22 (2007) 1948–1954. doi:10.1016/j.bios.2006.08.017.
- [227] C. Baggiani, C. Giovannoli, L. Anfossi, C. Passini, P. Baravalle, G. Giraudi, A Connection between the Binding Properties of Imprinted and Nonimprinted Polymers: A Change of Perspective in Molecular Imprinting, *J. Am. Chem. Soc.* 134 (2012) 1513–1518. doi:10.1021/ja205632t.
- [228] I. Tsyrlneva, O. Zaporozhets, E. Piletska, S. Piletsky, Molecular modelling and synthesis of a polymer for the extraction of amiloride and triamterene from human urine, *Anal. Methods*. 6 (2014) 3429. doi:10.1039/c4ay00318g.
- [229] G.A. Jeffrey, *An introduction to hydrogen bonding*, Oxford University Press, New York, 1997.
- [230] K. Farrington, E. Magner, F. Regan, Predicting the performance of molecularly imprinted polymers: Selective extraction of caffeine by molecularly imprinted solid phase extraction, *Anal. Chim. Acta.* 566 (2006) 60–68. doi:10.1016/j.aca.2006.02.057.
- [231] A. Lasagabáster-Latorre, M.C. Cela-Pérez, S. Fernández-Fernández, J.M. López-Vilariño, M.V. González-Rodríguez, M.J. Abad, et al., Insight into BPA–4-vinylpyridine interactions in molecularly imprinted polymers using complementary spectroscopy techniques, *Mater. Chem. Phys.* 141 (2013) 461–476. doi:10.1016/j.matchemphys.2013.05.045.

- [232] S. Subrahmanyam, K. Karim, S.A. Piletsky, Computational Approaches in the Design of Synthetic Receptors, in: S.A. Piletsky, M.J. Whitcombe (Eds.), *Des. Recept. Gener. Biosens.*, Springer Berlin Heidelberg, Berlin, Heidelberg, 2012: pp. 131–165.  
[http://link.springer.com/10.1007/5346\\_2012\\_22](http://link.springer.com/10.1007/5346_2012_22) (accessed June 10, 2015).
- [233] K. Golker, B.C.G. Karlsson, J.G. Wiklander, A.M. Rosengren, I.A. Nicholls, Hydrogen bond diversity in the pre-polymerization stage contributes to morphology and MIP-template recognition – MAA versus MMA, *Eur. Polym. J.* 66 (2015) 558–568.  
doi:10.1016/j.eurpolymj.2015.03.018.
- [234] A. Molinelli, J. O'Mahony, K. Nolan, M.R. Smyth, M. Jakusch, B. Mizaikoff, Analyzing the Mechanisms of Selectivity in Biomimetic Self-Assemblies via IR and NMR Spectroscopy of Prepolymerization Solutions and Molecular Dynamics Simulations, *Anal. Chem.* 77 (2005) 5196–5204. doi:10.1021/ac050525f.
- [235] I.A. Nicholls, S. Chavan, K. Golker, B.C.G. Karlsson, G.D. Olsson, A.M. Rosengren, et al., Theoretical and Computational Strategies for the Study of the Molecular Imprinting Process and Polymer Performance, in: B. Mattiasson, L. Ye (Eds.), *Mol. Imprinted Polym. Biotechnol.*, Springer International Publishing, Cham, 2015: pp. 25–50.  
[http://link.springer.com/10.1007/10\\_2015\\_318](http://link.springer.com/10.1007/10_2015_318) (accessed April 7, 2016).
- [236] M.P. Allen, D.J. Tildesley, *Computer simulation of liquids*, Clarendon Press, Oxford, 2009.
- [237] Z. Chen, R. Chen, B. Shan, *Nanomaterial Design and Computational Modeling*, in: Y. Ge, S. Li, S. Wang, R. Moore (Eds.), *Nanomed.*, Springer New York, New York, NY, 2014: pp. 63–82. [http://link.springer.com/10.1007/978-1-4614-2140-5\\_4](http://link.springer.com/10.1007/978-1-4614-2140-5_4) (accessed April 8, 2016).
- [238] M. Clark, R.D. Cramer, N. Van Opdenbosch, Validation of the general purpose tripos 5.2 force field, *J. Comput. Chem.* 10 (1989) 982–1012. doi:10.1002/jcc.540100804.
- [239] D.A. Case, T.E. Cheatham, T. Darden, H. Gohlke, R. Luo, K.M. Merz, et al., The Amber biomolecular simulation programs, *J. Comput. Chem.* 26 (2005) 1668–1688.  
doi:10.1002/jcc.20290.
- [240] B.R. Brooks, R.E. Bruccoleri, B.D. Olafson, D.J. States, S. Swaminathan, M. Karplus, CHARMM: A program for macromolecular energy, minimization, and dynamics calculations, *J. Comput. Chem.* 4 (1983) 187–217. doi:10.1002/jcc.540040211.
- [241] W.R.P. Scott, P.H. Hünenberger, I.G. Tironi, A.E. Mark, S.R. Billeter, J. Fennen, et al., The GROMOS Biomolecular Simulation Program Package, *J. Phys. Chem. A.* 103 (1999) 3596–3607. doi:10.1021/jp984217f.
- [242] W.L. Jorgensen, D.S. Maxwell, J. Tirado-Rives, Development and Testing of the OPLS All-Atom Force Field on Conformational Energetics and Properties of Organic Liquids, *J. Am. Chem. Soc.* 118 (1996) 11225–11236. doi:10.1021/ja9621760.
- [243] M. Möllhoff, U. Sternberg, Molecular mechanics with fluctuating atomic charges – a new force field with a semi-empirical charge calculation, *Molecular Model. Annu.* 7 (2001) 90–102.
- [244] R.C. Martin, *Smells and Heuristics*, in: *Clean Code Handb. Agile Softw. Craftsmanship*, Prentice Hall, Upper Saddle River, NJ, 2009: pp. 285–315.

- [245] M. Mihailescu, M.K. Gilson, On the theory of noncovalent binding, *Biophys. J.* 87 (2004) 23–36. doi:10.1529/biophysj.103.031682.
- [246] O. Trott, A.J. Olson, AutoDock Vina: Improving the speed and accuracy of docking with a new scoring function, efficient optimization, and multithreading, *J. Comput. Chem.* (2009) NA-NA. doi:10.1002/jcc.21334.
- [247] G.M. Morris, R. Huey, W. Lindstrom, M.F. Sanner, R.K. Belew, D.S. Goodsell, et al., AutoDock4 and AutoDockTools4: Automated docking with selective receptor flexibility, *J. Comput. Chem.* 30 (2009) 2785–2791. doi:10.1002/jcc.21256.
- [248] L.S. Ahlstrom, A. Dickson, C.L. Brooks, Binding and Folding of the Small Bacterial Chaperone HdeA, *J. Phys. Chem. B.* 117 (2013) 13219–13225. doi:10.1021/jp403264s.
- [249] J. Zhang, Y. Hou, Y. Wang, C. Wang, X. Zhang, The LBFGS quasi-Newtonian method for molecular modeling prion AGAAAAGA amyloid fibrils, *Nat. Sci.* 4 (2012) 1097–1108. doi:10.4236/ns.2012.412A138.
- [250] C. Chen, P. Depa, V.G. Sakai, J.K. Maranas, J.W. Lynn, I. Peral, et al., A comparison of united atom, explicit atom, and coarse-grained simulation models for poly(ethylene oxide), *J. Chem. Phys.* 124 (2006) 234901. doi:10.1063/1.2204035.
- [251] M.S. Daw, M.I. Baskes, Embedded-atom method: Derivation and application to impurities, surfaces, and other defects in metals, *Phys. Rev. B.* 29 (1984) 6443–6453. doi:10.1103/PhysRevB.29.6443.
- [252] E.V. Piletska, M. Romero-Guerra, I. Chianella, K. Karim, A.P.F. Turner, S.A. Piletsky, Towards the development of multisensor for drugs of abuse based on molecular imprinted polymers, *Anal. Chim. Acta.* 542 (2005) 111–117. doi:10.1016/j.aca.2005.03.067.
- [253] T. Takeuchi, A. Seko, J. Matsui, T. Mukawa, Molecularly imprinted polymer library on a microtiter plate. high-throughput synthesis and assessment of cinchona alkaloid-imprinted polymers, *Instrum. Sci. Technol.* 29 (2001) 1–9. doi:10.1081/CI-100001402.
- [254] M.P. Hacker, W.S. Messer, K.A. Bachmann, *Pharmacology: principles and practice*, Elsevier/Academic Press, Amsterdam ; Boston, 2009.
- [255] K. Balamurugan, K. Gokulakrishnan, T. Prakasam, Preparation and evaluation of molecularly imprinted polymer liquid chromatography column for the separation of Cathine enantiomers, *Saudi Pharm. J.* 20 (2012) 53–61. doi:10.1016/j.jsps.2011.06.004.
- [256] X. Dong, H. Sun, X. Lü, H. Wang, S. Liu, N. Wang, Separation of ephedrine stereoisomers by molecularly imprinted polymers—influence of synthetic conditions and mobile phase compositions on the chromatographic performance, *The Analyst.* 127 (2002) 1427–1432. doi:10.1039/B202295H.
- [257] S.A. Piletsky, K. Karim, E.V. Piletska, A.P.F. Turner, C.J. Day, K.W. Freebairn, et al., Recognition of ephedrine enantiomers by molecularly imprinted polymers designed using a computational approach, *The Analyst.* 126 (2001) 1826–1830. doi:10.1039/b102426b.

- [258] O. Ramstroem, L.I. Andersson, K. Mosbach, Recognition sites incorporating both pyridinyl and carboxy functionalities prepared by molecular imprinting, *J. Org. Chem.* 58 (1993) 7562–7564. doi:10.1021/jo00078a041.
- [259] Z. Meng, J. Wang, L. Zhou, Q. Wang, D. Zhu, High Performance Cocktail Functional Monomer for Making Molecule Imprinting Polymer., *Anal. Sci.* 15 (1999) 141–144. doi:10.2116/analsci.15.141.
- [260] W. Tang, G. Li, K.H. Row, T. Zhu, Preparation of hybrid molecularly imprinted polymer with double-templates for rapid simultaneous purification of theophylline and chlorogenic acid in green tea, *Talanta*. 152 (2016) 1–8. doi:10.1016/j.talanta.2016.01.046.
- [261] F. Duan, C. Chen, X. Zhao, Y. Yang, X. Liu, Y. Qin, Water-compatible surface molecularly imprinted polymers with synergy of bi-functional monomers for enhanced selective adsorption of bisphenol A from aqueous solution, *Env. Sci Nano.* (2016). doi:10.1039/C5EN00198F.
- [262] F. Breton, R. Delépée, L.A. Agrofoglio, Molecular imprinting of AMP by an ionic-noncovalent dual approach, *J. Sep. Sci.* 32 (2009) 3285–3291. doi:10.1002/jssc.200900226.
- [263] M. Khajeh, S.A. Moghaddam, M. Bohlooli, M. Ghaffari-Moghaddam, Application of the artificial neural network and imperialist competitive algorithm for optimization of molecularly imprinted solid phase extraction of methylene blue, *E-Polym.* 0 (2016). doi:10.1515/epoly-2016-0009



## **Chapter 2 – Objectives**

---





## 2. Objectives

The objectives of this thesis were:

1. To study the core principles of the field of molecular imprinting to devise and design synthetic protocols to be used within the Sensors and Biosensors research group at the Autonomous University of Barcelona on an on-going basis.
2. To investigate appropriate transduction mechanisms for the synthesised imprinted polymers.
3. To devise and test imprinted sensor apparatus for applicability to a sensor array such as would be used in robust Electronic Tongue systems.
4. Provide scope and perspective for the research trajectory toward more efficient and stable polymer sensor arrays to be used for future Electronic Tongue systems.



## **Chapter 3 – Experimental**

---



### 3. Experimental

All materials, methods and protocols listed herein are related to the work reported in the following journal articles:

*Article 1* - **F. Bates** and M. del Valle, *Voltammetric sensor for theophylline using sol–gel immobilized molecularly imprinted polymer particles*, Microchimica Acta. 182 (2015) 933–942.

*Article 2* - **F. Bates**, M. Busato, E. Piletska et al., *Computational design of molecularly imprinted polymer for direct detection of melamine in milk*, Separation Science and Technology [Manuscript submitted]

Article 3 - **F. Bates**, M.C. Cela-Pérez, K. Karim et al., *Virtual Screening of Receptor Sites for Molecularly Imprinted Polymers*, Macromolecular Bioscience (2016). doi:10.1002/mabi.201500461.

### 3.1 Materials

In *article 1*, 50  $\mu\text{m}$  particle size graphite powder (Merck, Darmstadt, Germany) was used in the preparation of the sol–gel membranes and of the epoxy- graphite electrodes. Epotek H77 resin and its corresponding hardener (Epoxy Technology, Billerica, MA, USA) were also used in the electrode fabrication. All reagents used in *article 1* were analytical reagent grade. All solvents were purchased from Scharlab, (Scharlab, Barcelona, Spain). The radical initiator 2,2'-Azobis (2,4-dimethylvaleronitrile) (AIVN) was purchased from Wako Chemicals GmbH (Wako Chemicals GmbH, Neuss, Germany). All other acids pertaining to *article 1* and potassium hydrogen phthalate were purchased from Panreac (Panreac, Barcelona, Spain).

The following chemicals for *articles 1 & 2* were purchased from Sigma-Aldrich (Sigma-Aldrich, St. Louis, MO): 1,7-dimethylxanthine, theophylline, theobromine, caffeine, melamine, acetoguanamine, cyanuric acid, urea, triazine, methacrylic acid (MAA), itaconic acid (IA), divinylbenzene (DVB), ethylene glycol dimethyl acrylate (EGDMA), dimethyl sulfoxide (DMSO), formic acid, tetraethyl orthosilane (TEOS), 1,1' azobis-cyclohexanecarbonitrile (AICN) and 2,2'-azobis 2-methylpropionitrile (AIBN).

All reagents and solvents used in *article 2* were analytical or HPLC grade and were used without any additional purification except for DVB which was technical grade and the referenced real milk samples were purchased at random at local supermarkets in Leicester, UK.

All water used in all referenced articles was triple distilled and deionised by Milli-Q purification systems (Millipore, Billerica, MA, USA).



## 3.2 Instrumentation

### 3.2.1 Laboratory instrumentation

Polymerisations in *Article 1* were done in a water bath controlled with a Huber CC1 thermoregulation pump (Huber Kaeltemaschinenbau GmbH, Offenburg, Germany). Polymerisations in *Article 2* were performed a silicone oil bath on a feedback-controlled hot plate or in a UV reactor using a Hönle 100 UV lamp (intensity 0.157 W/cm<sup>2</sup>) (Hönle UV, UK).

All *Article 1* experiments were conducted using a commercial 52–61 platinum combined Ag/AgCl reference and counter electrode (Crison Instruments, Barcelona Spain). All voltammetric measurements were carried out using a DropSens  $\mu$ Stat8000 multi-potentiostat/galvanostat and processed using Dropview 8400 computer software (Dropsens, Oviedo, Spain). Chronoamperometry measurements were executed using an Autolab PGStat 20 (Metrohm Autolab B.V, Utrecht, The Netherlands).

Analyses detailed in *Article 2* were done using the following instruments. Pore size and surface area analyses were carried out using a NOVA 1000 E Series Gas Sorption Analyser (Quantachrome Instruments, FL, USA) and interpreted using nitrogen BET theory (23) via the NovaWin software package. HPLC columns were packed using a Slurry Packer model 1666 (Alltech, UK). All HPLC experiments were conducted using an Agilent 1100 HPLC and recorded using Chemstation package (Agilent, CA, USA).

All SEM analyses were done using a MERLIN FE-SEM (Zeiss GmbH, Jena, Germany). Confocal microscopy was done with a Leica DCM-3D system (Wetzlar, Germany).

### **3.2.2 Computational instrumentation**

All SYBYL calculations and simulations were done using SYBYL v.7.3 (Tripos Inc. St. Louis, MO, USA) in conjunction with the SPECTRE operating system at the University of Leicester.

All other computational calculations were done on the Linux-based Ubuntu 15.04 (VividVervet) 64 bit OS ([releases.ubuntu.com/15.04/](http://releases.ubuntu.com/15.04/)), installed with default settings on to a Lenovo S540 Think Pad laptop computer with an Intel Core i7-4500U CPU system of 4×1.80 GHz processors @7.5GiB RAM. A modelling environment was constructed exclusively using open source, freely available software packages. Table 3.1 shows a brief summary of the principal items installed.

Table 3.1: Itinerary of the main open source software programs installed on the Lenovo S540 Think Pad laptop computer

Software name	Description	Reference
Marvin Sketch	Platform for 2D chemical sketching and visualisation	[1]
Openbabel	Open Babel is a chemical toolbox designed to speak the many languages of chemical data. It's an open, collaborative project allowing anyone to search, convert, analyse, or store data from molecular modelling, chemistry, solid-state materials, biochemistry, or related areas.	[2]
Acypype	Acypype (AnteChamber PYthon Parser interfacE) is a wrapper script around the ANTECHAMBER software that simplifies the generation of small molecule topologies and parameters for a variety of molecular dynamics programmes like GROMACS, CHARMM and CNS.	[3]
VMD	The VMD (Visual Molecular Viewer) allows for real-time visualisation of molecular dynamics calculations. It has been integrated into the default configuration of Gromacs from v 5.0 on.	[4]
Gromacs-5.0	(GRONingen MACHine for Chemical Simulations) is a molecular dynamics package primarily designed for simulations of proteins, lipids and nucleic acids.	[5]
Chimera 1.10.2	Chimera Molecular Visualisation package is compatible with gromacs .gro files for post-simulation viewing and conversion	[6]
Autodock Tools	AutoDockTools (ADT) is the free GUI for AutoDock developed by the private biomedical research non-profit, Scripps institute. It is used to prepare, submit and analyse AutoDock experiments.	[7]
Autodock VINA	AutoDock is a suite of automated docking tools. It is designed to predict how small molecules, such as substrates or drug candidates, bind to a receptor of known 3D structure.	[8]
PyMol 1.7.2	PyMol Molecule Graphics System; compatible with Autodock.pdbqt files	[9]

### 3.3 Polymerisation Protocols

#### *Article 1*

The protocol for the precipitation polymerisation synthesis of the MIP particles was taken from the literature [10]. In brief, inhibitor in the MAA and EGDMA was removed immediately prior to use via passage through separate inhibitor removal columns (Sigma-Aldrich, St. Louis, MO). 0.255 mmol of Theophylline was combined with 0.911 mmol of MAA in 40 mL of acetonitrile in a round bottomed flask. The mixture was then stirred gently at low temperature for 10 min. 3.64 mmol of EGDMA and 0.0852 mmol of AIVN were then added and mixed briefly. The solution was sonicated under vacuum and then purged with nitrogen for 10 min, at which point the flask was sealed and placed in a 60 °C water bath for 16 h. A control non-imprinted polymer was also created using an identical procedure with the omission of theophylline. The MIP particles were then removed from the porogen via centrifugation at 4500 RPM for 10 min and then equally divided between three 15 mL Falcon tubes. The particles were washed using 10 mL of 9:1 methanol: acetic acid solution for 1 h, at which point the washing solvent was refreshed; next, the tubes were centrifuged and the supernatant replaced. This process was repeated 5 times to ensure the complete removal of the template molecule; the particles were then rinsed again with methanol only and dried in an oven at 70 °C. A new technique for screening of “virtually imprinted receptors” for rebinding of the molecular template as well as secondary structures, correlating the virtual predictions with experimentally acquired data in three case studies. This novel technique is particularly applicable to the evaluation and prediction of molecularly imprinted polymer (MIP) receptor specificity and efficiency in complex aqueous systems.

#### *Article 2*

To test the miscibility of DVB in DMSO and its suitability as a porogen, 4 mL of chloroform, MeCN and DMSO were each mixed with an equal volume of DVB and 44 mg of AIBN initiator in glass vials. The solutions were then agitated, degassed, sealed and polymerised at 60°C for 24 hours. The resulting polymers were ground, sieved, washed in MeOH and compared with respect to pore structure using SEM.

All volumes or masses used in the imprinting protocol used in *Article 2* were calculated and confirmed using the MIP database's online polymer calculator [11]. For the preparation of the MIP, 1 mmol of melamine was combined with 8 mmol of itaconic acid in 4 mL (4.4 g) of DMSO in a 20

mL screw-topped glass vial. The mixture was then sonicated until all solids were dissolved. 24.8 mmol of DVB was then added and mixed to homogeneity followed by 44 mg, 0.268 mmol of the initiator was added. This was AICN for UV and 80°C polymerisations and AIBN for the 60°C polymerisation. The mixture was purged with nitrogen for 5 minutes following thorough mechanical mixing. The vial was then sealed. Control polymers were synthesised in an identical process with the omission of the melamine template. Thermally mediated polymerisations were carried out in an oil bath for 24 hours. For UV mediated polymerisations, the vials were placed into a UV reactor until turbidity was observed at which point these vials were transferred to an 80°C oil bath for 24 hours. Following polymerisation, all vials were removed and broken. Then the polymer was collected, ground and sieved to extract the 25 to 106  $\mu\text{m}$  fraction which was washed with methanol for 24 hours in a Soxhlet (30 minutes approx. per cycle) and dried at 70°C until a stable weight was observed.

### 3.4 MIP immobilisation

#### *Article 1*

The electrodes used for experimentation were epoxy-graphite composite electrodes of normal use in the laboratory of the authors and were prepared using a previously published in-house, established protocol [12]. Briefly, as shown in Figure 3.1, a gold-coated electrical connector was soldered to a 6 mm diameter copper disk after which a section of PVC tubing was placed over the setup to create a small cavity and a final geometric surface area of 0.28 mm<sup>2</sup>. Epoxy resin and its corresponding hardener was the combined with 50  $\mu\text{m}$  graphite particles and thoroughly mixed to a homogeneous paste. The electrode was then cured in an 80°C oven for 2 – 3 days. Following the curing duration, the electrodes were wet-polished with 400 grit abrasive-paper and degreased with acetone.

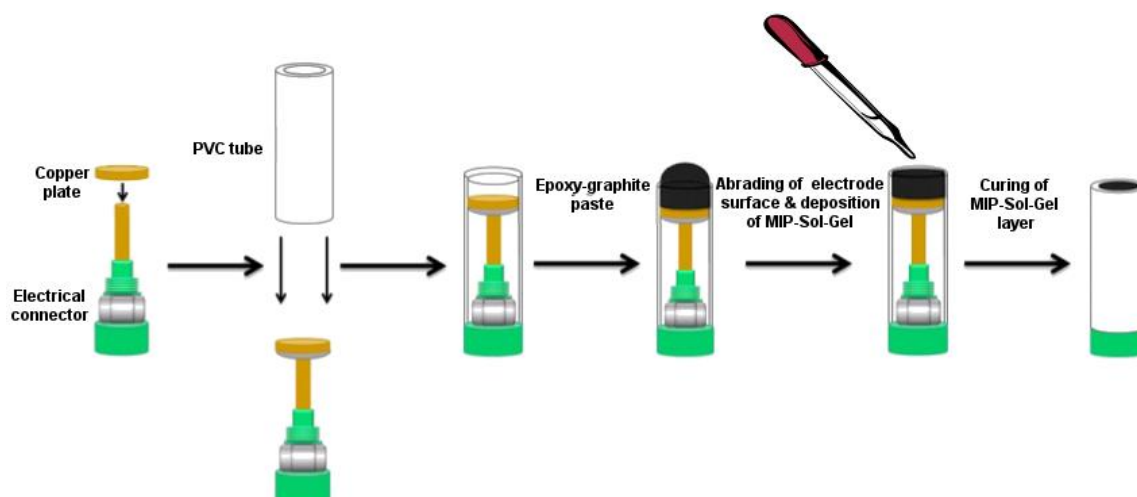


Figure 3.1: Schematic summary of the preparation of the epoxy-graphite composite electrode-immobilised MIP-sol-gel layer

The immobilisation of the MIP particles onto the surface of the epoxy-graphite electrode was modified from a previously published protocol [13]. 0.5 mL TEOS, 0.5 mL ethanol, 0.25 mL water and 25  $\mu$ L of 0.1 M hydrochloric acid (HCl) were combined and stirred vigorously for 35 min and rested for approximately 45 min to arrive at the syneresis stage. This liquid was combined with graphite and a MIP- DMF suspension in the ratio 200  $\mu$ L to 7 mg to 40  $\mu$ L respectively. The MIP-DMF suspension consisted of 15 mg of MIP particles and 1 mL of DMF; the experimental control consisted of particles polymerised in the absence of the template, a non-imprinted polymer (NIP). This mixture was shaken for 10 min at 1400 RPM. 10  $\mu$ L of this solution was deposited in the centre of each electrode and evenly distributed via a homemade spin coater at 1400 RPM for 60 s. The electrodes were dried at atmospheric pressure at 5  $^{\circ}$ C overnight and conditioned in water for 1 h before use. For regeneration experiments, the electrodes were immersed in 0.05 M HCl at 60–65 $^{\circ}$ C for 10 min and then conditioned in water for 1 h before subsequent use.

#### Article 2

The HPLC columns used were stainless steel (50 mm $\times$  4.6 mm) into which the polymer was packed using Slurry Packer model 1666 (Alltech, UK). This process entailed mixing the polymer particles in methanol and packing the column to a pressure of 100 bar. The columns were then tightly closed and washed with the mobile phase until a steady baseline was observed. When not in use, the columns were washed with a neutral (acid free) variant of the standard mobile phase.

### 3.5 Detection parameters

#### *Article 1*

Differential Pulse Voltammetry in all experiments was performed with a scan range between 1 and 1.7 V, a pulse potential of 0.01 V, duration of 300 ms and a scan rate of  $0.04 \text{ V} \cdot \text{s}^{-1}$ . A base line measurement was taken at  $t = 0$  ( $t_0$ ) from which all proceeding measures were subtracted. While chronoamperometry experiments were performed at +1.18 V. All measurements were done in pH = 3 phthalate buffer with the pH adjusted using 0.1 M HCl. An accumulation time of 5 min was used in all experiments unless otherwise stated whereby the electrode was immersed in the analyte ahead of the measurement event.

#### *Article 2*

All HPLC experiments were conducted using a Agilent 1100 HPLC and recorded using Chemstation package (Agilent, CA, USA) and performed in triplicate ( $n=3$ ). Polymer characterisation was executed using a mobile phase consisting of 50:50:0.05 water: MeCN: formic acid.

All milk samples were prepared identically. For powdered samples, they were mixed with water to a concentration of 1 gram in 10 mL. Samples were then mixed in falcon tubes at a ratio of 1:1 with the acetonitrile and spiked with melamine to a concentration of 10  $\mu\text{M}$  and agitated for several minutes. The solids were then separated from the liquid via centrifugation at 5000 RPM for 5 minutes. For adequate separation to occur, the organic fraction of the mobile phase was increased so that it was then 25:75:0.05, water: MeCN: formic acid. All samples were also prepared and analysed without adulteration with melamine to confirm their purity and also to establish a base line.

UV detectors were set to wavelengths of 204 and 240 nm. The dead volume,  $t_0$ , of the column was determined by the retention time of an injection of the mobile phase containing 10% acetone. Recovery fraction was calculated as the area under the curve of the peak relative to the area under the curve created by the analyte when injected without a column present given by equation 1.

$$Recovery = \frac{Recovered\ concentration}{Injected\ concentration} \times \frac{100}{1}$$

(1)

The retention factor 'k' was calculated using the formula give in equation 2.

$$k = \frac{t_r - t_0}{t_0}$$

(2)

Where  $t_r$  is the retention time of the analyte taken at maximum peak height and  $t_0$  is the dead volume of the column. The separation factor ' $\sigma$ ' of the polymer was calculated by equation 3.

$$\sigma = \frac{k_{melamine}}{k_2}$$

(3)

Where the subscript denotes the k value for each respective analyte; all calculations were done relative to  $k_{melamine}$ . The imprint factor ' $\alpha$ ' of the polymer was determined using equation 4.

$$\alpha = \frac{k_{MIP}}{k_{NIP}}$$

(4)

The theoretical plate number, representing the degree of interaction between the analyte and the polymer, was calculated by equation 5.

$$N = 5.545 \left( \frac{t_r}{w_h} \right)^2$$

(5)



Where  $t_r$  is the retention time of the analyte and  $w_h$  is the peak width at half height; this was normalised with respect to the length of the column by calculating the height equivalent to a theoretical plate (H) given by equation 6.

$$H = \frac{L}{N}$$

(6)

Where L is the length of the column.

### 3.6 Computational Chemistry

#### 3.6.1 Preparation of virtual molecules

##### Determination of 3D molecular structures

To attain the appropriate molecule files used in *Article 3*, 2-dimensional .mol files were either downloaded from online databases, such, as chemspider, or drawn directly using the Marvin Sketch program. This file can then be imported into the Chimera molecular visualisation software package, converted to the .mol2 format and opened in a text editor. The atom and bond types of the molecule were then inspected and modified where appropriate to ensure structural accuracy following the energy minimisation (Figure 3.2).

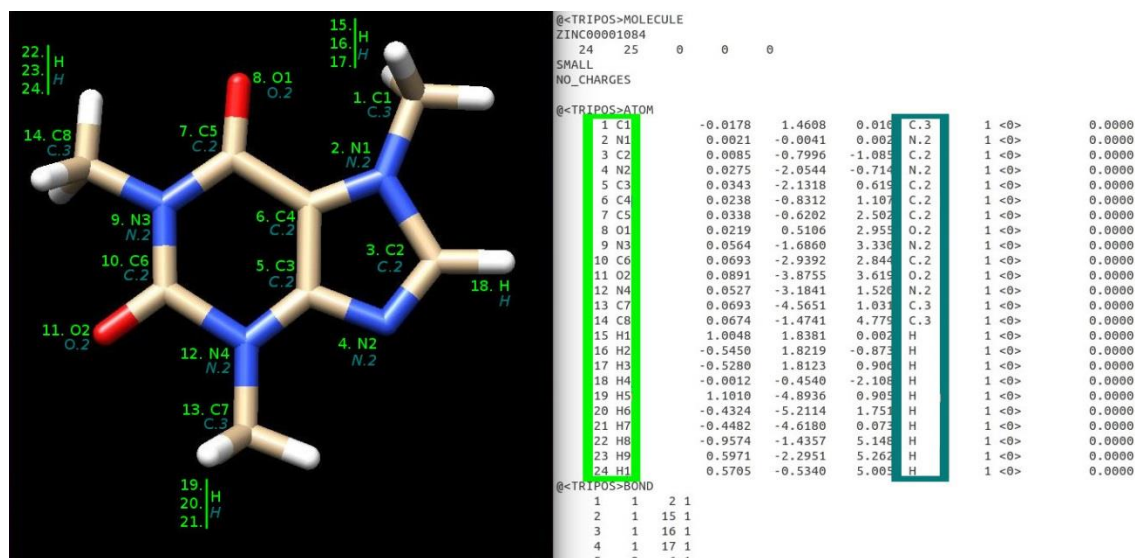


Figure 3.2: Inspection of a caffeine.mol2 file for correct molecular structure using Chimera visualisation software (left) and a text editor (right) via confirmation of atom number, element number (green) and atom type (blue)

As atom types cannot be assigned at in .mol format and structural errors are common in downloaded molecular structures, it is of paramount importance that details such as atom and bond definitions are double and triple checked to ensure accuracy of the energy minimisation, (Figure 3.3).

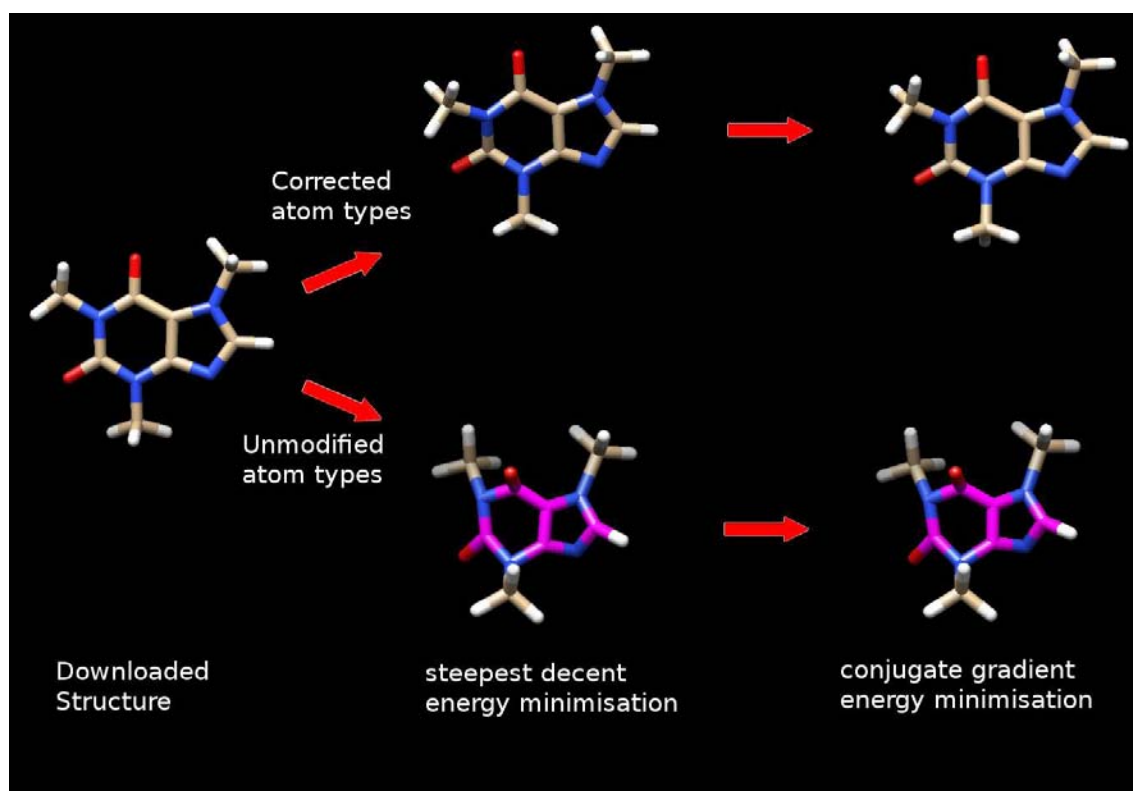


Figure 3.3: Graphic detailing the potential negative effect that incorrectly defined atom and bond types can have on the energy minimisation process

A two-step energy minimisation was then initiated through using the Openbabel software package via the 'obminimise' command through the terminal window. This minimisation was done within the integrated Generalised Amber Force Field (GAFF), employing the steepest decent and conjugate gradient optimisation algorithms receptively for a maximum of 200,000 iterations as shown below for the molecule 'input.mol2'.

```
obminimize -ff GAFF -n 200000 -sd -omol2 [>input<].mol2 > [>input_sd<].mol2
```

press ↵

```
obminimize -ff GAFF -n 200000 -cg -omol2 input_sd.mol2 > input_minimised.mol2
```

press ↵

### **Preparation of Autodock .pdbqt files**

For the experiments described in *Article 3*, all molecules were opened in Autodock Tools 1.5.6 [7, 14]. The automatic function of merging the non-polar hydrogen atoms (NPHS) to their heavier parent atom was disabled. For ligand molecules, a torsion tree was created by the detection of the number of rotatable bonds within the structure. Certain other structural features, capable of forming bonds were also identified and assigned specific autodock atom types; these were oxygen (OA) and nitrogen (NA) atoms capable of being acceptor atoms and polar hydrogen atoms (HD) capable of being donor atoms within hydrogen bonds. Aromatic carbon (AC) atoms were also identified and specifically defined.

The torsional degrees of freedom (TORSDOF) of each of these bonds were defined relative to a preselected root atom which acted as a mobility reference within the ligand structure. Gasteiger charges and NPHS energy was then assigned to each atom where appropriate within the structure while atom types were simultaneously defined by the bond types associated with said atom. For the molecule defined as the receptor, an identical assignment process was conducted with the omission of the torsion tree thus rendering the receptor molecule static and rigid.

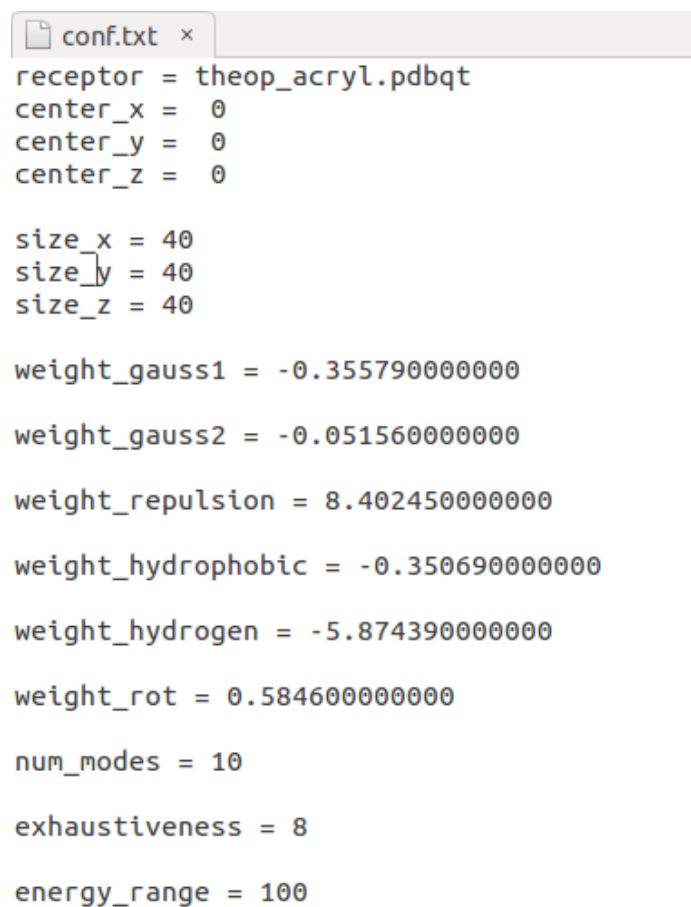
### **Preparation of Gromacs files**

Ahead of molecular dynamics experiments detailed in *Article 2*, on the Gromacs platform, topology and parameter files were prepared using the ACPYPE under default program parameters through the terminal window. This was repeated for each molecule to be included in the dynamic simulation. This process produced 3 files for each input molecule; a .gro, an .itp and a .top file using the AMBER99sb force field [15]. For a binary simulation to calculate the maximum stoichiometric ratio, both .itp files were opened in the text editor. The atom types of the FM were moved to the template file and duplicates were deleted. For both .top files were similarly combined and the resulting file was saved as a universal *topol.top* topology file. These files were then ready for use within a Gromacs simulation.

### 3.6.2 Virtual Screening

#### Autodock VINA

For docking analysis of files using the Autodock VINA algorithm described in *Article 3*, all structures were prepared in a manner identical to the preparatory steps for AD4 screening. The *ligand.pdbqt* files were named numerically id est, ligand\_01, ligand\_02 et cetera. A terminal window was opened and directed to the appropriate working directory containing the VINA executable file, configuration file and shell script file. A configuration file, a typical example of which can be seen in Figure 3.4, specified the centre and boundary conditions of the search space and the receptor file. Additional information such as cut-off energy, maximum number of docking conformations and search exhaustive could also be included in addition to user-modified parameter weights. Large ligand libraries could be screened automatically using a basic shell script (Figure 3.5) by submitting ligand files with generic, numerically increasing names. The results of this analysis could be opened in the PyMol molecular graphics system or directly in the text editor.



```
conf.txt x
receptor = theop_acryl.pdbqt
center_x = 0
center_y = 0
center_z = 0

size_x = 40
size_y = 40
size_z = 40

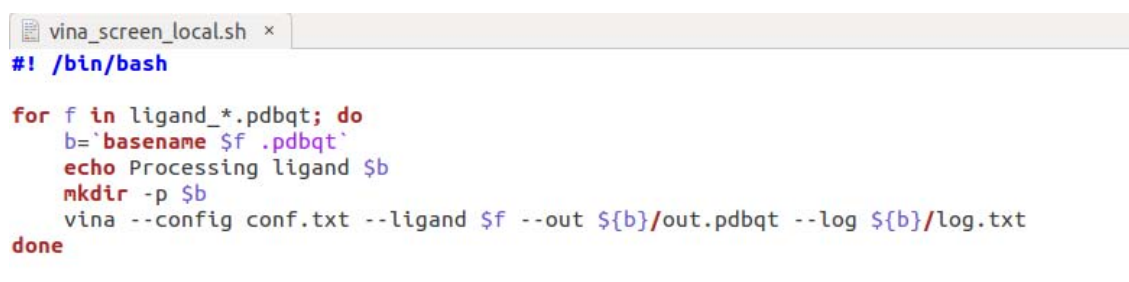
weight_gauss1 = -0.355790000000
weight_gauss2 = -0.051560000000
weight_repulsion = 8.402450000000
weight_hydrophobic = -0.350690000000
weight_hydrogen = -5.874390000000
weight_rot = 0.584600000000

num_modes = 10

exhaustiveness = 8

energy_range = 100
```

Figure 3.4: Screen shot showing a typical VINA configuration file



```
vina_screen_local.sh x
#!/bin/bash

for f in ligand_*.pdbqt; do
    b=`basename $f .pdbqt`
    echo Processing ligand $b
    mkdir -p $b
    vina --config conf.txt --ligand $f --out ${b}/out.pdbqt --log ${b}/log.txt
done
```

Figure 3.5: Screen shot of the shell script used for high throughput screening of molecules using the Autodock VINA algorithm

## **SYBYL**

The molecular modelling protocol employed to determine and rank candidate monomer molecules for effective binding with the template has been extensively documented elsewhere [16, 17]. This method used the DREAM operational mode of the LEAPFROG algorithm, a component of SYBYL (v. 7.3) modelling suite (Tripos Inc., St. Louis, MO, USA) to predict maximum docking affinity between two molecules. The parameters and relative move frequencies (Table 3.2) upon which the binding score was calculated, have been optimised to favour hydrogen bonding capacity between small, finite molecules, and thus place less weight on other interactions such as hydrophobic,  $\pi$ - $\pi$  or aromatic bonds [18]. All libraries screened consisted of molecular structures minimised to an energy of  $0.01 \text{ kcal}\cdot\text{mol}^{-1}$  using the MAXMIN2 command [19].

Table 3.2: Description of the relative move frequencies used by the Leapfrog algorithm to assign a docking mode and affinity score to the intermolecular complex

Parameter name	Description	Default weight	Optimised weight
Join	Join different fragments	2	0
Fuse	Fuse candidate fragments	0	0
New	new ligand is started by aligning fragments	5	10
Fly	Alternative minimum energy ligand orientations	2	0
Twist	Conventional minimisation	2	5
Refine	Improves newly identified ligands	2	0
Bridge	Considers all fragments as bridges	2	0
Complement	Chooses moiety complementary to a cavity group as a ligand	2	0
Save	Saves ligands that satisfy specifications	2	5
Weed	Discards all but the 10 best ligands	0	1
Crossover	Generates best hybridizations among similar molecules	0	0
Prune	Can delete moieties of a known ligand on the basis of their energy with the receptor	0	0

For the experiments detailed in *Article 2*, three libraries were compiled to be used in the MIP design process. A range of acidic, basic and neutral FMs were modelled with additional charged structures where appropriate. These were acrylamido-2-methyl-1-propanesulfonic acid (AMPSA), acrylic acid (AA), itaconic acid (IA), methacrylic acid (MAA), trifluoromethylacrylic acid (TFAA), allylamine, 1-vinylimidazole (VD), 2- & 4-vinylpyridine (VP), *N,N*-diethylamino ethyl methacrylate (DEAEM), *N,N'*-Methylenebisacrylamide (MBAA), Ethylene glycol methacrylate phosphate (EGMP), acrylamide, 2-hydroxyethyl methacrylate (HEMA) and styrene. The cross-linking monomers modelled were selected to include range of compounds: *m*- & *p*- divinylbenzene (DVB), *mono*-, *di*-, *tri* & *tetra*- ethylene glycol dimethacrylate (EGDMA), trimethylolpropane

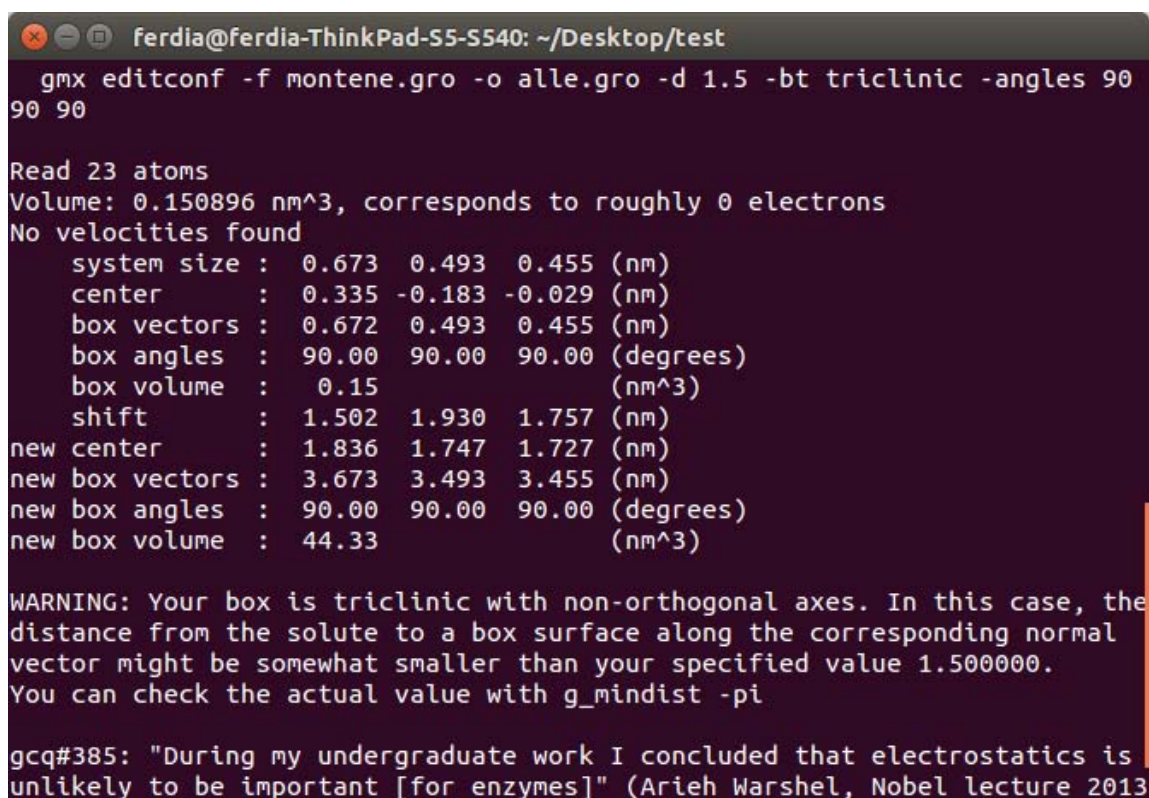


trimethylacrylate (TRIM). A combination of commonly used porogens and solvents with known melamine solubility were modelled; these were dimethylformamide (DMF), acetonitrile, chloroform, ethanol, methanol, acetone, ethylene glycol, DMSO and water.

### 3.6.3 Simulation of molecular dynamics

#### Gromacs

Using the molecule files prepared using the ACPYPE program, a virtual triclinic virtual box with right angled vertices and 3 nm edges was created using the editconf command through a terminal window using the Gromacs 5.0 molecular dynamics software package (Figure 3.6).



```

ferdia@ferdia-ThinkPad-S5-S540: ~/Desktop/test
gmx editconf -f montene.gro -o alle.gro -d 1.5 -bt triclinic -angles 90
90 90

Read 23 atoms
Volume: 0.150896 nm^3, corresponds to roughly 0 electrons
No velocities found
  system size : 0.673 0.493 0.455 (nm)
    center    : 0.335 -0.183 -0.029 (nm)
  box vectors : 0.672 0.493 0.455 (nm)
  box angles  : 90.00 90.00 90.00 (degrees)
  box volume  : 0.15 (nm^3)
    shift     : 1.502 1.930 1.757 (nm)
new center    : 1.836 1.747 1.727 (nm)
new box vectors : 3.673 3.493 3.455 (nm)
new box angles  : 90.00 90.00 90.00 (degrees)
new box volume  : 44.33 (nm^3)

WARNING: Your box is triclinic with non-orthogonal axes. In this case, the
distance from the solute to a box surface along the corresponding normal
vector might be somewhat smaller than your specified value 1.500000.
You can check the actual value with g_mindist -pi

gcq#385: "During my undergraduate work I concluded that electrostatics is
unlikely to be important [for enzymes]" (Arie Warshel, Nobel lecture 2013)

```

Figure 3.6: Gromacs report following the creation of the virtual box alle.gro

This box was then filled to capacity with the FM molecule using the insert-molecule command which typically amounted to approximately 150 molecules or 2-3000 atoms in total. The system's energy was minimised in 4 minimisation steps. The first two processes employed the steepest decent and conjugate gradient algorithms respectively. The DPOSRES option was specified within

the .mdp parameter files to apply position restraints to the system-atoms to initially maintain the template the centre of the box, in contact with the maximum quantity of molecules. A further 2 minimisation processes were conducted with full atomic mobility for all molecules (id est without the DPOSRES confinement). Following these 4 energy minimisation processes, 2 further geometric optimisation (GO) processes were implemented. The first of these was carried out at 1 atm by performing 1 ns of gradual annealing, thus the temperature was gradually increased from 0 to 300°K. The second GO simulation, a relaxation step, was conducted under a constant temperature and pressure 300°K and 1 atm for 200 ps. The system was geometry optimised in two cycles comprising 800 steps of steepest descent followed by 3,000 steps of conjugate gradient. During the GO phases, Berendsen thermostat and barostat [20] were applied to control the temperature and pressure, respectively. The LINCS algorithm [21] as used to constrain all bond lengths involving hydrogen atoms and an integration time step of 2 fs was used, to be well inside the frequency of typical light organic bonded atoms. Periodic boundary conditions (PBC) were applied. Long-range electrostatic interactions were treated using the particle mesh Ewald (PME) method [22]. The cut-off radius for the real part of the electrostatic interactions, as well as for the van der Waals interactions was set to 1 nm. At the end of these GOs, The virtual box (Figure 3.7) the hydrogen bonds involving the template molecule were identified using the hydrogen-bond analyser (Hbonanza) python script [23]. The resulting complex was then isolated and saved as a separate file with the appropriate extension for further use or analysis.

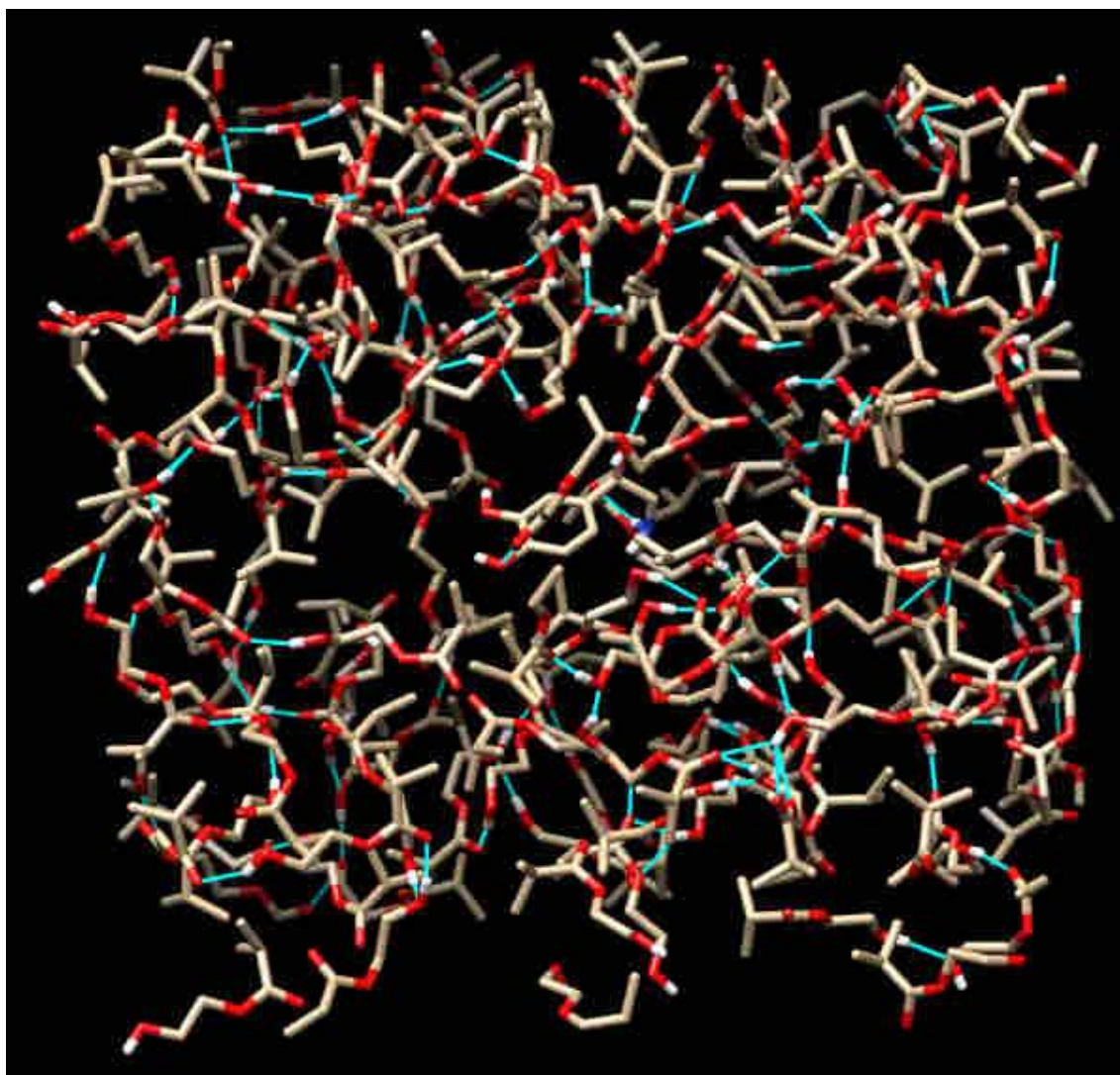


Figure 3.7: A typical virtual box containing 1 molecule of norepinephrine and 147 molecules of the FM, HEMA, following the molecular dynamics, simulation detailed above, with the resulting hydrogen bonds being shown in blue

## SYBYL

Determination of the stoichiometric ratio of template-FM was done via an established simulated annealing process using the SYBYL molecular modelling suite. A virtual cubic box containing one template molecule was packed with monomers until saturation capacity. The box was then reduced to its minimal dimensions to guard against excessive expansion of the mass as a result of repulsion between the molecules during the simulation. This box was then heated to 600°K and temperature



was reduced in four 25 femtosecond steps to 300°K during which time the initially high mobility of the molecules had decreased to a relaxed state of lowest energy and thus permitting the formation of a complex with the template molecule. Once the simulation was complete, shown in Figure 3.8 the stoichiometric ratio was determined visually by observing the number of monomers bonded to the template molecule.

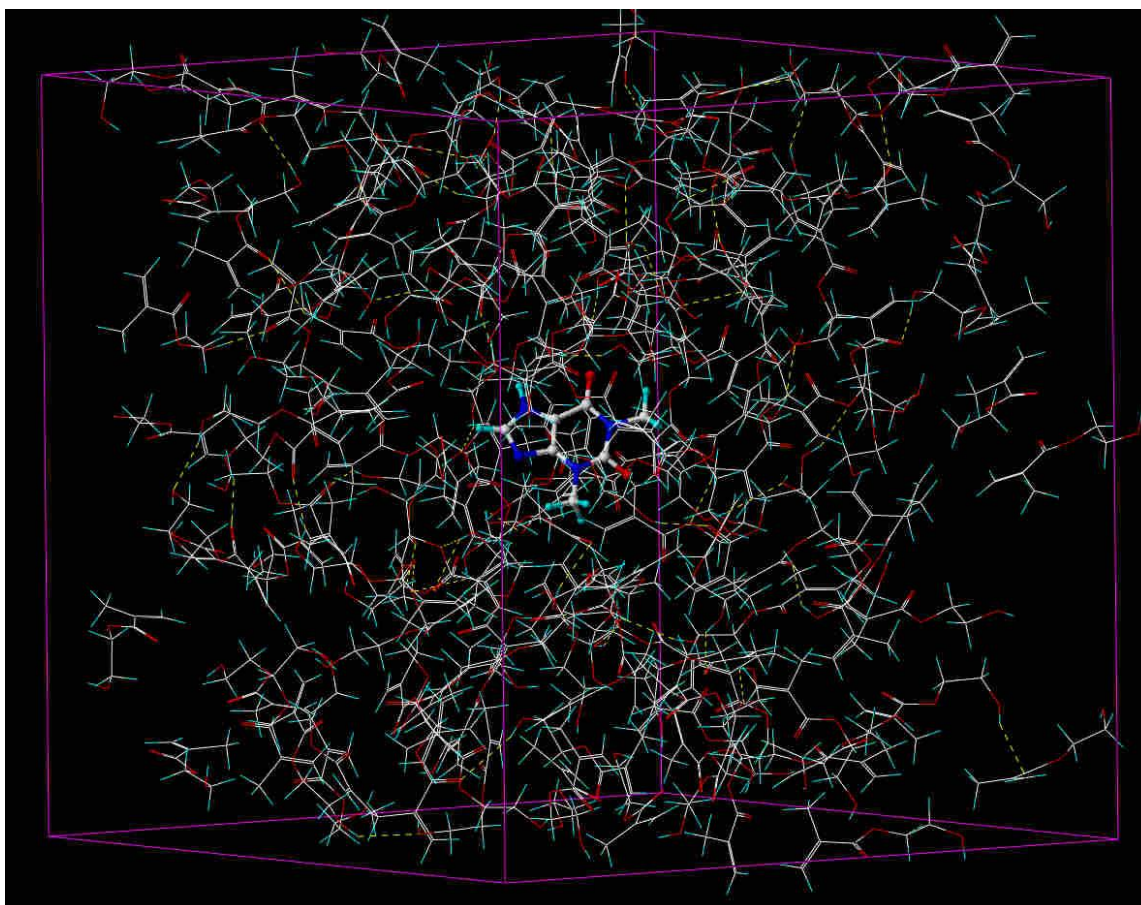


Figure 3.8: Example of a typical molecular dynamics simulation using the SYBYL molecular dynamics suite containing 1 molecule of theophylline and 153 molecules of the FM, HEMA

### 3.7 References

- [1] MarvinSketch – advanced chemical drawing software « ChemAxon – cheminformatics platforms and desktop applications, (2016).  
<https://www.chemaxon.com/products/marvin/marvinsketch/> (accessed April 18, 2016).
- [2] N.M. O’Boyle, M. Banck, C.A. James, C. Morley, T. Vandermeersch, G.R. Hutchison, Open Babel: An open chemical toolbox, J. Cheminformatics. 3 (2011) 33. doi:10.1186/1758-2946-3-33.

- [3] A.W. Sousa da Silva, W.F. Vranken, ACPYPE - AnteChamber PYthon Parser interfacE, BMC Res. Notes. 5 (2012) 367. doi:10.1186/1756-0500-5-367.
- [4] W. Humphrey, A. Dalke, K. Schulten, VMD: Visual molecular dynamics, J. Mol. Graph. 14 (1996) 33–38. doi:10.1016/0263-7855(96)00018-5.
- [5] M.J. Abraham, T. Murtola, R. Schulz, S. Páll, J.C. Smith, B. Hess, et al., GROMACS: High performance molecular simulations through multi-level parallelism from laptops to supercomputers, SoftwareX. 1–2 (2015) 19–25. doi:10.1016/j.softx.2015.06.001.
- [6] E.F. Pettersen, T.D. Goddard, C.C. Huang, G.S. Couch, D.M. Greenblatt, E.C. Meng, et al., UCSF Chimera--A visualization system for exploratory research and analysis, J. Comput. Chem. 25 (2004) 1605–1612. doi:10.1002/jcc.20084.
- [7] G.M. Morris, R. Huey, W. Lindstrom, M.F. Sanner, R.K. Belew, D.S. Goodsell, et al., AutoDock4 and AutoDockTools4: Automated docking with selective receptor flexibility, J. Comput. Chem. 30 (2009) 2785–2791. doi:10.1002/jcc.21256.
- [8] O. Trott, A.J. Olson, AutoDock Vina: Improving the speed and accuracy of docking with a new scoring function, efficient optimization, and multithreading, J. Comput. Chem. (2009) NA-NA. doi:10.1002/jcc.21334.
- [9] PyMOL Molecular Graphics System, Version 1.7.2 Schrödinger, LLC, (2014).
- [10] L. Ye, R. Weiss, K. Mosbach, Synthesis and Characterization of Molecularly Imprinted Microspheres, Macromolecules. 33 (2000) 8239–8245. doi:10.1021/ma000825t.
- [11] M.J. Whitcombe, MIPdatabase – Polymer Calculator, 2016. <http://mipdatabase.com/calc/calc.php> (accessed April 15, 2016).
- [12] C. Ocaña, E. Arcay, M. del Valle, Label-free impedimetric aptasensor based on epoxy-graphite electrode for the recognition of cytochrome c, Sens. Actuators B Chem. 191 (2014) 860–865. doi:10.1016/j.snb.2013.10.040.
- [13] A.K. Patel, P.S. Sharma, B.B. Prasad, Development of a Creatinine Sensor Based on a Molecularly Imprinted Polymer-Modified Sol-Gel Film on Graphite Electrode, Electroanalysis. 20 (2008) 2102–2112. doi:10.1002/elan.200804294.
- [14] M.F. Sanner, Python: a programming language for software integration and development, J. Mol. Graph. Model. 17 (1999) 57–61.
- [15] V. Hornak, R. Abel, A. Okur, B. Strockbine, A. Roitberg, C. Simmerling, Comparison of multiple Amber force fields and development of improved protein backbone parameters, Proteins Struct. Funct. Bioinforma. 65 (2006) 712–725. doi:10.1002/prot.21123.
- [16] I. Chianella, M. Lotierzo, S.A. Piletsky, I.E. Tothill, B. Chen, K. Karim, et al., Rational Design of a Polymer Specific for Microcystin-LR Using a Computational Approach, Anal. Chem. 74 (2002) 1288–1293. doi:10.1021/ac010840b.

- 
- [17] S.A. Piletsky, K. Karim, E.V. Piletska, A.P.F. Turner, C.J. Day, K.W. Freebairn, et al., Recognition of ephedrine enantiomers by molecularly imprinted polymers designed using a computational approach, *The Analyst*. 126 (2001) 1826–1830. doi:10.1039/b102426b.
- [18] E.V. Piletska, M. Romero-Guerra, I. Chianella, K. Karim, A.P.F. Turner, S.A. Piletsky, Towards the development of multisensor for drugs of abuse based on molecular imprinted polymers, *Anal. Chim. Acta*. 542 (2005) 111–117. doi:10.1016/j.aca.2005.03.067.
- [19] J. Labanowski, I. Motoc, C.B. Naylor, D. Mayer, R.A. Dammkoehler, Three-Dimensional Quantitative Structure-Activity Relationships. 2. Conformational Mimicry and Topographical Similarity of Flexible Molecules, *Quant. Struct.-Act. Relatsh.* 5 (1986) 138–152. doi:10.1002/qsar.19860050403.
- [20] H.J.C. Berendsen, J.P.M. Postma, W.F. van Gunsteren, A. DiNola, J.R. Haak, Molecular dynamics with coupling to an external bath, *J. Chem. Phys.* 81 (1984) 3684. doi:10.1063/1.448118.
- [21] B. Hess, H. Bekker, H.J.C. Berendsen, J.G.E.M. Fraaije, LINCS: A linear constraint solver for molecular simulations, *J. Comput. Chem.* 18 (1997) 1463–1472. doi:10.1002/(SICI)1096-987X(199709)18:12<1463::AID-JCC4>3.0.CO;2-H.
- [22] D.M. York, A. Wlodawer, L.G. Pedersen, T.A. Darden, Atomic-level accuracy in simulations of large protein crystals, *PNAS*. 91 (1994) 8715–8718. doi:10.1073/pnas.91.18.8715.
- [23] J.D. Durrant, J.A. McCammon, HBonanza: A computer algorithm for molecular-dynamics-trajectory hydrogen-bond analysis, *J. Mol. Graph. Model.* 31 (2011) 5–9. doi:10.1016/j.jmgm.2011.07.008



## **Chapter 4 – Results and Discussion**





## 4. Results and discussion

The aim of this thesis, as has been stated in the preceding chapters, is to explore the possibility using MIPs in high longevity sensing systems and sensor arrays. This line of research was begun in January of 2012 with the replication of already optimised imprinting protocols from the literature and then the immobilisation of the MIPs produced onto a voltammetric sensor surface. The results of this research were finally published in 2015 in the *Microchimica Acta* journal (Article 1). While the molecularly imprinted electrochemical sensor reported in this article was successful as a standalone sensor, it has inherent disadvantages which provided very valuable insights into the requirements of both imprinted sensors and sensor arrays.

Following this first project, a secondment in the laboratory of Professor Sergey Piletsky at the University of Leicester (UoL) was undertaken which took place during the calendar year of 2014. The work of this secondment focused in greater depth on the imprinting process itself and the effects of each individual component used in the synthesis on the MIP. Within this work, the highly developed molecular modelling resources of the research group were also taken advantage of. These were the computationally assisted selection of an optimal combination of functional and crosslinking monomers for both the selectivity and specificity of the MIP receptors, and also molecular dynamics computational protocols which were used in the optimisation of the MIP protocol. A further collaboration with the computational chemistry research group within the

University of Verona was also instigated during this time. This group, through the expertise of PhD student Mr Mirko Busato, replicated UoL's dynamics protocol using the open source 'Gromacs' software package. The MIP produced from this effort was then used to create an imprinted HPLC column sensor. In contrast to the first imprinted electrochemical sensor, the imprinted HPLC column sensor had none of the issues of sensor regeneration which had been one of the principal issues of that prior attempt. The results of this secondment have been written up and have been submitted to the Separation Science and Technology journal and are currently pending acceptance (Article 2).

Following on from the experience gained in the UoL with respect of computational molecular modelling, a novel protocol was developed using the open-source molecular docking software, Autodock. The ability to define receptors as rigid structures allowed for a totally new method of evaluating template-FM combinations as candidates for imprinting protocols. This predictions made by this technique have been correlated with experimentally acquired results extracted from the literature and published in the Macromolecular Bioscience journal this year (Article 3).

The results and discussion coming from this research has been arranged into Article sections with each section relating to a unique line of research. Sections 4.1, 4.2 and 4.3 detail the results coming from Articles 1, 2 and 3 respectively. All published Articles are reprinted in chapter 6, while all Articles submitted and pending decision are reprinted in the Annex. Following the presentation of the results in this chapter, the proceeding chapter will detail the currently on-going and future work which has been instigated and inspired by the effort of this thesis.

Article 1 - **F. Bates** and M. del Valle, *Voltammetric sensor for theophylline using sol-gel immobilized molecularly imprinted polymer particles*, Microchimica Acta. 182 (2015) 933–942.

Article 2 - **F. Bates**, M. Busato, E. Piletska et al., *Computational design of molecularly imprinted polymer for direct detection of melamine in milk* [Manuscript submitted to Separation Science and Technology]

Article 3 - **F. Bates**, M.C. Cela-Pérez, K. Karim et al., *Virtual Screening of Receptor Sites for Molecularly Imprinted Polymers*, Macromolecular Bioscience (2016).  
doi:10.1002/mabi.201500461

#### 4.1 Voltammetric sensor for theophylline using sol-gel immobilised molecularly imprinted polymer particles

The synthesis of sensors incorporating MIPs is feasible though the reproducibility of such techniques can be difficult due to the large number of interdependent steps. For this reason the attention of laboratories, both specialist and non-specialist alike, tend to focus more frequently on the synthesis of MIP particles. There is, however, a lack of protocols for immobilization of these particles. Herein is presented a sol-gel based method for immobilisation of MIP particles for use in an electrochemical sensor. The macroporous particles were prepared using precipitation-polymerisation and imprinted with theophylline. The sol-gel was combined with graphite microparticles (50  $\mu\text{m}$ ) and the composite was deposited on the surface of an epoxy-graphite electrode. The sensor was then tested for its response to theophylline using differential pulse voltammetry. A limit of detection of 1  $\mu\text{M}$  was observed and a relative standard deviation of 6.85%. The electrode can be regenerated via a thermal washing process which is accompanied by signal loss of 29.3%. Any further regeneration caused a signal loss of 2.4% only.

##### 4.1.1 Particle synthesis and sol-gel immobilisation

Microspheres were chosen for sol-gel immobilisation due to their small size and high homogeneity. Traditional monolith particles from a bulk polymerisation procedure was rejected due to the thickness of the membrane relative to the particle size which was seen to greatly reduce the availability of the MIP on the electrode surface and thus cause poor inter-electrode reproducibility. A larger particle size of a methacrylate based polymer would also greatly reduce the surface area available for electron transfer between the MIP recognition element and the conducting graphite thus reducing the electrode-signal. The synthesis protocol used employed a ratio of 1:4 MAA:EGDMA to ensure high crosslinking and optimal rigidity to maintain binding site morphology within the polymer matrix and thus maximise the selectivity of the final sensor. The yield following template removal was 563 mg, calculated as an efficiency of 64% by weight, 24% less than that given by Ye *et al.* [1]. This drop in yield efficiency is speculated to have originated from the lower centrifugation speeds that were used during the template removal process of the synthesis. SEM analysis confirmed the formation of highly uniform spherical particles (Figure 4.1 a & b). A superficial roughness or 'wrinkled' surface was observed on the MIP particles; an advantageous feature of macroporous particles due to the increment in surface area it provides. This surface area is permanent both in the dry state and does not require solvent-related swelling to provide access to the pores [2]. A subsequent statistical analysis (Figure 4.1 c) found the particle size distribution to

be in keeping with that published in the literature. 54% of the particle yield was made up of sizes at 970 nm while 96% of the yield was above 665 nm. In contrast to the large positive skew seen in the distribution of the MIP particle synthesis, the NIP control saw a quite narrow ( $\sigma = 33.1$  nm), normal distribution of particle sizes; with 46% of the yield being sized at the mean value and 86% of the total being at or above the mean of 116 nm, shown in Figure 4.1 d. The greatly diminished particle size demonstrates the sensitivity of precipitation polymerisation protocols to the choice of template.

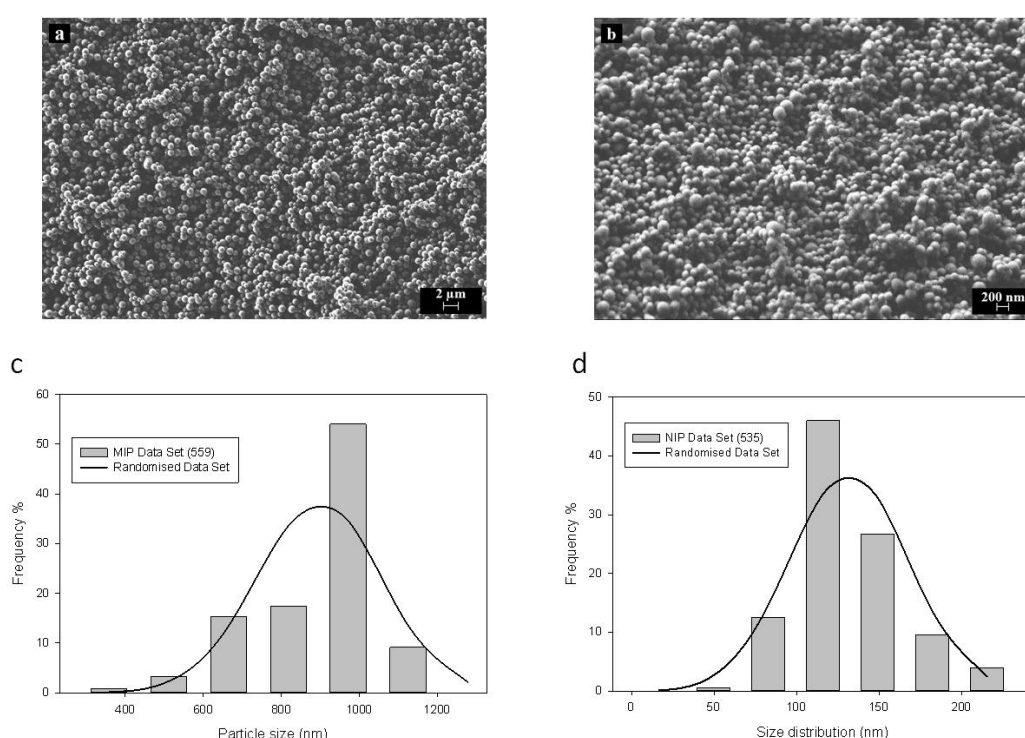


Figure 4.1: SEM of uniform spherical Theophylline-Imprinted Polymer particles (a) and the NIP control (b); Statistical analysis of MIP particle size distribution with a mean of 819 nm and standard deviation of 153 nm (c) and statistical analysis of NIP particle size distribution with a mean of 116 nm and standard deviation of 33 nm (d)

#### 4.1.2 Optimisation and determination of deposition, drying and regeneration sol-gel conditions

In order to obtain a sensing surface usable for voltammetry, it was decided to immobilise the obtained MIP microspheres within a sol-gel matrix. The necessity to modify the original protocol,

as optimized by Patel *et al.* [3–5], stemmed from the need to shift from a ‘MIP coated’ sol-gel to sol-gel-immobilised MIP particle. The increase in the graphite particle size, from 1-2  $\mu\text{m}$ , as was used in the original protocol, to 50  $\mu\text{m}$ , obliged the modification of the deposition method and electrochemical procedure. In contrast to the robustness of the gel of the original protocol, the newly devised concoction was found to be prone to cracking when dried at low-pressure as recommended by Patel *et al.* Optimal results were seen when the electrodes were chilled following the deposition and distribution (spin coating) and allowed to dry over night at ambient pressure. Though signal intensity was seen to be proportional to gel thickness, an optimised deposition volume of 10  $\mu\text{L}$  on the graphite-epoxy composite electrode was chosen as larger deposition volumes were seen to increase the instance of crack formation on the gel surface, a finding consistent with the literature [6]. Though it is possible to negate the instance of crack altogether as well as achieve extremely high film uniformity via multiple depositions [7], the high surface area seen to occur from a single deposition caused by the surface roughness was not replicated when multiple layers were built up on the electrode surface. The reduction in the deposition volume from that originally used was also motivated by the decrease in solution thickness that was seen with the use of an increased grain size of graphite. The increased liquidity of the solution predisposed it to spill from the surface of the electrode during spin-coating and thus a higher volume was not used.

The reduced density of the gel relative to original protocol caused the aggressive electrochemical cycling or sustained high-voltage pre-treatments to be detrimental to the structural integrity. This came contrary to the robustness the previously published gel presented by Patel *et al.* [5] where it was endured repeated and extended durations at 2 V without degradation.

The other strategies for signal augmentation of methylxanthines also were discounted. In the system reported by Alizadeh *et al.* [8], an extraction of the analyte from the sample solution by the electrode was followed by its immersion in strong acid which served to greatly augment the signal strength. Such a technique was not possible as the use of strong acids during voltammetric measurements caused the deterioration of the gel through the continuation of hydrolysis in the sol-gel within the membrane.

In the first instance, a standard phosphate salt buffer was chosen as a detection medium. Though binding and extraction of the imprinted template is most effective in neutral to slightly basic pH buffers, acidic pH buffers are also widely used for signal augmentation. Electrochemical sensor for folic acid based on a hyperbranched molecularly imprinted polymer-immobilized sol-gel-modified pencil graphite electrode [9, 10] and indeed, a low measuring pH was chosen in keeping with the

recommendations of Spataru *et al.* [11]. The use of such a buffer combines the binding and signal augmentation requirements to allow for a facile single step detection process without losing the imprinting effect of the MIP relative to its control.

Upon deposition, the sol mixture was evenly distributed using a home-made spin coater. The time period, 60 seconds was chosen as it was observed that excessive time spend in this fashion caused uneven evaporation of the solvent and thus crack-formation. When dried, the thickness of the membrane was measured using a 3D confocal microscope (Figure 4.2 a). It was observed that though the greatest thickness remained at the centre of the electrode at the site of the deposition, the overall distribution of membrane thickness was relatively uniform varying from approximately 200  $\mu\text{m}$  at the extreme peripheries of the electrode to 300  $\mu\text{m}$  at the original deposition point. This variation was seen to arise from the decrease in solution thickness, as well as graphite particle quantity, which occurred when the graphite particle size was increased while the mass proportion remained constant thus decreasing the *in-situ* availability of the graphite causing a radial gradient to be observed. Increasing the mass proportion of the graphite in order to compensate this reduction, though aiding in the homogeneous distribution of the gel upon disposition, provoked an increased occurrence of crack formation in the sol-gel surface upon drying which obliged a reduction in deposition volume and decreased signal strength.

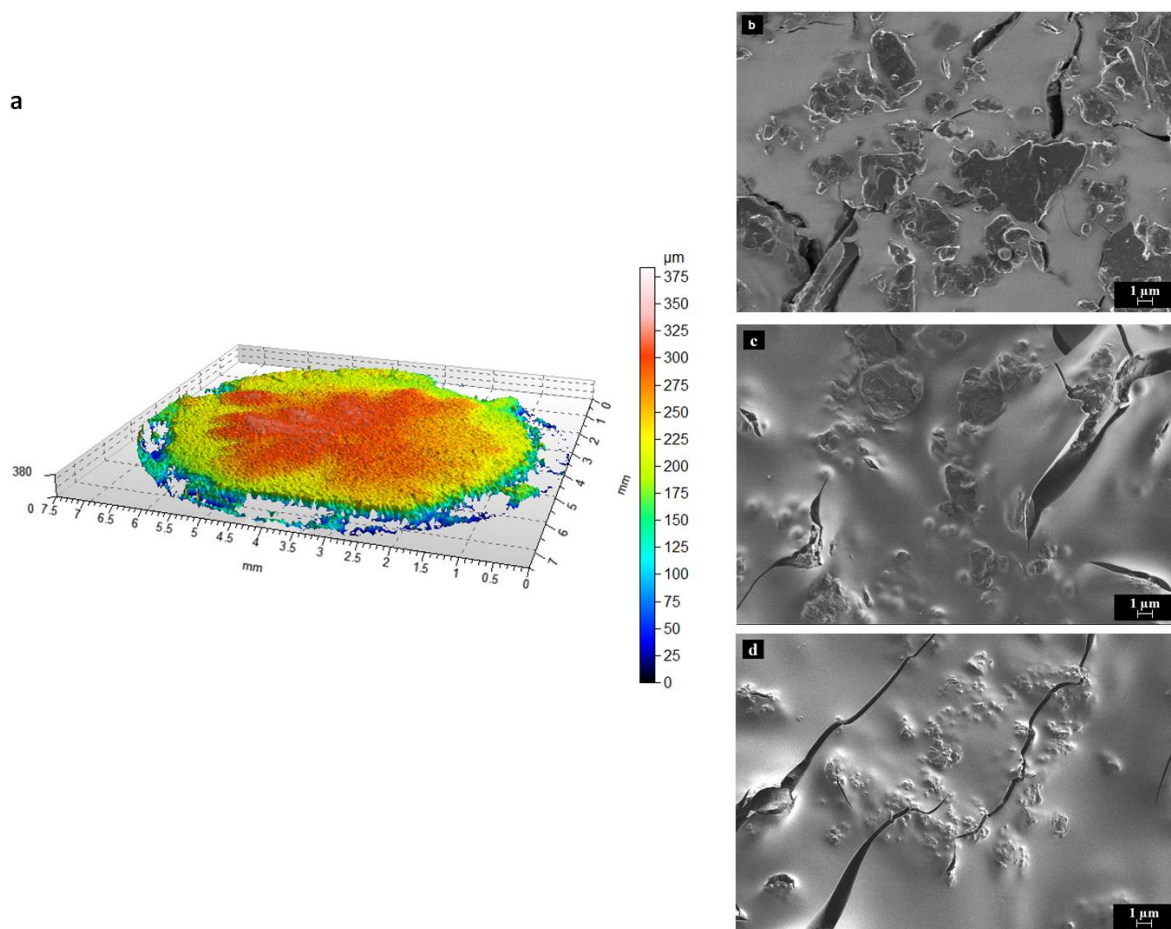


Figure 4.2: 3-dimensional surface profile and film-thickness of sol-gel on electrode surface obtained by confocal microscopy examination (a) SEM images of a deposited sol-gel membranes containing graphite only (b) and the sol-gel immobilised MIP and NIP microspheres (c & d)

It was seen that the MIP particles preferentially occupied the surface of the sol-gel electrode, clustering around the graphite particles (Figure 4.2 b – d). This orientation is advantageous as it reduces the incidence of non-specific interactions between the analyte solution and the graphite particles and thus maximises the specific binding events between the MIP particles and the target analyte. The high availability of the MIP particles at the surface of the sensor also allows for a reduction in the immersion time in the analyte required before measurement can occur as well as allowing the sensor to be regenerated as will be discussed below.



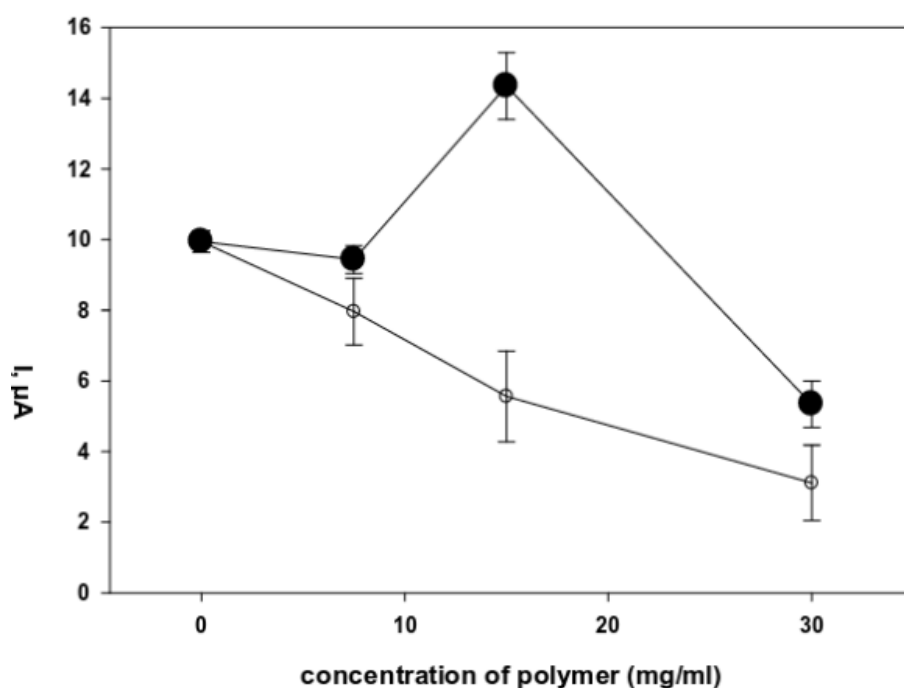


Figure 4.3: Optimisation of the concentration of polymer particles in the MIP-DMF suspension used in the synthesis of the MIP-sol-gel membrane (●) and NIP-sol-gel control electrode (○) up to 30 mg/mL for 0.27 mmol of theophylline

The volume of MIP particles in the sol-gel membrane was determined through varying their concentration in the MIP-DMF suspension that was used during the synthesis of the sol-gel membrane (Figure 4.3). It was found that 15 mg/mL caused the greatest augmentation in signal strength for the MIP-sol-gel electrode after which point the insulating effect of the methacrylate particles overrode the imprinting effect of the MIP. Interestingly, a linear decrease in oxidation potential was observed with respect to polymer concentration in the sol-gel. In the case of Theophylline this decrease was from 1.22 V the lowest concentrations tested (0 - 7.5 mg/mL) to 1.09 V for the highest (30 mg/mL).

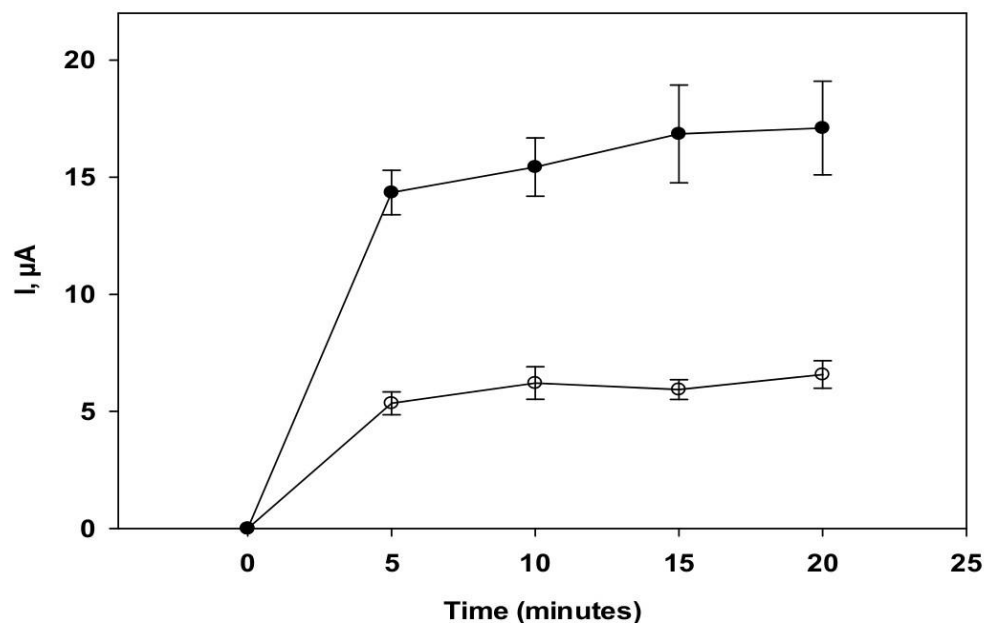


Figure 4.4: Dynamic response of MIP-sol-gel electrode (●) and NIP-sol-gel control electrode (○) toward theophylline in a pH =3 phosphate buffer solution at a concentration of 0.27 mmol

#### 4.1.3 Electrochemical Characterisation

The devised theophylline sensor made by the immobilisation of MIP microspheres employing a sol-gel matrix was subsequently used in adsorptive stripping voltammetric determination of the alkaloid using DPV. An accumulation time of five minutes was chosen for measurements, as a minimal signal increase occurred subsequent to this which was also accompanied by an increased inter-electrode signal heterogeneity which caused (Figure 4.4).

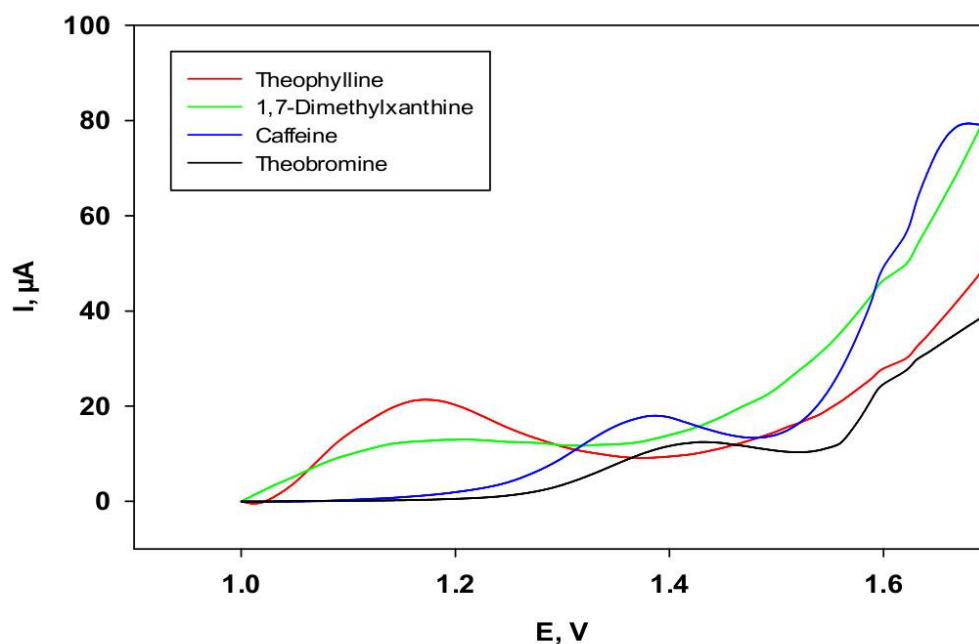


Figure 4.5: DPV voltammograms of the MIP-sol-gel electrode for caffeine, theophylline, theobromine and 1,7-dimethylxanthine at a concentration of 0.27 mmol/l,  $t = 5$  minutes, range 1 - 1.7 V, a duration of 300 ms, pulse potential of 0.01 V and scan rate of 0.04 V/s

When different methylxanthines were assayed with the prepared electrode, oxidation peaks of 1.14, 1.18, 1.36 and 1.4 V were observed for 1,7-dimethylxanthine, theophylline, caffeine and theobromine respectively (Figure 4.5). The peak cross-responses of Theobromine and Caffeine at pH = 3 were consistent with that set forward by Spataru *et al.* [11]. The buffer pH was specifically selected with a view to both maximise the oxidation potential of the target analyte itself and the performance of the receptor itself, an often tricky balance to find [12]. A buffer pH of 3 was seen to be the optimal balance between the electrochemical signal produced by the sensor and the enhancement of the affinity MAA-based imprinted receptor towards its target, theophylline [13]. The peaks observed for the secondary analytes were broader than that of theophylline most probably due to the lower incidence of binding events occurring at the surface of the MIPs.

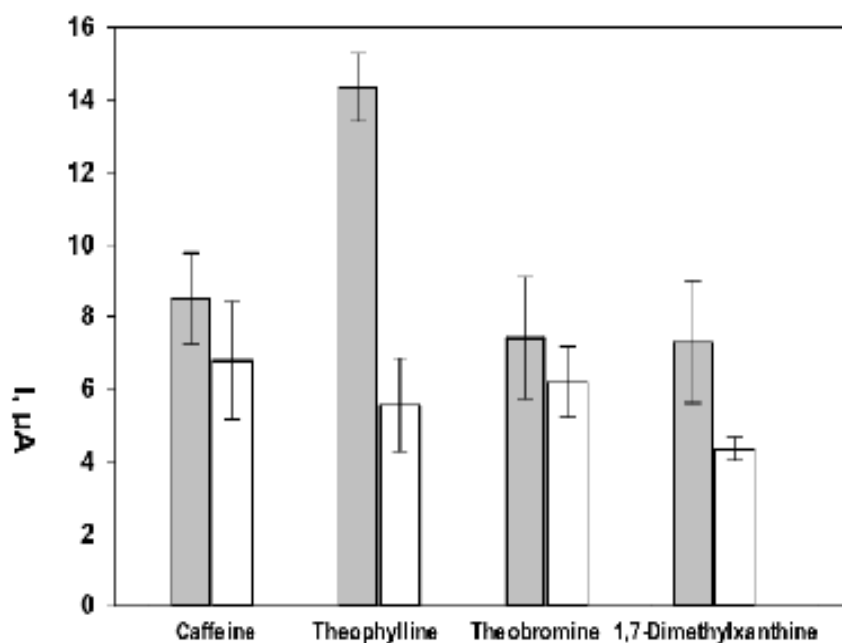


Figure 4.6: Oxidation peak heights of the MIP-sol-gel electrode (solid bars) and NIP-sol-gel electrode (white bars) for caffeine, theophylline, theobromine and 1,7-dimethylxanthine at an analyte concentration of 0.27mmol/l

Signal intensities were extracted from the profiles using the Dropview 8400 computer software and averages were made ( $n=5$ ). Relative standard deviation (RSD) was calculated as 6.85% for the primary target and an intensity of 258.1% (relative to control NIP-sol-gel electrode) (Figure 4.6). Lesser differentiation was seen between 1, 7-dimethylxanthine, caffeine and theobromine which yielded intensities being only 168.1%, 125.6% and 119.7% with respect to their controls. Though uric acid, acetaminophen, ascorbic acid and glucose were also tested, no oxidation peaks were produced within the measurement range.

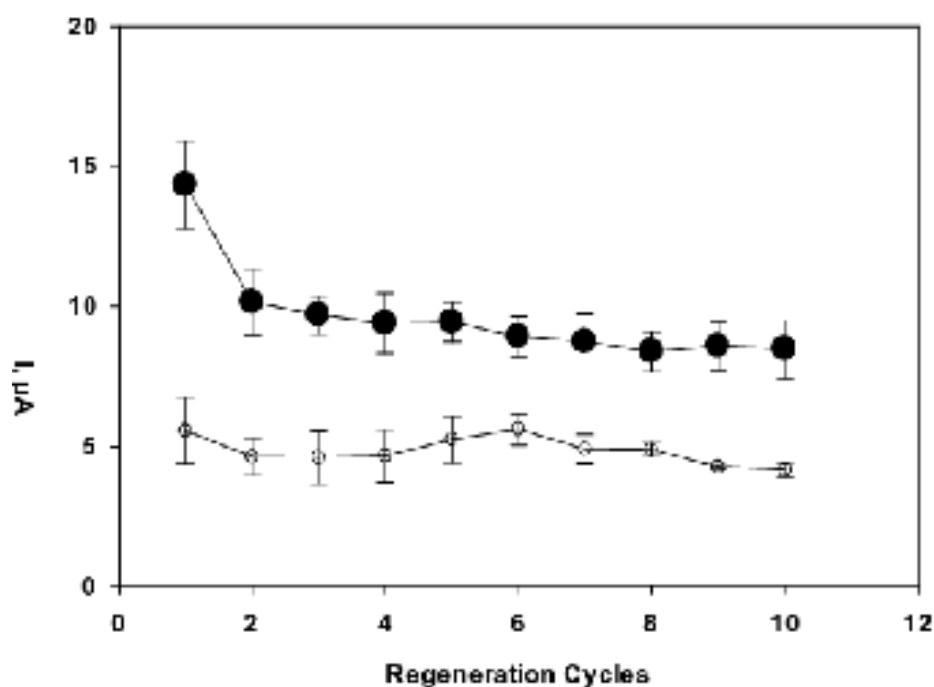


Figure 4.7: Regeneration of MIP-sol-gel electrode (●) and NIP-sol-gel control electrode (○) using thermal-acidic treatment calculated from  $n = 5$  replications

Regeneration of the MIP-sol-gel immobilised electrode was attempted. The temperatures, 60–65°C, duration of 10 minutes, and acidic strength of 0.05 M HCl, were optimised. Similar to that found during the optimisation of the deposition of the gel, strong acid and sustained augmented temperatures were detrimental to the integrity of the sol-gel structure; thus the parameters were determined. It was also seen that use of the electrode immediately following regeneration caused erratic results; this is believed to be due to the electrode body acting as a thermal battery, thus a relaxation period was required to return the electrodes to a base level.

As was observed by Alizadeh *et al.* [8], measurements subsequent to the initial binding event decreased in intensity. Such was the behaviour seen in the MIP-sol-gel electrode whereby all measures following the first were approximately 70.7% of the initial measurement (Figure 4.7). It was seen, however, that the linear pattern seen from the first regeneration cycle one was consistent for up to 40 regeneration cycles (not shown) with an average signal loss of 2.35% per cycle. The initial 29.3% decrease, followed by a greatly reduced loss of signal is due to the occupation of the deeply-seated, high affinity binding sites within the MIP particle structure which cannot be completely cleaned following the initial binding event. The subsequent preferential recognition of the analyte exhibited by the MIP-sol-gel electrode can be attributed to binding sites located on the

aforementioned ‘wrinkled’ surface of the particles which are not present on the surface of the NIP particles. The efficacy of the regeneration of the sensor hinges on the use of macroporous microparticles instead of a bulk-polymerised monolith whereby a permanent and heterogeneous pore structure allows the unhindered removal of the template from the particle surface

The limit of detection (LOD) of the sol-gel immobilised MIP was seen to be 1  $\mu\text{M}$  ( $y = 53.436x + 0.0053$ ;  $R^2 = 0.984$ ), consistent with the LODs of conductive sensors employing similarly synthesised un-specialised MIP particles (Table 4.1). A lower LOD was not possible to confirm due to the increasingly poor signal-to-noise ratio caused by the aforementioned interference originating from background currents created by the electrode inherent to the detection of methylxanthines. The authors believe that lower LOD would be possible with the incorporation of a conducting core into the MIP particles during their synthesis so as to augment the signal within the sensor rather than in the solution.

Table 4.1: Comparative table of different immobilisation methods for unmodified MIP particles onto conductive electrodes

Template	Monomers	MIP format	Immobilisation method	LOD	Operational lifetime	Ref.
Hydroquinone	MAA/TRIM	Macroporous microspheres	Agarose gel on glassy carbon electrode	1 $\mu$ M	N/A	[14]
1-hydroxypyrene	Styrene/DVB	Macroporous microspheres	Carbon ink on screen printed electrode	0.1 mM	N/A	[15]
Caffeine	MAA/EGDMA	Monolith	Integrated in carbon paste electrode	0.6 nM	N/A	[8]
Theophylline	MAA/EGDMA	Macroporous microspheres	sol-gel on carbon paste electrode	1 $\mu$ M	40 cycles	This work

## **4.2 Computational design of molecularly imprinted polymer for direct detection of melamine in milk**

Following the initial attempt to create a reusable imprinted sensor with limited success, a further study was carried out into both the fundamentals of the design process of an imprinted receptor and selection mechanism of each of the components which form the MIP, namely the FM, crosslinker, porogenic solvent and radical initiator. The fact that the analytes targeted by ET sensor arrays are often low solubility and present in trace quantities can put the requirements of the traditional imprinting process at odds with the specifications of the detection environment. With this in mind, a novel protocol for the imprinting of melamine was devised. The design of the MIP was achieved using a combination of computational techniques developed by the UoL and in-house laboratory trials, with the former greatly reducing the duration of the latter. The compatibility and mutual effect of monomer and solvent candidates were also investigated from the perspective of maximising the imprinting factor (IF) and minimising the negative interfering effects of the molecules supporting the actual imprinted receptor, id est, the crosslinker, porogenic solvent and radical initiator. Two novel open source tools were presented which are: the online polymer calculator from [and](#) and the application of the Gromacs modelling suite to determine the ideal stoichiometric ratio between template and functional monomer. The MIP binding was characterised for several structural analogues at 1-100  $\mu\text{M}$  concentrations. The use of DVB as cross-linking polymer and itaconic acid as functional monomer allowed synthesis of MIP with factor for melamine  $\text{IF}=2.25$ . This polymer was used in HPLC for the rapid detection of melamine in spiked milk samples with an experimental run taking 7-8 minutes. . This approach introduced and demonstrated the power of virtual tools in accelerated design of MIPs into this research project.

### **4.2.1 Solvation of melamine into the porogen and the use of computational modelling**

As the objective of this work was to produce a molecularly imprinted bulk porous polymer resin, suitable for use as a HPLC column packing media, several criteria had to be satisfied. The first and foremost of these is to find a combination of template, FM and solvent which may facilitate the formation of template-FM complexes which could then be physically secured in place via subsequent polymerisation of a co-monomer. Computer modelling offers an accurate way to accelerate the selection process by creating a short list of candidates from larger libraries which may then be tested in the laboratory. In bulk imprinting, the template must be dissolved in the



porogen at a concentration somewhere in the range of  $0.25 - 0.4 \text{ mol}\cdot\text{L}^{-1}$ . This concentration ensures a high number of binding sites while still ensuring a high percentage of cross-linking polymer to maintain structural rigidity. However, the high template concentrations typically present in the MIP solution can also significantly affect its thermodynamic stability and cause significant differences in all families pore morphology relative to the NIP control as summarised in Figure 1.13 in the introductory chapter.

Ahead of laboratory tests, melamine was screened against virtual libraries of common FMs, cross-linkers and solvents. This was done primarily due to the exceptionally poor solubility of the molecule in the conventionally used porogenic solvents. A search of the literature for melamine non-covalent imprinting protocols showed the most commonly used solvating porogen was either pure methyl alcohol [16,17] or a mixture of water and methyl or ethyl alcohol [18,19]. Two further works reported the successful detection of melamine using cyromazine, a structural analogue of melamine, as a template and water-alcohol binary porogenic solvent [20, 21]. One additional work also reported the successful use of benzene [22] as the porogen. All these cited works used the methacrylate monomers MAA and EGDMA and relied on strong solvent interactions in addition to the enhancement of template solubility provided by the FM. While it is clear that such attempts have yielded favourable results, the apparent necessity to employ solvents of high polarity and hydrogen-bonding capacity must be assumed to be a significant source of disruption to the formation of high affinity template-FM complexes in the solution [23, 24].

An alternative to this approach is the use of ethylene glycol as a porogen in order to dissolve the melamine [25]. While melamine has comparatively high solubility in ethylene glycol, it also has extremely high hydrogen bonding capacity and viscosity making it a challenging candidate for use as a porogenic solvent [23]. The solution employed by Yusof et al. was to use an imprinting mechanism based on aromatic and Van der Waals interactions between melamine and 9-vinylcarbazole. Mechanical mixing was used to facilitate radical mobility within the solution and to reduce autoacceleration.

### **Computational modelling and laboratory trials**

Since the existing protocols did not satisfy the requirements of this work, methodical laboratory pre-polymerisation trials were conducted to find an optimal combination of FM and solvent which would facilitate the solvation of melamine at a sufficient concentration and ultimately produce an

effective MIP. The *ab initio* use of virtual screening models in concert with laboratory trials to confirm these predictions ahead of any polymerisation event allows for the negation of any intermolecular differences in monomer reactivity which might otherwise affect the apparent results if the affinity of the FM candidates were compared in their polymerised form. Computationally determined affinity rankings were used to create a logical order of candidates. A summary of these results can be seen Figure 4.8.

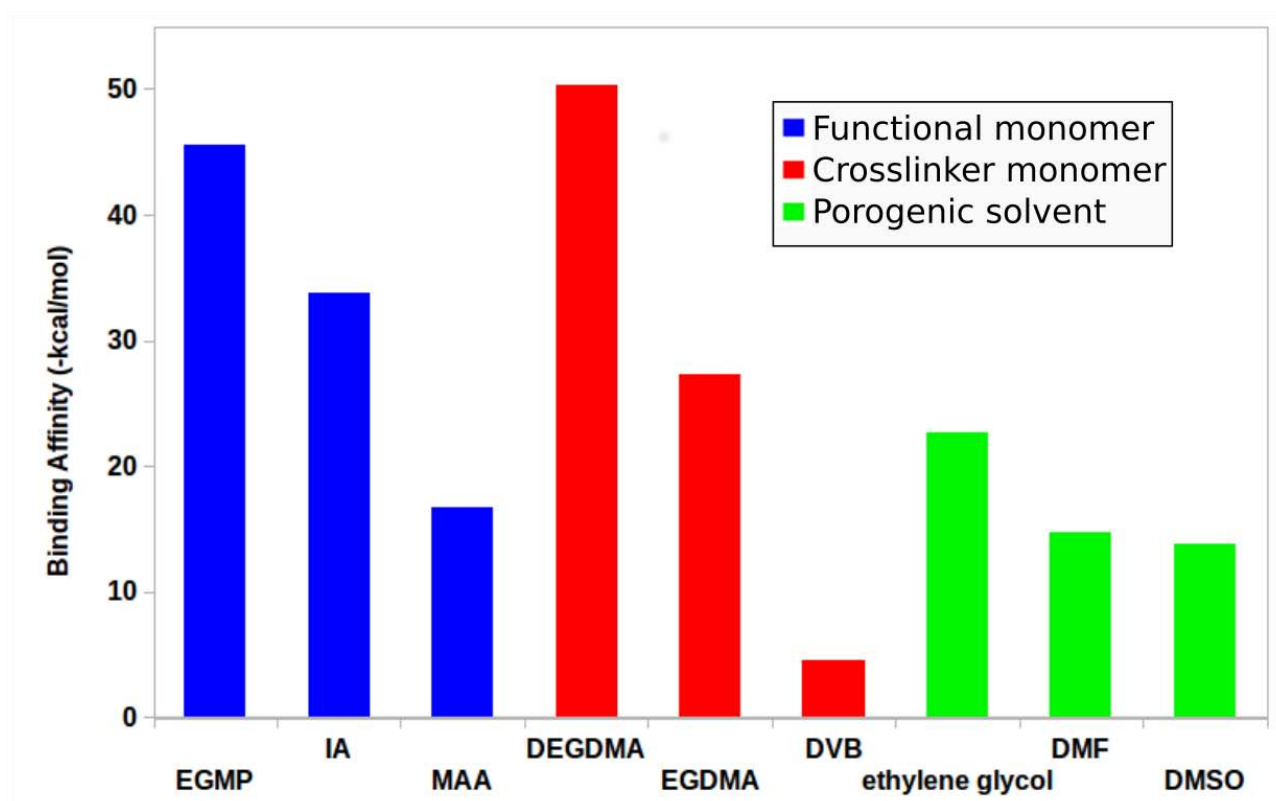


Figure 4.8: Histogram summarising the binding affinities of functional monomer, cross-linker monomer and solvent molecules for melamine as calculated by the SYBYL molecular modelling platform

Though the virtual scoring algorithm employed (described in detail elsewhere [26]), is optimised to predict the probability of hydrogen bond formation and strength, it cannot predict to what degree the intermolecular affinity and the formed complex will affect or augment the individual solubilities of each of the two molecules when combined in a solvent. Due to the poor solubility of melamine in organic solvents, the enhancing effect of the FM was heavily relied on its ability to dissolve it. Melamine's three amine groups, causing it to have a weakly basic nature, are most disposed to complex with acidic functional groups with respect to the enhancement of its solubility. Monomers

HEMA and acrylamide were unable to dissolve melamine in any solvent to the degree where conventional methods of molecular imprinting would be feasible.

Having failed to dissolve melamine in several conventional porogenic solvents, it was observed that each of the three acidic FMs, shown in Figure 4.8, could enhance the solubility of the template in DMSO to a level of 0.25 mol·L or 1 mmol in 4 mL. This implies e.g. an increase of template solubility by one order of magnitude for melamine, caused by the addition of the IA [27]. DMSO, though less commonly used than porogens such as DMF, acetonitrile or chloroform due to its relatively high polarity in addition to its augmented hydrogen bonding capacity and Hansen solubility parameters ( $\delta_T$ ) [23,24] may be acceptable where the template-FM complex is sufficiently durable. This is also reflected in the similar melamine-affinity scores given to both of these solvents by the molecular model (Figure 4.8).

### **Selection of the cross linking monomer**

For bulk synthesised MIPs, the addition of the cross-linking monomer can significantly alter the equilibrium of the solution. This equilibrium shift is especially apparent when the template molecule is present at saturated levels or if the complex between the FM and template is weak. Such a change in solution parameters can lead to the precipitation of the template in solution through the breakage of the stabilising bonds within the dissolved complex. While the use of a cross-linking monomer with higher template affinity may guard against this precipitation of low solubility templates, the consequence of this may be a higher incidence of non-specific interactions during post-polymerisation testing and use of the MIP.

*Di-*, *Tri-*, and *Tetra-* EGDMA exhibit increasing hydrophilic character. These monomers can be used as cross-linkers when a low solubility template or an unstable template-FM complex is being imprinted [28, 29]. The presence of an increasing number of oxygen atoms might also augment the probability of non-specific binding since they can each be employed as acceptor atoms in the formation of a hydrogen bond [30]. This can lead to lower specificity and poor imprint factors (IF). Conversely it is preferred to use cross-linking monomers which exhibit low affinity towards the template and thus does not compete with the binding mechanism of the template-FM complex. One combination of such a MIP is the use of MAA and DVB as FM and cross-linker respectively [31] whereby the VdW interactions between a template and cross-linker do not interfere with stronger

hydrogen-bonds formed by the template and FM at the receptor site as due to the nature of each's primary structural feature (Figure 4.9).

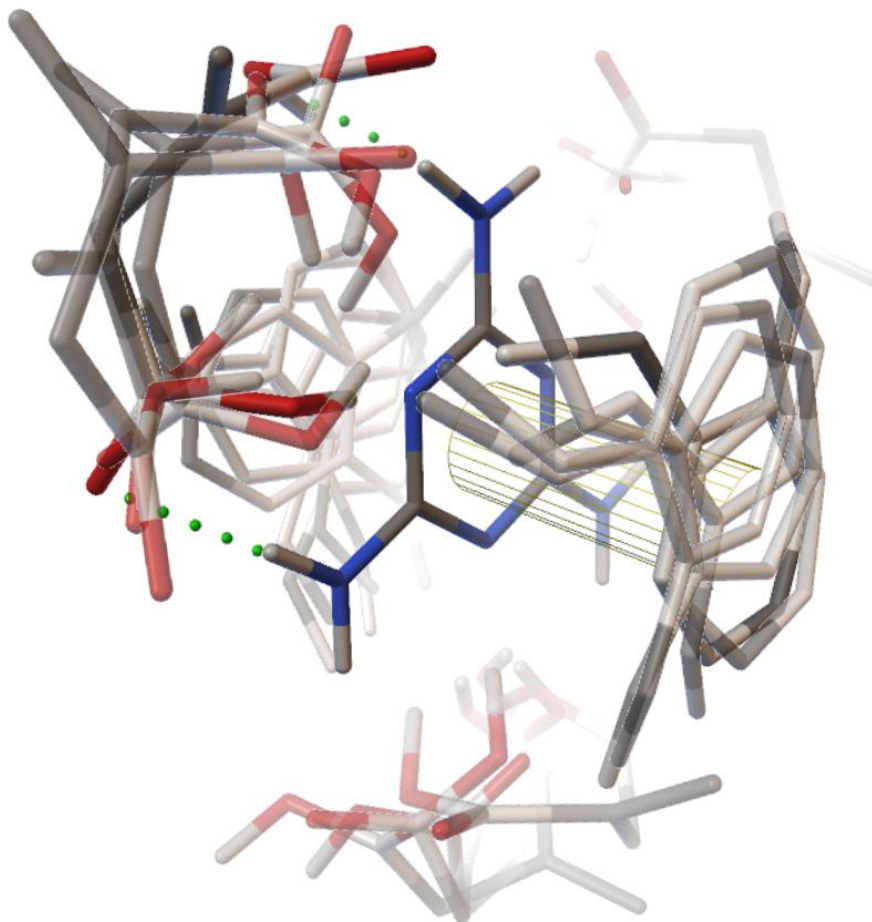


Figure 4.9: Superimposed docking modes of IA and DVB to melamine as predicted by the AD4 scoring algorithm with the latter exclusively interacting with the central aromatic ring and the former interacting solely with the peripheral amine groups

One of the most commonly used FMs, MAA, was rejected for this work because its predicted affinity was deemed too similar to that of the porogen DMSO. This has been confirmed by poor stability of melamine in a corresponding monomer mixture containing MAA. This precipitation did not occur when the higher affinity cross-linkers, EGDMA or DEGDMA, were added. These methacrylate monomers were also rejected as the affinity of these cross-linkers to melamine was interfering with the melamine-FM complex.

Ultimately, the combination of melamine, IA, DVB and DMSO for template, FM, cross-linker and porogen respectively, was considered to be optimal. The strength of the melamine-IA complex could also be immediately observed due to the stability of the solution upon the addition of the low affinity cross-linker DVB to monomer mixture, where no precipitation was observed.

Though IA and DVB was seen to be an excellent combination for the formation of a highly selective MIP, the necessity to use DMSO as a porogen in order to dissolve melamine raised concerns about the dynamic miscibility of the solution during polymerisation. Though the difference in  $\delta_T$  is an initially negligible issue due to the relatively low molecular weights of the (*mono*) DVB and DMSO, it becomes a hindrance to the homogeneous dispersion of DVB throughout the DMSO during polymerisation as the chain length and augmented molecular weight finally induces phase separation [32]. To confirm the feasibility of the use of DMSO as a porogen in this scenario, DVB polymer blanks were prepared using DMSO as well as the more commonly used porogens, chloroform and acetonitrile. SEM micrographs were taken to view the effect of the porogen on the formation of the second and third family pore structures with respect to increasing  $\delta_T$  [33].

As can be seen in Figure 4.10, the pore structure of the chloroform-DVB polymer shows high homogeneity with all microspheres completely merged. The intermediate  $\delta_T$  of the acetonitrile-DVB combination yielded adequate third family pore formation albeit with the merged microsphere-aggregates clearly visible in the morphology. Apparent puckering in the surface of the DMSO-DVB shows the endurance of the early stage microsphere-morphology due to a more abrupt phase transition. However, an acceptable third family pore structure is visible to a degree comparable to that of the acetonitrile-DVB polymer and was thus deemed satisfactory for use as a porogen for the DVB polymer.

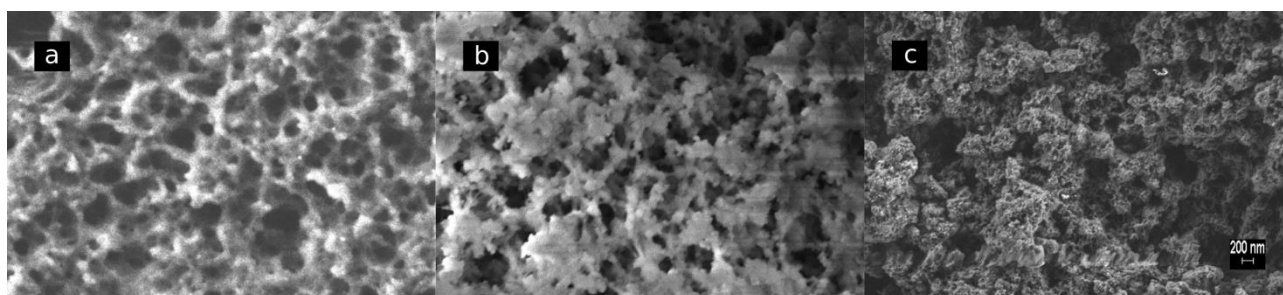


Figure 4.10: SEM micrographs showing the effect of differences in  $\delta_T$  and polymer-porogen miscibility on third family pore formation and homogeneity for (a) chloroform-DVB, (b) acetonitrile-DVB and (c) DMSO-DVB

### 4.2.2 Thermodynamic calculation of stoichiometric ratio and MIP composition

As an improvement on the standard 1:4 ratio generally employed in laboratory syntheses [34], determination of the ideal stoichiometry of a potential template-FM combination can allow for a greater deal of insight during the polymer and protocol design process. In order to optimise MIP composition, the knowledge of the ideal stoichiometric ratio between the template and FM, melamine and IA was required. By calculating the maximum number of FM molecules capable of forming high quality hydrogen bonds with the template, specificity and sensitivity can be maximised. This was achieved through minimisation of the formation of lower affinity binding sites [35].

The use of a computationally determined ratio alone, which is calculated under ideal conditions, has been reported to produce an inferior MIP with a high incidence of non-specific and heterogeneous binding behaviour caused by the disruption of the majority of the template-FM complexes by the solvent and cross-linker [36]. For this reason, an excess of monomer as a 'factor of safety' was added to the calculated ideal ratio. This factor of safety cannot be an unchecked saturation of the solution with the FM as this can also lead to FM-aggregation or dimerisation, also leading to a net reduction of receptors within the MIP [34, 37, 38].

Melamine-IA stoichiometric ratios of 6 were calculated by both computational methods attempted with both complexes showing identical bonds for each (Figure 4.11). This ratio of 6 with respect to the use of a carboxylic dipole is also independently confirmed by a third method recently published in the literature [17]. This ideal ratio of 6 was increased to 8 for the practical synthesis of the MIP.

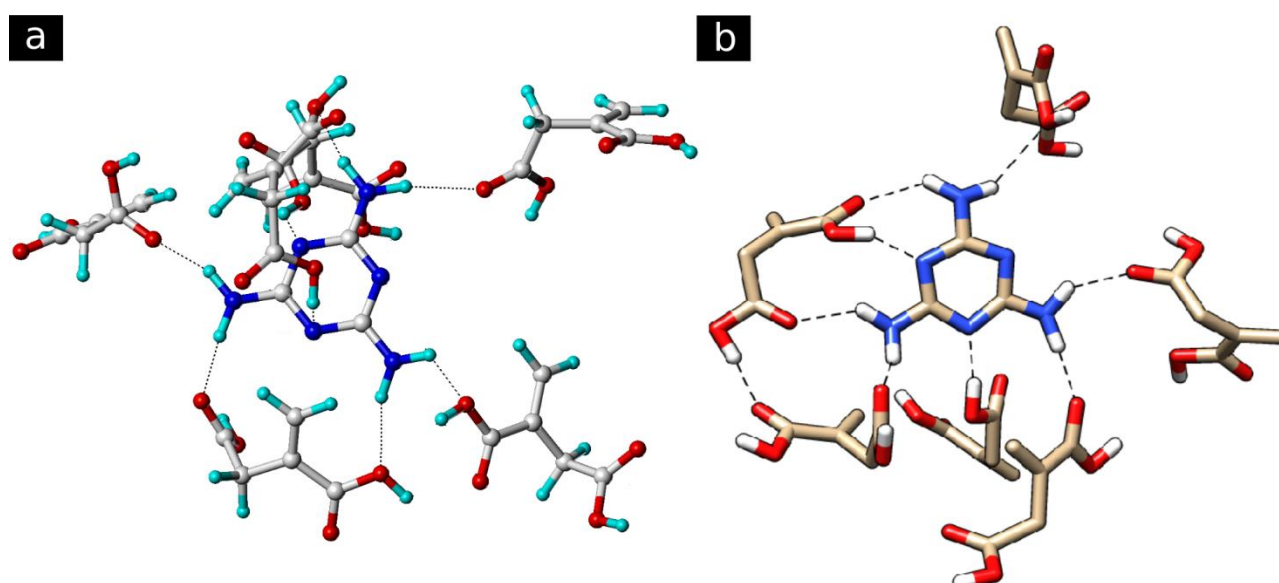


Figure 4.11: Image of ideal melamine-IA stoichiometric complexes calculated using parameters based on (a) the SYBYL modelling platform and (b) the open source Gromacs modelling platform

Thus the newly determined parameters for molecular dynamics protocol utilising the Gromacs open source molecular dynamics package were doubly confirmed. This confirmation of the Gromacs protocol is of added interest due to its departure from convention of the relaxation of the FM around the template via simulated annealing, from elevated to ambient temperature which has been the method of choice for the calculation of template-FM stoichiometric ratio to date. The Gromacs process, conversely, relies on a series of minimisation cycles followed by a final geometric optimisation and relaxation step all of which are conducted below physiological temperature limits and thus allow the calculation to be applied to thermally sensitive or biological molecules.

Having determined the optimal volumes of melamine, IA and DMSO which were dictated by stoichiometry and solubility limits, the calculation of the exact volume of cross-linker and initiator was calculated with the aid of the free online polymer calculator from the MIP database (see Materials and Methods). This allows for the facile calculation of all molecular and volumetric ratios with the inbuilt unit conversion facility. In this way, the masses or volumes of all of the polymerisation mixture can be balanced against the required volume of porogenic solvent, typically constituting to 50% of the total solution [34].

### 4.2.3 Selection of initiator and polymerisation temperature

The rate of radical propagation, of chain growth and the thermodynamic 'goodness' of the solvent all affect the point at which chain collapse and precipitation into the solution occurs. This precipitation point can be significantly delayed or advanced depending on the effect of the template. When the template has a high level of solubility in the porogen, the thermodynamic stabilisation of oligomer during chain growth leads to an enhancement in pore and precipitate size [39]. Alternatively, as is the case in this study, the decreased stability that melamine imbues to the growing oligomer was seen to force the precipitation of the chain at a shorter molecular weight and thus reduce the pore structure and net surface area of the polymer. Adding to the complexity of this effect is the enhancement of melamine solubility in DMSO with respect to increased temperature [40] which increases the stability of solvated melamine-IA complexes though any increase in temperature will have a similar effect on the rate of radical propagation [41]. A general rule of MIP synthesis with respect to the formation of selective binding sites is that the process should take place over a long period of time, at a low temperature and with a low concentration of initiator [42]. However, as is the present case, the final application of HPLC column packing media and the low thermodynamic stability of the melamine-IA complex required an elevated temperature to maintain sufficient mechanical rigidity and oligomer stability. The mass of the initiator was, however placed at a constant value of 44mg or 1% of the total monomer mass.

Two radical initiators were selected for polymerisation both of which had differing rates of decomposition ( $k_d$ ); AIBN at 60°C and AICN at 80°C decomposing at rates of approximately  $17 \times 10^{-5} \text{ s}^{-1}$  and  $6.5 \times 10^{-6} \text{ s}^{-1}$  respectively [41]. The latter can also be initiated via UV excitation at room temperature. The destabilising effect of melamine on the polymerisation process was most evident during room temperature polymerisation whereby phase separation was occurring 33% faster than in the case of the control. This clear and immediate demonstration of oligomer destabilisation in solution by melamine was reflected when the results of the porosity and surface area measurements were analysed (Table 4.2). Pore volume was reduced by one order of magnitude due to this effect with a similar reduction in total surface area. Due to the increased rate of radical propagation resulting from the AIBN-initiated polymerisation at 60°C, the pore volume was notably reduced from that of the slower radical production rate of the AICN-initiated polymerisation at 80°C. The pore volume of the NIP control was 140% that of the MIP. While the difference in surface area between the MIPs and NIPs of the two thermally initiated polymers was comparable, the very similar pore volume of the AIBN-initiated MIP and NIP cause it to be ultimately selected for further tests as it allowed for the most accurate analysis of the imprint factor.



Table 4.2: Summary of porosity and surface area measurements calculated using the N<sub>2</sub> BET method

Polymerisation type		Radical Initiator	Polymer ID	Pore Volume (cc·g <sup>-1</sup> )	Pore radius (Å)	Surface area (m <sup>2</sup> ·g <sup>-1</sup> )
temperature	Energy source					
20°C	UV	AICN	MIP	0.0077	9.6	24.61
			NIP	0.0265	9.3	75.88
60°C	Thermal	AIBN	MIP	0.1660	8.8	385.30
			NIP	0.1710	8.8	400.10
80°C	Thermal	AICN	MIP	0.6670	8.9	432.38
			NIP	0.9483	8.9	445.10

#### 4.2.4 Mobile phase selection and polymer characterisation

Following its selection as the polymer most comparable to its control, the AIBN-initiated MIP, polymerised at 60°C, was packed into HPLC columns. The use of the MIP as the stationary phase in a HPLC flow system has the distinct advantage of reducing the required detection time by decreasing the number of preparatory steps and negating the need for a separate regeneration process, as is the case with the more commonly used SPE method of detection. As a goal of this work was to create such an incorporated sensor, a comprehensive characterisation of the MIP was carried out under conditions typical to the detection of melamine-contaminated milk [43]. To facilitate the MIP's accurate characterisation, acidification of the mobile phase was necessary due to the failure of FM-FM dimerisation events during polymerisation. This dimerisation of surplus functional groups is essential to minimise non-specific interactions between the polymer and target, the absence of which may lead to the complete negation of any apparent imprinting event via the higher incidence of exposed functional groups at the surface of the polymer [34]. This phenomenon was made apparent by a high retention time, notably greater than that of the MIP, exhibited by the NIP toward melamine when a purely aqueous mobile phase was tested. This high retention time was accompanied by broad peak with extreme tailing caused by the exposure of IA-carboxylic groups on the surface of the NIP. Interestingly, in addition to the reduced retention time, the MIP column

also showed a greatly reduced level of tailing which was attributed to the higher level of order and reduced accessibility of the functional groups as more were engaged in a single receptor site at the MIP surface. The non-specific interactions exhibited by the NIP were disrupted with the acidification of the mobile phase with a weak acid. With the addition of 0.05% formic acid, the imprinting factor could be viewed and the polymer specificity characterised.

It was immediately notable that the peak tailing was still present in the NIP control even when the optimised mobile phase was implemented (Figure 4.12). Tailing was far less of an issue in the case of the MIP and its narrower peaks were accompanied with increased peak-symmetry. Optimisation of experimental conditions showed an increase in imprinting factor ( $\alpha$ ) with respect to reduced concentration and flow rate with a maximum value of 2.25 (Figure 4.13). A flow rate of 0.5 mL·min<sup>-1</sup> was ultimately selected due to practicality of the analysis.

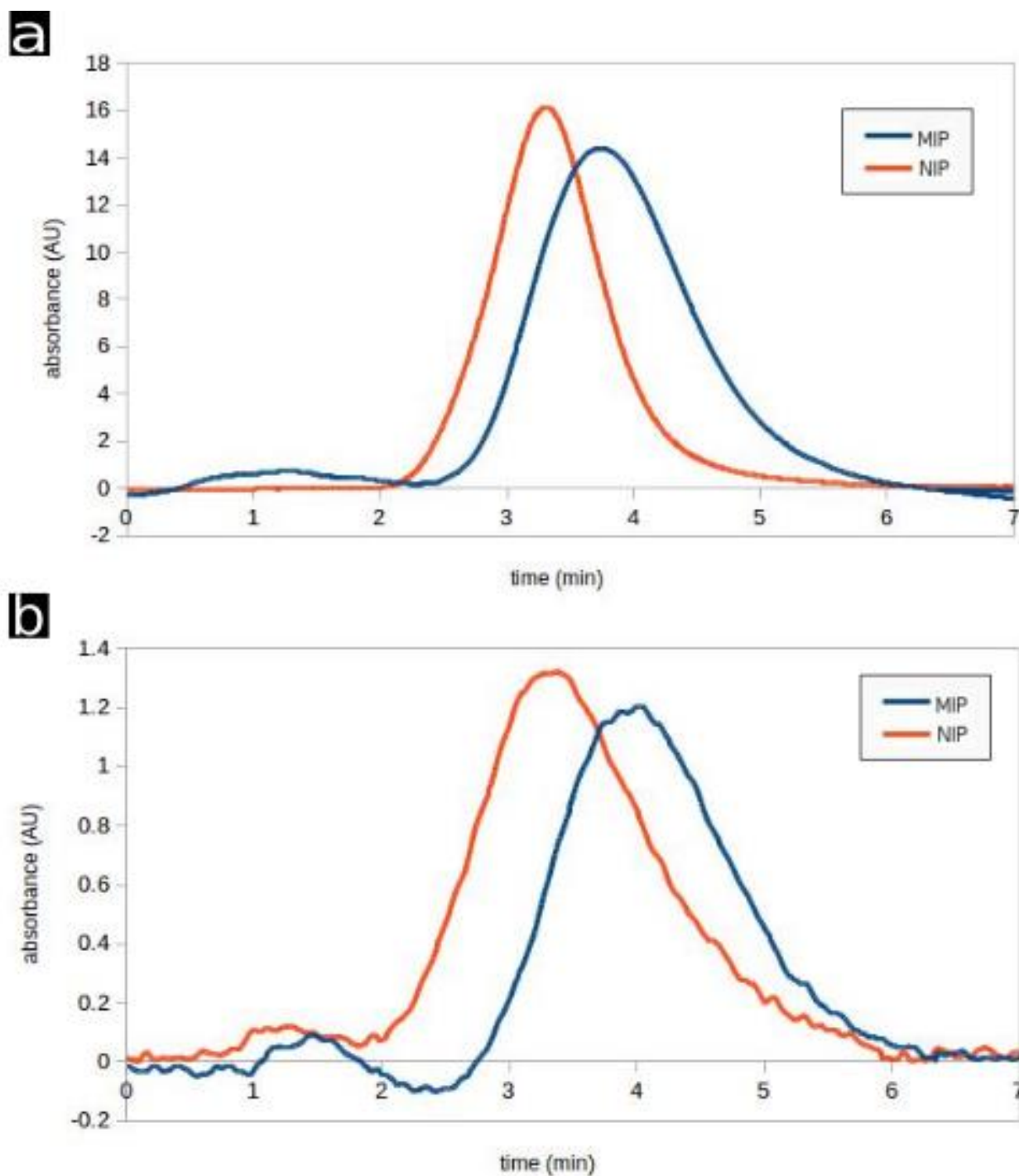


Figure 4.12: Chromatogram of the peak corresponding to a 10  $\mu\text{L}$  injection of (a) 100  $\mu\text{M}$  and (b) 10  $\mu\text{M}$  melamine solution in a 50:50:0.05 water, acetonitrile, formic acid and 0.5  $\text{mL}\cdot\text{min}^{-1}$  mobile phase

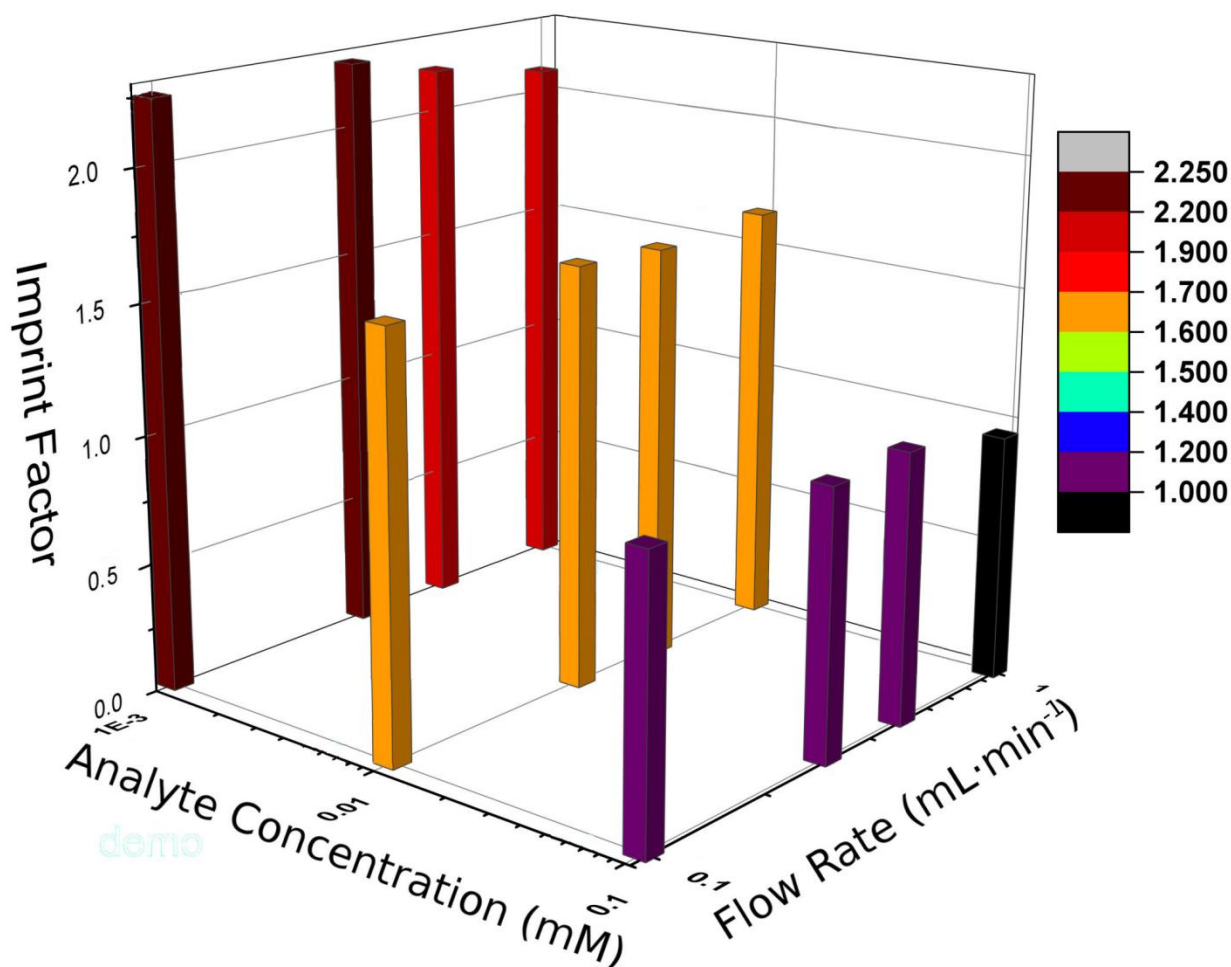


Figure 4.13: 3D histogram detailing imprint factor 'IF' as a function of flow rate and melamine concentration; injection volume was 10  $\mu\text{L}$

Cross-response of the polymer under these conditions could then be analysed. It was seen that due to the low affinity of the cross-linking polymer, DVB, specificity towards melamine could be rapidly achieved while secondary molecules were flushed through the column without any interaction (Table 4.3). Acetoguanamine, the molecule which exhibited a retention factor ( $k$ ) most similar to melamine, is retained notably longer on the non-imprinted polymer than melamine due to a higher primary affinity towards IA. This order is reversed on the MIP and must be attributed to the morphology of the imprinted receptors within its structure. Melamine recovery is also superior in the case of the MIP while for all other secondary molecules tested; the NIP control displayed improved recovery.

Table 4.3: Affinity and capacity factors characterising the (a) MIP and (b) NIP for cross response at a flow rate of  $0.5 \text{ mL} \cdot \text{min}^{-1}$  and a  $10 \text{ }\mu\text{L}$  injection volume of  $10 \text{ }\mu\text{M}$  concentration

(a)

	<b>Retention time (min)</b>	<b>k</b>	<b><math>\sigma</math></b>	<b><math>\alpha</math></b>	<b>% Recovery</b>	<b>N</b>	<b>H (mm)</b>
melamine	4.20	1.49	N/A	1.39	94.59	43.14	1.16
acetoguanamine	4.07	1.41	1.06	0.91	78.92	29.19	1.71
Cyanuric acid	1.55	-0.08	N/A	N/A	38.45	1.09	45.71
triazine	1.74	0.03	44.38	0.05	91.99	56.48	0.89
urea	1.60	-0.05	N/A	N/A	108.25	69.30	0.72

(b)

	<b>Retention time (min)</b>	<b>k</b>	<b><math>\sigma</math></b>	<b>% Recovery</b>	<b>N</b>	<b>H (mm)</b>
melamine	3.29	1.09	N/A	83.3	24.61	2.03
acetoguanamine	4.02	1.55	0.70	79.14	9.78	5.11
Cyanuric acid	1.53	-0.03	N/A	56.07	0.27	187.77
triazine	2.58	0.64	1.70	100.09	6.34	7.88
urea	1.79	0.14	7.91	114.77	22.31	2.24

#### 4.2.5 Testing on spiked real milk samples

Having confirmed the efficacy of the imprinting protocol and the resulting polymer, milk samples were prepared to test the ability of the MIP to detect melamine in its known role as an adulterant in dairy products. Five samples were selected from local supermarkets in order to encompass a range

of fat contents and product lifespans (Table 4.4). It was in the screening of these spiked samples that the limitation of the combined effect of the column length and polymer surface area was made apparent. The efficiency of separation power of MIP (as well as the Blank) columns did not allow separation of the melamine peak from all other compounds in all five samples tested (Table 4.3). For this reason, the organic fraction of the mobile phase was increased by 50% to improve peak separation. This had the desired effect and good recovery could be observed in four of the five samples tested (Table 4.5). The powdered samples showed greater levels of absorbance overall, possibly due to the presence of nondescript fibre within them, stated as being present at levels of 0.1% in sample 5. Improved recovery percentages using this polymer may be achieved with the use of a longer column which would compensate somewhat for the lower surface area observed in the MIP resulting from melamine's solubility issues.

Table 4.4: Description and content summary (g/100 mL) of milk samples tested

Sample	Description	Fats	Carbohydrate	Protein
1	Tesco everyday value British skimmed UHT milk	1.8	4.8	3.6
2	Pensworth Full fat whole milk	3.6	4.6	3.4
3	Pensworth low fat semi-skimmed milk	1.6	4.7	3.6
4	Tesco everyday value dried milk	0.06	3.0	2.1
5	Tesco Instant dried skimmed milk with added vitamins A & D	0.05	4.6	3.3

Table 4.5: Recoveries of melamine from the 5 milk samples detailed in Table 3

<b>Sample</b>	<b>% of total area</b>	<b>% Recovery</b>
1	17.22	94.16
2	17.39	96.11
3	17.28	66.91
4	16.17	90.07
5	14.78	88.87

### 4.3 Virtual Screening of Receptor Sites for Molecularly Imprinted Polymers

Using the experience gained from the research activities in UoL, further research into the use of computational models within the design process led to the identification of a unique feature of the open source Autodock model which was seen to have potential to provide an unprecedented new method of evaluating FM candidates with respect to the prospective receptors it could provide specifically for the design of receptors with a morphology to facilitate the cross reactive requirement of the Electronic tongue sensor array. This novelty manifested through a unique property of the virtual molecular docking suite, in concert with established thermodynamic calculation of the optimal stoichiometric template-FM complex already discussed and referenced in section 4.2.

The *modus operandi* of the Autodock algorithm is designed to reduce computational workload and processing time. To achieve this, the structures of receptors and ligands are independently defined. Bond types are defined only as connections between atoms while their effect is seen in the partial charge assigned to each atom when the molecule is save in the Autodock file format. The receptor is resolved to a static, rigid structure into which mobile ligands can be evaluated for dockability. The ligand structure is assigned a 'torsion tree' whereby a selected 'root' atom within its structure provides a reference point from which degrees of rotational freedom are assigned to 'branches'. The degree to which the receptor can restrict this ligand mobility, along with interactions between each molecule's structures, calculated via a number of superficially weighted, predefined parameters, allows Autodock to assign an affinity score to the receptor-ligand complex. This resolution of the receptor structure to a rigid body allows for the facile and rapid evaluation of these ideal stoichiometric complexes, created using more highly defined molecular modelling environments [44].

To demonstrate the potential of this technique, three case studies were selected to showcase scenarios in which visualization and interpretation of the model system might aid in the understanding and development of an experimental system. All results were obtained from independently conducted and experimental works, previously published by the UDC research group, allowing their findings to confirm the retrospective analysis. These systems are the detection of hypoxanthine, a metabolite of adenosine triphosphate (ATP) from food products [45, 46] using a selection of theophylline-imprinted polymers (section 4.3.1), Tetrahydrocannabinol (THC) using a Catechin-hydrate MIP with acrylamide as FM [47] (section 4.3.2) and the detection of Bisphenol A and Bisphenol F using a Bisphenol A MIP with 4-vinylpyridine as the FM [48, 49] (section 4.3.3). The structures for these molecules can be seen in Figure 4.14.



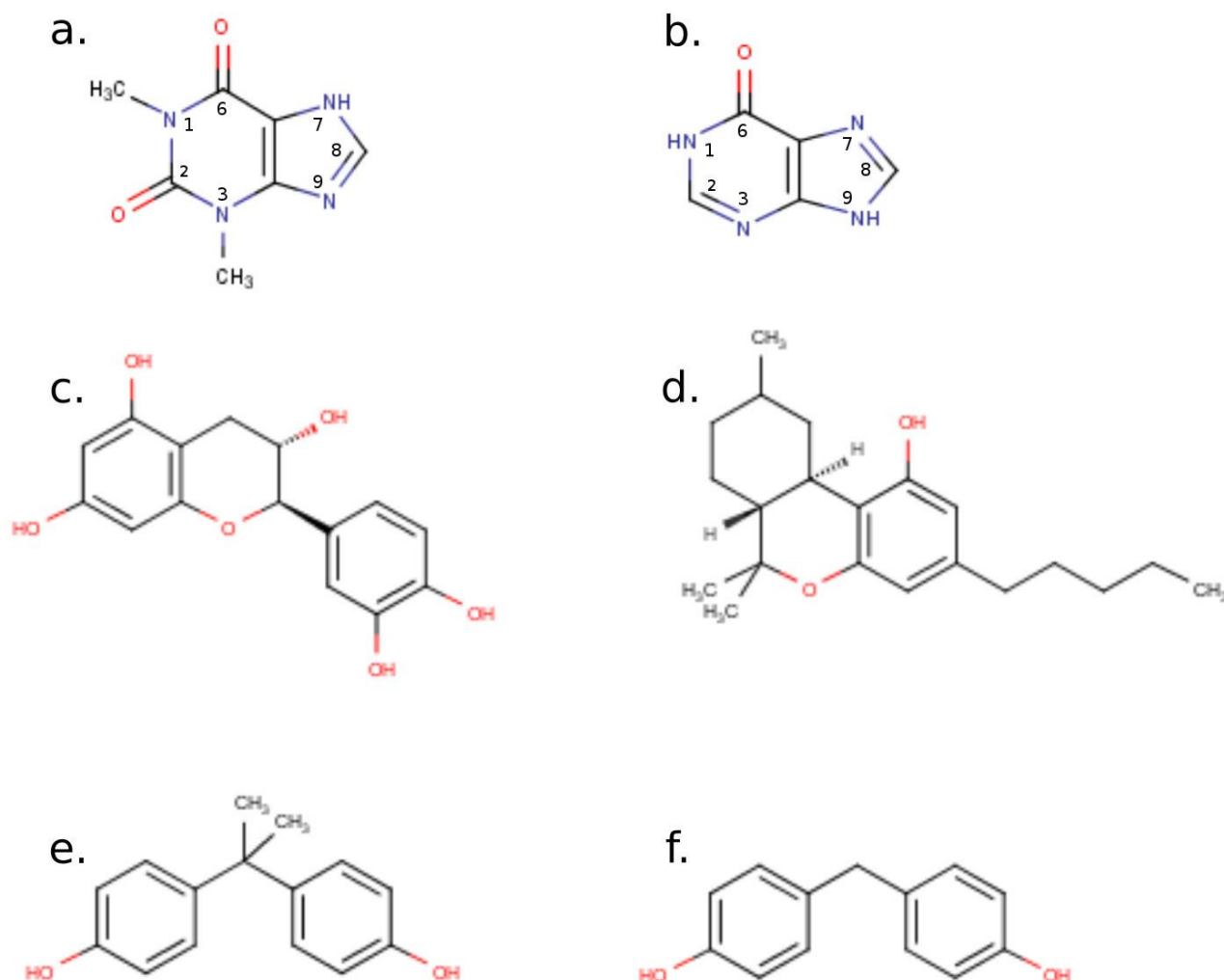


Figure 4.14: Two dimensional templates and structures of interest corresponding to the three case studies detailed in this work which were (a.) Theophylline, (b.) Hypoxanthine (section 4.3.1), (c.) Catechin-hydrate, (d.) Tetrahydrocannabinol (section 4.3.2), (e.) Bisphenol A and (f.) Bisphenol F (section 4.3.3); the numbering shown in (a) Theophylline and (b) Hypoxanthine structures are numbered using standard nomenclature convention, as referenced in Table 4.6

#### 4.3.1 Detection of hypoxanthine using a theophylline-imprinted polymer

The stoichiometric complexes between the MIP template (theophylline) and the FMs, acrylamide, HEMA and MAA were created using an established thermodynamic simulation protocol as detailed in the chapter 3. FM ratios of 5, 3, and 3 were attained for acrylamide, HEMA and MAA respectively (Figure 4.15) and the sites where hydrogen bonds were formed on the template were noted using standard nomenclature convention [50] (Table 4.6 b, Figure 4.14). This complex could

then be imported into the Autodock GUI, Autodock Tools [51] where the template could be removed; the remaining FMs were then saved as a rigid receptor file, thus securing the exact topology of the FMs and creating a “virtually imprinted” receptor site. The target and tautomeric structural analogue of theophylline, hypoxanthine, could then be docked as a ligand into this receptor using the Autodock “VINA” scoring function. [52]. The docking affinity score, re-formation of hydrogen bonds and the spacial “dockability” of hypoxanthine to the receptor was compared both between receptor sites and also with that of theophylline (Figure 4.15, Tables 4.6 and 4.11). As expected, acrylamide provided the strongest docking affinity in both the predicted and experimental models due to the combined effect of a high stoichiometric ratio with the dummy-template and highest rate of hydrogen bond re-formation with the target. In addition to this, the affinity of the primary template–FM complex was experimentally determined to be an order of magnitude higher than the other two FM candidates [45] thus ensuring a high probability of imprinting success during polymerization.

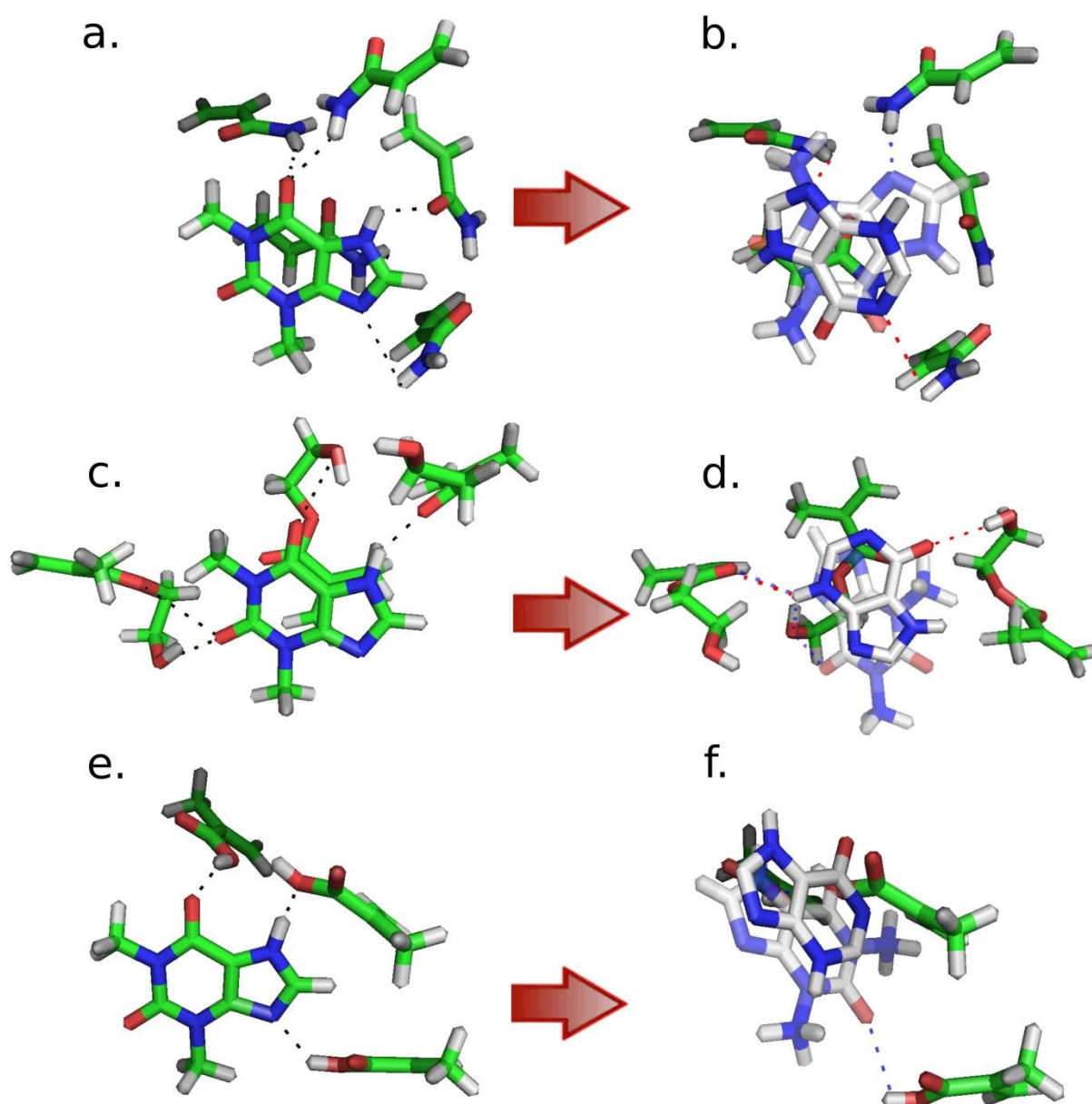


Figure 4.15: Predicted stoichiometric complexes between theophylline and acrylamide (a), HEMA (c), and MAA (e) formed through thermodynamic simulation performed in SYBYL, and the primary docking modes predicted by VINA for hypoxanthine and theophylline (transparent) for the acrylamide (b), HEMA (d) and MAA (f) receptor; hydrogen bonds are shown for hypoxanthine (red) and theophylline (blue)

Table 4.6: Sites of the hydrogen bonds formed on the template and ligand structures for primary template–FM complexes (i.e., the location of the strongest and most probable hydrogen bonds) (a), and for the predicted stoichiometric complex (b) and the redocking event (c).

(a)

	<b>Theophylline<sup>a</sup></b>	<b>Hypoxanthine<sup>a</sup></b>
<b>Acrylamide</b>	7N-H; 6-O	1N
<b>HEMA</b>	7N-H; 6-O	7N-H; 6-O
<b>MAA</b>	7N-H; 6-O	7N-H

(b)

	<b>Theophylline-FM stoichiometric ratio</b>	<b>Site of hydrogen bonds<sup>a, b</sup></b>
<b>Acrylamide</b>	5	(6-O [2.3], 6-O [2.2]); 7N-H [2.5]; (9N [2.8], 9N [3.1])
<b>HEMA</b>	3	2-O [1.8]; 6-O [1.9]; 7N-H [2.8]
<b>MAA</b>	3	6-O [1.7]; 7N-H [1.8]; 9N [2]

(c)

	<b>Theophylline<sup>a, b</sup></b>	<b>Hypoxanthine<sup>a, b</sup></b>
<b>Acrylamide</b>	9N [1.9]	1N [3.6]; 9N [4.2]
<b>HEMA</b>	(6-O [2.3], 7N-H [2.6]); 7N [2.8]	3N-H [2.3]; 6-O [2.8]
<b>MAA</b>	6-O [2.7]; 2-O [2.7]	N/A

*a) Sites of hydrogen bonds are defined on the template and ligand structures using standard nomenclature convention [50] (Figure 4.14); b) parentheses indicate that multiple FMs bonding with the same ligand atom while semicolons separate sites on the ligand structure with bond length of each given in [Å] after each entry.*

Table 4.7: Docking affinity scores ( $\text{kcal}\cdot\text{mol}^{-1}$ ) for theophylline-imprinted receptors shown in Figure 4.14 predicted by the VINA scoring function and by laboratory experimentation.

	<b>Hypoxanthine</b>		<b>Theophylline</b>
	<b>Experimental</b>	<b>VINA Score</b>	<b>VINA Score</b>
<b>Acrylamide</b>	5.34	25.	16.8
<b>HEMA</b>	5.09	24.1	16.4
<b>MAA</b>	2.75	22.8	14.7

The novelty of this technique, however, is not seen in the confirmation of the highest affinity template–FM combination, but rather in the explanation that it provides for the sizable difference in performance for the HEMA- and MAA-based MIPs. Though both FMs shower comparable primary affinity scores, with MAA actually out-performing HEMA, the HEMA-based MIP exhibited affinity towards hypoxanthine closer to the acrylamide- based MIP while the MAA-based MIP displaying the poorest hypoxanthine-affinity of all (Table 4.7). As this cannot be explained by the calculated primary affinity of the template–FM complex, it must then be assumed that the enhancement must come, instead from the topology of the imprint created template–FM stoichiometric complex and the orientation of the FM dipoles within the imprinted receptor. Visualization of the redocking event and of the imprinted-receptor itself clearly shows that hypoxanthine docks most efficiently into the receptor created by HEMA, aligning the molecule most closely to the imprinted template, theophylline, of the three receptors examined (Table 4.6 c). This can be specifically attributed to the HEMA molecule interacting with the “2-O” oxygen atom on theophylline’s structure; this interaction is unique to HEMA, with the acrylamide and MAA stoichiometric complexes forming around the opposite side of the template. Furthermore, regarding the HEMA receptor, the alignment of the interacting donor–acceptor atoms during the imprinting of theophylline and the hydrogen bonds formed upon the docking of hypoxanthine are the most similar of the three. Additionally, hydrogen bonds predicted to form between hypoxanthine and the theophylline-imprinted HEMA receptor involve the functional groups of the primary hypoxanthine–HEMA complex (Table 4.6 a) thus providing the highest probability of such docking event occurring homogeneously en-mass, thus making them experimentally detectable in practice. The poor experimental performance of MAA receptor can be attributed to its inability to form hydrogen bonds with hypoxanthine upon redocking. In the absence of such strong directional bonds, the potential energy between the MAA functional groups and hypoxanthine may not be strong enough

to desolvate the molecule out of its solvent cage and into the receptor cavity. This issue is compounded by the hydrophobia of the crosslinking polymer which further reduces the aqueous performance and experimental affinity of the MIP-receptors. An aspect discussed at greater length in section 4.3.2. In the case of the acrylamide receptor, whose monomers were in positions similar to those of the MAA receptor, the increased stoichiometric ratio and higher primary affinity both serve to position the hypoxanthine molecule in an orientation which is then more favourable to hydrogen bond formation, thus providing sufficient energy to capture the target molecule from the solution through the concerted effect of the functional groups of the FMs. The increased level of insight which the technique detailed in this communication provides, not only serves to rapidly evaluate the imprinting efficiency and performance of a receptor, but also can greatly reduce laboratory man-hours and costs due to its ability to rapidly simulate docking events for large numbers of both ligand and monomer libraries. This allows the user to make an accurate prediction of the specificity of the MIP using specific template–FM combinations, thus eliminating poor combinations *ab initio*. This, in turn, reduces the laboratory workload and screening time whilst also decreasing negative environmental impact through a reduction of harmful waste products resulting from laboratory synthesis and experimentation.

#### **4.3.2 Detection of Tetrahydrocannabinol using Catechin-Imprinted Polymers**

Tetrahydrocannabinol (THC), the psychedelic compound responsible for the associated effects of marijuana consumption, is present in its metabolized form in blood, saliva and urine for a duration following its initial ingestion and has been claimed to impair various bodily faculties essential for many professional activities. It is often present at low levels and thus can be difficult to detect [53]. As a potential template for molecular imprinting, it also is a poor candidate due the low number of functional groups on its surface and thus is an excellent candidate for dummy imprinting or, rather, as a molecule of interest to be targeted by a MIP, imprinted with a dummy template.

In this case, contrary to that of the detection of hypoxanthine as an ATP derivative detailed in section 4.3.1 above, testing of effluent and bodily excretions in the form of urine and saliva brings the sensing mechanism into contact with a vastly increased array of potential molecules as they potentially contain any and all metabolites and xenobiotics ingested and created by the candidate. Given that the accurate and positive detection of THC in human samples is of such interest with respect to illicit activity in many countries, it is seen as a molecule of high interest within the field of sensors.

Within this following section is detailed a computational analysis correlated with the experimental work carried out, looking at the imprinted receptor cavity created using catechin-hydrate (CAT) and acrylamide (ACR) as the template and functional monomer respectively; EGDMA was used as the crosslinking co-polymer and the low volatile solvent triethylene glycol dimethyl ether (TRIGLYME) and a non-reactive linear polymer, poly (vinyl acetate) as co-porogens. The experimental results detailed and used in this study are discussed in greater detail in the published article [47].

### **Experimental description**

In order to test the experimental efficiency of CAT as a dummy template for THC, two practical experiments were conducted [47]. The first of these was to determine the effect of the imprint on the binding behaviour, or rather, the suitability of CAT-imprinted receptor for the detection of THC; to test this hypothesis, THC at a concentration equivalent to physiological levels, 2.5 ppm, was dissolved in a 6:4 solution of water and ethanol and saturation binding experiments were performed using the MIP and NIP. The second experiment was conducted to investigate the effect of interferent molecules on the binding mode and the degree to which the docking event into the imprinted cavity could be disrupted by common, legal pharmaceuticals (i.e. caffeine and acetaminophen). In this second experiment, THC, caffeine (CAF) and acetaminophen (ACE) were each added in equal quantities to the level of 2.5 ppm in an identical solution of water and ethanol. Saturation binding experiments were then performed under identical conditions. The results of these experiments are shown in Table 4.8.

Table 4.8: (a) THC binding results as a percentage and proportion per polymer unit mass of total THC present in the binding solutions (2.5 ppm); (b) binding results of the ternary mixture of THC, CAF and ACE present at concentrations of 2.5 ppm each, given as percentages of their respective concentration, proportion of total concentration, and total bound concentration per polymer unit mass

(a)

	<b>MIP</b>	<b>NIP</b>
<b>THC (% total concentration)</b>	75.45	55.23
<b>Total bound concentration (mg/L/unit polymer mass)</b>	1.886	1.38

(b)

		<b>MIP</b>	<b>NIP</b>
<b>Bound molecules (% total concentration)</b>	THC	45.59	39.94
	CAF	10.67	11.65
	ACE	3.31	3.85
<b>Bound concentration (mg/L/unit polymer mass)</b>	THC	0.25	0.291
	CAF	0.069	0.096
	ACE	1.139	0.9985
<b>Total bound concentration (mg/L/unit polymer mass)</b>		1.458	1.385

### Complexation mode and receptor evaluation

Following the thermal annealing protocol described above, the ideal stoichiometric ratio between CAT and ACR was calculated; the maximum ratio of 7 can be seen in Figure 4.16. As expected, formation of the stoichiometric complex was concentrated at the extremities of the molecular structure and only a moderate strength hydrogen bond predicted to form at the central ring. Analysis of bond length and location, shown in Table 4.9, indicated the formation of a strong complex with a high probability of survival through the polymerization process.

It is interesting to note the apparent absence of interaction at the centre of the molecule though it must also be recalled that large hydrophobic areas on the template structure may create



complementary features within the receptor cavity through hydrophobically driven interactions between the FM, co-polymer and template.

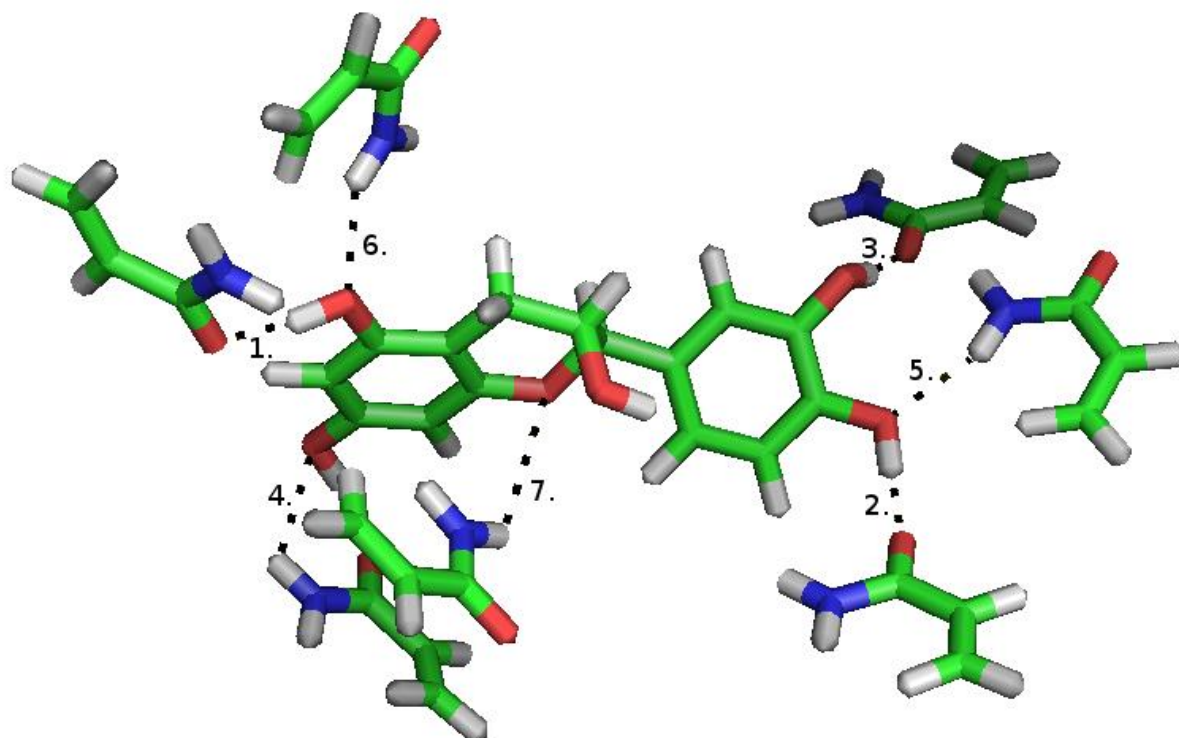


Figure 4.16: Ideal stoichiometric complex between CAT and ACR as calculated using the SYBYL modelling suite; hydrogen bonds are numbered in order of increasing distance, and corresponding strength, between the involved donor and acceptor atoms (Table 4.9)

Table 4.9: Bond distances and strengths [30] corresponding to the complex shown in Figure 4.16

	<b>Donor- Acceptor Distance (Å)</b>	<b>Bond strength</b>
<b>1.</b>	1.653	Strong
<b>2.</b>	1.667	Strong
<b>3.</b>	1.682	Strong
<b>4.</b>	1.746	Strong
<b>5.</b>	2.219	Moderate
<b>6.</b>	2.322	Moderate
<b>7.</b>	3.097	Moderate

### Interpretation of rebinding modes and correlation with experimental results

The binding modes predicted by the Autodock algorithm can be seen in Figure 4.17. For the template, CAT, an effective rebinding mode can be seen with functional groups from several monomers being engaged in strong to moderate hydrogen bonds. THC, the target molecule, successfully formed only one high energy hydrogen bond though at least one further bond can be seen in the optimal docking mode thus demonstrating a specific imprint effect. The potential interferants, CAF and ACE however, formed complexes which engaged only one hydrogen bond indicating a significant potential non-specific interaction due to the comparative size of the receptor. The predicted affinities of these interferants are also significantly higher than that of THC thus raising the concern that in a physiological environment where competitive binding was an issue, effective capture of the target, THC, would be blocked.

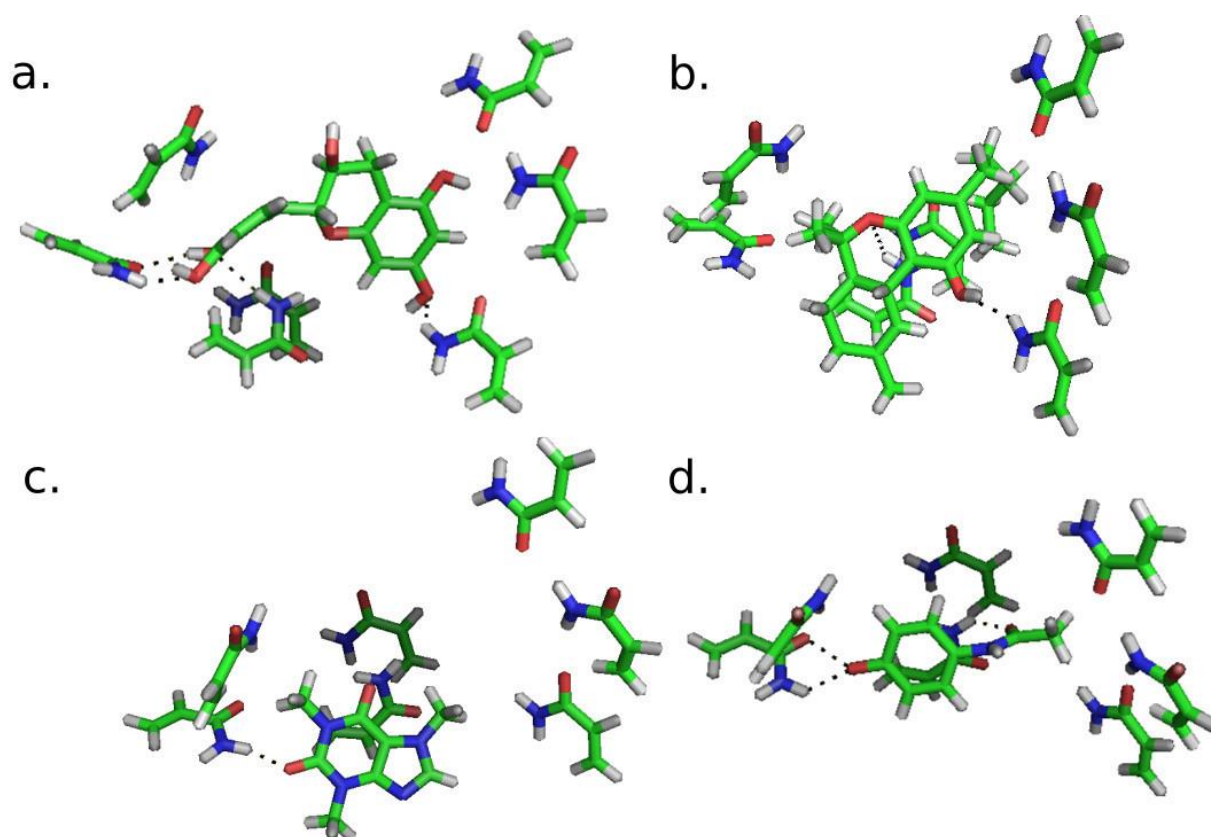


Figure 4.17: Aqueous binding modes predicted by the Autodock VINA algorithm into the CAT-ACR receptor site created from the stoichiometric complex shown in Figure 4.16; ligand molecules shown are CAT (a.), THC (b.), CAF (c.) and ACE (d.)

Viewing the projected modes and more specifically, the formation of strong hydrogen bonds, the template of the imprinted receptor, CAT, was able to dock most efficiently with the receptor site, forming hydrogen bonds with the highest number of individual FM. Additionally, the mode was relatively symmetrical when compared with those of the other molecules tested. This can be seen in the quite uniform contribution that each ACR monomer made to the overall predicted docking affinity (Figure 4.18). THC, the structural analogue and primary target of this study, succeeded in forming 2 favourable hydrogen bonds and also in displaying some imprint-related docking affinity though the molecule, notably, does not have the same homogeneous primary docking mode as CAT, the original template (Figure 4.17). The smaller interferent molecules, CAF and ACE both had significant asymmetry in their predicted binding modes, indicative of a nonspecific, poorly docked molecule.

Viewing the aqueous solubilities of each of these three molecules, however, reveals a differential of several orders of magnitude between THC and the interferants (Table 4.6). The significant hydrophilic nature of the interferants is an indication that these molecules will be more disposed to disrupt binding rather than participate in or be captured by such events. This was reflected in the

practical laboratory results. It can be seen that, though the control NIP bound an almost identical quantity of molecules in both cases (Table 4.8), the quantity bound by the MIP in the pure THC solution (Table 4.8 a) and that of the ternary mixture of molecules (Table 4.8 b) differed by a significant amount, amounting to a 23% net reduction in particles bound per unit mass of polymer. While this sensitivity displayed by the MIP relative to the NIP can be explained by the increased order of exposed functional groups within the MIP which tend to form FM-FM dimers in the NIP. This results in the decreased exposure of molecular dipoles to the polar aqueous solvent at the polymer surface and thus makes high affinity hydrophilic molecules more likely to block and disrupt docking events within the confined pores of the MIP and simultaneously less likely to bind themselves within the hydrophobic cavities of the MIP, remaining in their higher energy solvent cages.

Table 4.10: Aqueous and ethanol solubilities of the components of the ternary mixture

	<b>Water (g.L<sup>-1</sup>)</b>	<b>Ethanol (g.L<sup>-1</sup>)</b>
<b>ACE</b>	12.78 [54]	190.61 [54]
<b>CAF</b>	20 [55]	15 [55]
<b>THC</b>	0.001 – 0.002 [56]	35 [57]

The proportion of THC bound by the MIP was reduced by double that of the NIP indicating a significantly higher disruption in the case of the MIP rather than the NIP. In addition to this, though the disruption seen by the MIP was significantly higher than that of the NIP, the proportion of interferent molecules captured was in fact higher for the NIP than the MIP, pointing to an increased hydrophilic interface at the NIP surface resulting from a greater number of exposed FM functional groups and thus causing an increased incidence of hydrophilic interaction.

#### **Effect of the number of monomers in the receptor on docking affinity**

Given that the initial aqueous docking modes utilized only one half of the predicted ideal binding site, a further investigation into the effect of the number of FM molecules within the receptor site the predicted binding affinity. In this manner, 7 receptor sites were created containing from 7 to 1 ACR monomers; the order in which the monomers were deleted was determined by distance from the CAT template molecule which, in turn could be approximated to a hierarchy of hydrogen bond strength (Table 4.19) and thus probability of *in situ* formation in the presence of solvent and co-polymer molecules.

These 7 sites were then screened against the 4 molecules of interest, CAT, THC, CAF and ACE. As shown in Figure 4.18, the original template showed the greatest and most linear decline in affinity with respect to the reduction of functional groups and thus showing the greatest sensitivity to the shape and aspect of the receptor site. Two intermediate slopes can be seen corresponding to stoichiometric ratios from 3 to 4 and then from 5 to 7, while there is no imprint-related behaviour at ratios between 1 and 2. It is highly interesting to note that the initial four molecules of ACR, which formed strong hydrogen bonds in the initial complex (Figure 4.16), constitute the most integral part of the imprint-related specificity receptor site as seen in the steep increase in receptor affinity for CAT. This sharp slope then tapers off at the increased stoichiometric ratios. This highly apparent imprint-effect within the receptor sites formed from strong hydrogen bonds during synthesis ensure a high probability of a good imprinting factor for the MIP when compared to the NIP control.

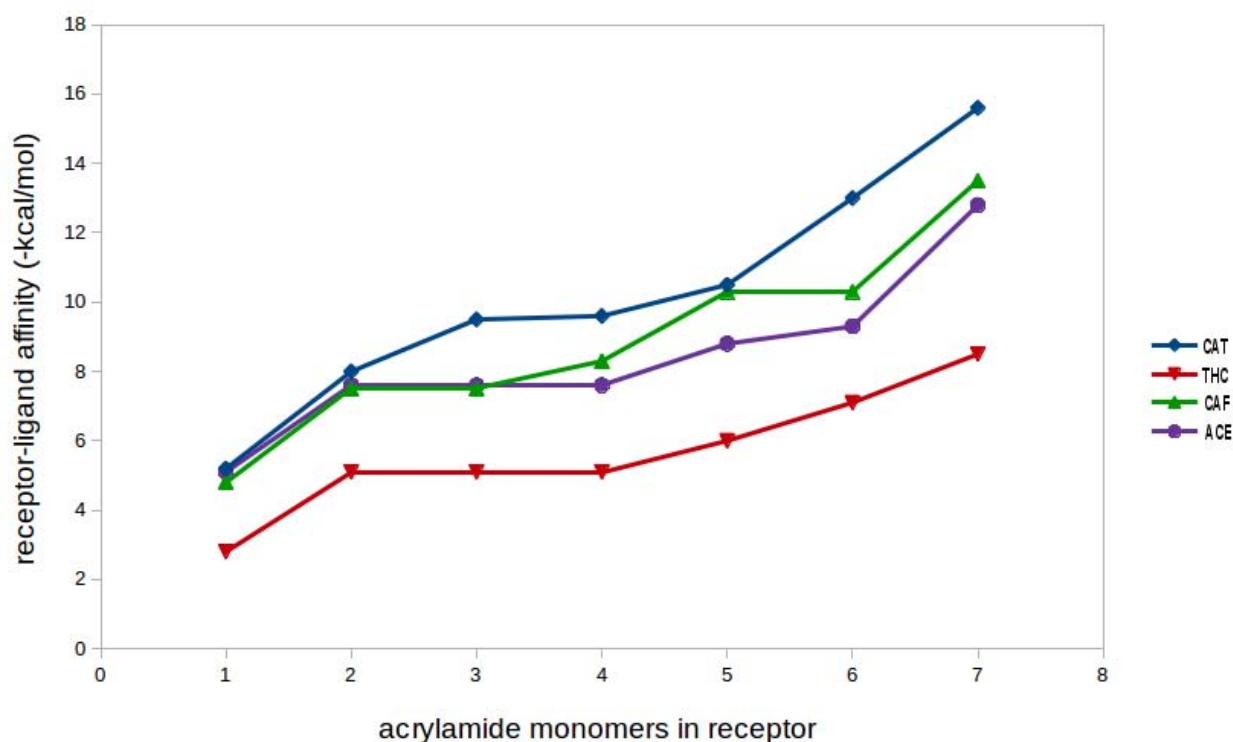


Figure 4.18: Receptor-ligand affinities calculated by Autodock VINA for the four molecules of interest, CAT, THC, CAF and ACE. 7 receptor cavities were tested, each of contained an additional ACR molecule which were added in order of distance from the template molecule (Figure 4.16; Table 4.9)

In the case of the actual target molecule for the MIP, THC showed a consistently lower affinity than that of the interferants, CAF and ACE. Relatively parallel slopes for each of these three molecules may also be used as a confirmation of a consistent and high potential for the disruption of THC docking events when attempted in the presence of these secondary molecules.

The final notable point from this study comes from the plateau of docking affinities seen between FM ratios of between 5 and 6 which is not present for the template molecule thus indicating the asymmetry of the docking modes for the secondary molecules into the receptor cavity relative to the actual template, CAT, which is inherently better suited for docking into the receptor (Figure 4.18).

### Correlation of virtual and experimental results

It must be remembered at all times that the docking modes and affinities predicted by the VINA virtual model neglects the effect of the crosslinking co-polymer on the binding event. While the evaluation of the interactions between the functional groups of the receptor site are highly applicable to the prediction of the specificity and performance of the receptor sites, the effect of the co-polymer must be recalled when interpreting the virtual data. In other words, favourable ligand docking and receptor affinity is not necessarily indicative of net capture of the ligand by the MIP throughout its structure.

To explain this behaviour, it must be recalled that the co-polymer typically constitutes approximately 70 – 80% of the MIP's overall mass. The monomer from which this co-polymer is formed is ideally devoid of functional groups or has low interaction potential in order to minimize its interference with the primary template-functional monomer complex. The apolar nature which is imparted to the MIP upon polymerization results in a hydrophobic character and an overall reduced aqueous performance of the MIP [58]. It follows that this hydrophobic nature, inherent to conventional MIPs, would also promote hydrophobic interactions thus increasing performing when the targeted molecule is also hydrophobic.

It is at this point that a misinterpretation of the experimental data may occur whereby a low instance of capture may be taken to indicate low affinity between that molecule and the imprinted receptor cavities within the MIP. On the contrary, the more hydrophilic molecules interact to a great extent with the receptor sites even if the overall hydrophobia of the MIP cavity does not allow desolvation of the molecules into the receptor cavity. This high interaction between the functional groups at the receptor cavity and highly soluble molecules serve to greatly disrupt the docking of the primary target; in this case the docking of THC into the dummy-imprinted (CAT) receptor cavity being disrupted by CAF and ACE.

The results of the experimental study of the competitive binding between THC, CAF and ACE can be seen in Table 4.8 b Equal concentrations (2.5 ppm) of the three molecules were dissolved in a binary mixture of water and ethanol in the proportion of 6:4 respectively. While the solubility of THC increases significantly from water to ethanol, CAF's solubility reduces slightly while remaining relatively static. ACE solubility, however, increased from 12 to 190 mg.ml<sup>-1</sup> when solvated in ethanol rather than water; this extremely large difference in the solubilities of the molecules of interest complicates the interpretation of the experimental data (Table 4.10).

Though the initial binding experiment (Table 4.8 a) indicated a favourable imprint-related preference of the MIP for THC, binding approximately 30% more of the total concentration of THC

present in the solution, when this experiment was repeated in the presence of ACE and CAF, this differential for THC was reduced to just a few percent relative to the NIP while the quantity of ACE and CAF did not replace the THC inhibited from binding by these interferants (Table 4.8 b). The result of this is that, though the NIP bound an almost identical quantity of molecules for the single and competitive binding experiments,  $1.38 - 1.385 \text{ mg.L}^{-1}$  per unit mass of polymer, the MIP suffered a significant loss in performance between the two experiments with its specific binding capacity falling from  $1.886 - 1.458 \text{ mg.L}^{-1}$  per unit mass of polymer.

This significant reduction in performance must only be due to the disruption of THC-receptor docking events by the interferent molecules with higher docking affinities towards the receptor cavity as predicted by the VINA algorithm (Figure 4.18). This disruption of primary docking events is, however, not accompanied by the capture of these secondary molecules which the MIP fails to capture, thus resulting in the significantly poorer performance of the MIP in the presence of these interferants.

Viewing the percentage of CAF and ACE bound, one is confronted with an additional conundrum which is that, whereas the virtual model predicts comparable affinity scores for both of these molecules, ACE is bound in a significantly lower quantity than CAF, having only 3.31% and 10.67% of their total concentration bound to the MIP. This discrepancy can be explained when the solubilities of these molecules are taken into account (Table 4.10). Though they both have comparable aqueous solubilities, their solubilities in ethanol differ by an order of magnitude thus making ACE far more resistant to desolvation than CAF.

It is thus finally confirmed both computationally and experimentally that CAF and ACE serve as significant interferants to the binding and capture of THC by the CAT-ACR MIP through the disruption of THC-receptor docking events via the superior affinity of CAF and ACE to the receptor.

This disruption was not accompanied by the capture of these interferants due to high aqueous and ethanol solubility in which these experiments were conducted. It is thus accepted that the use of the virtual model, VINA, can be used to indicate docking events in a competitive setting though, as the co-polymer is not included in the receptor file, VINA cannot be used as a predictor of molecular capture by the MIP. Instead it may be used as a predictor of preferential interaction with the receptor site while the degree to which the docked molecule is captured by the MIP as a whole must be estimated by the solubility of the molecule in question in the solvent.



#### 4.4.3 Design of a Bisphenol A –Imprinted Polymers

Bisphenol A (BPA) is a molecule of high interest due to its potential carcinogenic nature and low dose toxicity. This has encouraged the development of detection methods given its high prevalence in baby bottles, food-storage containers, medical equipment, and consumer electronics [59, 60].

As low concentration chronic exposure is the most common and dangerous type of potential risk, the use of MIPs to detect BPA is logical. In addition, BPA has low and high solubility in aqueous and organic solvents respectively and so, it should be highly favourable for conventional non-covalent molecular imprinting protocols as such imprinting events are typically carried out in an apolar organic environment at relatively high concentrations.

The challenge of imprinting BPA manifests itself in the low number of functional groups within its structure which consists of two hydroxyl groups and two aromatic rings. The polymer research group at the University of Coruña (UDC) has already published a detailed account of the design and development of a BPA-MIP with a substantial body of experimental data including extensive study of the intermolecular interactions between BPA and the selected FM, 4-vinylpyridine (4VP) [48]. A further report on the binding behaviour and performance of the MIP for the capture and detection of BPA in water samples has also been published [49]. In this case study, the experimental results were accurately predicted by the virtual modelling protocol detailed in this present communication.

The experiments of Zhu et al. [61] showed the primary interaction between BPA and several phenolic molecules containing carboxylic and hydroxyl functional groups to be based on hydrogen bonding. An additional report on virtual and practical experiments on the molecular imprinting of phenol, using 4VP as the FM, found that the primary mode of that system in an aqueous environment was hydrophobically driven via van der Waals forces and  $\pi$ - $\pi$  stacking [62]. The authors of this report contend that both of these bond types are present within the BPA-4VP receptor. The reduction in receptor affinity seen between the pre- and post-polymerization studies comes from a change in the binding mode which occurs when the environment is changed from apolar organic porogen to aqueous solvent. It is believed that the immobilization of 4VP in a receptor cavity within a MIP allows for the initial bonding of the BPA molecule to the 4VP aromatic functionality via hydrophobically driven forces. This initial interaction allows the donor and acceptor atoms to align within the two molecules, facilitating the formation of a hydrogen bond of moderate energy. The receptor cavity, being highly hydrophobic due to the nature of the crosslinking co-polymer, allows for the creation of pores that favour these hydrophobic, electrostatic interactions.

**Experimental results and description**

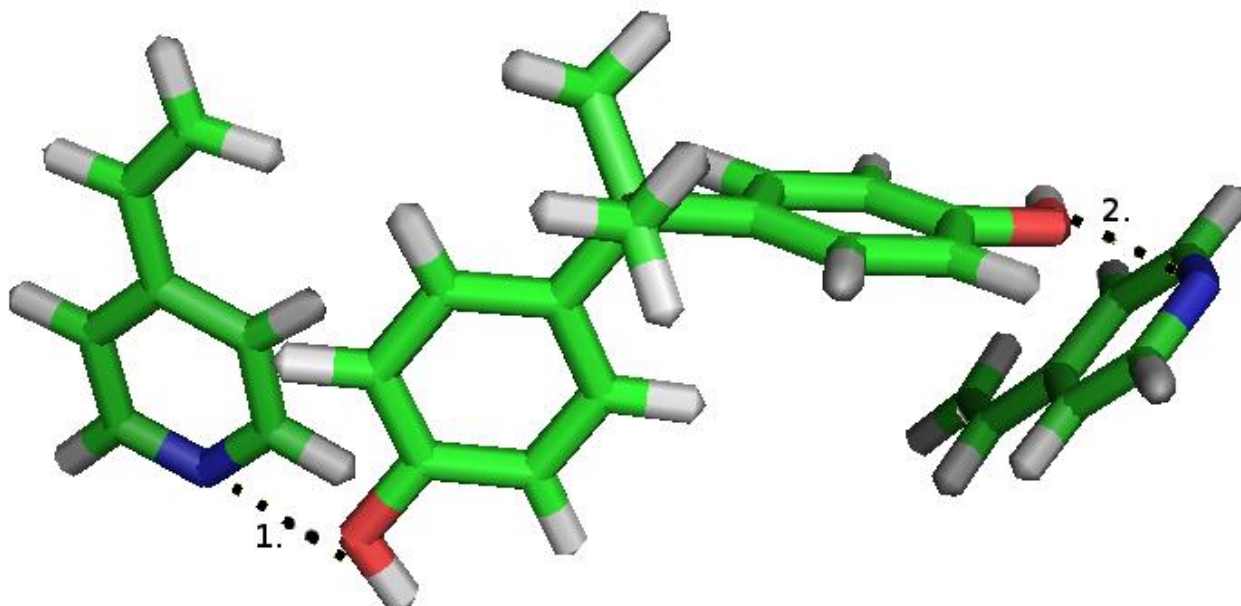
All referenced experimental data can be found in previously published works [48, 49]. BPA, 4VP and EGDMA were combined at a ratio of 1:6:6 with the low volatile solvent triethylene glycol dimethyl ether (TRIGLYME) and a non-reactive linear polymer, poly-(vinyl acetate) as porogen. The polymerization process was then thermally initiated and maintained for 24 hours. Rebinding and adsorption experiments were conducted across 12 different concentrations in water from 22.41 – 4482  $\mu\text{mol.L}^{-1}$ . Adsorption isotherms were calculated using the Freundlich equation which yielded precise affinity constants ( $R^2 > 0.99$ ). These constants can be seen in Table 4.11. These calculated constants showed Bisphenol F (BPF), the structural analogue of BPA, to have the highest binding affinity constant, BPA, the template and primary target to have the second highest affinity constant while caffeine (CAF) and acetaminophen (ACE), the interferents tested, had lowest affinities.

Table 4.11: Maximum and minimum Freundlich affinity constants calculated for the BPA MIP for the primary target, BPA, structural analogue, BPF and the interferants, CAF and ACE [49]

	$K_{\max}$	$K_{\min}$
<b>BPA</b>	$6.25 \times 10^5$	$6.41 \times 10^2$
<b>BPF</b>	$1.09 \times 10^6$	$2.45 \times 10^3$
<b>CAF</b>	$6.72 \times 10^4$	$2.65 \times 10^2$
<b>ACE</b>	$5.76 \times 10^4$	$4.95 \times 10^2$

### Correlation of pre-polymerization studies with virtual prediction

The ideal stoichiometric complex that was created by the thermal annealing method was poor compared to the other two case studies detailed in this work. Steric hindrance created by the structure of BPA did not allow high energy hydrogen-bonds to form between BPA and the 4VP molecules functional groups. Instead, the closest distances between the donor and acceptor atoms of the template and FM molecules respectively were 3 – 4.2 Å with large bond angles, thus indicating poorly formed, weak hydrogen bonds, largely electrostatic in nature. The binding energies of these



hydrogen bonds are typically less than 4 kcal·mol<sup>-1</sup> [30] (Figure 4.19; Table 4.12).

Figure 4.19: Stoichiometric complex for BPA and 4VP as calculated by the thermal annealing method

Table 4.12: Characteristics of Bonds shown in Figure 4.19

<b>Bond ID</b>	<b>Bond length (Å)</b>	<b>Bond angle</b>	<b>Bond strength</b>
<b>1</b>	3.035	90°	weak
<b>2</b>	4.242	111°	weak

The formation of multiple low energy hydrogen bonds around the BPA molecule was observed in the experimental data of the UAC research group via Infrared transmission spectroscopy though not fully understood until the results from this simulation were viewed. During the study of BPA-4VP interactions in the organic solvents tested, which were  $\text{CCl}_4$ ,  $\text{HCCl}_3$ ,  $\text{CH}_2\text{Cl}_2$  and acetonitrile (ACN); for the three chlorinated solvents tested, binding constants of  $2.15 - 4.95 \times 10^3 \text{ M}^{-1}$  in free solution were observed which indicated the formation of stable complexes though, most importantly for this work, were not high enough to indicate the formation of strong 1:2 BPA-4VP complexes based on two or more point cooperative hydrogen bonds. These binding energies were sufficient to indicate the formation of the lower energy, weak 1:2 hydrogen bonded complexes in low polarity solvents. This complex was disrupted by the increased polarity of ACN and thus was not detected outside of the chlorine-based solvents [48].

Regarding the experimental determination of the low binding affinity of the 1:2 BPA-4VP complexes discussed above and in addition to the visualization of the complex which the virtual modelling protocol allowed, it is not surprising that the imprinting effect within the MIP would be lost at mid to high BPA concentrations. To elaborate, when the polymer was experimentally tested for capacity in saturation binding experiments, it was seen that the imprinting effect was only visible until a concentration of 0.5 mM after which point any imprint effect was obscured by non-specific adsorption of molecules to the polymer surface [48]. This implies a low binding capacity within the MIP. From this it may be inferred that there was a high failure rate of the BPA-4VP complexes during the thermally mediated polymerization. The increased mobility that this thermal polymerization process gave to the molecules within the stoichiometric complexes allowed them to break free from comparatively their fragile constraints.

#### Post polymerization correlation of virtual docking modes and experimental results

During the MIP design process the majority of the attention of the research is placed often on the initial formation and maintenance of hydrogen bonds between the template and FM. Generally less attention is placed on the rebinding mode of the template and secondary analogues into the receptor cavity as it is assumed to be largely identical to the pre-polymerization complex. However, it has been demonstrated that ideal template-FM complexes observed in free solution and present during receptor synthesis were not representative of the rebinding mode [63]. Additionally, given that the polymerization process is most often carried out in an organic solvent whilst rebinding most often be in an aqueous environment, such calculations of ideal complex orientation alone cannot suffice. With the use of the VINA computational model, rebinding behaviour can be predicted and used to estimate efficiency and specificity of the receptor. Additionally, it is possible to evaluate the quality and durability of the imprint site through the creation of a hierarchy of bond strength using dipole distance as the determining factor.

The docking modes predicted by VINA, shown in Figure 4.20, were consistently shown to be primarily driven by hydrophobic interactions between the aromatic rings within the receptor and ligand molecule. Additionally, all docking modes for all the molecules were between single 4VP molecules, and none incorporated the two 4VP molecules present within the receptor site. The most intriguing observation from the results of the virtual docking experiment was the formation of low energy hydrogen bonds through the alignment of the donor and acceptor atoms within the receptor-ligand docking modes. This alignment was caused by the initial parallelization of aromatic rings and did not occur in the docking mode of CAF, in which there was no available donor atoms. This apparent  $\pi$ - $\pi$  stacking of the aromatic rings and additional reduction in the stoichiometry from 2 to 1 in an aqueous environment was also experimentally confirmed through shifts in the  $^1\text{H}$  NMR spectrum which were interpreted as being the main driving force for complexation in aqueous environments. This interpretation has now been confirmed by the virtual model. The hydrophobic ring alignment within the virtual docking modes may be used as an indication as to the contribution of the aromatic functionalities to the total docking affinity. This was specifically referred to during the experimental rebinding study in which the main driving force for binding in water was attributed to intermolecular hydrophobic interactions. Further confirmation of the importance of the hydrophobic contribution to the docking mode came when rebinding was additionally investigated in an apolar (chloroform) medium and MIP performance was significantly reduced [48].

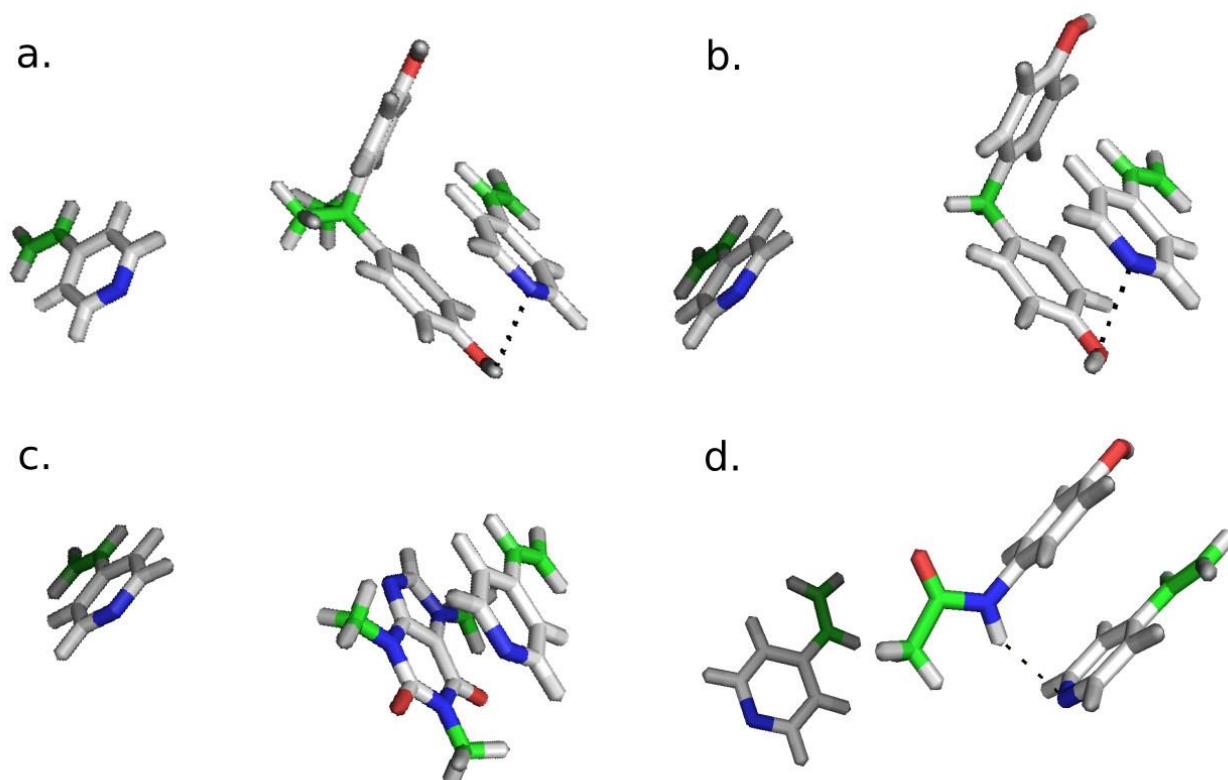


Figure 4.20: Predicted binding modes for BPA (a.), BPF (b.), CAF (c.) and ACE (d.)

As the aqueous rebinding mode substantially differed from the imprinting mode, it is not surprising that selectivity was mediated by aqueous solubility rather than any apparent imprinting effect. Overall, the affinities predicted by VINA (Table 4.13) reflected the order in which rebinding performance was observed in the laboratory study with BPF showing the greatest affinity constant (Table 4.11), followed by BPA and then the interferants, CAF and ACE, both with high aqueous solubilities (Table 4.10), performed most poorly.

Table 4.13: Docking affinities and bond distances for modes shown in Figure 4.20

	VINA predicted affinity (-kcal.mol <sup>-1</sup> )	Hydrogen bond length (Å)	$\pi$ - $\pi$ bond distance (Å)
<b>BPA</b>	9.1	3.5	3.8 – 4.0
<b>BPF</b>	10.6	3.9	3.7 – 4.1
<b>CAF</b>	8.6	N/A	3.7 – 3.8
<b>ACE</b>	8.4	2.5	3.8 – 4.0

While the performance of the interferants may be attributed to the combined effect of their being non-imprinted molecules and high aqueous solubility, this is not the case with the two structural analogues, BPF and BPA. These structural analogues, both having the same aqueous solubility of 360 mg.L<sup>-1</sup> and very similar chemical properties [64], may be assumed to have an equal opportunity for adsorption to the MIP receptor sites from the solution, especially given the predicted ideal docking modes shown above. For this reason, in a competitive binding situation, in which no other exterior interferent is present, the molecule with the higher primary binding affinity, in this case BPF, will preferentially form a complex with the MIP receptor site.

In this way, when the solubilities of both molecules are comparable, the capture probability can be predicted solely from the docking affinity calculated by the VINA algorithm which, in this case correctly placed BPF as having the highest receptor-ligand affinity.

#### 4.4 References

- [1] L. Ye, R. Weiss, K. Mosbach, Synthesis and Characterization of Molecularly Imprinted Microspheres, *Macromolecules*. 33 (2000) 8239–8245. doi:10.1021/ma000825t.
- [2] D.C. Sherrington, Preparation, structure and morphology of polymer supports, *Chem. Commun.* (1998) 2275–2286. doi:10.1039/a803757d.
- [3] A.K. Patel, P.S. Sharma, B.B. Prasad, Development of a Creatinine Sensor Based on a Molecularly Imprinted Polymer-Modified Sol-Gel Film on Graphite Electrode, *Electroanalysis*. 20 (2008) 2102–2112. doi:10.1002/elan.200804294.
- [4] A.K. Patel, P.S. Sharma, B.B. Prasad, Trace-level sensing of creatine in real sample using a zwitterionic molecularly imprinted polymer brush grafted to sol-gel modified graphite electrode, *Thin Solid Films*. 518 (2010) 2847–2853. doi:10.1016/j.tsf.2009.09.009.
- [5] A.K. Patel, P.S. Sharma, B.B. Prasad, Electrochemical sensor for uric acid based on a molecularly imprinted polymer brush grafted to tetraethoxysilane derived sol-gel thin film graphite electrode, *Mater. Sci. Eng. C*. 29 (2009) 1545–1553.

doi:10.1016/j.msec.2008.12.008.

- [6] J. Liu, M.K. Chaudhury, D.H. Berry, J.E. Seebergh, J.H. Osborne, K.Y. Blohowiak, Effect of Surface Morphology on Crack Growth at a Sol-Gel Reinforced Epoxy/Aluminum Interface, *J. Adhes.* 82 (2006) 487–516. doi:10.1080/00218460600713725.
- [7] M.M. Viana, T.D.S. Mohallem, G.L.T. Nascimento, N.D.S. Mohallem, Nanocrystalline titanium oxide thin films prepared by sol-gel process, *Braz. J. Phys.* 36 (2006) 1081–1083. doi:10.1590/S0103-97332006000600075.
- [8] T. Alizadeh, M.R. Ganjali, M. Zare, P. Norouzi, Development of a voltammetric sensor based on a molecularly imprinted polymer (MIP) for caffeine measurement, *Electrochimica Acta.* 55 (2010) 1568–1574. doi:10.1016/j.electacta.2009.09.086.
- [9] B.B. Prasad, R. Madhuri, M.P. Tiwari, P.S. Sharma, Electrochemical sensor for folic acid based on a hyperbranched molecularly imprinted polymer-immobilized sol-gel-modified pencil graphite electrode, *Sens. Actuators B Chem.* 146 (2010) 321–330. doi:10.1016/j.snb.2010.02.025.
- [10] B.B. Prasad, D. Kumar, R. Madhuri, M.P. Tiwari, Sol-gel derived multiwalled carbon nanotubes ceramic electrode modified with molecularly imprinted polymer for ultra trace sensing of dopamine in real samples, *Electrochimica Acta.* 56 (2011) 7202–7211. doi:10.1016/j.electacta.2011.04.090.
- [11] N. Spătaru, B.V. Sarada, D.A. Tryk, A. Fujishima, Anodic Voltammetry of Xanthine, Theophylline, Theobromine and Caffeine at Conductive Diamond Electrodes and Its Analytical Application, *Electroanalysis.* 14 (2002) 721. doi:10.1002/1521-4109(200206)14:11<721::AID-ELAN721>3.0.CO;2-1.
- [12] C.-L. Choong, W.I. Milne, Dynamic modulation of detection window in conducting polymer based biosensors, *Biosens. Bioelectron.* 25 (2010) 2384–2388. doi:10.1016/j.bios.2010.03.023.
- [13] C. Baggiani, F. Trotta, G. Giraudi, G. Moraglio, A. Vanni, Chromatographic characterization of a molecularly imprinted polymer binding theophylline in aqueous buffers, *J. Chromatogr. A.* 786 (1997) 23–29. doi:10.1016/S0021-9673(97)00537-2.
- [14] X. Kan, Molecularly imprinted polymers microsphere prepared by precipitation polymerization for hydroquinone recognition, *Talanta.* 75 (2008) 22–26. doi:10.1016/j.talanta.2007.08.038.
- [15] N. Kirsch, J.P. Hart, D.J. Bird, R.W. Luxton, D.V. McCalley, Towards the development of molecularly imprinted polymer based screen-printed sensors for metabolites of PAHs, *The Analyst.* 126 (2001) 1936–1941. doi:10.1039/b108008n.
- [16] L. Zhu, G. Xu, F. Wei, J. Yang, Q. Hu, Determination of melamine in powdered milk by molecularly imprinted stir bar sorptive extraction coupled with HPLC, *J. Colloid Interface Sci.* 454 (2015) 8–13. doi:10.1016/j.jcis.2015.05.008.
- [17] Y. Wang, J.-B. Liu, S.-S. Tang, R.-F. Jin, Preparation of melamine molecularly imprinted polymer by computer-aided design, *J. Sep. Sci.* 38 (2015) 2647–2654. doi:10.1002/jssc.201500375.
- [18] D. He, X. Zhang, B. Gao, L. Wang, Q. Zhao, H. Chen, H. Wang, C. Zhao, Preparation of magnetic molecularly imprinted polymer for the extraction of melamine from milk followed by liquid chromatography-tandem mass spectrometry, *Food Control.* 36 (2014) 36–41.



doi:10.1016/j.foodcont.2013.07.044.

- [19] H.-H. Yang, W.-H. Zhou, X.-C. Guo, F.-R. Chen, H.-Q. Zhao, L.-M. Lin, X.-R. Wang, Molecularly imprinted polymer as SPE sorbent for selective extraction of melamine in dairy products, *Talanta*. 80 (2009) 821–825. doi:10.1016/j.talanta.2009.07.067.
- [20] L. He, Y. Su, X. Shen, Y. Zheng, H. Guo, Z. Zeng, Solid-phase extraction of melamine from aqueous samples using water-compatible molecularly imprinted polymers, *J. Sep. Sci.* 32 (2009) 3310–3318. doi:10.1002/jssc.200900407.
- [21] H. Yan, X. Cheng, N. Sun, T. Cai, R. Wu, K. Han, Rapid and selective screening of melamine in bovine milk using molecularly imprinted matrix solid-phase dispersion coupled with liquid chromatography-ultraviolet detection, *J. Chromatogr. B.* 908 (2012) 137–142. doi:10.1016/j.jchromb.2012.09.022.
- [22] R. Liang, R. Zhang, W. Qin, Potentiometric sensor based on molecularly imprinted polymer for determination of melamine in milk, *Sens. Actuators B Chem.* 141 (2009) 544–550. doi:10.1016/j.snb.2009.05.024.
- [23] A.F.M. Barton, *CRC handbook of solubility parameters and other cohesion parameters*, 2nd ed, CRC Press, Boca Raton, 1991.
- [24] C. Reichardt, T. Welton, *Solvents and solvent effects in organic chemistry*, 4th, updated and ed ed., Wiley-VCH, Weinheim, Germany, 2011.
- [25] N. Yusof, S. Rahman, M. Hussein, N. Ibrahim, Preparation and Characterization of Molecularly Imprinted Polymer as SPE Sorbent for Melamine Isolation, *Polymers*. 5 (2013) 1215–1228. doi:10.3390/polym5041215.
- [26] I. Nicholls, S. Piletsky, B. Chen, I. Chianella, A. Turner, Thermodynamic Considerations and the Use of Molecular Modeling as a Tool for Predicting MIP Performance, in: M. Yan, O. Ramström (Eds.), *Mol. Imprinted Mater.*, CRC Press, 2004: pp. 363–393.
- [27] L.H. Keith, D.B. Walters, National Toxicology Program (U.S.), eds., *National Toxicology Program's chemical solubility compendium*, Lewis Publishers, Boca Raton, 1992.
- [28] M.-M. Zheng, R. Gong, X. Zhao, Y.-Q. Feng, Selective sample pretreatment by molecularly imprinted polymer monolith for the analysis of fluoroquinolones from milk samples, *J. Chromatogr. A.* 1217 (2010) 2075–2081. doi:10.1016/j.chroma.2010.02.011.
- [29] A. Gryshchenko, C. Bottaro, Development of Molecularly Imprinted Polymer in Porous Film Format for Binding of Phenol and Alkylphenols from Water, *Int. J. Mol. Sci.* 15 (2014) 1338–1357. doi:10.3390/ijms15011338.
- [30] G.A. Jeffrey, *An introduction to hydrogen bonding*, Oxford University Press, New York, 1997.
- [31] F.A. Villamena, A.A. De La Cruz, Caffeine selectivity of divinylbenzene crosslinked polymers in aqueous media, *J. Appl. Polym. Sci.* 82 (2001) 195–205. doi:10.1002/app.1839.
- [32] C.M. Hansen, *Hansen solubility parameters: a user's handbook*, 2nd ed, CRC Press, Boca Raton, 2007.
- [33] D. Spivak, Optimization, evaluation, and characterization of molecularly imprinted polymers, *Adv. Drug Deliv. Rev.* 57 (2005) 1779–1794. doi:10.1016/j.addr.2005.07.012.
- [34] J. Li, G. Wei, Y. Zhang, Molecularly imprinted polymers as recognition elements in sensors,

- in: S. Li, Y. Ge, S.A. Piletsky, J. Lunec (Eds.), *Mol. Imprinted Sens. Overv. Appl.*, 1st ed, Elsevier, Amsterdam ; Boston, 2012: pp. 35–56.
- [35] O.K. Castell, D.A. Barrow, A.R. Kamarudin, C.J. Allender, Current practices for describing the performance of molecularly imprinted polymers can be misleading and may be hampering the development of the field, *J. Mol. Recognit.* 24 (2011) 1115–1122. doi:10.1002/jmr.1161.
- [36] M. Schauperl, D.W. Lewis, Probing the Structural and Binding Mechanism Heterogeneity of Molecularly Imprinted Polymers, *J. Phys. Chem. B.* 119 (2015) 563–571. doi:10.1021/jp506157x.
- [37] S.A. Piletsky, K. Karim, E.V. Piletska, A.P.F. Turner, C.J. Day, K.W. Freebairn, C. Legge, Recognition of ephedrine enantiomers by molecularly imprinted polymers designed using a computational approach, *The Analyst.* 126 (2001) 1826–1830. doi:10.1039/b102426b.
- [38] K. Farrington, E. Magner, F. Regan, Predicting the performance of molecularly imprinted polymers: Selective extraction of caffeine by molecularly imprinted solid phase extraction, *Anal. Chim. Acta.* 566 (2006) 60–68. doi:10.1016/j.aca.2006.02.057.
- [39] F. Bates, M. del Valle, Voltammetric sensor for theophylline using sol–gel immobilized molecularly imprinted polymer particles, *Microchim. Acta.* 182 (2015) 933–942. doi:10.1007/s00604-014-1413-4.
- [40] B. Ren, C. Li, X. Yuan, F. Wang, Determination and correlation of melamine solubility, *Huagong Xuebao J. Chem. Ind. Eng. China.* 54 (2003) 1001–1003.
- [41] Sigma Aldrich, Free radical initiators - thermal initiators, 2015. [http://www.sigmaaldrich.com/content/dam/sigma-aldrich/docs/Aldrich/General\\_Information/thermal\\_initiators.pdf](http://www.sigmaaldrich.com/content/dam/sigma-aldrich/docs/Aldrich/General_Information/thermal_initiators.pdf) (accessed September 24, 2015).
- [42] I. Mijangos, F. Navarro-Villoslada, A. Guerreiro, E. Piletska, I. Chianella, K. Karim, A. Turner, S. Piletsky, Influence of initiator and different polymerisation conditions on performance of molecularly imprinted polymers, *Biosens. Bioelectron.* 22 (2006) 381–387. doi:10.1016/j.bios.2006.05.012.
- [43] M. Ibáñez, J.V. Sancho, F. Hernández, Determination of melamine in milk-based products and other food and beverage products by ion-pair liquid chromatography–tandem mass spectrometry, *Anal. Chim. Acta.* 649 (2009) 91–97. doi:10.1016/j.aca.2009.07.016.
- [44] S. Subrahmanyam, K. Karim, S.A. Piletsky, Computational Approaches in the Design of Synthetic Receptors, in: S.A. Piletsky, M.J. Whitcombe (Eds.), *Des. Recept. Gener. Biosens.*, Springer Berlin Heidelberg, Berlin, Heidelberg, 2012: pp. 131–165. [http://link.springer.com/10.1007/5346\\_2012\\_22](http://link.springer.com/10.1007/5346_2012_22) (accessed June 10, 2015).
- [45] A.L. Latorre, M. Concepción Cela Pérez, S.F. Fernández, J.M. López Vilariño, M.V. González Rodríguez, Selective removal of ATP degradation products from food matrices I: Design and characterization of a dummy molecularly imprinted specific sorbent for hypoxanthine, *React. Funct. Polym.* 91–92 (2015) 51–61. doi:10.1016/j.reactfunctpolym.2015.04.004.
- [46] M.C. Cela-Pérez, L. Barbosa-Pereira, X. Vecino, M. Pérez-Ameneiro, A.L. Latorre, J.M. López-Vilariño, M.V. González Rodríguez, A.B. Moldes, J.M. Cruz, Selective removal of ATP degradation products from food matrices II: Rapid screening of hypoxanthine and inosine by molecularly imprinted matrix solid-phase dispersion for evaluation of fish

- freshness, *Talanta*. 135 (2015) 58–66. doi:10.1016/j.talanta.2014.12.037.
- [47] M.C. Cela-Pérez, F. Bates, C. Jiménez-Morigosa, E. Lendoiro, A. de Castro, A. Cruz, M. López-Rivadulla, J.M. López-Vilariño, M.V. González-Rodríguez, Water-compatible imprinted pills for sensitive determination of cannabinoids in urine and oral fluid, *J. Chromatogr. A*. 1429 (2016) 53–64. doi:10.1016/j.chroma.2015.12.011.
- [48] A. Lasagabáster-Latorre, M.C. Cela-Pérez, S. Fernández-Fernández, J.M. López-Vilariño, M.V. González-Rodríguez, M.J. Abad, L.F. Barral-Losada, Insight into BPA–4-vinylpyridine interactions in molecularly imprinted polymers using complementary spectroscopy techniques, *Mater. Chem. Phys.* 141 (2013) 461–476. doi:10.1016/j.matchemphys.2013.05.045.
- [49] M.C. Cela-Pérez, M.M. Castro-López, A. Lasagabáster-Latorre, J.M. López-Vilariño, M.V. González-Rodríguez, L.F. Barral-Losada, Synthesis and characterization of bisphenol-A imprinted polymer as a selective recognition receptor, *Anal. Chim. Acta*. 706 (2011) 275–284. doi:10.1016/j.aca.2011.09.002.
- [50] J.J. Christensen, J.H. Rytting, R.M. Izatt, Thermodynamic  $pK$ ,  $\Delta H^\circ$ ,  $\Delta S^\circ$ , and  $\Delta C_p^\circ$  values for proton dissociation from several purines and their nucleosides in aqueous solution, *Biochemistry (Mosc.)*. 9 (1970) 4907–4913. doi:10.1021/bi00827a012.
- [51] G.M. Morris, R. Huey, W. Lindstrom, M.F. Sanner, R.K. Belew, D.S. Goodsell, A.J. Olson, AutoDock4 and AutoDockTools4: Automated docking with selective receptor flexibility, *J. Comput. Chem.* 30 (2009) 2785–2791. doi:10.1002/jcc.21256.
- [52] O. Trott, A.J. Olson, AutoDock Vina: Improving the speed and accuracy of docking with a new scoring function, efficient optimization, and multithreading, *J. Comput. Chem.* (2009) NA-NA. doi:10.1002/jcc.21334.
- [53] S.B. Karch, ed., Marijuana, in: *Drug Abuse Handb.*, CRC Press, Boca Raton, Fla, 1998: p. 806.
- [54] R.A. Granberg, Å.C. Rasmuson, Solubility of Paracetamol in Pure Solvents, *J. Chem. Eng. Data*. 44 (1999) 1391–1395. doi:10.1021/jc990124v.
- [55] A. Shalmashi, F. Golmohammad, Solubility of caffeine in water, ethyl acetate, ethanol, carbon tetrachloride, methanol, chloroform, dichloromethane, and acetone between 298 and 323 K, *Lat. Am. Appl. Res.* 40 (2011) 283–285.
- [56] P. Jarho, D.W. Pate, R. Brenneisen, T. Järvinen, Hydroxypropyl- $\beta$ -cyclodextrin and its combination with hydroxypropyl-methylcellulose increases aqueous solubility of  $\Delta^9$ -tetrahydrocannabinol, *Life Sci.* 63 (1998) PL381–PL384. doi:10.1016/S0024-3205(98)00528-1.
- [57] Product Information;  $\Delta^9$ -THC, 2014. <https://www.caymanchem.com/pdfs/12068.pdf> (accessed July 23, 2015).
- [58] S. Li, ed., *Molecularly imprinted sensors: overview and applications*, 1st ed, Elsevier, Amsterdam ; Boston, 2012.
- [59] R.A. Keri, S.-M. Ho, P.A. Hunt, K.E. Knudsen, A.M. Soto, G.S. Prins, An evaluation of evidence for the carcinogenic activity of bisphenol A, *Reprod. Toxicol.* 24 (2007) 240–252. doi:10.1016/j.reprotox.2007.06.008.
- [60] N. Benachour, A. Aris, Toxic effects of low doses of Bisphenol-A on human placental cells,

Toxicol. Appl. Pharmacol. 241 (2009) 322–328. doi:10.1016/j.taap.2009.09.005.

- [61] F.-D. Zhu, K.-H. Choo, H.-S. Chang, B. Lee, Interaction of bisphenol A with dissolved organic matter in extractive and adsorptive removal processes, *Chemosphere*. 87 (2012) 857–864. doi:10.1016/j.chemosphere.2012.01.026.
- [62] Y.-Q. Lv, Z. Lin, W. Feng, T. Tan, Evaluation of the Polymerization and Recognition Mechanism for Phenol Imprinting SPE, *Chromatographia*. 66 (2007) 339–347. doi:10.1365/s10337-007-0336-1.
- [63] H. Kim, D.A. Spivak, New Insight into Modeling Non-Covalently Imprinted Polymers, *J. Am. Chem. Soc.* 125 (2003) 11269–11275. doi:10.1021/ja0361502.
- [64] L.M.L. Nollet, Bisphenol-A and Bisphenol-F, in: *Chromatogr. Anal. Environ.*, CRC/Taylor & Francis, Boca Raton, 2006: p. 1244. <http://www.crcnetbase.com/isbn/9780824726294> (accessed August 2, 2015).



# **Chapter 5 – Conclusions and Future Work**

---



### 5. Conclusions and future work

#### 5.1 Conclusions

1. The key issues and challenges pertaining to the molecular imprinting process were identified; including the specific effects of each of the required components have on both the polymerisation process and on the final imprinted polymer (Articles 1 & 2). Template solubility and comparability was seen to be the greatest factor with respect to the selection of monomers, porogen and polymerisation mechanism and rate.

2. A number of factors were identified regarding the selection of an appropriate immobilisation and transduction method for a MIP. For electrochemical transduction (Article 1), the key disadvantages identified were as follows:

a. The requirement to use up to 80% of inert, crosslinking polymer in the MIP in order to rigidly support the imprinted receptor significantly retarded the electron transfer rate which caused peak broadening and a reduction in sensitivity in contrast to a



bare electrode. The MIP did, however allow does allow for the differentiation between compositionally identical structural analogues.

b. While regeneration of the sensor was possible and, indeed, greatly enhanced relative to analogous electrochemical MIP sensors in the literature due to the use of precipitated polymer particles rather than bulk polymer monoliths, the imprinted sensor's life time was finite, with each consecutive use producing a signal of decreasing strength.

c. The inability to regenerate the MIP sensor was attributed to the location of the high affinity receptors within deep-seated recesses of the pore structure of the MIP. These receptors could not be regenerated by diffusion forces alone, which was the only possible regenerative force available following the immobilisation of the MIP onto the sensor surface.

d. The issue of regeneratibility can be solved by integrating a flow system into the sensor (Article 2) or by using the MIP in free solution during a pre-concentration step, ahead of electrochemical detections

3. With respect to the development of a polymer sensor array for use in an Electronic Tongue, the issues of electron transfer reduction and regeneratibility can be solved with the computational matching of the functional monomer to the analyte(s) of interest or 'virtually imprinting' and redocking a template molecule to design and evaluate the receptor ahead of synthesis (Article 2 & 3).

4. Several outcomes, both expected and unforeseen, have stemmed from this doctoral research project. Though the application of MIPs to sensor arrays and electronic tongues is contentious due to the apparent divergence of the two paradigms, it is possible to bring together the two technologies so as to produce an enhanced and more cost effective sensing system to be applied to complex, real-world solutions and mixtures.

## **5.2 On-going and future work**

A clear sign to the productivity of this doctoral research project, the progress it has made and the research lines it has created, is the currently on-going projects as well as the potential collaborations and future work which is waiting to be capitalised upon. What follows is a brief description of the most relevant of these projects.

### **5.2.1 Virtually matched, triggerable polymer sensor arrays for electronic tongues**

A currently on-going research line at the UAB, carried out in the laboratory by Ms Anna Herrera, is the modification of electrochemical sensors with polyelectrolytes which have been computationally matched to an analyte of interest.

Polyelectrolytes are polymers which contain an electrolyte group in their repeating subunits (monomer). These groups can dissociate in water and at a specific pH to give the polymer a charge. This pH sensitivity can be used as a 'trigger' so that, at neutral pH, there is low affinity which permits the complex (the target molecules and the polyelectrolyte functional group) to be separated and the sensor to be regenerated. This family of molecules is often used in water treatment. At a specific pH (below the  $pK_a$ ), the ionic charge and structural affinity of the functional group can be used to target a specific molecule. Specifically for electrochemical, especially voltammetric, systems, polyelectrolytes are highly promising because they are conductive.

Additionally, because these electrolytes are already matched to the analyte of interest and selected accordingly, the polymer used to modify the electrode surface does not need to be imprinted and consequently does not need to support a receptor within its structure. This allows for the drastic reduction if not the complete removal of the crosslinking polymer from the polymerisation process and thus the polymer's electrically insulating properties can be minimised.

The use of a 'trigger' as opposed to an imprinted receptor to attract and capture the targeted analyte allows for the reverse to also happen; the removal of this trigger, such as the returning of the pH of the solution to a neutral value, allows for the rapid and facile regeneration of the sensor surface. This advantage is magnified by the fact that

there is no longer the issue of tailored, high affinity receptor sites seated deeply within a complex and tiny pore structure on the immobilised sensor surface.

A proof of concept experiment has already been conducted by the author using the proton conducting polyelectrolyte EGMP, already referenced in the introductory chapter of this work (Figure 1.10). This was computationally matched for affinity to the common analgesic, acetaminophen, using the SYBYL scoring algorithm at UoL. As can be seen in figure 5.1, a clear and strong modification to the signal profile occurs when the anionic EGMP-modified electrode comes into contact with the alkaloidal structure of the acetaminophen in contrast to the cations of uric and ascorbic acid.

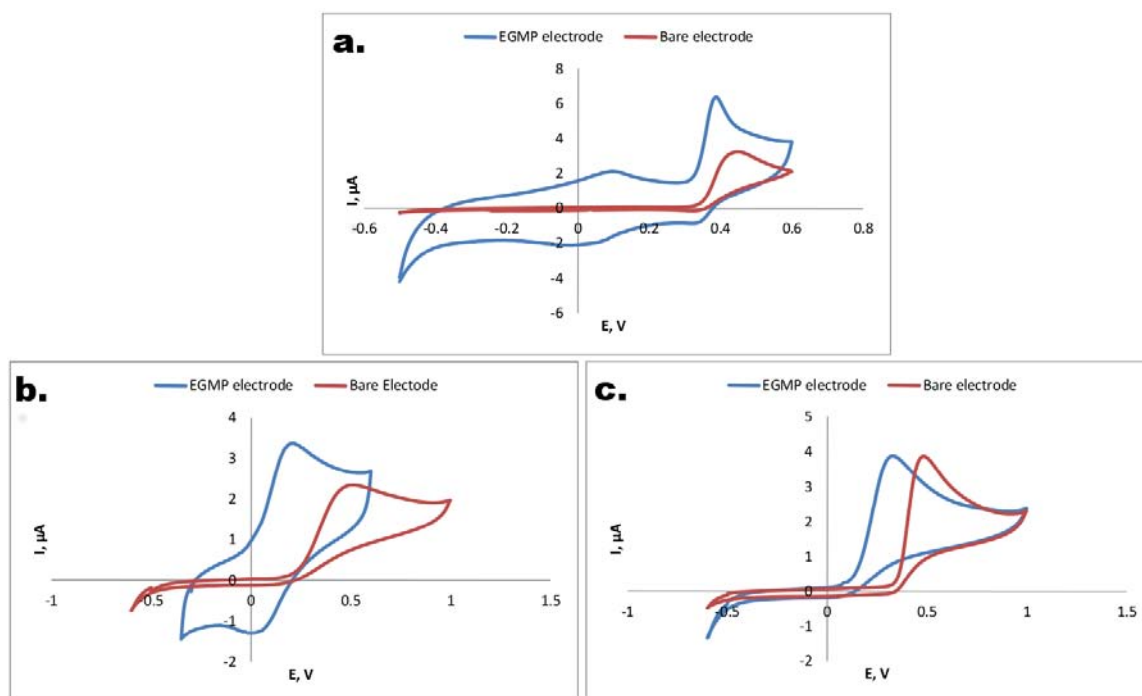


Figure 5.1: Cyclic voltammograms produced by the unmodified and EGMP-modified electrodes in pH 2 Britton-Robinson buffer in the presence of 0.2 mmol•L<sup>-1</sup> of acetaminophen (a.), ascorbic acid (b.) and uric acid (c.)

### 5.2.2 Augmentation of the computational power

Following the success of the research documented in *Articles 2 & 3*, the research team at UDC has moved to increase the computing capacity at their disposal through significant investment in both on-site computing resources as well as potential collaborations with local supercomputing facilities. The quadrupling of processing

power within this computing system, with respect to that used for the experimentation of this thesis ,can allow for the execution of simulations on a massively more complex scale for a greater duration than have been described in this thesis thus far. An interesting example of the benefits of this investment in computational power is the ability to create a more realistic prediction of MIP receptor topologies which in turn can be screened using the protocol detailed in Article 3.

For an idea of the scale of the increase in capacity, whereas the simulation for this thesis were done using an 8 Gb CPU, typically consisting of approximately 150 molecules or 2000 atoms, the new computer resource boasts 32 Gb of RAM and has been seen to stably support and run simulations of 1000 molecules or 20,000 atoms. Screen shots of this experiment are shown in Figure 5.2.

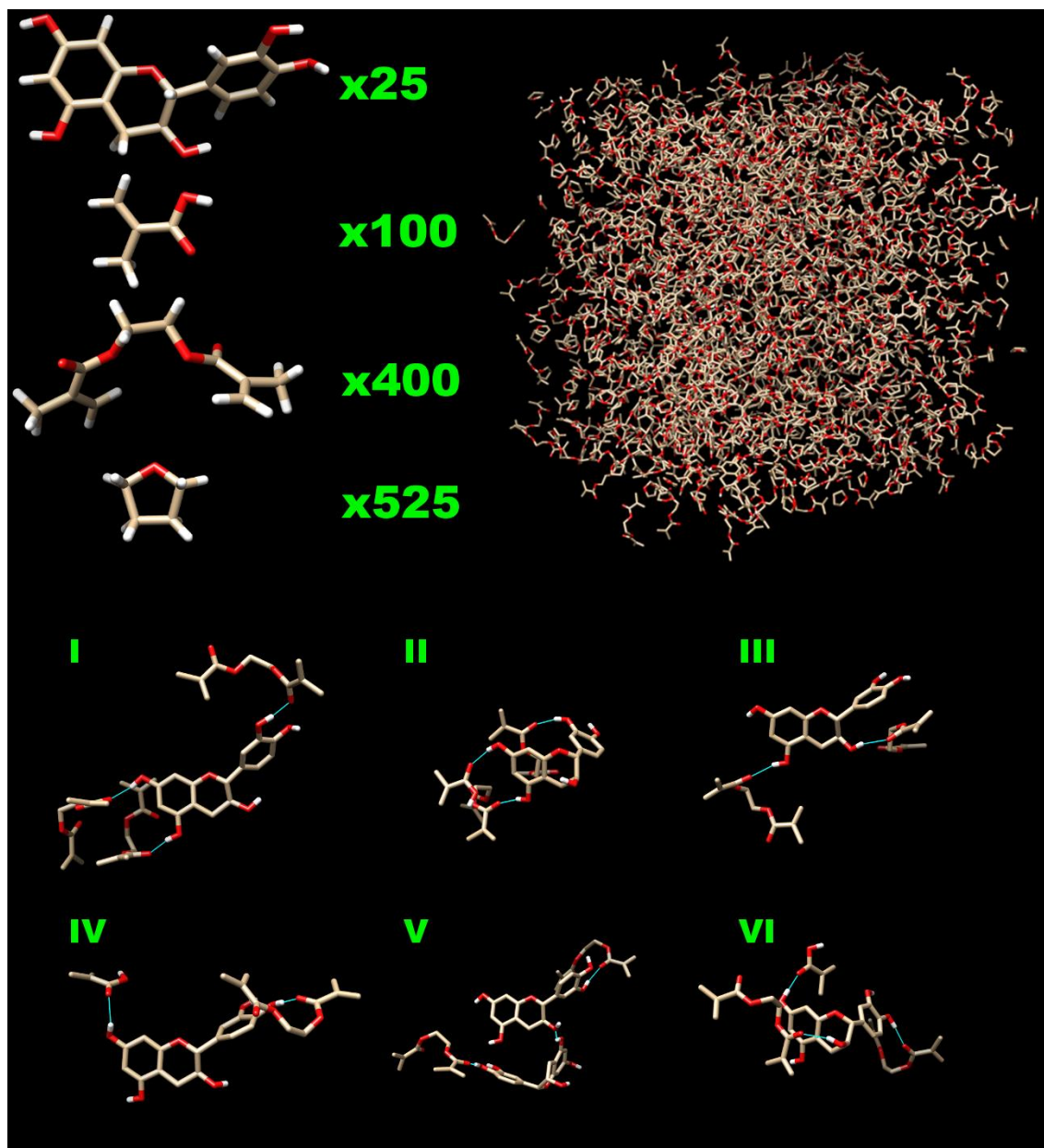


Figure 5.2: Dynamic simulation imprinting solution with representative quantities of template, FM, cross-linker and porogenic solvent at polymerisation temperature (60°C) for 10 ns done in the Gromacs molecular modelling suite (top); this type of large scale simulation can be used to create more realistic and diverse imprinted receptors (bottom)

### 5.2.3 Improvement of virtual screening of imprinted receptors

A currently on-going topic of research within the UoL research group is the application of the novel receptor screening method detailed in Article 3. PhD student Ms Julie

Settipani has seen excellent results in their attempts to create and screen rigid receptor topologies within the much more highly detailed Tripos force field of the SYBYL modelling suite with the intention of incorporating such a tool into their world renowned imprinted polymer laboratory.

### **5.2.4 Incorporation of Open-Source Modelling Techniques into Online screening platform for MIP design**

A further effort is being simultaneously made within the Computational Biophysics research group at the University of Verona by the hand of Mr Mirko Busato to take advantage of the Autodock screening technique for MIP receptor design. Mr Busato is incorporating the prediction tools developed and detailed in this thesis into the online platform that will be the topic of his thesis. This work is currently on-going though an initial view of what it will look like can be seen in Figure 5.3. A paper detailing this platform is also being written and is intended to be submitted for publication in the coming months.

**Upload the search space parameters**

**CALCULATE THE BOX (VMD)**

OR

center x	
center y	
center z	
size x	
size y	
size z	
<div style="border: 1px solid black; padding: 2px 10px;">DONE</div>	

**Download the search space parameters**

**Upload the Advanced/Misc parameters**

**USE PAPER PARAMETERS**

OR

weight gauss1	-0.035579
weight gauss2	-0.005156
weight repulsion	0.8402450000000002
weight hydrophobic	-0.03506900000000003
weight hydrogen	-0.5874390000000004
weight rot	0.05845999999999998
exhaustiveness	8
num_modes	9
energy range	3
<div style="border: 1px solid black; padding: 2px 10px;">DONE</div>	

**Download the Advanced/Misc parameters**

submit

\*\*\*\* in the window the default VINA values\*\*\*\*

Figure 5.3: Screen shot of the job submission page of the online prediction tool currently under construction within the Computational Biophysics research group at the University of Verona

### **5.2.5 Application of an array of CIT imprinted polymer pastilles to a GSB artificial neural network**

The final scope for future collaboration and work comes in the combination of efforts made by the Technological Research Centre (CIT) at UDC and the Sensors and Biosensors Research group (GSB) at UAB. The research lines on both of these groups run in parallel and stand to be, if combined, stronger than the sum of their parts. As has been laid out throughout this thesis, a key attenuator to the use of MIPs in sensor arrays is the difficulty in regenerating the MIP sensor, especially after the immobilisation of the MIP onto a sensor surface. The use of the MIP in free solution or in a flow system can remove this issue of regenerability entirely and indeed, this is exactly what the Ms Anna Herrera is currently undertaking in the GSB laboratory in Barcelona with the use of SPE cartridges, packed with monolithic MIP particles, in concert with in-house electrochemical sensors replacing the more expensive chromatographic methods.

In the CIT laboratory in the Ferrol campus of UDC, imprinted polymer 'pastilles' have been perfected; these have already been referenced in the introductory chapter of this thesis. These pastilles remove the need for post polymerisation grinding of the MIP as well as making the polymer highly convenient to transport, use and regenerate. To date, these pastilles have been characterised and exploited using spectroscopic and chromatographic methods only. As laid out in Figure 5.4, this collaboration would take minimal effort for both parties involved and would allow for the rapid progression toward a MIP-incorporating Electronic Tongue while also providing more scope for the application and testing of the Autodock-based virtual screening method for the design of MIP receptors, customised to the cross-responsive requirements of the Electronic Tongue imprinted sensor array.



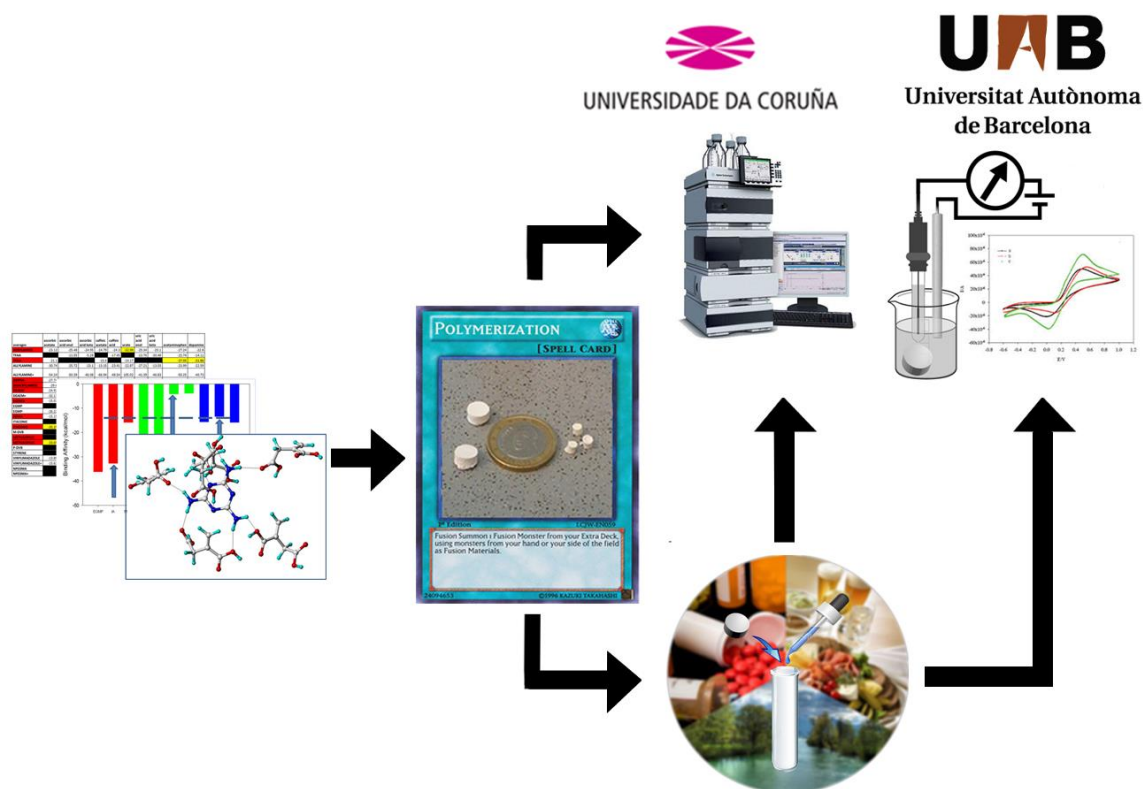


Figure 5.4: Proposed collaboration to combine the synthetic expertise of the CIT polymer research group at UDC with the analytical expertise of the GSB group at UAB entailing the use of an array of imprinted polymer 'pastilles' to pre-concentrate analytes in real samples which could then be analysed using an electronic tongue

# **Chapter 6 – Publications**

---



**Article 1:**

*Voltammetric sensor for theophylline using sol–gel immobilized molecularly imprinted polymer particles*

**Ferdia Bates** and Manel del Valle., *Microchimica Acta*. 182 (2015) 933–942.



## Voltammetric sensor for theophylline using sol–gel immobilized molecularly imprinted polymer particles

Ferdia Bates · Manel del Valle

Received: 1 August 2014 / Accepted: 10 November 2014 / Published online: 19 November 2014  
© Springer-Verlag Wien 2014

**Abstract** Sensors incorporating molecularly imprinted polymers (MIPs) are feasible in concept though the reproducibility of such devices can be compromised by the large number of interdependent steps. For this reason, many researchers have focused on the synthesis of MIP particles only, not on their immobilization. Herein is presented a sol–gel based method for immobilization of unmodified MIP particles for use in an electrochemical sensor. The macroporous particles were prepared using precipitation-polymerization and imprinted with theophylline. The sol–gel was combined with graphite micro-particles (50  $\mu\text{m}$ ) and the composite was deposited on the surfaced of an epoxy-graphite electrode. The sensor was then tested for its response to theophylline using differential pulse voltammetry. A limit of detection of 1  $\mu\text{M}$  was observed and a relative standard deviation of 6.85 %. The electrode can be regenerated via a thermal washing process which was accompanied by an initial signal loss of 29.3 %. Any further regeneration caused a signal loss of 2.4 % only.

**Keywords** Molecularly imprinted polymers (MIP) · Sol–gel · Graphite · Theophylline · Differential pulse voltammetry

### Introduction

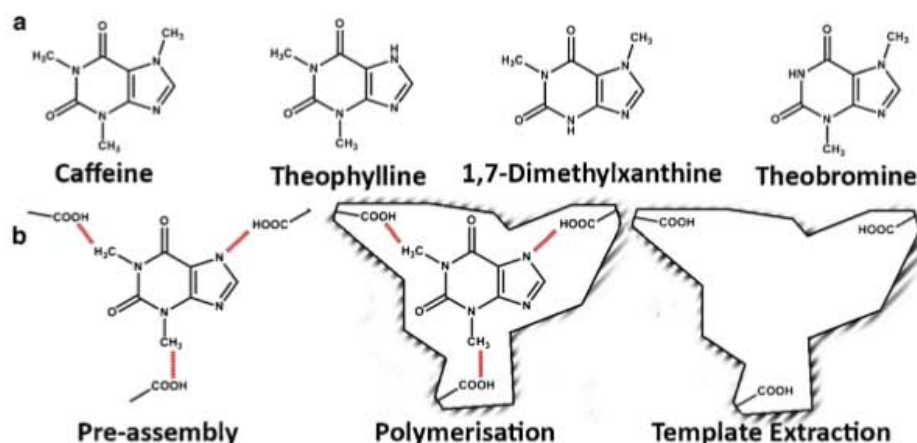
The necessity for novel qualitative sensor systems with the capacity to detect targeted molecular compounds is ever-present. For several decades, sensors based on biological recognition, such as those utilizing enzymes, antibodies, microorganisms or aptamers, have received a majority of interest within

this field thanks to their superior recognition properties [1]. Biomolecules do, however, suffer from a generally poor chemical and physical stability as well as being costly to synthesize or refine and thus in more recent years, artificial receptors have been garnered with an increasing degree of attention [2].

Molecular imprinting embodies the creation of a tailored binding site for a selected template molecule. The binding sites that are created can be highly specific and have the ability to discriminate between structurally similar compounds as well as chiral molecules [3]. This field is most commonly manifested in the paradigm of Molecularly Imprinted Polymers (MIPs) which has exhibited exponential growth with respect to annual publications over the course of the last two decades [4]. Though there are two main imprinting strategies, covalent and non-covalent, the non-covalent approach is afforded greater attention due to the speed and ease of synthesis, facile post-binding regeneration and the greater level of functionality at the binding site [5]. The synthesis of such MIPs, generally consists of a preassembly step whereby the template molecule is mixed with a functional monomer to form complexes with the template at its local dipoles. The spatial orientation of these binding sites is then secured via the crosslinking of the functional monomer with a secondary copolymer, which fixes at proper distance and geometry the binding sites; at this point, the template can be extracted from the newly-formed cavities [6] and usages of the MIP can be developed; a schematic of this process, using theophylline as a template, can be seen in Fig. 1. The popularity of MIPs comes from their low cost, ease of preparation and high stability [7]; these attributes have garnered them with the title ‘plastic antibodies’ [8].

Given their advantages, molecular imprinting appears equally enticing to laboratories regardless of the level of in-house synthetic expertise. There are, however, some drawbacks and discouragements while attempting to imprint polymers. Of the two most common structural forms of MIPs,

F. Bates · M. del Valle (✉)  
Sensors and Biosensors Group, Department of Chemistry,  
Universitat Autònoma de Barcelona, Bellaterra,  
Barcelona 08193, Spain  
e-mail: manel.delvalle@uab.es



**Fig. 1** Molecular structure of caffeine, theophylline theobromine and 1,7-dimethylxanthine (a); schematic of the creation of a theophylline-imprinted binding site consisting of the pre-assembly of the functional

monomer and the template, polymerization of the crosslinking polymer and the subsequent removal of the template to leave a functional binding site (b)

particles and deposited films, both are accompanied by disadvantages which hinder the exploitation of molecular imprinting as an analytical technique. While particles are easier to synthesize compared to films [9], the number of immobilization methods for MIP particles available in the literature is limited. This low level of available protocols can be noticed as those referenced in a 2010 review of the state-of-the-art of molecular imprinting in electrochemistry [10]. Of 61 papers reporting the immobilization of MIPs onto sensors only five of these, less than 10 %, employed unmodified MIP particles as the sensing mechanism. Four additional citations reported the use of packed columns or flow systems though such strategies suffer from drawbacks of slow rebinding of the target within the cavities of the MIP, leading to long extraction times [11].

Theophylline, the molecule chosen as molecular template for this work, is a methylxanthine alkaloid of the purine family and is present in cocoa beans, teas and a range of other beverages and plant materials along with its structural analogues caffeine and theobromine. For over 70 years it has been used to treat maladies of the airway such as asthma and chronic obstructive pulmonary disease (COPD). Its low cost and high availability have both contributed to make it one of the most widely prescribed drugs for such pathologies [12]. Its simple structure and close similarity to its analogues (Fig. 1) make it an attractive molecule to study in the field of molecular imprinting. Its low cost and toxicity also increases the attraction of using it in prototype studies [13, 14].

Conventional methods for the detection of methylxanthines are based on gas and liquid chromatography, the advantages of which are clouded by the requirement of bulky, expensive equipment, complicated sample pretreatments and trained operators to run the analysis [15, 16]. Electrochemical methods on the other hand, embodied by voltammetric,

potentiometric, amperometric and piezoelectric devices, were until relatively recently not commonly used for their detection [17]. This is due to their extremely high oxidation potentials, observed with common electrochemical systems incorporating metallic and/or carbon-based electrodes, which make the final signal poorer, with background noise created from oxidative currents and limited reproducibility [13, 18].

Synthesis techniques of particulate MIPs consist of bulk, suspension, emulsion, two-step swelling and/or precipitation polymerizations [19]. The disadvantage of bulk imprinting, the most commonly used technique, lies in the high volume of material and template that is required by the synthesis. The monolith particles obtained can also have a low capacity due to binding-site heterogeneity and poor site accessibility stemming from the grinding process needed to break the polymer brick [20], thus there is a need to investigate alternative synthesis strategies.

Though MIPs have already been successfully applied to the majority of the contemporary transduction mechanisms [21], there is instead a deficit in the availability of facile immobilization methods for particulate MIPs onto the surface of available transducers for rapid sensing of the targeted molecule; such methods would allow for the rapid substitution of the molecule targeted by the sensor via a change in the imprinted template rather than the laborious redesign of the sensor, thus greatly increasing the versatility of the systems.

The key difficulty in the search for an effective immobilization method for particulate MIPs lies in the compromise between extraction or measurement time and reproducibility. When using monolithic MIP particles, a large quantity must be used in order to negate the potential heterogeneity of the measurement due to the aforementioned accessibility issues. When such particles are immobilized in lower quantities, in a



membrane for example, the decreased availability of the binding sites lead to undesirably high variability between measurements [14]. Incorporation of the monoliths inside the electrode increases the robustness of the sensor and allows the use of more aggressive strategies to be used for signal amplification [13] though this method does not allow for the removal of the template upon re-binding and thus effective regeneration of the sensor is not possible.

Though the use of an agarose membrane for the immobilization of MIP particles onto a sensor surface is well documented [20, 22], it was rejected due to the slow response time with respect to membrane thickness, an increase of which is required with respect to increased oxidation potential of analyte. Also, the complete coverage of the MIP particles by a membrane would also negate the possibility of electrode regeneration.

Sol-gel immobilized MIPs have been reported in which high voltage potentials (1.4–2.0 V) are incorporated into the sensing [23]. Further work by the same laboratory immobilizes hyper-branched MIP particles inside an identical sol-gel membrane [24]. While the non-conventional imprinting strategy employed, known as the Takagishi method is effective [25], the elevated temperatures used during the polymerization process renders it unsuitable for imprinting many organic molecules. It should also be noted that it is also possible to imprint directly into a sol-gel matrix, using its polymeric structure to replace one or both of the functional and crosslinking monomers [26] though this strategy was also rejected in favour of maintaining the segregation between the imprinting and immobilization events.

In this work, a theophylline-imprinted polymer-incorporating voltammetric sensor is presented. Microspherical macroporous MIP particles were immobilized using the sol-gel technique together with graphite as the conducting medium on the surface of a carbon electrode. The theophylline-imprinted polymer was synthesized using standard protocols of precipitation polymerisation and their morphology and size distribution was confirmed via Scanning Electron Microscopy (SEM). Prepared sol-gel membranes were also characterised using confocal microscopy. Primary response and electrode regeneration was investigated using adsorptive stripping voltammetry (ASV) employing the differential pulse technique. Cross response to other methylxanthines: 1,7-dimethylxanthine, caffeine and theobromine was fully characterised. The limit of detection of the electrode was also demonstrated using chronoamperometry.

## Experimental

### Reagents and chemicals

50  $\mu\text{m}$  particle size graphite powder (Merck, Darmstadt, Germany; <http://www.merck.com/>) was used in the

preparation of the sol-gel membranes and of the epoxy-graphite electrodes. Epotek H77 resin and its corresponding hardener (Epoxy Technology, Billerica, MA, USA; <http://www.epotek.com/>) were also used in the electrode fabrication. All reagents were analytical reagent grade. All solvents were purchased from Scharlab, (Scharlab, Barcelona, Spain; <http://www.scharlab.com/>). 1,7-dimethylxanthine, theophylline, theobromine, caffeine, methacrylic acid (MAA), ethylene glycol dimethyl acrylate (EGDMA) and tetraethyl orthosilane (TEOS) were purchased from Sigma-Aldrich (Sigma-Aldrich, St. Louis, MO; <https://www.sigmaaldrich.com/>). The radical initiator 2,2'-Azobis (2,4-dimethylvaleronitrile) (AIVN) was purchased from Wako Chemicals GmbH (Wako Chemicals GmbH, Neuss, Germany; <http://www.wako-chemicals.de/>). All other acids and potassium hydrogen phthalate were purchased from Panreac (Panreac, Barcelona, Spain; <http://www.panreac.es/>).

### Apparatus

All polymerisations were done in a water bath controlled with a Huber CCI thermoregulation pump (Huber Kaeltemaschinenbau GmbH, Offenburg, Germany; <http://www.huber-online.com/>). All experiments were conducted using a commercial 52–61 platinum combined Ag/AgCl reference and counter electrode (Crison Instruments, Barcelona Spain; <http://www.crisoninstruments.com/>). All voltammetric measurements were carried out using a DropSens  $\mu\text{Stat}8000$  multi-potentiostat/galvanostat and processed using Dropview 8400 computer software (Dropsens, Oviedo, Spain; <http://www.dropsens.com/>). Chronoamperometry measurements were executed using an Autolab PGStat 20 (Metrohm Autolab B.V, Utrecht, The Netherlands; <http://www.ecochemie.nl/>). SEM analysis was executed using a MERLIN FE-SEM (Zeiss GmbH, Jena, Germany; <http://www.zeiss.com/>). Confocal microscopy was done with a Leica DCM-3D system (Wetzlar, Germany; <http://www.leica-microsystems.com/>).

### Preparation of theophylline-imprinted polymer particles

The protocol for the precipitation polymerisation synthesis of the MIP particles was taken from the literature [27]. In brief, inhibitor in the MAA and EGDMA was removed immediately prior to use via passage through separate inhibitor removal columns (Sigma-Aldrich, St. Louis, MO; <https://www.sigmaaldrich.com/>). 0.255 mmol of Theophylline was combined with 0.911 mmol of MAA in 40 mL of acetonitrile in a round bottomed flask. The mixture was then stirred gently at low temperature for 10 min. 3.64 mmol of EGDMA and 0.0852 mmol of AIVN were then added and mixed briefly. The solution was sonicated under vacuum and then purged with nitrogen for 10 min, at which point the flask



was sealed and placed in a 60 °C water bath for 16 h. A control non-imprinted polymer was also created using an identical procedure with the omission of theophylline. The MIP particles were then removed from the porogen via centrifugation at 4500 RPM for 10 min and then equally divided between three 15 mL Falcon tubes. The particles were washed using 10 mL of 9:1 methanol: acetic acid solution for 1 h, at which point the washing solvent was refreshed; next, the tubes were centrifuged and the supernatant replaced. This process was repeated 5 times to ensure the complete removal of the template molecule; the particles were then rinsed again with methanol only and dried in an oven at 70 °C.

#### Electrode preparation and MIP-sol-gel immobilization and regeneration

The electrodes used for experimentation were epoxy-graphite composite electrodes of normal use in the laboratory of the authors and were prepared using a previously published in-house protocol with a final geometric surface area of 0.28 mm<sup>2</sup> [28]. Following the curing duration, the electrodes were wet-polished with 400 grit abrasive-paper and degreased with acetone. The immobilization of the MIP particles onto the surface of the epoxy-graphite electrode was modified from a previously published protocol [29]. 0.5 mL TEOS, 0.5 mL ethanol, 0.25 mL water and 25 µL of 0.1 M hydrochloric acid (HCl) were combined and stirred vigorously for 35 min and rested for approximately 45 min to arrive at the syneresis stage. This liquid was combined with graphite and a MIP-DMF suspension in the ratio 200 µL to 7 mg to 40 µL respectively. The MIP-DMF suspension consisted of 15 mg of MIP particles and 1 mL of DMF; the experimental control consisted of particles polymerised in the absence of the template, a non-imprinted polymer (NIP). This mixture was shaken for 10 min at 1400 RPM. 10 µL of this solution was deposited in the centre of each electrode and evenly distributed via a home-made spin coater at 1400 RPM for 60 s. The electrodes were dried at atmospheric pressure at 5 °C overnight and conditioned in water for 1 h before use. For regeneration experiments, the electrodes were immersed in 0.05 M HCl at 60–65 °C for 10 min and then conditioned in water for 1 h before subsequent use.

#### Electrochemical measurements

Differential Pulse Voltammetry in all experiments was performed with a scan range between 1 and 1.7 V, a pulse potential of 0.01 V, duration of 300 ms and a scan rate of 0.04 V·s<sup>-1</sup>. A base line measurement was taken at  $t=0$  ( $t_0$ ) from which all proceeding measures were subtracted. Chronoamperometry experiments were performed at +1.18 V. All measurements were done in pH=3 phthalate buffer with the pH adjusted using 0.1 M HCl. An

accumulation time of 5 min was used in all experiments unless otherwise stated whereby the electrode was immersed in the analyte ahead of the measurement event.

## Results and discussion

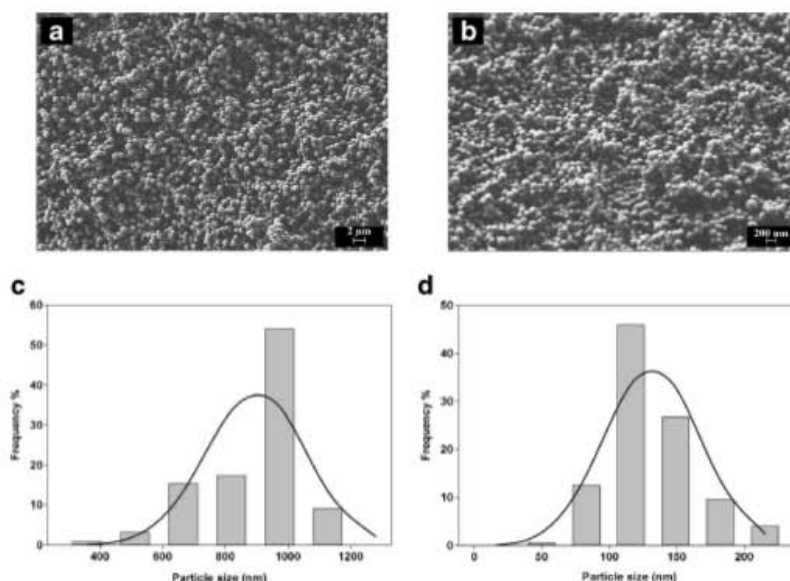
### Particle synthesis and sol-gel immobilization

Precipitated microspheres were used for sol-gel immobilization due to their small size and high homogeneity. The synthesis protocol used employed a molar ratio of 1:4 MAA:EGDMA to ensure high crosslinking and optimal rigidity to maintain binding-site morphology within the polymer matrix.

The yield following template removal was 563 mg, calculated as an efficiency of 64 % by weight, 24 % less than that given by Ye et al. [27]. This drop in yield efficiency is speculated to originate in the lower centrifugation speeds used during the template removal process. SEM analysis confirmed the formation of highly uniform spherical particles (Fig. 2a and b). A superficial roughness or 'wrinkled' aspect was observed on the surface of the polymers; an advantageous feature of macroporous particles due to the increment in surface area it provides. This surface area is permanent both in the dry state and is not susceptible to solvent-related swelling, a feature of traditional monolith MIPs which can place stress on both the polymer and the supporting matrix, a phenomenon which can affect rebinding performance [30]. A subsequent statistical analysis (Fig. 2c) found the particle size distribution to be in keeping with that published in the literature. 54 % of the particle yield was made up of sizes at 970 nm while 96 % of the yield was above 665 nm. In contrast to the large positive skew seen in the distribution of the MIP particle synthesis, the NIP control saw a quite narrow ( $\sigma=33.1$  nm), normal distribution of particle sizes; with 46 % of the yield being sized at the mean value and 86 % of the total being at or above the mean of 116 nm, shown in Fig. 2d.

The greatly diminished particle size demonstrates the sensitivity of precipitation polymerisation protocols to the choice of template due to the augmented solubility parameter which the presence of the template, theophylline, provides relative to the control. In brief, the solubility parameter is a term in polymer chemistry used to describe solvent-monomer compatibility based on the absolute sum total of the dipole-dipole, hydrogen bond and dispersion forces between the solvent and the dissolved monomer (s). When polymerisation is induced, the resultant chain becomes progressively more unstable until the point of phase separation which causes the collapse and subsequent precipitation of the polymer chain into the solvent and thus the formation of a polymer particle. In the case of MIPs, the additional polar surface area of the template molecule provides substantial additional thermodynamic stability during chain growth which can significantly delay polymer

**Fig. 2** SEM of uniform spherical Theophylline-Imprinted Polymer particles (a) and the NIP control (b); Statistical analysis of MIP particle size distribution with a mean of 819 nm and standard deviation of 153 nm (c) and statistical analysis of NIP particle size distribution with a mean of 116 nm and standard deviation of 33 nm (d)



precipitation into the solvent phase, resulting in a large size difference between the MIP and its control [31, 32]; in this case, this size difference is 7-fold. The increase in particle size distribution observed in the MIP relative to its control can be minimised with decreased mechanical agitation, which is the main source of turbulence within the solvent phase during the polymerisation process.

#### Optimisation and determination of deposition, drying and regeneration sol-gel conditions

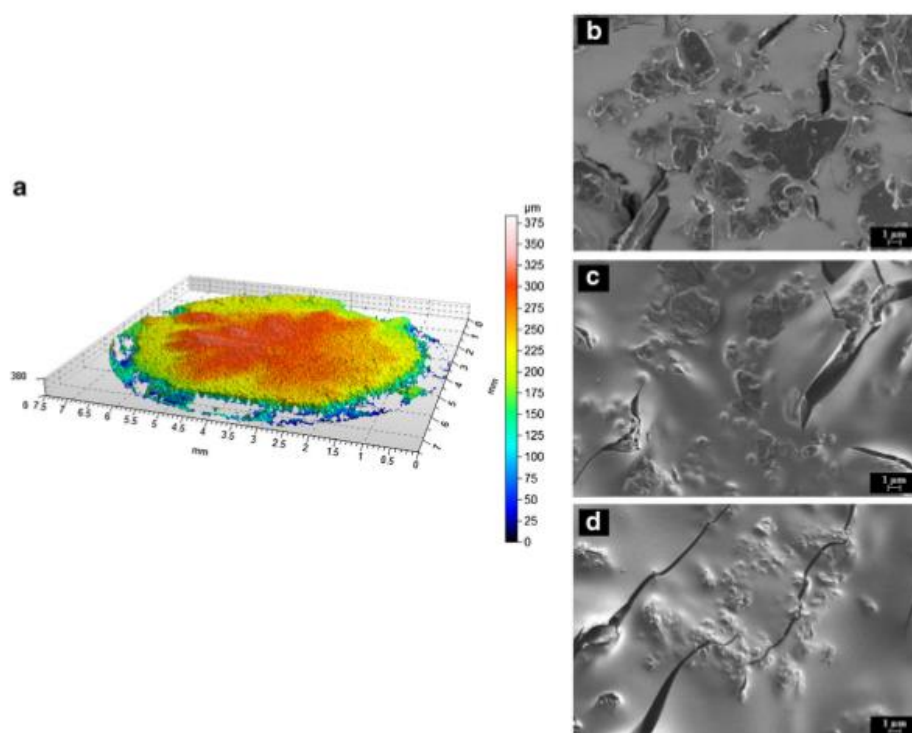
In order to obtain a sensing surface usable for voltammetry, it was decided to immobilize the obtained MIP microspheres within a sol-gel matrix. This was done by modifying a procedure determined by Patel et al. [23, 29, 33, 34]. Optimal results were seen when the electrodes were chilled immediately following the deposition and distribution (spin coating) and allowed to dry over night at ambient pressure. Though signal intensity was seen to be related to the final gel thickness, an optimised deposited volume of 10  $\mu$ L on the graphite-epoxy composite electrode was chosen as larger deposition volumes were seen to increase the instance of crack formation on the gel surface, a finding consistent with the literature [35]. Though it is possible to negate the instance of crack altogether as well as to achieve extremely high film uniformity via multiple layered depositions [36], the signal augmentation that was seen with the single deposition was not replicated when multiple layers were built up on the electrode surface. The use of high-potential voltammetric cycling or sustained high voltage pre-treatments were seen to be detrimental to the structural

integrity of the sol-gel and thus obliged the subtraction of interfering background currents prior to each measurement. Performance of measurements in strong acids in order to increase the signal to noise ratio, as used for the detection of similar compounds [13], also was not feasible as the acid caused the gel deterioration due to continued hydrolysis of the sol-gel membrane.

To elaborate on the choice made for buffer pH, theophylline exhibits a sharp approximately linear increase in oxidative current with acidifying pH values [18]. However, with respect to the MIP recognition element, this augmentation in signal intensity can only be exploited until a point before the degree of ionisation of the target molecule in the buffer renders it unfit for the imprinted cavity and thus dropping selectivity [24]; high relative standard deviation (RSD) also occurs when detection is attempted at pH values too close to the  $pK_a$  of the target. Accordingly, pH 3 was chosen as the detection pH sufficiently distanced from the dissociation points of theophylline given as 5.6 and 2.5 [37]. The use of such a buffer combines the binding and signal augmentation requirements to allow for a facile single step detection process without losing the imprinting effect of the MIP relative to its control.

Upon deposition, the sol mixture was evenly distributed using a home-made spin coater. When dried, the thickness of the membrane was measured using a 3D confocal microscope (Fig. 3a). It was observed that though the greatest thickness remained at the centre of the electrode at the site of the deposition, the overall distribution of membrane thickness was relatively uniform varying from approximately 200  $\mu$ m at the extreme peripheries of the electrode to 300  $\mu$ m at the





**Fig. 3** 3-dimensional surface profile and film-thickness of sol-gel on electrode surface obtained by confocal microscopy examination (a); SEM images of a deposited sol-gel membranes containing graphite only (b) and the sol-gel immobilized MIP and NIP microspheres (c & d)

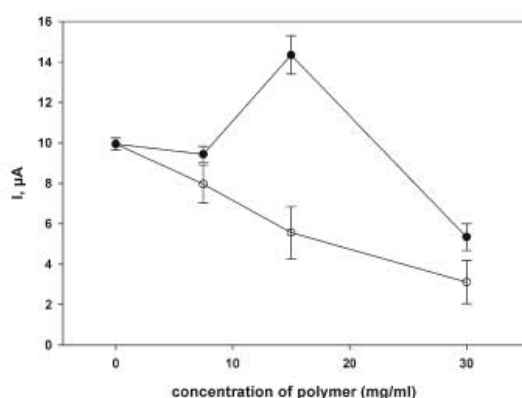
original deposition point. This variation was seen to arise from the decrease in solution thickness, as well as graphite particle quantity, which occurred when the graphite particle size was increased while the mass proportion remained constant; this fact decreasing the in-situ availability of the graphite causing a substantial gradient to be observed. Increasing the mass proportion of the graphite in order to compensate this reduction, though aiding in the homogeneous distribution of the gel upon disposition, provoked an increased incidence of crack formation in the sol-gel surface upon drying; this obliged a reduction in deposition volume and decreased signal strength.

It was seen that the MIP particles preferentially occupied the surface of the sol-gel electrode, clustering around the graphite particles (Fig. 3b–d). This orientation is advantageous as it reduces the incidence of non-specific interactions between the analyte solution and the graphite particles and thus maximises the specific binding events between the MIP particles and the target analyte. The high availability of the MIP particles at the surface of the sensor also allows for a reduction in the immersion time in the analyte required before measurement can occur as well as allowing the sensor to be regenerated as will be discussed below.

The volume of MIP particles in the sol-gel membrane was determined through varying their concentration in the MIP-DMF suspension that was used during the synthesis of the sol-gel membrane (Fig. 4). It was found that 15 mg/mL caused the greatest augmentation in signal strength for the MIP-sol-gel electrode after which point the insulating effect of the methacrylate particles overrode the imprinting effect of the MIP. Interestingly, a linear decrease in oxidation potential was observed with respect to polymer concentration in the sol-gel. In the case of theophylline this decrease was from +1.22 V the lowest concentrations tested ( $0\text{--}7.5\text{ mg}\cdot\text{mL}^{-1}$ ) to +1.09 V for the highest ( $30\text{ mg}\cdot\text{mL}^{-1}$ ).

#### Electrochemical characterization

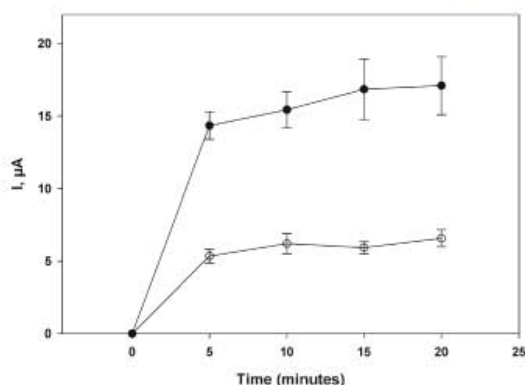
The devised theophylline sensor made by the immobilization of MIP microspheres in a sol-gel matrix was subsequently used in adsorptive stripping voltammetric determination of the alkaloid using DPV. A baseline was taken at  $t_0$  so as to negate any nonspecific interactions between the graphite support and the analyte; all subsequent measurements were subtracted from this initial level. An accumulation time of 5 min was



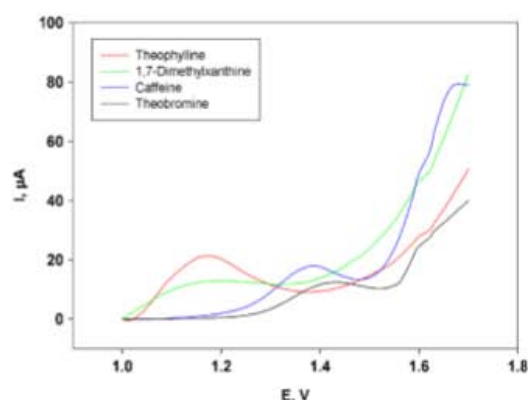
**Fig. 4** Optimisation of the concentration of polymer particles in the MIP-DMF suspension used in the synthesis of the MIP-sol-gel membrane (●) and NIP-sol-gel control electrode (○) up to 30 mg/mL for 0.27 mmol of theophylline

chosen for measurements due to the minimal signal increase which occurred thereafter; additionally, this low increase was accompanied by an increased inter-electrode signal heterogeneity causing a substantial rise in RSD (Fig. 5).

When different methylxanthines were assayed with the prepared electrode, oxidation peaks of +1.14, +1.18, +1.36 and +1.4 V were observed for 1,7-dimethylxanthine, theophylline, caffeine and theobromine respectively (Fig. 6). An increase in oxidative peak width observed in the MIP-sol-gel electrode is due to a decrease in the rate of electron transfer, a problem synonymous with sensors incorporating non-conductive monomers. Though oxidation peaks can be sharpened by reducing the scan rate used, this in turn increases the duration of measurement and cannot be an ultimate solution to this phenomenon [23]; the peak width is in keeping with other voltammetric MIP-incorporating systems [13].



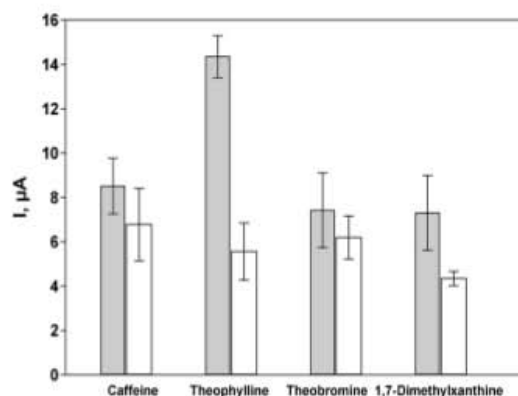
**Fig. 5** Dynamic response of MIP-sol-gel electrode (●) and NIP-sol-gel control electrode (○) toward the primary imprinted methylxanthine (Theophylline) in a pH=3 phosphate buffer solution at a concentration of 0.27 mmol·L<sup>-1</sup>



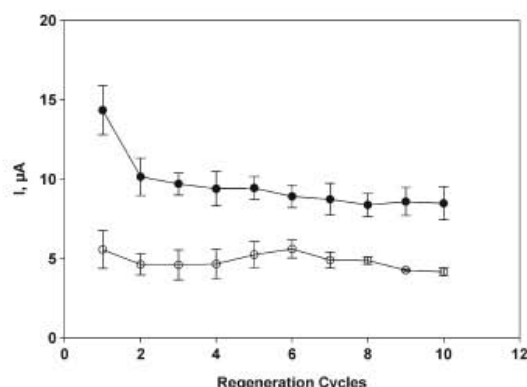
**Fig. 6** DPV voltammograms of the MIP-sol-gel electrode for caffeine, theophylline, theobromine and 1,7-dimethylxanthine at a concentration of 0.27 mmol·L<sup>-1</sup>,  $t=5$  min, range 1–1.7 V, a pulse duration of 300 ms, pulse potential of 0.01 V and scan rate of 0.04 V·s<sup>-1</sup>

Current intensities were extracted from the profiles by subtracting the background signal and averages were made ( $n=5$ ). RSD was calculated as 6.85 % for the primary target and an intensity of 258.1 % (relative to control NIP-sol-gel electrode) (Fig. 7). Lesser differentiation was seen between 1,7-dimethylxanthine, caffeine and theobromine which yielded intensities being only 168.1, 125.6 and 119.7 % with respect to their controls. Though uric acid, acetaminophen, ascorbic acid and glucose were also tested, no oxidation peaks were produced within the measurement range, demonstrating a reduced interference from non-xanthine compounds.

Regeneration of the MIP-sol-gel immobilized electrode was attempted. The temperature of 60–65 °C, duration of 10 min, and acidic strength of 0.05 M HCl, were optimised. Similar to that found during the optimisation of the deposition



**Fig. 7** Oxidation peak heights of the MIP-sol-gel electrode (solid bars) and NIP-sol-gel electrode (white bars) for caffeine, theophylline, theobromine and 1,7-dimethylxanthine at an analyte concentration of 0.27 mmol·L<sup>-1</sup>



**Fig. 8** Regeneration of MIP-sol-gel electrode (●) and NIP-sol-gel control electrode (○) using thermal-acidic treatment calculated from  $n = 5$  replications

of the gel, strong acid and sustained augmented temperatures were detrimental to the integrity of the sol-gel structure; thus the parameters were determined. It was also seen that use of the electrode immediately following regeneration caused erratic results; this is believed to be due to the electrode body acting as a thermal battery, thus a relaxation period was required to return the electrodes to a base level.

As was observed by Alizadeh et al. [13], measures subsequent to the initial binding event decreased in intensity. Such was the behaviour seen in the MIP-sol-gel electrode whereby all measures following the first were approximately 70.7 % of

the initial measurement (Fig. 8). It was seen, however, that the linear pattern seen from the first regeneration cycle one was consistent for up to 40 regeneration cycles (not shown) with an average signal loss of 2.35 % per cycle. The initial 29.3 % decrease, is due to the occupation of the deeply-seated, high affinity binding sites within the MIP particle structure which cannot be completely cleaned following the initial binding event. This decrease from the initial signal intensity could be reduced with the use of a MIP synthesized via photo-activated polymerisation rather than thermal polymerisation; this would greatly increase the number of lower affinity binding sites; such sites would be suitable for template recognition whilst also facilitating a more thorough regeneration of the sensor though conversely, could reduce the accuracy of the resulting sensor by facilitating secondary structural analogues to bind in these lower energy sites [38]. The subsequent preferential recognition of the analyte exhibited by the MIP-sol-gel electrode can be attributed to binding sites located on the aforementioned 'wrinkled' surface of the particles. The efficacy of the regeneration of the sensor hinges on the use of macroporous microparticles, rather than bulk-polymerised monoliths, whereby a permanent and heterogeneous pore structure allows the unhindered removal of the template from the binding sites on the particle surface.

The limit of detection (LOD) of the sol-gel immobilized MIP was seen to be 1 μM ( $y = 53.436x + 0.0053$ ;  $R^2 = 0.984$ ), consistent with the LODs of conductive sensors employing similarly synthesised un-specialised MIP particles as well as being in keeping with other contemporary electrochemical systems for the detection of theophylline (Table 1). A lower

**Table 1** Summary of different immobilisation methods for unmodified MIP particles onto conductive electrodes devices/biosensors with MIP materials for theophylline and related compounds

Template	Monomer composition	Polymer type	Immobilisation method	Sensing principle	LOD	Operational lifetime	Reference
Hydroquinone	MAA/TRIM	Macroporous microsphere	Agarose gel on glassy carbon electrode	Voltammetry	1 μM	N/A	[20]
1-hydroxypyrene	Styrene/DVB	Macroporous microsphere	Carbon ink on screen printed electrode	Voltammetry	0.1 mM	N/A	[39]
Caffeine	MAA/EGDMA	Monolith	Integrated in carbon paste electrode	Voltammetry	0.6 nM	N/A	[13]
Theophylline	MAA/EGDMA	Film	Adhered layer	Surface Plasmon resonance	0.2 mM	N/A	[40]
Theophylline	Electropolymerized phenol	Conducting polymer	Electropolymerization	Capacitance	1 μM	N/A	[41]
Theophylline	Poly (acrylic acid)	Layer by layer	Langmuir-Blodgett film	Gravimetric	N/A	N/A	[42]
Theophylline	Electropolymerized phenylenediamine + gold nanoparticles	Conducting polymer	Electropolymerization	Voltammetry	3 μM	N/A	[43]
Theophylline	Electropolymerized polypyrrole	Conducting polymer	Electropolymerization	Gravimetric	1 μM	N/A	[44]
Theophylline	MAA/ethylene glycol maleic rosinat acrylate	Film	Direct polymerization	Voltammetry	0.1 μM	N/A	[45]
Theophylline	MAA/EGDMA	Macroporous microsphere	Sol-gel on carbon paste electrode	Voltammetry	1 μM	40 cycles	this work



LOD was not possible to confirm due to the increasingly poor signal-to-noise ratio thought to be caused by interference originating from the aforementioned background currents created by the graphite electrode, inherent to the detection of methylxanthines. The authors believe that lower LOD would be possible with the incorporation of a conducting core into the MIP particles during their synthesis so as to augment the signal within the sensor rather than in the solution.

## Conclusions

A MIP-incorporating voltammetric sensor, responsive to the alkaloid theophylline has been presented. A modified sol-gel protocol was exploited to immobilize MIP microspherical particles onto epoxy-graphite electrodes which were synthesised in-house. Primary response, cross response to other alkaloids, 1,7-dimethylxanthine, caffeine and theobromine, and electrode regeneration was investigated using DPV. The preferential occupation of the surface of the sol-gel membrane by the MIP particles allowed both a quick measurement time and regeneration of the electrode. It was found a limit of detection consistent with sensors incorporating similarly synthesised MIP particles using chronoamperometry. To the authors' knowledge, this is the first report of a standard methacrylate-based MIP being used for quantitative electrochemical measurements using sol-gel immobilization methods.

**Acknowledgments** This research was supported by the Research Executive Agency (REA) of the European Union under Grant Agreement number PITN-GA-2010-264772 (ITN CHEBANA), by the Ministry of Science and Innovation (MCINN, Madrid, Spain) through the project CTQ2010-17099 and by the Catalonia program ICREA Academia.

## References

- Mello LD, Kubota LT (2002) Review of the use of biosensors as analytical tools in the food and drink industries. *Food Chem* 77(2): 237–256
- Kroger S, Turner APF, Mosbach K, Haupt K (1999) Imprinted polymer based sensor system for herbicides using differential-pulse voltammetry on screen printed electrodes. *Anal Chem* 71(17):3698–3702
- Wulff G (2013) Forty years of molecular imprinting in synthetic polymers: origin, features and perspectives. *Microchim Acta* 180(15–16):1359–1370
- Whitcombe MJ, Kirsch N, Nicholls IA (2014) Molecular imprinting science and technology: a survey of the literature for the years 2004–2011. *J Mol Recog* 27(6):297–401
- Yan HY, Row KH (2006) Characteristic and synthetic approach of molecularly imprinted polymer. *Int J Mol Sci* 7(5–6):155–178
- Wulff G, Knorr K (2001) Stoichiometric noncovalent interaction in molecular imprinting. *Bioseparation* 10(6):257–276
- Yoshimi Y, Ohdaira R, Iiyama C, Sakai K (2001) "Gate effect" of thin layer of molecularly-imprinted poly (methacrylic acid-co-ethyleneglycol dimethacrylate). *Sensors Actuators B Chem* 73(1): 49–53
- Sellergren B (1997) Noncovalent molecular imprinting: antibody-like molecular recognition in polymeric network materials. *Trend Anal Chem* 16(6):310–320
- Comack PAG, Elorza AZ (2004) Molecularly imprinted polymers: synthesis and characterisation. *J Chromatogr B* 804(1): 173–182
- Suryanarayanan V, Wu CT, Ho KC (2010) Molecularly imprinted electrochemical sensors. *Electroanalysis* 22(16):1795–1811
- Sellergren B, Shea KJ (1995) Origin of peak asymmetry and the effect of temperature on solute retention in enantiomer separations on imprinted chiral stationary phases. *J Chromatogr A* 690(1):29–39
- Bames PJ (2010) Theophylline. *Pharma* 3(3):725–747
- Alizadeh T, Ganjali MR, Zare M, Norouzi P (2010) Development of a voltammetric sensor based on a molecularly imprinted polymer (MIP) for caffeine measurement. *Electrochim Acta* 55(5):1568–1574
- Ebarvia BS, Binag CA, Sevilla F 3rd (2004) Biomimetic piezoelectric quartz sensor for caffeine based on a molecularly imprinted polymer. *Anal Bioanal Chem* 378(5):1331–1337
- Aranda M, Morlock G (2007) Simultaneous determination of caffeine, ergotamine, and metamizol in solid pharmaceutical formulation by HPTLC-UV-FLD with mass confirmation by online HPTLC-ESI-MS. *J Chromatogr Sci* 45(5):251–255
- Tzanavaras PD, Themelis DG (2007) Development and validation of a high-throughput high-performance liquid chromatographic assay for the determination of caffeine in food samples using a monolithic column. *Anal Chim Acta* 581(1):89–94
- Svorc L (2013) Determination of caffeine: a comprehensive review on electrochemical methods. *Int J Electrochem Sci* 8(4):5755–5773
- Spataru N, Sarada BV, Tryk DA, Fujishima A (2002) Anodic voltammetry of xanthine, theophylline, theobromine and caffeine at conductive diamond electrodes and its analytical application. *Electroanalysis* 14(11):721–728
- Perez-Moral N, Mayes AG (2004) Comparative study of imprinted polymer particles prepared by different polymerisation methods. *Anal Chim Acta* 504(1):15–21
- Kan X, Zhao Q, Zhang Z, Wang Z, Zhu JJ (2008) Molecularly imprinted polymers microsphere prepared by precipitation polymerization for hydroquinone recognition. *Talanta* 75(1):22–26
- Adhikari B, Majumdar S (2004) Polymers in sensor applications. *Prog Polym Sci* 29(7):699–766
- Kriz D, Mosbach K (1995) Competitive amperometric morphine sensor-based on an agarose immobilized molecularly imprinted polymer. *Anal Chim Acta* 300(1–3):71–75
- Patel AK, Sharma PS, Prasad BB (2009) Electrochemical sensor for uric acid based on a molecularly imprinted polymer brush grafted to tetraethoxysilane derived sol-gel thin film graphite electrode. *Mater Sci Eng C* 29(5):1545–1553
- Prasad BB, Madhuri R, Tiwari MP, Sharma PS (2010) Electrochemical sensor for folic acid based on a hyperbranched molecularly imprinted polymer-immobilized sol-gel-modified pencil graphite electrode. *Sensors Actuators B Chem* 146(1):321–330
- Takagishi T, Klotz IM (1972) Macromolecule-small molecule interactions - introduction of additional binding-sites in polyethyleneimine by disulfide crosslinkages. *Biopolymers* 11(2): 483–8
- Mujahid A, Lieberzeit PA, Dickert FL (2010) Chemical sensors based on molecularly imprinted sol-gel materials. *Mater* 3(4): 2196–2217
- Ye L, Weiss R, Mosbach K (2000) Synthesis and characterization of molecularly imprinted microspheres. *Macromolecules* 33(22):8239–8245

28. Ocaña C, Arcay E, del Valle M (2014) Label-free impedimetric aptasensor based on epoxy-graphite electrode for the recognition of cytochrome c. *Sensors Actuators B Chem* 191:860–865
29. Patel AK, Shama PS, Prasad BB (2008) Development of a creatinine sensor based on a molecularly imprinted polymer-modified sol-gel film on graphite electrode. *Electroanalysis* 20(19):2102–2112
30. Sherrington DC (1998) Preparation, structure and morphology of polymer supports. *Chem Commun* 21:2275–2286
31. Castell OK, Allender CJ, Barrow DA (2006) Novel biphasic separations utilising highly selective molecularly imprinted polymers as biorecognition solvent extraction agents. *Biosens Bioelectron* 22(4): 526–533
32. Mohamed MH, Wilson LD (2012) Porous copolymer resins: tuning pore structure and surface area with non reactive porogens. *Nanomater* 2(2):163–186
33. Patel AK, Sharma PS, Prasad BB (2009) Electrochemical sensor for uric acid based on a molecularly imprinted polymer brush grafted to tetraethoxysilane derived sol-gel thin film graphite electrode. *Mat Sci Eng C-Bio S* 29(5):1545–1553
34. Patel AK, Shama PS, Prasad BB (2009) Voltammetric sensor for barbituric acid based on a sol-gel derived molecularly imprinted polymer brush grafted to graphite electrode *Int J Pharm* 371(1–2): 47–55
35. Liu J, Chaudhury MK, Berry DH, Seebergh JE, Osborne JH, Blohowiak KY (2006) Effect of surface morphology on crack growth at a sol-gel reinforced epoxy/aluminum interface. *J Adhes* 82(5): 487–516
36. Viana MM, Mohallem TDS, Nascimento GLT, Mohallem NDS (2006) Nanocrystalline titanium oxide thin films prepared by sol-gel process. *Braz J Phys* 36(3B):1081–1083
37. Brittain HG (2007) Profiles of drug substances, excipients and related methodology: critical compilation of pKa values for pharmaceutical substances, vol 33. Academic, San Diego CA
38. Castell OK, Barrow DA, Kamarudin AR, Allender CJ (2011) Current practices for describing the performance of molecularly imprinted polymers can be misleading and may be hampering the development of the field. *J Mol Recog* 24(6):1115–1122
39. Kirsch N, Hart JP, Bird DJ, Luxton RW, McCalley DV (2001) Towards the development of molecularly imprinted polymer based screen-printed sensors for metabolites of PAHs. *Analyst* 126(11): 1936–1941
40. Lai EPC, Fafara A, VanderNoot VA, Kono M, Polsky B (1998) Surface plasmon resonance sensors using molecularly imprinted polymers for sorbent assay of theophylline, caffeine, and xanthine. *Can J Chem* 76(3):265–273
41. Wang Z, Kang J, Liu X, Ma Y (2007) Capacitive detection of theophylline based on electropolymerized molecularly imprinted polymer. *Int J Polym Anal Charact* 12(2):131–142
42. Niu J, Liu Z, Fu L, Shi F, Ma H, Ozaki Y, Zhang X (2008) Surface-imprinted nanostructured layer-by-layer film for molecular recognition of theophylline derivatives. *Langmuir* 24(20):11988–11994
43. Kan X, Liu T, Zhou H, Li C, Fang B (2010) Molecular imprinting polymer electrosensor based on gold nanoparticles for theophylline recognition and determination. *Microchim Acta* 171(3–4):423–429
44. Kim J-M, Lee U-H, Chang S-M, Park JY (2014) Gravimetric detection of theophylline on pore-structured molecularly imprinted conducting polymer. *Sensors Actuators B Chem* 200:25–30
45. Tan X, Wang L, Li P, Gong Q, Liu L, Zhao D, Lei F, Huang Z (2012) Electrochemical sensor for the determination of theophylline based on molecularly imprinted polymer with ethylene glycol maleic rosinate acrylate as cross-linker. *Acta Chim Sin* 70(9):1088–1094

**Article 3:**

*Virtual Screening of Receptor Sites for Molecularly Imprinted Polymers*

**Ferdia Bates**, María Concepción Cela-Pérez, Kal Karim, Sergey Piletsky, José Manuel López-Vilariño, *Macromolecular Bioscience* (2016). doi:10.1002/mabi.201500461.

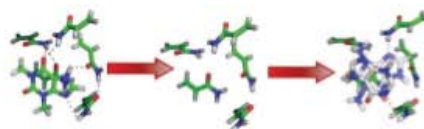




# Virtual Screening of Receptor Sites for Molecularly Imprinted Polymers

Ferdia Bates, María Concepción Cella-Pérez, Kal Karim,  
Sergey Piletsky, José Manuel López-Vilariño\*

Molecularly Imprinted Polymers (MIPs) are highly advantageous in the field of analytical chemistry. However, interference from secondary molecules can also impede capture of a target by a MIP receptor. This greatly complicates the design process and often requires extensive laboratory screening which is time consuming, costly, and creates substantial waste products. Herein, is presented a new technique for screening of “virtually imprinted receptors” for rebinding of the molecular template as well as secondary structures, correlating the virtual predictions with experimentally acquired data in three case studies. This novel technique is particularly applicable to the evaluation and prediction of MIP receptor specificity and efficiency in complex aqueous systems.



MIPs embody an exciting and dynamic research field with many hundreds of articles being published annually in all areas of analytical chemistry.<sup>[1]</sup> In conventional non-covalent imprinting scenarios using the bulk imprinting, whereby the target analyte is imprintable and there is minimal control over binding site heterogeneity, the functional monomer (FM) selection process can be resolved to the primary affinity of the template monomer complex; in other words, a high affinity primary template–FM complex indicates a high-affinity and efficiently imprinted polymer.<sup>[2]</sup>

Regardless of the efficiency of the imprinting and polymerization process, the efficacy of the artificial receptor can be severely reduced when the receptor is evaluated in real samples, in the presence of structural analogues and interferent molecules. An additional attenuator to progress may arise when the targeted analyte is not imprintable due to high price, low solubility, terminal double bonds, thermal sensitivity, or tautomeric structure. In this latter case, it may be viable to attempt the use of a “dummy template” whereby a structurally similar, imprintable molecule is used to form binding sites within the polymer.<sup>[3]</sup> It is thus possible to selectively capture an otherwise unimprintable molecule whilst still profiting from the improved stability and lower cost that MIPs relative to their biological counterparts. While this “dummy” strategy can be quite effective, the added level of complexity that it adds to the design process is significant. Even binding sites of low specificity may be unsuitable for docking and detection of the target molecule as they are imprinted around unsuitable functional groups on the dummy-template due to the structural activity relationship (SAR) paradox whereby structurally similar molecules may have significantly differing properties and complexing behavior with the FM.<sup>[4]</sup> These complications oblige lengthy laboratory screening processes to

Mr. F. Bates, Dr. M. C. Cella-Pérez, Dr. J. M. López-Vilariño  
Technological Research Centre (CIT)  
University of Coruña  
15403 Ferrol, Spain  
E-mail: iquimica@udc.es  
Mr. F. Bates  
Sensors and Biosensors Group  
Department of Chemistry Autonomous University of Barcelona  
08193 Barcelona, Spain  
Dr. K. Karim, Prof. S. Piletsky  
Department of Chemistry  
University of Leicester  
Leicester LE1 7RH, UK

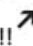
Macromol. Biosci. 2016, DOI: 10.1002/mabi.201500461

© 2016 WILEY-VCH Verlag GmbH & Co. KGaA, Weinheim

wileyonlinelibrary.com

DOI: 10.1002/mabi.201500461

1

Early View Publication; these are NOT the final page numbers, use DOI for citation !! 

determine the optimal template–FM combination and even then, the level of insight into the docking mode of an analyte or interferent, or the root cause of MIP specificity, is limited. Needless to say, any method to reduce this workload would not only save man-hours but also reduce the consumption and production of expensive chemicals and waste byproducts respectively, thus allowing further streamlining the design process and further aligning it with the green chemistry ethos.<sup>[5]</sup>

Though computational modeling has been thoroughly applied to MIPs for ranking of primary template–FM affinity with excellent results,<sup>[6–9]</sup> there has been, to date, no non-superficial way to evaluate the rebinding ability of MIPs, taking into account the cumulative steric effect of multiple FMs within the receptor site; a unique property of the open source “Autodock” virtual molecular docking suite,<sup>[10,11]</sup> in concert with established thermodynamic calculation of the optimal stoichiometric template–FM complex<sup>[9]</sup> allows for exactly this.

The *modus operandi* of the Autodock algorithm is designed to reduce the required computational workload and processing time. To achieve this, receptors and ligands are independently defined. Bond types are defined only as connections between atoms while their energy is represented within the partial charge assigned to each atom when the molecule is saved in the Autodock file format. The receptor is resolved to a static, rigid structure into which mobile ligands can be evaluated for dockability. The ligand structure is assigned a “torsion tree” whereby a selected “root” atom within its structure provides a reference point from which degrees of rotational freedom are assigned to “branches.” The degree to which the receptor can restrict this ligand mobility, along with interactions between each molecule’s structures, calculated via a number of superficially weighted, predefined parameters, allows Autodock to assign an affinity score to the receptor–ligand complex. This resolution of the receptor structure to a rigid body allows for the facile and rapid evaluation of these ideal stoichiometric complexes, created using more highly defined molecular modeling environments.<sup>[9]</sup>

To demonstrate the potential of this technique, three case studies have been selected in which visualization and interpretation of the model system may significantly aid in the understanding and development of the experimental system. All results were obtained from independently conducted and previously published works, allowing their findings to confirm the retrospective analysis. These systems are the detection of tetrahydrocannabinol (THC) using a Catechin–hydrate MIP with acrylamide as FM<sup>[12]</sup> (case study 2) and the detection of Bisphenol A and Bisphenol F using a Bisphenol A MIP with 4-vinylpyridine as the FM<sup>[13,14]</sup> (case study 3) both of which are discussed in detail in the supporting information. The

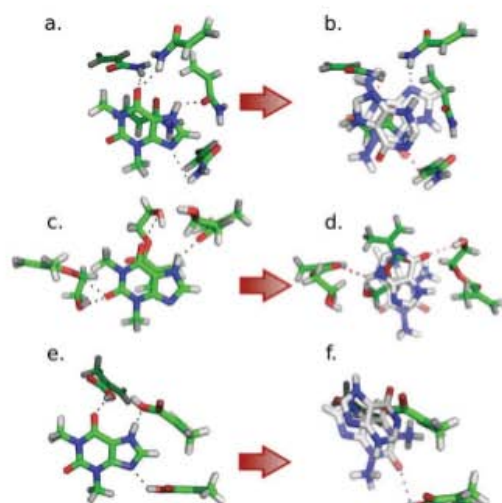
first case, involving the detection of hypoxanthine, a metabolite of adenosine triphosphate (ATP) from food products<sup>[15,16]</sup> using a selection of theophylline MIPs is detailed in brief below.

The two former studies were specifically selected due to their significance in demonstrating notable aspects of this application of the virtual docking technique. In case study 2, the scenario in which detection takes place, interferents in the form of other pharmaceuticals, caffeine and acetaminophen, serve to disrupt the primary docking event between the MIP receptor and the target, THC, rendering the MIP unable to bind it. When evaluating the affinity score, especially in a scenario where several molecules with differing characteristics and solubilities are present, it is important to keep in mind the abstract nature of the receptor model, consisting of the FM molecules of the MIP receptor only. Disregarding the crosslinking co-polymer, which can constitute upwards of 80% of the total mass of the MIP, leaves the virtual model unable to penalize the receptor for the hydrophobic contribution it makes to the net capture of the molecule of interest. For this reason, especially when modeling high solubility ligands, the scores presented cannot be directly used as an indication of capture efficiency. Instead, highly soluble molecules may interact with the receptor site while not leaving their strong solvent cage, thus blocking other lower affinity docking events from occurring. In other words, though the predicted affinity cannot always be directly equated to successful capture, it can be used to indicate the disruption of lower affinity docking events.

Evaluation of the bond distances within the ideal stoichiometric complex, such as are shown in Figure 1 and Table 1, can be used to create a hierarchy of bond strength and thus a rudimentary indication as to the probability of each bond enduring the polymerization process. Using this ranking method, incomplete imprinted sites, implying those with less than the maximum stoichiometric ratio, can be screened for respective contribution to the imprint-effect; particularly applicable in cases where there is a high stoichiometric ratio whereby the maximum ratio is unlikely to occur (case study 2).

This presented method of receptor site screening can also be used to investigate any change in binding mode when the solvent medium is changed from the typically apolar porogenic solvent to the aqueous environment for which the default Autodock scoring algorithm is optimized and in which the majority of physiological processes take place. This is particularly apparent in case study 3 where the ideal hydrogen bond-based complex was weak and so, was unable to re-form when rebinding was attempted; forming instead a hydrophobically driven complex which facilitated the alignment of the complementary donor and acceptor atoms within the receptor and ligand. In addition to this change in binding mode, the formation of only





**Figure 1.** Predicted stoichiometric complexes between theophylline and acrylamide (top-left), HEMA (middle-left), and MAA (bottom-left) formed through a thermodynamic simulation (supporting information), and the primary docking modes predicted by VINA for hypoxanthine and theophylline (transparent) for the acrylamide (top-right), HEMA (middle-right) and MAA (bottom-right) receptor; hydrogen bonds are shown for hypoxanthine (red) and theophylline (blue)

low energy hydrogen bonds between the template and FM also led to a high failure rate of these complexes, thus reducing the imprint effect and consequently the capacity of the MIP relative to the control polymer.

In this first case study, stoichiometric complexes between the MIP template (theophylline) and the FMs, acrylamide, hydroxyethyl methacrylate (HEMA) and methacrylic acid (MAA) were created using an established thermodynamic simulation protocol (supporting information). FM ratios of 5, 3, and 3 were attained for acrylamide, HEMA and MAA respectively (Figure 1) and the sites where hydrogen bonds were formed on the template were noted using standard nomenclature convention<sup>[17]</sup> (Table 1b, Figure S1, Supporting Information). This complex could then be imported into the Autodock GUI, Autodock Tools,<sup>[11]</sup> where the template could be removed; the remaining FMs were then saved as a rigid receptor file, thus securing the exact topology of the FMs and creating a “virtually imprinted” receptor site. The target and tautomeric structural analogue of theophylline, hypoxanthine, could then be docked as a ligand into this receptor using the Autodock “VINA” scoring function.<sup>[10]</sup> The docking affinity score, re-formation of hydrogen bonds and the spacial “dockability” of hypoxanthine to the receptor was compared both between receptor sites and also with that of theophylline (Figure 1, Tables 1 and 2).

As expected, acrylamide provided the strongest docking affinity in both the predicted and experimental models due to the combined effect of a high stoichiometric ratio with the dummy-template and highest rate of hydrogen bond re-formation with the target. In addition to this, the affinity of the primary template–FM complex was experimentally determined to be an order of magnitude higher than the other two FM candidates<sup>[16]</sup> thus ensuring a high probability of imprinting success during polymerization.

**Table 1.** Sites of the hydrogen bonds formed on the template and ligand structures for primary template–FM complexes (i.e., the location of the strongest and most probable hydrogen bonds) (a), and for the predicted stoichiometric complex (b) and the redocking event (c).

(a)	Theophylline <sup>a)</sup>	Hypoxanthine <sup>a)</sup>
Acrylamide	7N-H; 6-O	1N
HEMA	7N-H; 6-O	7N-H; 6-O
MAA	7N-H; 6-O	7N-H
(b)	Theophylline-FM stoichiometric ratio	Site of hydrogen bonds <sup>a,b)</sup>
Acrylamide	5	(6-O [2.3], 6-O [2.2]); 7N-H [2.5]; (9N [2.8], 9N [3.1])
HEMA	3	2-O [1.8]; 6-O [1.9]; 7N-H [2.8]
MAA	3	6-O [1.7]; 7N-H [1.8]; 9N <sup>[2]</sup>
(c)	Theophylline <sup>a,b)</sup>	Hypoxanthine <sup>a,b)</sup>
Acrylamide	9N [1.9]	1N [3.6]; 9N [4.2]
HEMA	(6-O [2.3], 7N-H [2.6]); 7N [2.8]	3N-H [2.3]; 6-O [2.8]
MAA	6-O [2.7]; 2-O [2.7]	

<sup>a)</sup>Sites of hydrogen bonds are defined on the template and ligand structures using standard nomenclature convention<sup>[17]</sup> (Figure S1, Supporting Information); <sup>b)</sup>parentheses indicate that multiple FMs bonding with the same ligand atom while semicolons separate sites on the ligand structure with bond length of each given in [Å] after each entry.

**Table 2.** Docking affinity scores (kcal mol<sup>-1</sup>) for theophylline-imprinted receptors shown in Figure 1 predicted by the VINA scoring function and by laboratory experimentation.

	Hypoxanthine		Theophylline
	Experimental <sup>[13]</sup>	VINA Score	VINA Score
Acrylamide	5.34	25.6	16.8
HEMA	5.09	24.1	16.4
MAA	2.75	22.8	14.7

The novelty of this technique, however, is not seen in the confirmation of the highest affinity template–FM combination, but rather in the explanation that it provides for the sizable difference in performance for the HEMA- and MAA-based MIPs. Though both FMs show comparable primary affinity scores, with MAA actually out-performing HEMA, the HEMA-based MIP exhibited affinity towards hypoxanthine closer to the acrylamide-based MIP while the MAA-based MIP displaying the poorest hypoxanthine-affinity of all (Table 2). As this cannot be explained by the calculated primary affinity of the template–FM complex, it must then be assumed that the enhancement must come, instead from the topology of the imprint created template–FM stoichiometric complex and the orientation of the FM dipoles within the imprinted receptor.

Visualization of the redocking event and of the imprinted-receptor itself clearly shows that hypoxanthine docks most efficiently into the receptor created by HEMA, aligning the molecule most closely to the imprinted template, theophylline, of the three receptors examined (Table 1c). This can be specifically attributed to the HEMA molecule interacting with the “2-O” oxygen atom on theophylline’s structure; this interaction is unique to HEMA, with the acrylamide and MAA stoichiometric complexes forming around the opposite side of the template.

Furthermore, regarding the HEMA receptor, the alignment of the interacting donor–acceptor atoms during the imprinting of theophylline and the hydrogen bonds formed upon the docking of hypoxanthine are the most similar of the three. Additionally, hydrogen bonds predicted to form between hypoxanthine and the theophylline-imprinted HEMA receptor involve the functional groups of the primary hypoxanthine–HEMA complex (Table 1a) thus providing the highest probability of such docking event occurring homogeneously en-mass, thus making them experimentally detectable in practice.

The poor experimental performance of MAA receptor can be attributed to its inability to form hydrogen bonds with hypoxanthine upon redocking. In the absence of such strong directional bonds, the potential energy between the MAA functional groups and hypoxanthine

may not be strong enough to desolvate the molecule out of its solvent cage and into the receptor cavity. This issue is compounded by the hydrophobia of the crosslinking polymer which further reduces the aqueous performance and experimental affinity of the MIP-receptors. An aspect discussed at greater length in case study 2 (Supporting Information). In the case of the acrylamide receptor, whose monomers were in positions similar to those of the MAA receptor, the increased stoichiometric ratio and higher primary affinity both serve to position the hypoxanthine molecule in an orientation which is then more favorable to hydrogen bond formation, thus providing sufficient energy to capture the target molecule from the solution through the concerted effect of the functional groups of the FMs.

The increased level of insight which the technique detailed in this communication provides, not only serves to rapidly evaluate the imprinting efficiency and performance of a receptor, but also can greatly reduce laboratory man-hours and costs due to its ability to rapidly simulate docking events for large numbers of both ligand and monomer libraries. This allows the user to make an accurate prediction of the specificity of the MIP using specific template–FM combinations, thus eliminating poor combinations ab initio. This, in turn, reduces the laboratory workload and screening time whilst also decreasing negative environmental impact through a reduction of harmful waste products resulting from laboratory synthesis and experimentation. Given the specificity of this technique, it is expected to be of particular relevance to high affinity MIP nanoparticles<sup>[18]</sup> where affinity separations can isolate highly homogeneous receptors.

## Supporting Information

Supporting Information is available from the Wiley Online Library or from the author.

Received: December 21, 2015; Revised: March 11, 2016;  
Published online: DOI: 10.1002/mabi.201500461

Keywords: dummy template; green chemistry; imprinting; polymers; virtual screening

- [1] M. J. Whitcombe, N. Kirsch, I. A. Nicholls, *J. Mol. Recognit.* **2014**, 27, 297.
- [2] C. Baggiani, C. Giovannoli, L. Anfossi, C. Passini, P. Baravalle, G. Giraudi, *J. Am. Chem. Soc.* **2012**, 134, 1513.
- [3] *Designing Receptors for the Next Generation of Biosensors* (Eds: S. Piletsky, M. J. Whitcombe), Springer, Heidelberg, New York **2013**.
- [4] *Pharmacology: Principles and Practice* (Eds: M. P. Hacker, W. S. Messer, K. A. Bachmann), Elsevier/Academic Press, Amsterdam; Boston **2009**.

- [5] M. de la Guardia, S. Garrigues, *Handb. Green Anal. Chem.*, Wiley, Hoboken, N.J. **2013**, pp. 3–16.
- [6] S. A. Piletsky, K. Karim, E. V. Piletska, A. P. F. Turner, C. J. Day, K. W. Freebairn, C. Legge, *Analyst* **2001**, *126*, 1826.
- [7] I. Chianella, M. Lotierzo, S. A. Piletsky, I. E. Tothill, B. Chen, K. Karim, A. P. F. Turner, *Anal. Chem.* **2002**, *74*, 1288.
- [8] K. Karim, F. Breton, R. Rouillon, E. Piletska, A. Guerreiro, I. Chianella, S. Piletsky, *Adv. Drug Deliv. Rev.* **2005**, *57*, 1795.
- [9] S. Subrahmanyam, K. Karim, S. A. Piletsky, in *Des. Recept. Gener. Biosens.* (Eds.: S. A. Piletsky, M. J. Whitcombe), Springer Berlin Heidelberg, Berlin, Heidelberg **2012**, pp. 131–165.
- [10] O. Trott, A. J. Olson, *J. Comput. Chem.* **2010**, *31*, 455.
- [11] G. M. Morris, R. Huey, W. Lindstrom, M. F. Sanner, R. K. Belew, D. S. Goodsell, A. J. Olson, *J. Comput. Chem.* **2009**, *30*, 2785.
- [12] M. C. Cela-Pérez, F. Bates, C. Jiménez-Morigosa, E. Lendoiro, A. de Castro, A. Cruz, M. López-Rivadulla, J. M. López-Vilariño, M. V. González-Rodríguez, *J. Chromatogr. A* **2016**, *1429*, 53.
- [13] A. Lasagabáster-Latorre, M. C. Cela-Pérez, S. Fernández-Fernández, J. M. López-Vilariño, M. V. González-Rodríguez, M. J. Abad, L. F. Barral-Losada, *Mater. Chem. Phys.* **2013**, *141*, 461.
- [14] M. C. Cela-Pérez, M. M. Castro-López, A. Lasagabáster-Latorre, J. M. López-Vilariño, M. V. González-Rodríguez, L. F. Barral-Losada, *Anal. Chim. Acta* **2011**, *706*, 275.
- [15] M. C. Cela-Pérez, L. Barbosa-Pereira, X. Vecino, M. Pérez-Ameneiro, A. L. Latorre, J. M. López-Vilariño, M. V. González Rodríguez, A. B. Moldes, J. M. Cruz, *Talanta* **2015**, *135*, 58.
- [16] A. L. Latorre, M. Concepción Cela Pérez, S. F. Fernández, J. M. López Vilariño, M. V. González Rodríguez, *React. Funct. Polym.* **2015**, *91*–92, 51.
- [17] J. J. Christensen, J. H. Rytting, R. M. Izatt, *Biochemistry (Mosc.)* **1970**, *9*, 4907.
- [18] A. Poma, A. Guerreiro, M. J. Whitcombe, E. V. Piletska, A. P. F. Turner, S. A. Piletsky, *Adv. Funct. Mater.* **2013**, *23*, 2821.



## **Annex**

---





**Article 2:**

*Computational design of molecularly imprinted polymer for direct detection of melamine in milk*

**Ferdia Bates**, Mirko Busato, Elena Piletska, Michael J. Whitcombe, Kal Karim, Antonio Guerreiro, Manel del Valle, Alejandro Giorgetti, Sergey Piletsky, Separation Science and Technology, [Manuscript submitted]

## Computational design of molecularly imprinted polymer for direct detection of melamine in milk

Ferdia Bates<sup>1</sup>, Mirko Busato<sup>2</sup>, Elena Piletska<sup>3</sup>, Michael J. Whitcombe<sup>3</sup>, Kal Karim<sup>3</sup>, Antonio Guerreiro<sup>3</sup>, Manel del Valle<sup>1\*</sup>, Alejandro Giorgetti<sup>2</sup>, Sergey Piletsky<sup>3</sup>

1. Sensors & Biosensors Group, Department of Chemistry, Universitat Autònoma de Barcelona, 08193 Bellaterra, Spain

2. Department of Biotechnology, University of Verona, Strada le Grazie 15, 37134 Verona, Italy

3. Chemical Biology, Department of Chemistry, University of Leicester, Leicester LE1 7RH, UK

### Abstract

A novel protocol for use of molecularly imprinted polymer (MIP) in analysis of melamine is presented. Design of polymer for melamine has been achieved using a combination of computational techniques and laboratory trials, the former greatly reducing the duration of the latter. The compatibility and concerted effect of monomers and solvents were also investigated and discussed. Two novel open source tools were presented which are: the online polymer calculator from [mipdatabase.com](http://mipdatabase.com) and the application of the Gromacs modelling suite to determine the ideal stoichiometric ratio between template and functional monomer. The MIP binding was characterised for several structural analogues at 1-100  $\mu\text{M}$  concentrations. The use of DVB as cross-linking polymer and itaconic acid as functional monomer allowed synthesis of MIP with imprint factor for melamine  $\text{IF}=2.25$ . This polymer was used in HPLC for the rapid detection of melamine in spiked milk samples with an experimental run taking 7-8 minutes. This approach demonstrated the power of virtual tools in accelerated design of MIPs for practical applications.

**Keywords:** melamine, milk, molecularly imprinted polymer, molecular modelling, molecular dynamics

### 1. Introduction

Molecularly imprinted polymers (MIPs) have become a widely known and growing part of the field of polymer chemistry (1, 2). Their great advantage is that they can be used in a wide range of environments and applications due to their high thermal and chemical stability. Additionally, high specificity and affinity in MIPs can be achieved by tailoring of their binding site at a molecular level. Although there are several formats of imprinting protocols available, by far the most popular method used in practice remains bulk imprinting, where solution containing template and

monomers is polymerised to form a solid 'brick' which can then be broken, washed and used as the specific application requires such as the packing media of HPLC or SPE columns or as the detection element of molecular sensors (2). Though it is the most tried and tested technique with a minimal number of interdependent steps, a notable challenge of the traditional molecular imprinting strategy of bulk imprinting can be seen when the molecular template selected has a low solubility in organic solvents. The solubility of the template can be increased by the addition of an appropriate functional monomer (FM), as is done in this present study to great effect; however the phase separation during polymerisation still can lead to the precipitation of the template back into the solution. This danger of template precipitation can be further minimised by the use of a co-monomer with a higher affinity to the template, however this can reduce the specificity of the polymer. Indeed, the solubility of the template in the porogen and the manner in which it interacts with the functional monomers can markedly affect the efficiency of the imprinting process (3).

Melamine, a highly nitrogenous compound, is a heterocyclic triazine. It is used extensively in the synthesis of melamine formaldehyde resin which is, in turn, used in the fabrication of everyday products such as laminates, fabric coatings, commercial filters, glues and adhesives in addition to its general use in food containers and various common kitchenwares (4). Given its close proximity to food stuffs, the need to accurately detect and monitor it is paramount, especially when melamine combines with cyanuric acid (5–7). The hydrogen bonded complex of the two molecules is highly insoluble and precipitates in the kidneys to form stones which can lead to potentially fatal kidney failure (8).

Due to the aforementioned nitrogen content, counting for two thirds of its molecular mass, adulteration of dairy products with melamine has been employed as a method of artificially augmenting the apparent crude protein content (9) and as a cheap food supplement in cattle feed (10). Contamination of infant formula and pet food with melamine has caused a global scandal following the deaths of a number of babies and the hospitalisation of several thousand more (11). In 2004 the World Health Organisation (WHO) established a tolerable daily intake (TDI) of melamine of 0.2 mg/kg of body mass, a reduction from the previous level of 0.63 mg/kg set by the American FDA based on data collected in 1983 (4).

As a result the call was issued for more discriminating detection methods for melamine. For this reason, great efforts have been made in recent years to develop reliable methods for the detection

for this molecule. Exhaustive research has been performed on the application of aptamers, immunoassays, colorimetric and electrochemical sensors for analysis of melamine (4, 12). Unfortunately these approaches suffer from high price and limited dynamic and thermal stability of specific binders used in the assays and sensors. It is logical then that the application of MIPs for the detection of melamine has been attempted using several different imprinting and polymerisation methods.

The study herein details the design and development process of a melamine imprinted polymer utilising itaconic acid (IA) and divinylbenzene (DVB) as the functional monomer and cross-linker respectively. These components, along with the porogenic solvent, dimethyl sulfoxide (DMSO) were selected with the aid of a computational algorithm to rank monomers affinity toward melamine; the affinity rankings were confirmed with complimentary laboratory trials. Additionally, ideal stoichiometric ratios between melamine and IA were calculated using two independent protocols the second of which, utilising the open source modelling suite, Gromacs (13), has not been applied to this task prior to current work. The polymerisation method and temperature were optimised to produce a polymer most suitable for use as packing media for a HPLC column. HPLC mobile phase composition and isocratic flow rate was also optimised for separation efficiency, measurement time and resolution. The MIP was characterised for selectivity and specificity against several structural analogues before being used for the detection of melamine in liquid and powdered milk samples. Rapid and selective detection of melamine was achieved with the optimised process taking 7-8 minutes. The maximum imprint factor of the polymer column was calculated to be  $IF=2.25$  and this showed discriminative preference for melamine at concentrations from 1 to 100  $\mu\text{M}$ .

## **2. Experimental**

### **2.1 Reagents**

Melamine, acetoguanamine, cyanuric acid, urea, triazine, itaconic acid (IA), divinylbenzene (80% mixture of isomers) (DVB), dimethyl sulfoxide (DMSO), 1,1' azobis-cyclohexanecarbonitrile (AICN), 2,2'-azobis 2-methylpropionitrile (AIBN) and formic acid were all purchased from Sigma-Aldrich, UK. All reagents and solvents were analytical or HPLC grade and were used without any additional purification except for DVB which was technical grade. All water used was triple distilled and deionised to a resistivity of  $18.2 \text{ M}\Omega\cdot\text{m}^{-1}$  by a Milli-Q purification system (Millipore,

Billerica, MA, USA). Real milk samples were purchased at random at local supermarkets in Leicester, UK.

## 2.3 Molecular modelling

### 2.3.1 Virtual screening of molecules

The molecular modelling protocol employed to determine and rank candidate monomer molecules for effective binding with the template has been extensively documented elsewhere (14, 15). This method uses the DREAM method of the LEAPFROG algorithm, a component of SYBYL (v. 7.3) modelling suite (Tripos Inc., St. Louis, MO, USA). The parameters of the binding upon which the binding score is calculated, have been optimised to favour the ability of monomers to form strong molecular complex with the template. All libraries screened consisted of molecular structures minimised to an energy of  $0.01 \text{ kcal}\cdot\text{mol}^{-1}$ .

Three libraries were compiled to be used in the MIP design process. A range of acidic, basic and neutral FMs were modelled with additional charged structures where appropriate. These were acrylamido-2-methyl-1-propanesulfonic acid (AMPSA), acrylic acid (AA), IA, methacrylic acid (MAA), trifluoromethylacrylic acid (TFAA), allylamine, 1-vinylimidazole (VI), 2- & 4-vinylpyridine, *N,N*-diethylamino ethyl methacrylate (DEAEM), acrylamide, 2-hydroxyethyl methacrylate (HEMA) and styrene. The cross-linking monomers modelled were selected to include range of compounds: *m*- & *p*- DVB, *mono*-, *di*-, *tri* & *tetra*- ethylene glycol dimethacrylate (EGDMA), trimethylolpropane trimethylacrylate (TRIM). A combination of commonly used porogens and solvents with known melamine solubility were modelled; these were dimethylformamide (DMF), acetonitrile, chloroform, ethanol, methanol, acetone, ethylene glycol, DMSO and water.

## 2.4 Molecular dynamics

### 2.4.1 Method 1

Determination of the stoichiometric ratio of template-FM was done via an established simulated annealing process, described elsewhere (14, 15) using the SYBYL molecular modelling suite. A

virtual cubic box containing one template molecule is packed with monomers until saturation capacity. The box is then reduced to its minimal dimensions to guard against excessive expansion of the mass as a result of repulsion between the molecules during the simulation. This box is then heated to 600°K and temperature reduced in four 25 femtosecond steps to 300°K during which time the molecules will have initially high and then decreasing mobility, allowing them to relax and orientate themselves into the position of lowest energy and thus forming a complex with the template molecule. Once the simulation is complete, the stoichiometric ratio is determined by the number of monomers bonded to the template molecule.

#### **2.4.2 Method 2**

The structures of melamine and itaconic acid molecules were downloaded from ZINC database (16) and then minimized using tools from the Chimera program (17). The melamine molecule was placed in box (3.6×3.6×3.0 nm) with itaconic acid monomers. The resulting system consisted of ca. 2175 atoms. The AMBER99sb force field was applied (18). Parameters for itaconic acid and melamine molecules were derived using the ACPYPE program using default parameters (19). The system was energy minimised and then two cycles of geometry optimisation (GO) were applied using GROMACS 4.5.5 (13). The first GO was carried out at 300 K and 1 atm by performing 1 ns of gradual annealing, thus the temperature was gradually increased from 0 to 300 K. The second GO simulation was realised at 300 K and 1 atm by performing 200 ps. The system was geometry optimised in two cycles comprising 800 steps of steepest descent followed by 3,000 steps of conjugate gradient. During the GO phases, Berendsen thermostat and barostat (20) were applied to control the temperature and pressure, respectively. The LINCS algorithm (21) as used to constrain all bond lengths involving hydrogen atoms and an integration time step of 2 fs was used. Periodic boundary conditions (PBC) were applied. Long-range electrostatic interactions were treated using the particle mesh Ewald (PME) method (22). The cut-off radius for the real part of the electrostatic interactions, as well as for the van der Waals interactions was set to 1 nm. At the end of these GOs, the number of hydrogen bond interactions between melamine and itaconic acid molecules was extracted by using Chimera software.

#### **2.5 Preparation of polymers and MIPs**

The protocol for the synthesis of the MIP and control polymer was calculated with the aid of the MIP database's polymer calculator (<http://mipdatabase.com/calc/calc.php>). Using this calculator,

speedy and accurate conversion of the determined molar ratios to usable masses and volumes, were calculated using the built-in compound parameters, accessible from drop down menus.

Following the solubility trials for melamine which determined DMSO as porogenic solvent of choice with the most favourable solubility, miscibility trials were conducted to compare DMSO with other (more compatible) solvents. 4 mL of chloroform, MeCN and DMSO were mixed with an equal volume of DVB and 44 mg of AIBN initiator in glass vials. The solutions were then agitated, degassed, sealed and polymerised at 60°C for 24 hours.

For the preparation of the MIP, 1 mmol of melamine was combined with 8 mmol of itaconic acid in 4 mL (4.4 g) of DMSO in a 20 mL screw-topped glass vial. The mixture was then sonicated until all solids were dissolved. 24.8 mmol of DVB was then added and mixed to homogeneity followed by 44 mg, 0.268 mmol of the initiator was added. This was AICN for UV and 80°C polymerisations and AIBN for the 60°C polymerisation. The mixture was purged with nitrogen for 5 minutes following thorough mechanical mixing. The vial was then sealed. Control polymers were synthesised in an identical process with the omission of the melamine template.

Thermally mediated polymerisations were carried out in an oil bath for 24 hours. For UV mediated polymerisations, the vials were instead placed into a UV reactor using a Hönle 100 UV lamp (intensity 0.157 W/cm<sup>2</sup>) (Hönle UV, UK) until turbidity was observed at which point these vials were transferred to an 80°C oil bath for 24 hours. Following polymerisation, all vials were removed and broken. Then the polymer was collected, ground and sieved to extract the 25 to 106 µm fraction which was washed with methanol for 24 hours in a Soxhlet (30 minutes approx. per cycle) and dried at 70°C until a stable weight was observed.

## **2.6 SEM analysis**

SEM analysis was executed using a MERLIN FE-SEM (Zeiss GmbH, Jena, Germany).

## **2.7 N<sub>2</sub> Pore size analysis**



Pore size and surface area analyses were carried out using a NOVA 1000 E Series Gas Sorption Analyser (Quantachrome Instruments, FL, USA) and interpreted using nitrogen BET theory (23) via the NovaWin software package.

## 2.8 Column packing and HPLC calculations

The HPLC columns used were stainless steel (50 mm× 4.6 mm) into which the polymer was packed using Slurry Packer model 1666 (Alltech, UK). This process entailed mixing the polymer particles in methanol and packing the column to a pressure of 100 bar. The columns were then tightly closed and washed with the mobile phase until a steady baseline was observed.

All HPLC experiments were conducted using a Agilent 1100 HPLC and recorded using Chemstation package (Agilent, CA, USA) and performed in triplicate (n=3). Polymer characterisation was executed using a mobile phase consisting of 50:50:0.05 water: MeCN: formic acid.

UV detectors were set to wavelengths of 204 and 240 nm. The dead volume,  $t_0$ , of the column was determined by the retention time of an injection of the mobile phase containing 10% acetone. Recovery fraction was calculated as the area under the curve of the peak relative to the area under the curve created by the analyte when injected without a column present given by equation 1.

$$Recovery\% = \frac{Recovered\ concentration}{Injected\ concentration} \times \frac{100}{1} \quad (1)$$

The retention factor 'k' was calculated using the formula give in equation 2.

$$k = \frac{t_r - t_0}{t_0} \quad (2)$$

Where  $t_r$  is the retention time of the analyte taken at maximum peak height and  $t_0$  is the dead volume of the column. The separation factor ' $\sigma$ ' of the polymer was calculated by equation 3.

$$\sigma = \frac{k_{melamine}}{k_2} \quad (3)$$

Where the subscript denotes the  $k$  value for each respective analyte; all calculations were done relative to  $k_{melamine}$ . The imprint factor ' $\alpha$ ' of the polymer was determined using equation 4.

$$\alpha = \frac{k_{MIP}}{k_{NIP}} \quad (4)$$

The theoretical plate number, representing the degree of interaction between the analyte and the polymer, was calculated by equation 5.

$$N = 5.545 \left( \frac{t_r}{w_h} \right)^2 \quad (5)$$

Where  $t_r$  is the retention time of the analyte and  $w_h$  is the peak width at half height; this was normalised with respect to the length of the column by calculating the height equivalent to a theoretical plate ( $H$ ) given by equation 6.

$$H = \frac{L}{N} \quad (6)$$

Where  $L$  is the length of the column.

## **2.9 Milk sample preparation**

All milk samples were prepared identically. For powdered samples, they were mixed with water to a concentration of 1 gram in 10 mL. Samples were then mixed in falcon tubes at a ratio of 1:1 with the acetonitrile and spiked with melamine to a concentration of 10  $\mu\text{M}$  and agitated for several minutes. The solids were then separated from the liquid via centrifugation at 5000 RPM for 5 minutes. All samples were also prepared and analysed without adulteration with melamine to confirm their purity and also to establish a base line.

## **3. Results and discussion**

### **3.1 Solvation of melamine into the porogen and the use of computational modelling**

As the objective of this work was to produce a molecularly imprinted bulk porous polymer resin, suitable for use as a HPLC column packing media, several criteria had to be satisfied. The first and foremost of these is to find a combination of template, FM and solvent which may facilitate the formation of template-FM complexes which could then be physically secured in place via subsequent polymerisation of a co-monomer. Computer modelling offers an accurate way to accelerate the selection process by creating a short list of candidates from larger libraries which may then be tested in the laboratory. In bulk imprinting, the template must be dissolved in the porogen at a concentration somewhere in the range of 0.25 – 0.4  $\text{mol}\cdot\text{L}^{-1}$ . This concentration ensures a high number of binding sites while still ensuring a high percentage of cross-linking polymer to maintain structural rigidity. However, the high template concentrations typically present in the MIP solution can also significantly affect its thermodynamic stability and cause significant differences in all families of pore morphology relative to the NIP control (Figure 1).

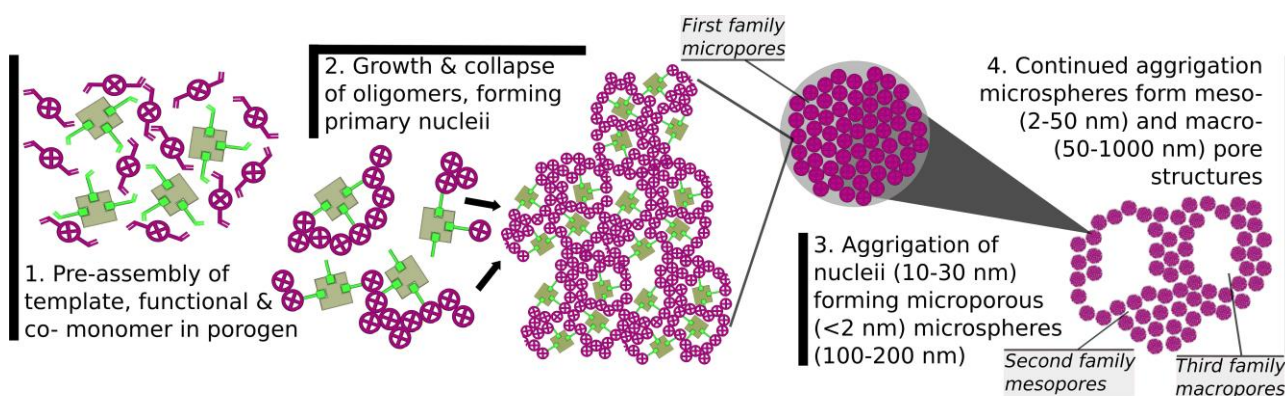


FIG 1: Schematic representation of the molecular imprinting and pore formation processes in the synthesis of a molecularly imprinted porous polymer resin

Ahead of laboratory tests, melamine was screened against virtual libraries of common FMs, cross-linkers and solvents. This was done primarily due to the exceptionally poor solubility of the molecule in the conventionally used porogenic solvents. A search of the literature for melamine non-covalent imprinting protocols showed the most commonly used solvating porogen was either pure methyl alcohol (24, 25) or a mixture of water and methyl or ethyl alcohol (26, 27). Two further works reported the successful detection of melamine using cyromazine, a structural analogue of melamine, as a template and water-alcohol binary porogenic solvent (28, 29). One additional work also reported the successful use of benzene (30) as the porogen. All these cited works used the methacrylate monomers MAA and EGDMA and relied on strong solvent interactions in addition to the enhancement of template solubility provided by the FM. While it is clear that such attempts have yielded favourable results, the apparent necessity to employ solvents of high polarity and hydrogen-bonding capacity must be assumed to be a significant source of disruption to the formation of high affinity template-FM complexes in the solution (31, 32).

An alternative to this approach is the use of ethylene glycol as a porogen in order to dissolve the melamine (33). While melamine has comparatively high solubility in ethylene glycol, it also has extremely high hydrogen bonding capacity and viscosity making it a challenging candidate for use as a porogenic solvent (31). The solution employed by Yusof et al. was to use an imprinting mechanism based on aromatic and Van der Waals interactions between melamine and 9-vinylcarbazole. Mechanical mixing was used to facilitate radical mobility within the solution and to reduce autoacceleration.

### 3.1.1 Computational modelling and laboratory trials

Since the existing protocols did not satisfy the requirements of this work, methodical laboratory pre-polymerisation trials were conducted to find an optimal combination of FM and solvent which would facilitate the solvation of melamine at a sufficient concentration and ultimately produce an effective MIP. The *ab initio* use of virtual screening models in concert with laboratory trials to confirm these predictions ahead of any polymerisation event allows for the negation of any intermolecular differences in monomer reactivity which might otherwise affect the apparent results if the affinity of the FM candidates were compared in their polymerised form. Computationally determined affinity rankings were used to create a logical order of candidates. A summary of these results can be seen Figure 2.

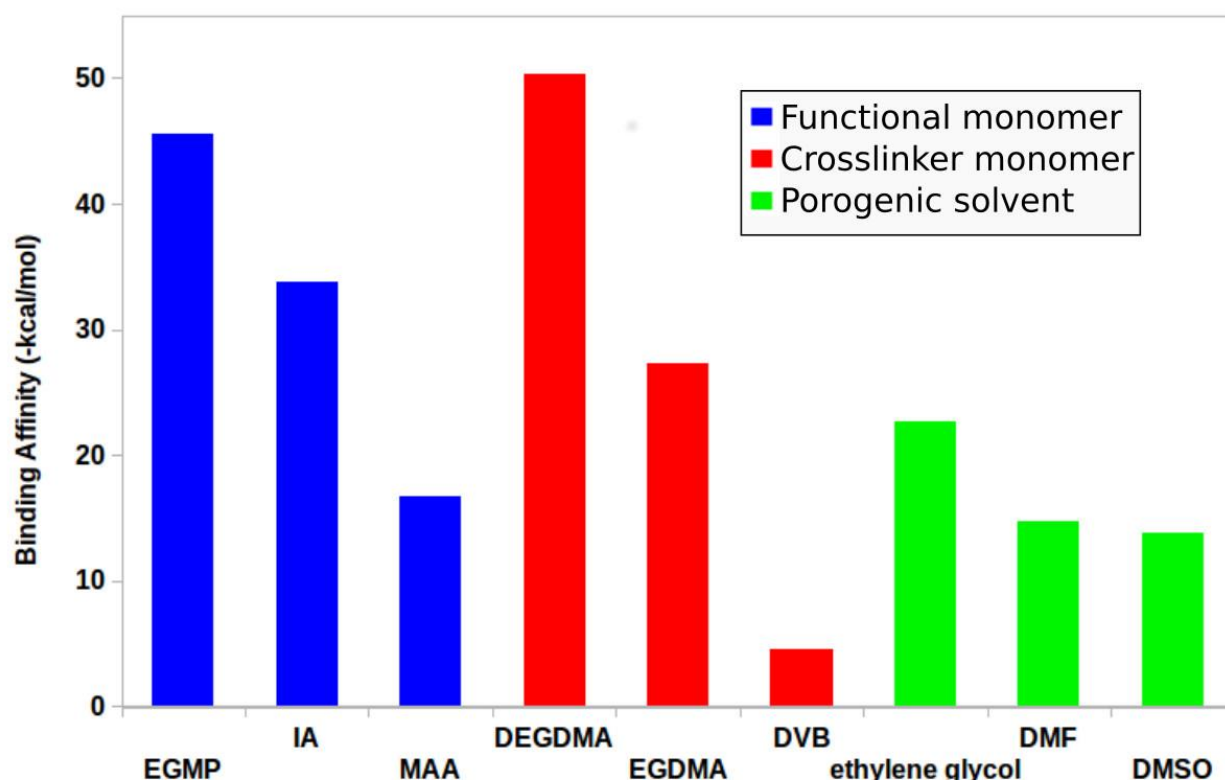


FIG 2: Histogram summarising the binding affinities of functional monomer, cross-linker monomer and solvent molecules for melamine as calculated by the SYBYL molecular modelling platform

Though the virtual scoring algorithm employed (described in detail elsewhere (34)), is optimised to predict the probability of hydrogen bond formation and strength, it cannot predict to what degree the intermolecular affinity and the formed complex will affect or augment the individual solubilities of each of the two molecules when combined in a solvent. Due to the poor solubility of melamine in organic solvents, the enhancing effect of the FM was heavily relied on its ability to dissolve it. Melamine's three amine groups, causing it to have a weakly basic nature, are most disposed to complex with acidic functional groups with respect to the enhancement of its solubility. Monomers

HEMA and acrylamide were unable to dissolve melamine in any solvent to the degree where conventional methods of molecular imprinting would be feasible.

Having failed to dissolve melamine in several conventional porogenic solvents, it was observed that each of the three acidic FMs, shown in Figure 2, could enhance the solubility of the template in DMSO to a level of 0.25 mol·L or 1 mmol in 4 mL. This implies e.g. an increase of template solubility by one order of magnitude for melamine, caused by the addition of the IA (35). DMSO, though less commonly used than porogens such as DMF, acetonitrile or chloroform due to its relatively high polarity in addition to its augmented hydrogen bonding capacity and Hansen solubility parameters ( $\delta_T$ ) (31, 32) may be acceptable where the template-FM complex is sufficiently durable. This is also reflected in the similar melamine-affinity scores given to both of these solvents by the molecular model (Figure 2).

### 3.1.2 Selection of the cross linking monomer

For bulk synthesised MIPs, the addition of the cross-linking monomer can significantly alter the equilibrium of the solution. This equilibrium shift is especially apparent when the template molecule is present at saturated levels or if the complex between the FM and template is weak. Such a change in solution parameters can lead to the precipitation of the template in solution through the breakage of the stabilising bonds within the dissolved complex. While the use of a cross-linking monomer with higher template affinity may guard against this precipitation of low solubility templates, the consequence of this may be a higher incidence of non-specific interactions during post-polymerisation testing and use of the MIP.

*Di*-, *Tri*-, and *Tetra*- EGDMA exhibit increasing hydrophilic character. These monomers can be used as cross-linkers when a low solubility template or an unstable template-FM complex is being imprinted (36, 37). The presence of an increasing number of oxygen atoms might also augment the probability of non-specific binding since they can each be employed as acceptor atoms in the formation of a hydrogen bond (38). This can lead to lower specificity and poor imprint factors (IF). Conversely it is preferred to use cross-linking monomers which exhibit low affinity towards the template and thus does not compete with the binding mechanism of the template-FM complex. One combination of such a MIP is the use of MAA and DVB as FM and cross-linker respectively (39) whereby the weaker van der Waals interactions between a template and cross-linker do not interfere with stronger hydrogen-bonds formed by the template and FM at the receptor site.

One of the most commonly used FMs, MAA, was rejected for this work because its predicted affinity was deemed too similar to that of the porogen DMSO. This has been confirmed by poor stability of melamine in a corresponding monomer mixture containing MAA. This precipitation did not occur when the higher affinity cross-linkers, EGDMA or DEGDMA, were added. These methacrylate monomers were also rejected as the affinity of these cross-linkers to melamine was interfering with the melamine-FM complex.

Ultimately, the combination of melamine, IA, DVB and DMSO for template, FM, cross-linker and porogen respectively, was considered to be optimal. The strength of the melamine-IA complex could also be immediately observed due to the stability of the solution upon the addition of the low affinity cross-linker DVB to monomer mixture, where no precipitation was observed.

Though IA and DVB was seen to be an excellent combination for the formation of a highly selective MIP, the necessity to use DMSO as a porogen in order to dissolve melamine raised concerns about the dynamic miscibility of the solution during polymerisation. Though the difference in  $\delta_T$  is an initially negligible issue due to the relatively low molecular weights of the (*mono*) DVB and DMSO, it becomes a hindrance to the homogeneous dispersion of DVB throughout the DMSO during polymerisation as the chain length and augmented molecular weight finally induces phase separation (40). To confirm the feasibility of the use of DMSO as a porogen in this scenario, DVB polymer blanks were prepared using DMSO as well as the more commonly used porogens, chloroform and acetonitrile. SEM micrographs were taken to view the effect of the porogen on the formation of the second and third family pore structures with respect to increasing  $\delta_T$  (41).

As can be seen in Figure 3, the pore structure of the chloroform-DVB polymer shows high homogeneity with all microspheres completely merged. The intermediate  $\delta_T$  of the acetonitrile-DVB combination yielded adequate third family pore formation albeit with the merged microsphere-aggregates clearly visible in the morphology. Apparent puckering in the surface of the DMSO-DVB shows the endurance of the early stage microsphere-morphology due to a more abrupt phase transition. However, an acceptable third family pore structure is visible to a degree comparable to that of the acetonitrile-DVB polymer and was thus deemed satisfactory for use as a porogen for the DVB polymer.

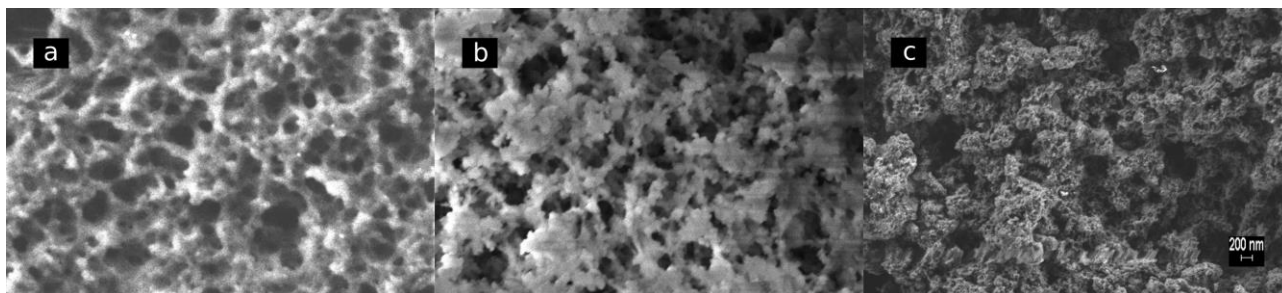


FIG 3: SEM micrographs showing the effect of differences in  $\delta_T$  and polymer-porogen miscibility on third family pore formation and homogeneity for (a) chloroform-DVB, (b) acetonitrile-DVB and (c) DMSO-DVB

### 3.2 Thermodynamic calculation of stoichiometric ratio and MIP composition

As an improvement on the standard 1:4 ratio generally employed in laboratory syntheses (42), determination of the ideal stoichiometry of a potential template-FM combination can allow for a greater deal of insight during the polymer and protocol design process. In order to optimise MIP composition, the knowledge of the ideal stoichiometric ratio between the template and FM, melamine and IA was required. By calculating the maximum number of FM molecules capable of forming high quality hydrogen bonds with the template, specificity and sensitivity can be maximised. This was achieved through minimisation of the formation of lower affinity binding sites (43).

The use of a computationally determined ratio alone, which is calculated under ideal conditions, has been reported to produce an inferior MIP with a high incidence of non-specific and heterogeneous binding behaviour caused by the disruption of the majority of the template-FM complexes by the solvent and cross-linker (44). For this reason, an excess of monomer as a 'factor of safety' was added to the calculated ideal ratio. This factor of safety cannot be an unchecked saturation of the solution with the FM as this can also lead to FM-aggregation or dimerisation, also leading to a net reduction of receptors within the MIP (15, 42, 45).

Melamine-IA stoichiometric ratios of 6 were calculated by both computational methods attempted with both complexes showing identical bonds for each (Figure 4). This ratio of 6 with respect to the use of a carboxylic dipole is also independently confirmed by a third method recently published in the literature (25). This ideal ratio of 6 was increased to 8 for the practical synthesis of the MIP.



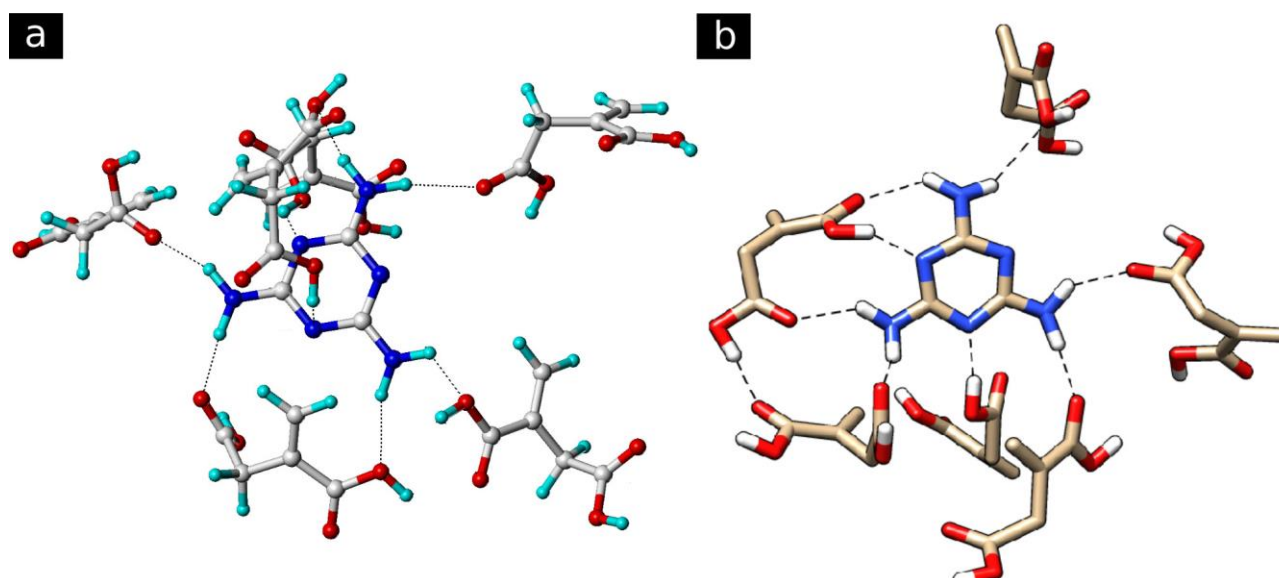


FIG 4: Image of ideal melamine-IA stoichiometric complexes calculated using parameters based on (a) the SYBYL modelling platform and (b) the open source Gromacs modelling platform

Thus the newly determined parameters for molecular dynamics protocol utilising the Gromacs open source molecular dynamics package were doubly confirmed. This confirmation of the Gromacs protocol is of added interest due to its departure from convention of the relaxation of the FM around the template via simulated annealing, from elevated to ambient temperature which has been the method of choice for the calculation of template-FM stoichiometric ratio to date. The Gromacs process, conversely, relies on a series of minimisation cycles followed by a final geometric optimisation and relaxation step all of which are conducted below physiological temperature limits and thus allow the calculation to be applied to thermally sensitive or biological molecules.

Having determined the optimal volumes of melamine, IA and DMSO which were dictated by stoichiometry and solubility limits, the calculation of the exact volume of cross-linker and initiator was calculated with the aid of the free online polymer calculator from the MIP database (see Materials and Methods). This allows for the facile calculation of all molecular and volumetric ratios with the inbuilt unit conversion facility. In this way, the masses or volumes of all of the polymerisation mixture can be balanced against the required volume of porogenic solvent, typically constituting to 50% of the total solution (42).

### 3.3 Selection of initiator and polymerisation temperature

The rate of radical propagation, of chain growth and the thermodynamic 'goodness' of the solvent all affect the point at which chain collapse and precipitation into the solution occurs. This precipitation point can be significantly delayed or advanced depending on the effect of the template.

When the template has a high level of solubility in the porogen, the thermodynamic stabilisation of oligomer during chain growth leads to an enhancement in pore and precipitate size (3). Alternatively, as is the case in this study, the decreased stability that melamine imbues to the growing oligomer was seen to force the precipitation of the chain at a shorter molecular weight and thus reduce the pore structure and net surface area of the polymer. Adding to the complexity of this effect is the enhancement of melamine solubility in DMSO with respect to increased temperature (46) which increases the stability of solvated melamine-IA complexes though any increase in temperature will have a similar effect on the rate of radical propagation (47). A general rule of MIP synthesis with respect to the formation of selective binding sites is that the process should take place over a long period of time, at a low temperature and with a low concentration of initiator (48). However, as is the present case, the final application of HPLC column packing media and the low thermodynamic stability of the melamine-IA complex required an elevated temperature to maintain sufficient mechanical rigidity and oligomer stability. The mass of the initiator was, however placed at a constant value of 44mg or 1% of the total monomer mass.

Two radical initiators were selected for polymerisation both of which had differing rates of decomposition ( $k_d$ ). AIBN at 60°C and AICN at 80°C decomposing at rates of approximately  $17 \times 10^{-5} \text{ s}^{-1}$  and  $6.5 \times 10^{-6} \text{ s}^{-1}$  respectively (47). The latter can also be initiated via UV excitation at room temperature. The destabilising effect of melamine on the polymerisation process was most evident during room temperature polymerisation whereby phase separation was occurring 33% faster than in the case of the control. This clear and immediate demonstration of oligomer destabilisation in solution by melamine was reflected when the results of the porosity and surface area measurements were analysed (Table 1). Pore volume was reduced by one order of magnitude due to this effect with a similar reduction in total surface area. Due to the increased rate of radical propagation resulting from the AIBN-initiated polymerisation at 60°C, the pore volume was notably reduced from that of the slower radical production rate of the AICN-initiated polymerisation at 80°C. The pore volume of the NIP control was 140% that of the MIP. While the difference in surface area between the MIPs and NIPs of the two thermally initiated polymers was comparable, the very similar pore volume of the AIBN-initiated MIP and NIP cause it to be ultimately selected for further tests as it allowed for the most accurate analysis of the imprint factor.

TABLE 1: Summary of porosity and surface area measurements calculated using the N<sub>2</sub> BET method

Polymerisation type		Radical Initiator	Polymer ID	Pore Volume (cc·g <sup>-1</sup> )	Pore radius (Å)	Surface area (m <sup>2</sup> ·g <sup>-1</sup> )
temperature	Energy source					
20°C	UV	AICN	MIP	0.0077	9.6	24.61
			NIP	0.0265	9.3	75.88
60°C	Thermal	AIBN	MIP	0.1660	8.8	385.30
			NIP	0.1710	8.8	400.10
80°C	Thermal	AICN	MIP	0.6670	8.9	432.38
			NIP	0.9483	8.9	445.10

### 3.4 Mobile phase selection and polymer characterisation

Following its selection as the polymer most comparable to its control, the AIBN-initiated MIP, polymerised at 60°C, was packed into HPLC columns. The use of the MIP as the stationary phase in a HPLC flow system has the distinct advantage of reducing the required detection time by decreasing the number of preparatory steps and negating the need for a separate regeneration process, as is the case with the more commonly used SPE method of detection. As a goal of this work was to create such an incorporated sensor, a comprehensive characterisation of the MIP was carried out under conditions typical to the detection of melamine-contaminated milk (49). To facilitate the MIP's accurate characterisation, acidification of the mobile phase was necessary due to the failure of FM-FM dimerisation events during polymerisation. This dimerisation of surplus functional groups is essential to minimise non-specific interactions between the polymer and target, the absence of which may lead to the complete negation of any apparent imprinting event via the higher incidence of exposed functional groups at the surface of the polymer (42). This phenomenon was made apparent by a high retention time, notably greater than that of the MIP, exhibited by the NIP toward melamine when a purely aqueous mobile phase was tested. This high retention time was accompanied by broad peak with extreme tailing caused by the exposure of IA-carboxylic groups on the surface of the NIP. Interestingly, in addition to the reduced retention time, the MIP column also showed a greatly reduced level of tailing which was attributed to the higher level of order and reduced accessibility of the functional groups as more were engaged in a single receptor site at the MIP surface. The non-specific interactions exhibited by the NIP were disrupted with the

acidification of the mobile phase with a weak acid. With the addition of 0.05% formic acid, the imprinting factor could be viewed and the polymer specificity characterised.

It was immediately notable that the peak tailing was still present in the NIP control even when the optimised mobile phase was implemented (Figure 5). Tailing was far less of an issue in the case of the MIP and its narrower peaks were accompanied with increased peak-symmetry. Optimisation of experimental conditions showed an increase in imprinting factor ( $\alpha$ ) with respect to reduced concentration and flow rate with a maximum value of 2.25 (Figure 6). A flow rate of  $0.5 \text{ mL} \cdot \text{min}^{-1}$  was ultimately selected due to practicality of the analysis.

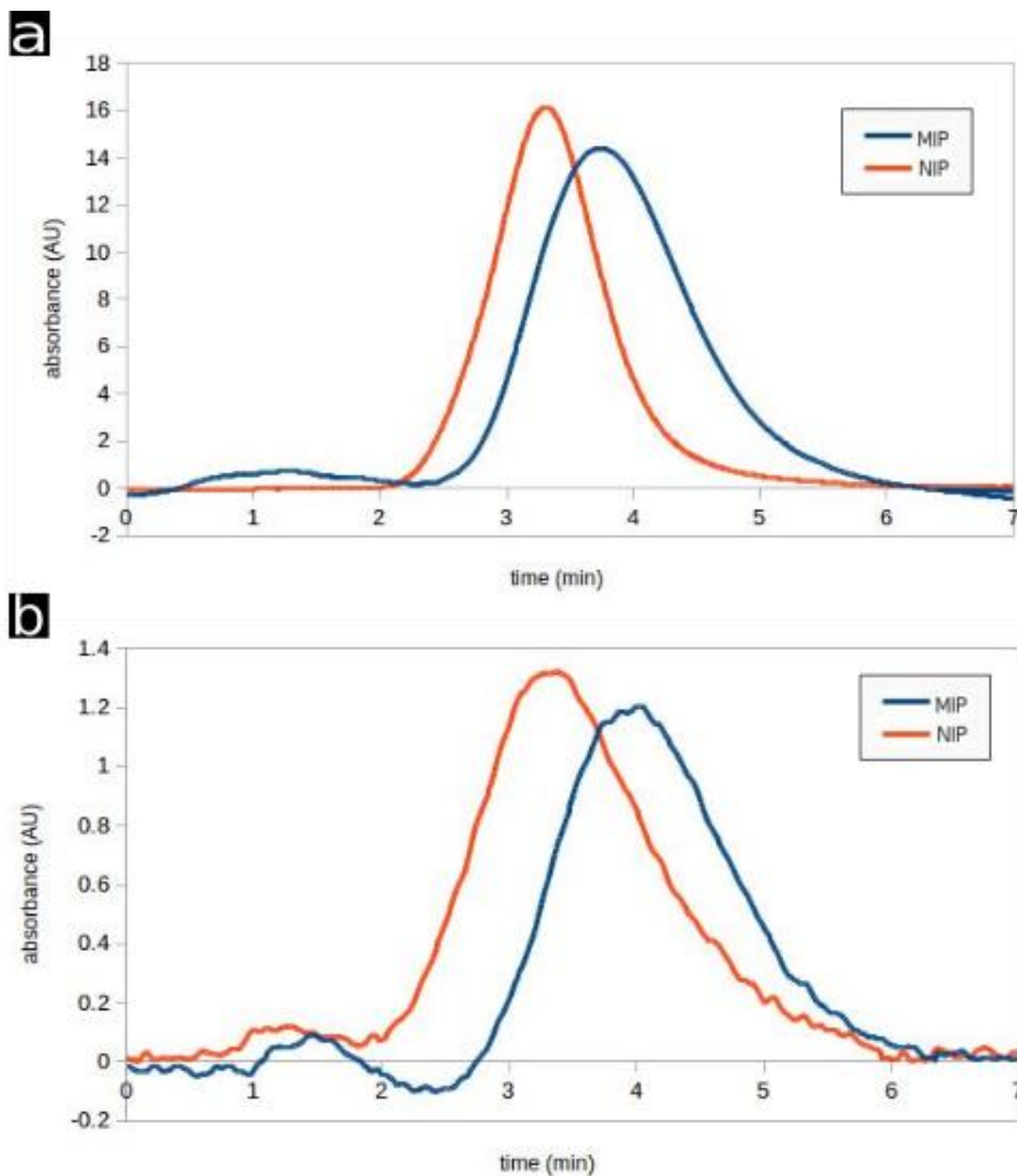


FIG 5: Chromatogram of the peak corresponding to a 10  $\mu\text{L}$  injection of (a) 100  $\mu\text{M}$  and (b) 10  $\mu\text{M}$  melamine solution in a 50:50:0.05 water, acetonitrile, formic acid and 0.5  $\text{mL}\cdot\text{min}^{-1}$  mobile phase

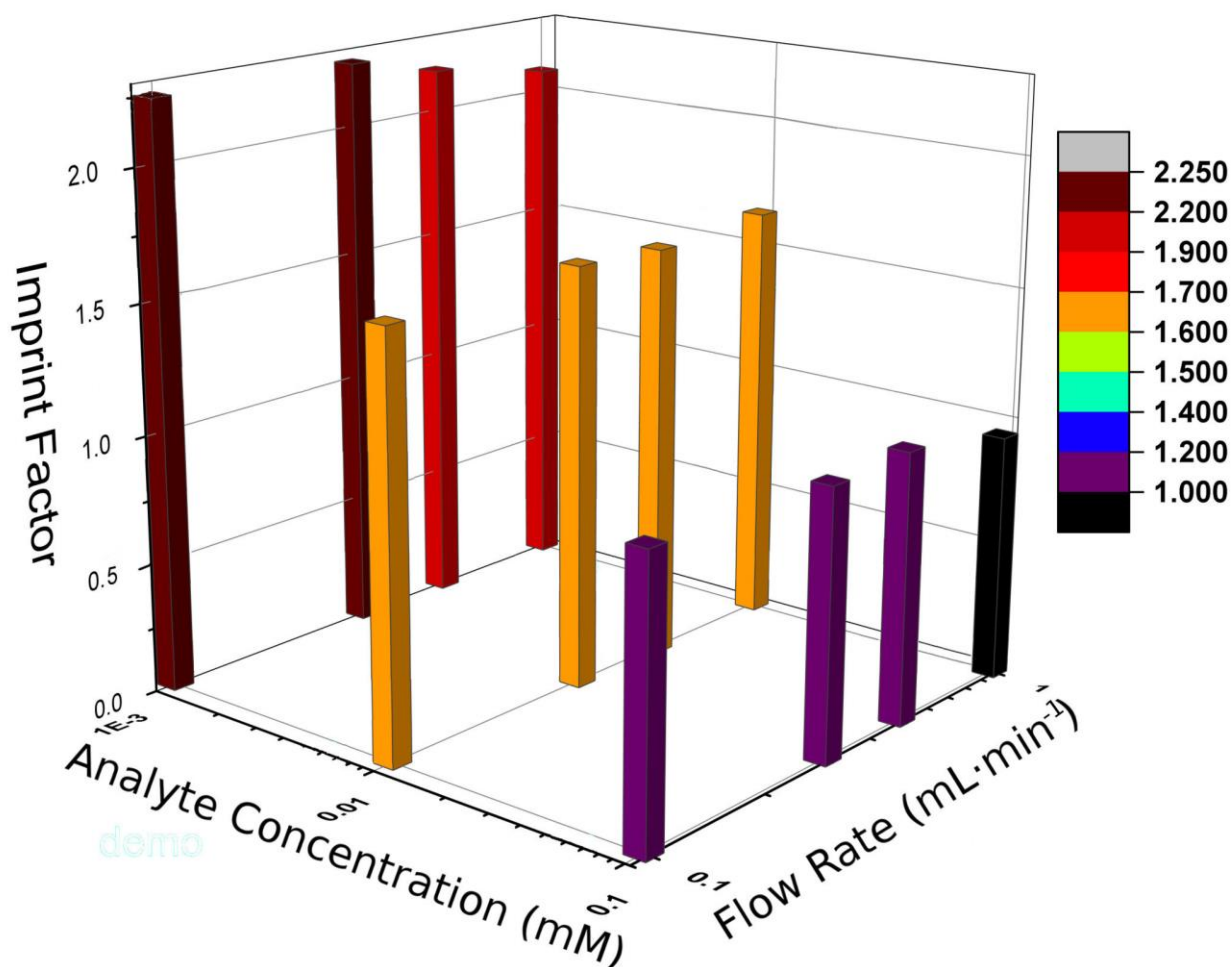


FIG 6: 3D histogram detailing imprint factor 'IF' as a function of flow rate and melamine concentration; injection volume was 10  $\mu\text{L}$

Cross-response of the polymer under these conditions could then be analysed. It was seen that due to the low affinity of the cross-linking polymer, DVB, specificity towards melamine could be rapidly achieved while secondary molecules were flushed through the column without any interaction (Table 2). Acetoguanamine, the molecule which exhibited a retention factor ( $k$ ) most similar to melamine, is retained notably longer on the non-imprinted polymer than melamine due to a higher primary affinity towards IA. This order is reversed on the MIP and must be attributed to the morphology of the imprinted receptors within its structure. Melamine recovery is also superior in the case of the MIP while for all other secondary molecules tested; the NIP control displayed improved recovery for all other secondary molecules tested.

TABLE 2: Affinity and capacity factors characterising the (a) MIP and (b) NIP for cross response at a flow rate of 0.5  $\text{mL}\cdot\text{min}^{-1}$  and a 10  $\mu\text{L}$  injection volume of 10  $\mu\text{M}$  concentration

(a)

	Retention time (min)	k	$\sigma$	$\alpha$	% Recovery	N	H (mm)
melamine	4.20	1.49	N/A	1.39	94.59	43.14	1.16
acetoguanamine	4.07	1.41	1.06	0.91	78.92	29.19	1.71
Cyanuric acid	1.55	-0.08	N/A	N/A	38.45	1.09	45.71
triazine	1.74	0.03	44.38	0.05	91.99	56.48	0.89
urea	1.60	-0.05	N/A	N/A	108.25	69.30	0.72

(b)

	Retention time (min)	k	$\sigma$	% Recovery	N	H (mm)
melamine	3.29	1.09	N/A	83.3	24.61	2.03
acetoguanamine	4.02	1.55	0.70	79.14	9.78	5.11
Cyanuric acid	1.53	-0.03	N/A	56.07	0.27	187.77
triazine	2.58	0.64	1.70	100.09	6.34	7.88
urea	1.79	0.14	7.91	114.77	22.31	2.24

### 3.5 Testing on spiked real milk samples

Having confirmed the efficacy of the imprinting protocol and the resulting polymer, milk samples were prepared to test the ability of the MIP to detect melamine in its known role as an adulterant in dairy products. Five samples were selected from local supermarkets in order to encompass a range of fat contents and product lifespans (Table 3). It was in the screening of these spiked samples that the limitation of the combined effect of the column length and polymer surface area was made apparent. The efficiency of separation power of MIP (as well as the Blank) columns did not allow separation of the melamine peak from all other compounds in all five samples tested (Table 2). For this reason, the organic fraction of the mobile phase was increased by 50% to improve peak

separation. This had the desired effect and good recovery could be observed in four of the five samples tested (Table 4). The powdered samples showed greater levels of absorbance overall, possibly due to the presence of nondescript fibre within them, stated as being present at levels of 0.1% in sample 5. Improved recovery percentages using this polymer may be achieved with the use of a longer column which would compensate somewhat for the lower surface area observed in the MIP resulting from melamine's solubility issues.

TABLE 3: Description and content summary (g/100 mL) of milk samples tested

Sample	Description	Fats	Carbohydrate	Protein
1	Tesco everyday value British skimmed UHT milk	1.8	4.8	3.6
2	Pensworth Full fat whole milk	3.6	4.6	3.4
3	Pensworth low fat semi-skimmed milk	1.6	4.7	3.6
4	Tesco everyday value dried milk	0.06	3.0	2.1
5	Tesco Instant dried skimmed milk with added vitamins A & D	0.05	4.6	3.3

TABLE 4: Recoveries of melamine from the 5 milk samples detailed in Table 3

Sample	% of total area	% Recovery
1	17.22	94.16
2	17.39	96.11
3	17.28	66.91
4	16.17	90.07
5	14.78	88.87

#### 4. Conclusions

A new MIP HPLC column for the detection of melamine in milk has been described. Using virtual screening methods, laboratory screening time was greatly reduced. Solvent-polymer compatibility,



template affinity and polymerisation conditions were confirmed through virtual and practical methods to produce an optimised imprinted polymer. A novel new protocol was presented for the determination of template-FM stoichiometric ratio using the open source molecular dynamics software suite, Gromacs. The minimisation of affinity between cross-linking polymer and melamine, the target, allowed for a rapid and selective analysis process which, under optimised conditions took 7 to 8 minutes. The maximum imprinting factor of the polymer column was calculated to be 2.25 and showed discriminative preference for melamine at concentrations from 100 to 1  $\mu$ M. This MIP-HPLC based analysis system is a promising tool for the detection of melamine in food products.

## 5. Acknowledgements

This research was supported by the Research Executive Agency (REA) of the European Union under Grant Agreement number PITN-GA-2010-264772 (ITN CHEBANA) and the Spanish ministry of economy MINECO (Project CTQ2013-41577-P). M. del Valle acknowledges support by the Catalonia program ICREA Academia.

## 6. References

1. Haupt K, Mosbach K (2000) Molecularly Imprinted Polymers and Their Use in Biomimetic Sensors. *Chem Rev* 100:2495
2. Whitcombe MJ, Kirsch N, Nicholls IA (2014) Molecular imprinting science and technology: a survey of the literature for the years 2004-2011. *J Mol Recognit* 27:297
3. Bates F, del Valle M (2015) Voltammetric sensor for theophylline using sol–gel immobilized molecularly imprinted polymer particles. *Microchim Acta* 182:933
4. Rovina K, Siddiquee S (2015) A review of recent advances in melamine detection techniques. *J Food Compos Anal* 43:25
5. National Toxicology Program (1983) NTP Carcinogenesis Bioassay of Melamine (CAS No. 108-78-1) in F344/N Rats and B6C3F1 Mice (Feed Study). *Natl Toxicol Program Tech Rep Ser* 245:1
6. Ogasawara H, Imaida K, Ishiwata H, et al (1995) Urinary bladder carcinogenesis induced by melamine in F344 male rats: correlation between carcinogenicity and urolith formation. *Carcinogenesis* 16:2773
7. Panuwet P, Wade EL, Nguyen JV, et al (2010) Quantification of cyanuric acid residue in human urine using high performance liquid chromatography–tandem mass spectrometry. *J Chromatogr B* 878:2916

8. Skinner CG, Thomas JD, Osterloh JD (2010) Melamine toxicity. *J Med Toxicol* 6:50
9. Lynch JM, Barbano DM (1999) Kjeldahl nitrogen analysis as a reference method for protein determination in dairy products. *J AOAC Int* 82:1389
10. Venkatasami G, Sowa JR (2010) A rapid, acetonitrile-free, HPLC method for determination of melamine in infant formula. *Anal Chim Acta* 665:227
11. Gossner CM-E, Schlundt J, Ben Embarek P, et al (2009) The Melamine Incident: Implications for International Food and Feed Safety. *Environ Health Perspect* 117:1803
12. Li Y, Xu J, Sun C (2015) Chemical sensors and biosensors for the detection of melamine. *RSC Adv* 5:1125
13. Pronk S, Pall S, Schulz R, et al (2013) GROMACS 4.5: a high-throughput and highly parallel open source molecular simulation toolkit. *Bioinformatics* 29:845
14. Chianella I, Lotierzo M, Piletsky SA, et al (2002) Rational Design of a Polymer Specific for Microcystin-LR Using a Computational Approach. *Anal Chem* 74:1288
15. Piletsky SA, Karim K, Piletska EV, et al (2001) Recognition of ephedrine enantiomers by molecularly imprinted polymers designed using a computational approach. *The Analyst* 126:1826
16. Irwin JJ, Sterling T, Mysinger MM, et al (2012) ZINC: A Free Tool to Discover Chemistry for Biology. *J Chem Inf Model* 52:1757
17. Pettersen EF, Goddard TD, Huang CC, et al (2004) UCSF Chimera--A visualization system for exploratory research and analysis. *J Comput Chem* 25:1605
18. Hornak V, Abel R, Okur A, et al (2006) Comparison of multiple Amber force fields and development of improved protein backbone parameters. *Proteins Struct Funct Bioinforma* 65:712
19. Sousa da Silva AW, Vranken WF (2012) ACPYPE - AnteChamber PYthon Parser interface. *BMC Res Notes* 5:367
20. Berendsen HJC, Postma JPM, van Gunsteren WF, et al (1984) Molecular dynamics with coupling to an external bath. *J Chem Phys* 81:3684
21. Hess B, Bekker H, Berendsen HJC, Fraaije JGEM (1997) LINCS: A linear constraint solver for molecular simulations. *J Comput Chem* 18:1463
22. York DM, Wlodawer A, Pedersen LG, Darden TA (1994) Atomic-level accuracy in

simulations of large protein crystals. *PNAS* 91:8715

23. McMillan WG, Teller E (1951) The Assumptions of the B.E.T. Theory. *J Phys Chem* 55:17
24. Zhu L, Xu G, Wei F, et al (2015) Determination of melamine in powdered milk by molecularly imprinted stir bar sorptive extraction coupled with HPLC. *J Colloid Interface Sci* 454:8
25. Wang Y, Liu J-B, Tang S-S, Jin R-F (2015) Preparation of melamine molecularly imprinted polymer by computer-aided design. *J Sep Sci* 38:2647
26. He D, Zhang X, Gao B, et al (2014) Preparation of magnetic molecularly imprinted polymer for the extraction of melamine from milk followed by liquid chromatography-tandem mass spectrometry. *Food Control* 36:36
27. Yang H-H, Zhou W-H, Guo X-C, et al (2009) Molecularly imprinted polymer as SPE sorbent for selective extraction of melamine in dairy products. *Talanta* 80:821
28. He L, Su Y, Shen X, et al (2009) Solid-phase extraction of melamine from aqueous samples using water-compatible molecularly imprinted polymers. *J Sep Sci* 32:3310
29. Yan H, Cheng X, Sun N, et al (2012) Rapid and selective screening of melamine in bovine milk using molecularly imprinted matrix solid-phase dispersion coupled with liquid chromatography-ultraviolet detection. *J Chromatogr B* 908:137
30. Liang R, Zhang R, Qin W (2009) Potentiometric sensor based on molecularly imprinted polymer for determination of melamine in milk. *Sens Actuators B Chem* 141:544
31. Barton AFM (1991) *CRC handbook of solubility parameters and other cohesion parameters*, 2nd ed. CRC Press, Boca Raton
32. Reichardt C, Welton T (2011) *Solvents and solvent effects in organic chemistry*, 4th, updated and enl. ed. Wiley-VCH, Weinheim, Germany
33. Yusof N, Rahman S, Hussein M, Ibrahim N (2013) Preparation and Characterization of Molecularly Imprinted Polymer as SPE Sorbent for Melamine Isolation. *Polymers* 5:1215
34. Nicholls I, Piletsky S, Chen B, et al (2004) Thermodynamic Considerations and the Use of Molecular Modeling as a Tool for Predicting MIP Performance. In: Yan M, Ramström O (eds) *Mol. Imprinted Mater.* CRC Press, pp 363–393
35. Keith LH, Walters DB, National Toxicology Program (U.S.) (1992) *National Toxicology Program's chemical solubility compendium*. Lewis Publishers, Boca Raton

- 
36. Zheng M-M, Gong R, Zhao X, Feng Y-Q (2010) Selective sample pretreatment by molecularly imprinted polymer monolith for the analysis of fluoroquinolones from milk samples. *J Chromatogr A* 1217:2075
  37. Gryshchenko A, Bottaro C (2014) Development of Molecularly Imprinted Polymer in Porous Film Format for Binding of Phenol and Alkylphenols from Water. *Int J Mol Sci* 15:1338
  38. Jeffrey GA (1997) *An introduction to hydrogen bonding*. Oxford University Press, New York
  39. Villamena FA, De La Cruz AA (2001) Caffeine selectivity of divinylbenzene crosslinked polymers in aqueous media. *J Appl Polym Sci* 82:195
  40. Hansen CM (2007) *Hansen solubility parameters: a user's handbook*, 2nd ed. CRC Press, Boca Raton
  41. Spivak D (2005) Optimization, evaluation, and characterization of molecularly imprinted polymers. *Adv Drug Deliv Rev* 57:1779
  42. Li J, Wei G, Zhang Y (2012) Molecularly imprinted polymers as recognition elements in sensors. In: Li S, Ge Y, Piletsky SA, Lunec J (eds) *Mol. Imprinted Sens. Overv. Appl.*, 1st ed. Elsevier, Amsterdam ; Boston, pp 35–56
  43. Castell OK, Barrow DA, Kamarudin AR, Allender CJ (2011) Current practices for describing the performance of molecularly imprinted polymers can be misleading and may be hampering the development of the field. *J Mol Recognit* 24:1115
  44. Schauperl M, Lewis DW (2015) Probing the Structural and Binding Mechanism Heterogeneity of Molecularly Imprinted Polymers. *J Phys Chem B* 119:563
  45. Farrington K, Magner E, Regan F (2006) Predicting the performance of molecularly imprinted polymers: Selective extraction of caffeine by molecularly imprinted solid phase extraction. *Anal Chim Acta* 566:60
  46. Ren B, Li C, Yuan X, Wang F (2003) Determination and correlation of melamine solubility. *Huagong Xuebao J Chem Ind Eng China* 54:1001
  47. Sigma Aldrich Free radical initiators - thermal initiators.  
[http://www.sigmaaldrich.com/content/dam/sigma-aldrich/docs/Aldrich/General\\_Information/thermal\\_initiators.pdf](http://www.sigmaaldrich.com/content/dam/sigma-aldrich/docs/Aldrich/General_Information/thermal_initiators.pdf) . Accessed 24 Sep 2015
  48. Mijangos I, Navarro-Villoslada F, Guerreiro A, et al (2006) Influence of initiator and different polymerisation conditions on performance of molecularly imprinted polymers. *Biosens Bioelectron* 22:381

49. Ibáñez M, Sancho JV, Hernández F (2009) Determination of melamine in milk-based products and other food and beverage products by ion-pair liquid chromatography–tandem mass spectrometry. *Anal Chim Acta* 649:91